FR- 2475- 101

A Krueger

JUN 2 9 1970

FINAL REPORT
FOR THE
BACKSCATTER ULTRAVIOLET (BUV) INSTRUMENT

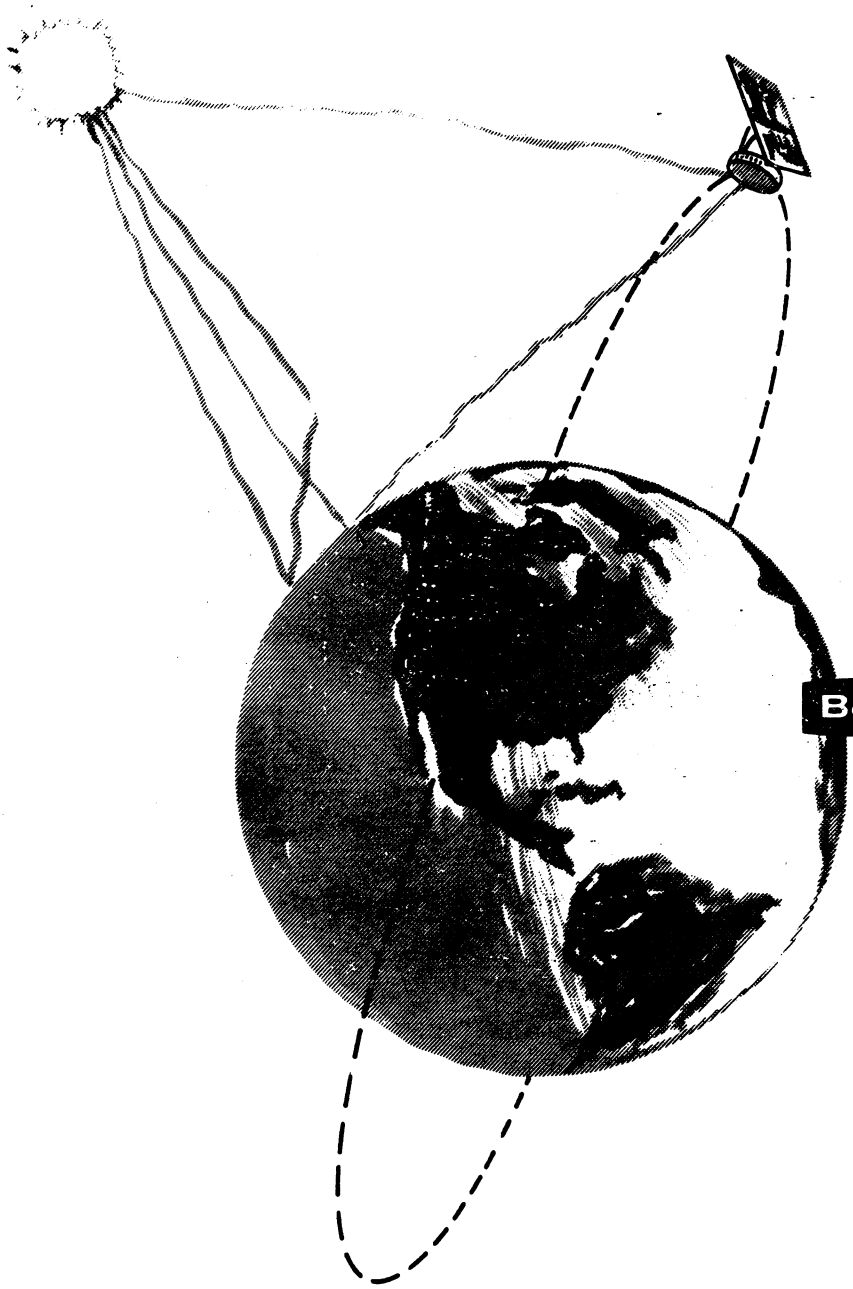

VOLUME 1

Prepared by

Beckman INSTRUMENTS, INC.
ADVANCED TECHNOLOGY OPERATIONS
FULLERTON, CALIFORNIA • 92634

for

Goddard Space Flight Center
Greenbelt, Maryland

FR-2475-101

Volume I

Final Report

for the

BACKSCATTER ULTRAVIOLET (BUV) INSTRUMENT

Contract No. NAS5-10381

Covering the Period:

(April 1967 to June 1970)

Goddard Space Flight Center

Contracting Officer: Henry Arista
Technical Monitor: Arlin J. Krueger

Prepared By:

Beckman® INSTRUMENTS, INC.
ADVANCED TECHNOLOGY OPERATIONS
FULLERTON, CALIFORNIA • 92634

Project Manager: Merton A. Robinson

Prepared For

GODDARD SPACE FLIGHT CENTER
Greenbelt, Maryland

Volume I

TABLE OF CONTENTS

PARAGRAPH		PAGE
SECTION I	INTRODUCTION	
1.1	General	1-1
1.2	Program Results	1-1
1.3	Description and Purpose of the BUV Instrument	1-2
SECTION II	SYSTEM DESCRIPTION	
2.1	System Functional Description	2-1
2.2	Specification Summary	2-9
SECTION III	OPTICS	
3.1	Design Study Analysis	3-1
3.2	Optical Tests and Results	3-46

LIST OF ILLUSTRATIONS

FIGURE NO.	NAME	PAGE
1-1	Optical Diagram of the BUV Photometer and Monochromator	1-3
1-2	Schematic Representation of the Satellite Viewing Attitude at Various Orbital Positions	1-6
2-1	BUV Instrument, Simplified Functional Block Diagram	2-4
2-2	Data Format	2-7
2-3	Bench Test Unit	2-8
3-1	Fastie-Ebert Monochromator	3-21
3-2	Common Bearing Axis with Identical Angular Orientation	3-22
3-3	BUV Monochromator Imaging Characteristics (Horizontal Beam)	3-24
3-4	Double Ebert Mono-f/5 250 mm Fl, 2400 1/mm Grating--Double Prism	3-30
3-5	Double Ebert Mono-f/5 250 mm Fl, 2400 1/mm Grating--Double Prism	3-32
3-6	Double Ebert Mono-f/5 250 mm Fl, 2400 1/mm Grating--Corner Mirror	3-33
3-7	Double Ebert Mono-f/5 250 mm Fl, 2400 1/mm Grating--Two Mirror	3-34
3-8	81 Ray Spot Diagram at Intermediate Slit for Y = 0 Double Ebert Mono-f/5 250 mm Fl, 2400 1/mm Grating--Corner Mirror	3-36
3-9	81 Ray Spot Diagram at Intermediate Slit for Y = 6.25 MM Double Ebert Mono-f/5 250 mm Fl, 2400 1/mm Grating--Corner Mirror	3-37
3-10	81 Ray Spot Diagram at Intermediate Slit for Y = 12.5 MM Double Ebert Mono-f/5 250 mm Fl, 2400 1/mm Grating--Corner Mirror	3-38
3-11	81 Ray Spot Diagram at Exit Slit for Y = 0. Double Ebert Mono-f/5 250 mm Fl, 2400 1/mm Grating--Corner Mirror	3-39
3-12	81 Ray Spot Diagram at Exit Slit for Y = 6.25 MM. Double Ebert Mono-f/5 250 mm Fl, 2400 1/mm Grating--Corner Mirror	3-40
3-13	81 Ray Spot Diagram at Exit Slit for Y = 12.5 MM. Double Ebert Mono-f/5 250 mm Fl, 2400 1/mm Grating--Corner Mirror	3-41
3-14	81 Ray Spot Diagram at Exit Slit for Y = 0. Double Ebert Mono-f/5 250 mm Fl, 2400 1/mm Grating--Two Mirror	3-42
3-15	81 Ray Spot Diagram at Exit Slit for Y = 6.25 MM. Double Ebert Mono-f/5 250 mm Fl, 2400 1/mm Grating--Two Mirror	3-43
3-16	81 Ray Spot Diagram at Exit Slit for Y = 12.5 MM. Double Ebert Mono-f/5 250 mm Fl, 2400 1/mm Grating--Two Mirror	3-44
3-17	Transmission Efficiency Test Setup	3-47

LIST OF ILLUSTRATIONS (continued)

FIGURE NO.	NAME	PAGE
3-18	DK-2 Transmission Bandwidth Scan of Filter Used for Measurements	3-49
3-19	BUV First Monochromator Collimating Mirror Percent of Energy Reflectance Vs. Wavelength	3-53
3-20	Wavelength Transfer Function 2537 Å, P103 Instrument	3-87
3-21	" " " 2537 Å, Engineering Model	3-88
3-22	" " " 2967 Å, Engineering Model	3-89
3-23	" " " 3341 Å, Engineering Model	3-90
3-24	Slit Transfer Function 2967 Å Scan I, P103 Instrument	3-91
3-25	" " " 2967 Å Scan G, " "	3-92
3-26	" " " 3341 Å Scan J, " "	3-93
3-27	" " " 3341 Å Scan H, " "	3-94
3-28	Field-of-View, Test Setup	3-100
3-29	" " P103 Instrument	3-102
3-30	" " F104 Instrument	3-103
3-31	Orientation of BUV for Field-of-View Measurements Perpendicular and Parallel to Outboard Surface of BUV	3-104
3-32	Traversal of Photometer Aperture for Field-of-View Measurements with BUV Outboard Surface Perpendicular and Parallel to Mounting Surface	3-105
3-33	Monochromator Field-of-View at 3398 Å, Parallel to Outboard Surface--F104 Instrument	3-106
3-34	Monochromator Field-of-View at 2537 Å, Parallel to Outboard Surface--F104 Instrument	3-107
3-35	Photometer Field-of-View Parallel to Outboard Surface--F104 Instrument	3-108
3-36	Field-of-View Perpendicular to Outboard Surface--F104 Instrument	3-109
3-37	Monochromator Field-of-View at 3398 Å, Parallel to Outboard Surface--P103 Instrument	3-110
3-38	Monochromator Field-of-View at 3398 Å, Perpendicular to Outboard Surface--P103 Instrument	3-111
3-39	Monochromator Field-of-View at 2537 Å, Parallel to Outboard Surface--P103 Instrument	3-112
3-40	Photometer Field-of-View at 3800 Å, Parallel to Outboard Surface--P103 Instrument	3-113
3-41	Photometer Field-of-View at 3800 Å, Perpendicular to Outboard Surface--P103 Instrument	3-114
3-42	BUV Test Fixture	3-115
3-43	P103 Instrument--MgO Plate	3-117
3-44	P103 Instrument--Zenith Sky	3-118
3-45	F104 Instrument--MgO Plate	3-119
3-46	F104 Instrument--Zenith Sky	3-120
3-47	Concentrated Beam of Light Directed into Photometer	3-122
3-48	Focused Sunlight Directed into Monochromator Horn	3-122

LIST OF ILLUSTRATIONS (continued)

FIGURE NO.	NAME	PAGE
3-49	Installation of Additional Stray-Light Shield	3-123
3-50	Orientation of Grating in Test Fixture (Equivalent of First Monochromator)	3-127
3-51	Orientation of Grating in BUV First Monochromator	3-128
3-52	BUV and Test Fixture--Second Monochromator	3-129
3-53	First Monochromator Blaze Orientation	3-130
3-54	Second Monochromator Blaze Orientation	3-131
3-55	Grating Selection	3-135
3-56	Calcite Depolarizer	3-137
3-57	Assembly of the Complete Depolarizer into the BUV Instrument	3-138
3-58	Polarization Sensitivity Experimental Equipment Layout	3-139
3-59	Polarization Sensitivity (P103 Instrument)	3-142
3-60	Polarization Sensitivity Interpolation Graph (P103 Instrument)	3-143
3-61	Polarization Sensitivity with Rotating Polarized Light Source (F104 Instrument)	3-146
3-62	Polarization Sensitivity--Manual Poladisk Rotation (F104 Instrument)	3-147
3-63	Polarization Sensitivity--Manual Data and Average (F104 Instrument)	3-150
3-64	Percent Transmission of Corning Filters (Before Irradiation) (1 of 2)	3-152
3-65	Percent Transmission of Corning Filters (Before Irradiation) (2 of 2)	3-153
3-66	Percent Transmission of Corning Filters (After Irradiation)	3-154
3-67	Percent Transmission of Cerium Doped Corning Filters (Before Irradiation) (1 of 2)	3-155
3-68	Percent Transmission of Cerium Doped Corning Filters (Before Irradiation) (2 of 2)	3-156
3-69	Percent Transmission of Cerium Doped Corning Filters (After Irradiation)	3-157
3-70	Percent Transmission of Interference Filter Cement (After Irradiation) (1 of 2)	3-158
3-71	Percent Transmission of Interference Filter Cement (After Irradiation) (2 of 2)	3-159
3-72	Percent Transmission of Interference Filter Peak (Before Irradiation)	3-160
3-73	Half-Bandwidth of Interference Filter (Before Irradiation)	3-161
3-74	Percent Transmission (Leakage) in Filter Sidebands (After Irradiation)	3-162
3-75	Half-Bandwidth of Interference Filter (After Irradiation)	3-163
3-76	Percent Transmission of Interference Filter Peak (After Irradiation)	3-164
3-77	Percent Transmission of Interference Filter Sidebands (Before Irradiation)	3-165

LIST OF ILLUSTRATIONS (continued)

FIGURE NO.	NAME	PAGE
3-78	Percent Transmission of Interference Filters (No Irradiation) (1 of 3)	3-167
3-79	Percent Transmission of Interference Filters (No Irradiation) (2 of 3)	3-168
3-80	Percent Transmission of Interference Filter (No Irradiation) (3 of 3)	3-169
3-81	Reflection Characteristics (1 of 4)	3-170
3-82	Reflection Characteristics (2 of 4)	3-171
3-83	Reflection Characteristics (3 of 4)	3-172
3-84	Reflection Characteristics (4 of 4)	3-173
3-85	Absolute Reflectance of Diffuser	3-177
3-86	Aluminum Diffuser Plate Reflectance vs. Wavelength	3-179
3-87	" " " " " Instrument Position	3-180
3-88	Barium Diffuser Plate--Reflectance vs. Wavelength	3-181
3-89	" " " " " Instrument Position	3-182
3-90	Angular Relationship Between Incident Energy and the BUV Breadboard	3-183
3-91	BUV in Vertical Position for Goniometric Sensitivity Measurements	3-184
3-92	BUV in Horizontal Position for Goniometric Sensitivity	3-185

LIST OF TABLES

TABLE NO.	NAME	PAGE
3-1	Performance Characteristics of a Littrow Monochromator with a 250 mm Focal Length and a Grating with 2400 grooves/mm	3-6
3-2	Performance Characteristics of a Prism Littrow Monochromator with a 250 mm Focal Length and a Fused Silica Reflecting Prism with Prism Angle of 36°	3-9
3-3	BUV Transmission Efficiency; P103 Instrument	3-50
3-4	BUV Transmission Efficiency; F104 Instrument	3-51
3-5	Slit Functions, P103 Instrument	3-95
3-6	Typical Monochromator Checkout Procedure	3-97
3-7	Typical Monochromator Data Record	3-98
3-8	Typical Photometer Checkout Procedure	3-99
3-9	Results of Stray Light Shield Installation (2 sheets)	3-124
3-10	Grating Selection Criteria	3-133
3-11	Summary of Computer Printout Selection Matrix	3-134
3-12	Polarization Sensitivity, Manual and Lock-in Data--Two Different Geometries (P103)	3-141
3-13	Polarization Sensitivity Summary of Results, F104 (Expressed in Percent)	3-145
3-14	Polarization Sensitivity Summary of Results, F104 (Expressed in Percent)	3-149
3-15	Absolute Reflectance Diffuser	3-178

SECTION I

INTRODUCTION

1.1 GENERAL

This final project report covers the design, development, construction, testing and qualification of the NIMBUS D BUV (Backscatter Ultraviolet) instrument. The instrument was designed and constructed in accordance with GSFC specification S-623-P-1 and amendments.

1.2 PROGRAM RESULTS

The design phase consisted of activity in three areas of technology: (1) Optical, (2) Mechanical, and (3) Electrical. Beckman Instruments, Inc. performed the tasks concerned with optical and mechanical design while Analog Technology Corporation was the electronics subcontractor.

Initial studies resulted in the development of a breadboard model of the BUV instrument. Following extensive testing, additional mathematical analyses, and required modifications, preliminary and critical design reviews were performed. The results of these activities were the construction of an engineering model, used for extensive testing and demonstration of the final design features. Final design data resulted in the construction of two flight-rated instruments, serial numbers P103 and F104. On April 8, 1970, the P103 instrument was successfully launched into orbit on NIMBUS D and is presently fully operational.

1.3 DESCRIPTION AND PURPOSE OF THE BUV INSTRUMENT

The Backscatter Ultraviolet (BUV) Instrument is a satellite-borne scientific instrument which monitors the spatial distribution of atmospheric ozone by measuring the intensity of ultraviolet radiation backscattered from the earth's atmosphere. The knowledge of atmospheric ozone distribution on a global scale is needed for studies of the energy balance and photochemistry of the stratosphere, the mass exchange between the lower stratosphere and trophosphere, and general atmospheric circulation. To determine the ozone distribution, the BUV subsystem makes the following measurements:

1. Backscattered Ultraviolet Radiation from the daytime sun-illuminated atmosphere.
2. Direct solar radiation.
3. Reflected solar radiation from the lunar surface during gibbous and full phases of the moon.
4. Backscattered Ultraviolet Radiation from the night-time atmosphere illuminated by the moon.

The BUV Instrument, as shown in Figure 1-1, is basically a precision monochromator and photometer with supplementary optical, mechanical, and electronic equipment.

The monochromator has a wavelength range from 2500 Å to 3400 Å. Twelve steps in this range are selected for sample wavelengths. The instrument continuously scans the wavelength range and remains on the selected wavelength steps a certain time interval to take readings.

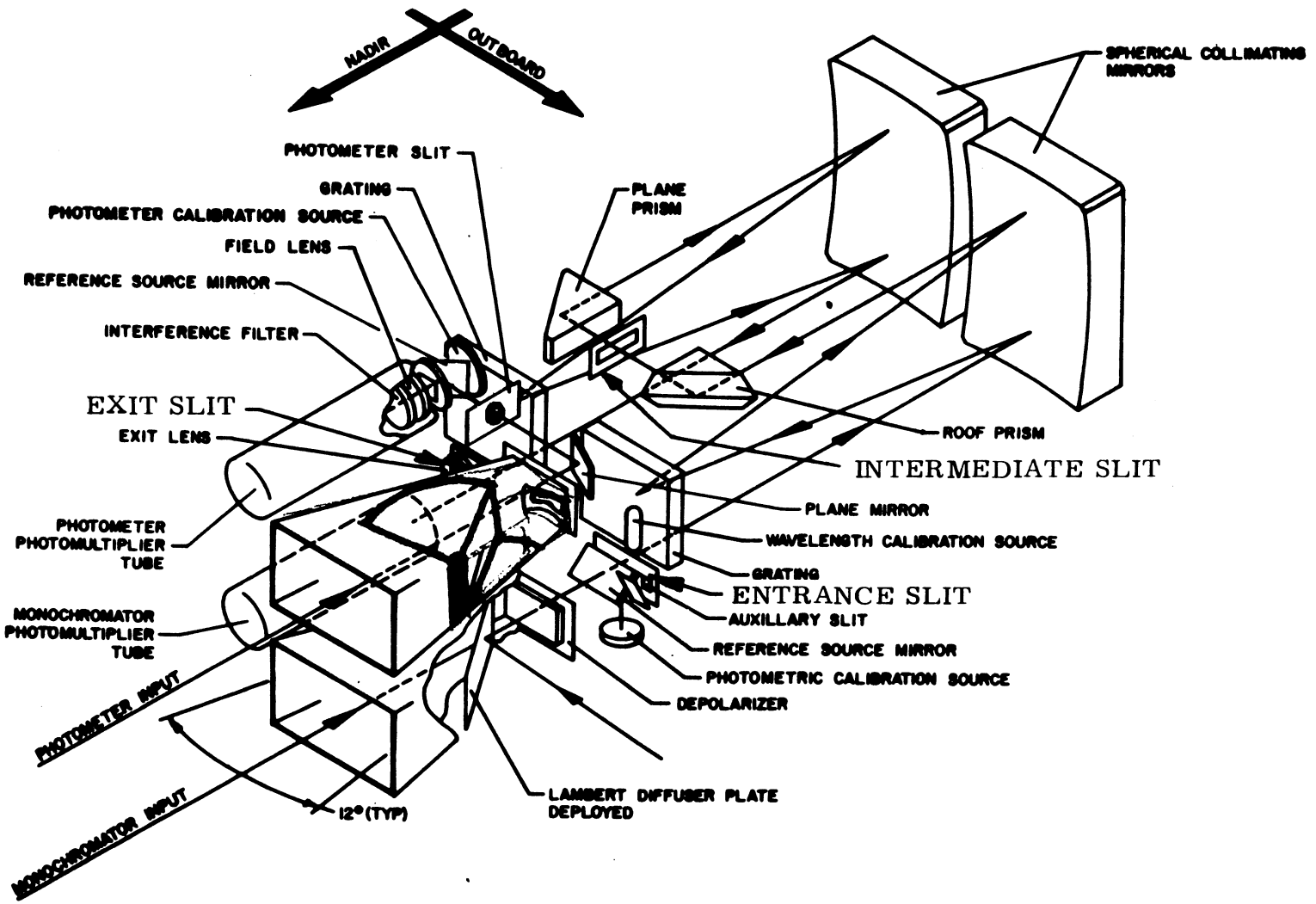

Figure 1-1. Optical Diagram of the BUV Photometer and Monochromator

The double monochromator allows maximum flux transfer for the wavelength range of interest and limits the total unwanted radiant flux output (stray light) to less than one percent of the wanted spectral radiant flux output. The wavelength resolution of the monochromator is 10 Å at all wavelengths, using gratings as the dispersive element.

The optical elements in the monochromator render the BUV Instrument selectively sensitive to polarized radiation. A depolarizer is installed in front of the entrance slit to minimize the polarization effect.

Wavelength calibration is provided by an internal mercury-argon lamp. The 2537 Å mercury line is scanned by the wavelength cam in seven discrete steps. The location of the line with respect to the steps indicates wavelength accuracy.

Photometric calibration is provided by an internal radioactive phosphor source. The broad emission band of the source covers almost the entire wavelength range of the Instrument. The response of the photomultiplier to the photometric source flux is used to monitor Instrument optical transmission efficiency.

A photometric calibration of the photometer is provided which is identical to the system employed in the monochromator, except for the different wavelength response of the phosphor.

Further calibration is provided which uses the sun's direct radiation. Upon command, diffuser plates for photometer and monochromator are deployed which direct the sun's radiation into the Instrument for comparison with the back-scattered ozone radiation from the earth's atmosphere.

The instrument is designed to perform trouble-free for a minimum of one year in orbit. Figure 1-2 is a schematic representation of the satellite viewing attitude at various orbital positions.

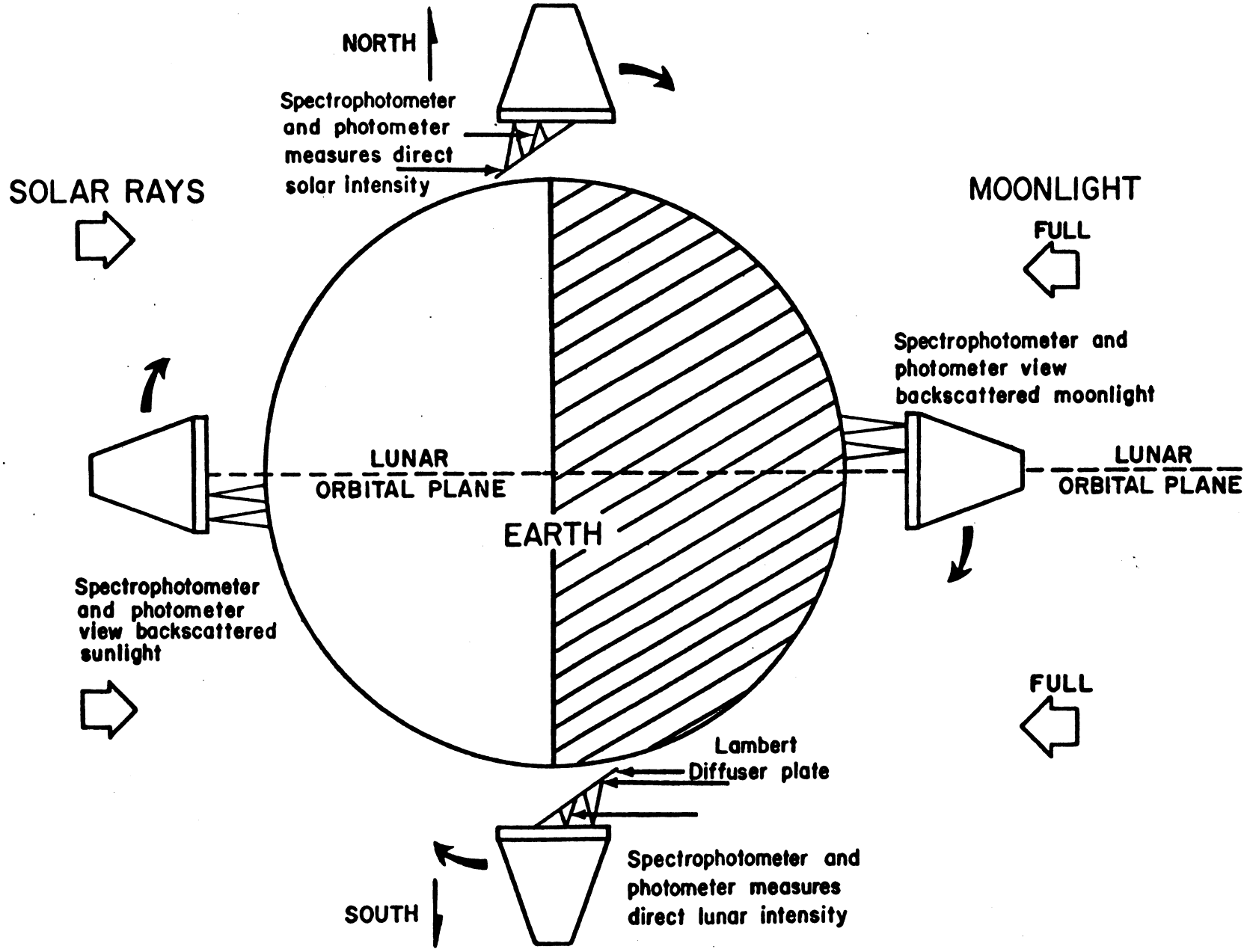

Figure 1-2. Schematic Representation of the Satellite Viewing Attitude at Various Orbital Positions

SECTION II

SYSTEM DESCRIPTION

2.1 SYSTEM FUNCTIONAL DESCRIPTION

The BUV subsystem is composed of two units:

1. Sensor or optical module
2. Electronics module

The sensor module houses the optical components of the subsystem, the high voltage power supplies and the first stages of the signal processing electronics.

The electronics module houses the bulk of the signal processing electronics plus the circuitry required to support the subsystem. The sensor module is located in bay 9 and is a 4/4 configuration unit, while the electronics module is located in bay 8 and is a 3/0 configuration unit. The total power consumption when operating in the normal mode is 13.181 watts.

2.1.1 Mechanical and Optical

The sensor module consists basically of a spectrometer (monochromator) and a photometer. As the spacecraft orbits the earth, the monochromator monitors sequentially the intensity of ultraviolet radiation backscattered and reflected from the earths atmosphere in 12 wavelengths in which ozone attenuation occurs. The photometer monitors the reflected ultraviolet radiation in a single wavelength span in which attenuation by ozone does not occur. During each orbit, the subsystem field of view is switched to the sun by deployment of a set of diffuser plates to provide a measurement of the intensity of the radiation

impinging on the earth. During those orbits in which night time measurements are made, the diffuser is deployed at the appropriate time to view the moon for similar reasons. These measurements of incident, scattered, and unattenuated light are transmitted to the ground, where appropriate processing combines them, resulting in a determination of the spatial distribution of atmospheric ozone over the surface of the earth.

Additional calibrations of the instrument are provided for wavelength, photometric, and electronic checking.

The wavelength calibration is provided by an internal mercury-argon lamp. The 2537 Angstroms mercury line is scanned by the wavelength cam in 7 discrete steps. The location of the maximum response point with respect to the steps indicates the wavelength accuracy. Photometric calibration of the monochromator and photometer is provided by two internal radioactive phosphor sources. The broad emission band of the sources covers almost the entire wavelength range of the instrument. The response of the photomultiplier to the photometric sources is used to monitor the optical transmission efficiency of the instrument. The radiation source for the photometer calibration is identical to that employed in the monochromator except for the different wavelength response of the phosphor.

The electronics calibration consists of a 9.2 second interval during which PMT dark current is measured; three pulse calibrations utilizing three different pulse heights; and two analog current calibrations where a precision current is injected into the electrometer input of both channels to allow verification of the proper operation in orbit.

2.1.2 Electronics

The BUV electronics consists of four separate electronic assemblies: The electronics module; sensor module 3, mounted on the optical sensor module; and two identical units, sensor modules 1 and 2, each mounted directly to the rear of their respective photomultiplier tube bases, also in the optical module.

The signal processing electronics of the monochromator and photometer are identical. Figure 2-1 is a block diagram of the signal processing electronics.

Light impinging upon the photocathode of either of the photomultiplier tubes produces electrons which are multiplied by the dynode structure of the tube as a function of the high voltage applied across the dynode structure. The output of the photomultiplier tube (PMT) is a series of current pulses. These current pulses are applied to an electrometer which provides two outputs: a dc level proportional to the average current input and a voltage pulse out for each current pulse in. The electrometer gain is controlled by the automatic range sequencer (ARS) which affords an automatic selection of three discrete electrometer gains by relay switching of the electrometer feedback network. In addition, two automatically switched gains are provided for PMT operation.

The analog output of the electrometer is fed to a logarithmic analog-to-digital converter whose output is sent to the data handling circuitry. The pulse output of the electrometer is connected to pulse amplifiers and shapers and sent to a discriminator and anti-coincidence circuit which routes the resultant accepted pulses either to a data register or an energetic particle register. These circuits also interface with the data handling circuits which

$$y = 10^{b} x^{m}$$

$$\frac{d}{dx}(a^{x})$$

$$\frac{\partial y}{\partial b} = x^{m} 10^{b} \ln b$$

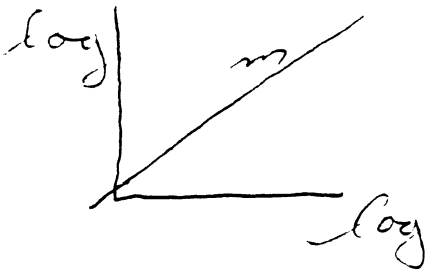

$$\Delta y = x^{m} 10^{b} \ln b \, \Delta b$$

$$= x^{m} 10^{-11.286} [\ln(-11.286)](.113)$$

$b = -11.286$
$\Delta b = .113$

$$\Delta y = N x^{m}$$

$$= N 2^{1.01}$$

$$= N$$

$$\frac{\Delta y}{y} \times 100 < 2\% \quad \text{good}$$

$$\frac{\Delta y}{1.017 \times 10^{-11}} \times 100 < 2\%$$

11.286
.113
11.399

$$m = \frac{\log 1}{\log I}$$

$$\alpha = \frac{OUT}{IN}$$

$$\hat{y} = 10^{b} \hat{x}^{m}$$

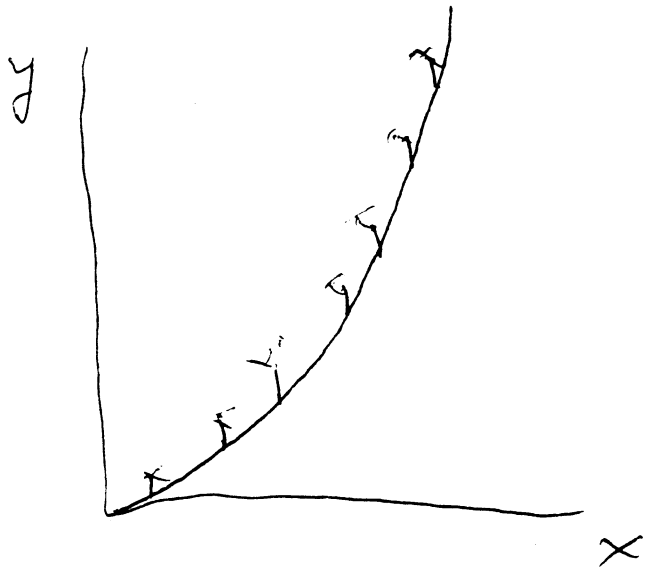

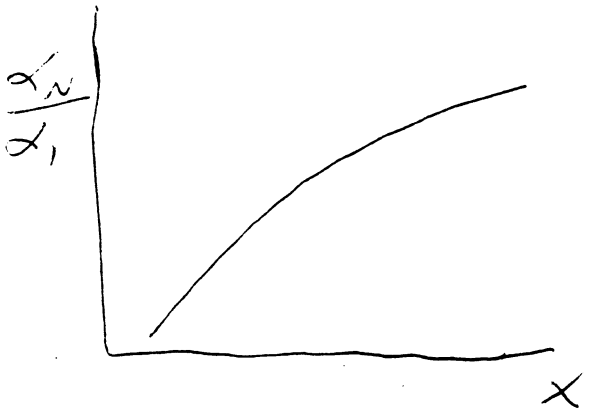

$$\frac{\alpha_N}{\alpha_1} = \log X \quad \text{OR} \quad \log \frac{\alpha_n}{\alpha_1} = \log X$$

$$\alpha_N = \log X \, \alpha_1$$

$$\frac{y_N}{x_N} = \log X \, \frac{y_1}{x_1}$$

$$\frac{y_N}{x_N} = 10^b \frac{x_N^m}{x_N}$$

$$\frac{\frac{y_N}{x_N}}{\frac{y_1}{x_1}} = \frac{10^b x_N^{m-1}}{\frac{y_1}{x_1}}$$

$$= \frac{10^b x_N^{m-1}}{\frac{10^b x_1^m}{x_1}}$$

$$y = 10^{b} x^{m}$$

is $\dfrac{\frac{y_N}{x_N}}{\frac{y_1}{x_1}} \overset{?}{=} \log x$

$$\begin{array}{r} 389 \\ 23 \\ \hline 2 \end{array}$$

$$\begin{array}{r} 99 \\ 70 \\ \hline 169 \\ \hline 175 \end{array}$$

$\frac{A_N}{\Phi_N} \frac{\Psi}{A_1} =$

$\frac{A_1}{\Phi_1}$

y = PMT i

x = lamp intensity

$\log y$ vs $\log x$

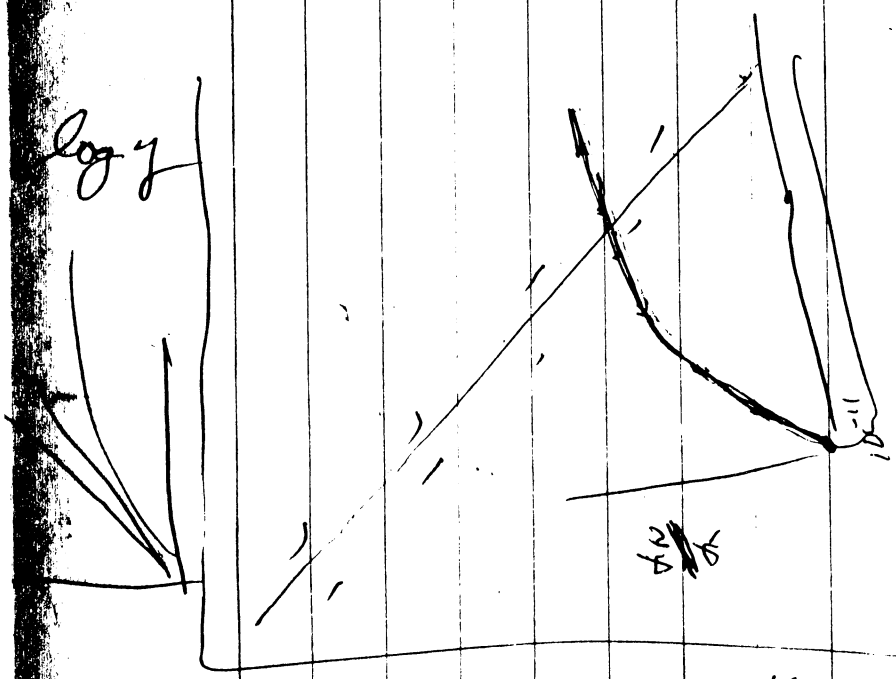

$\log \hat{y} = m \log \hat{x} + b$

$= \log \hat{x}^m + b$

$\log \hat{y} - \log \hat{x}^m = b$

$\log \left(\frac{\hat{y}}{\hat{x}^m} \right) = b$

$\frac{\hat{y}}{\hat{x}^m} = 10^b$

$\hat{y} = 10^b \hat{x}^m$

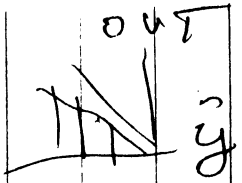

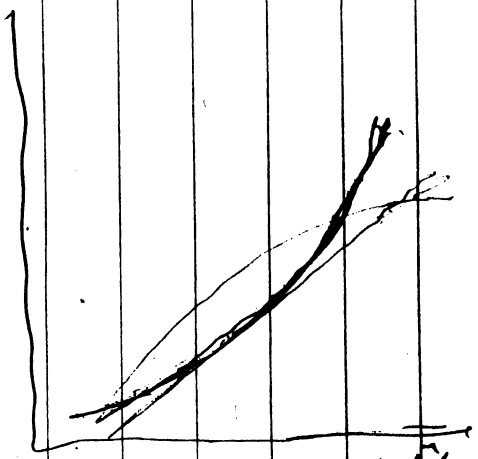

$-.5085 \times 10^{-11}$

$-.506 \times 10^{-11}$

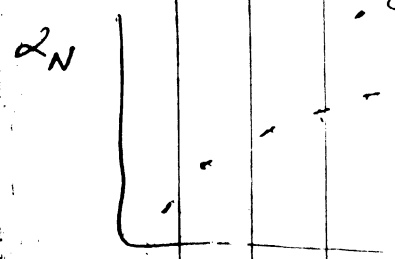

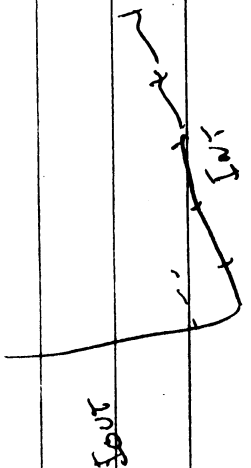

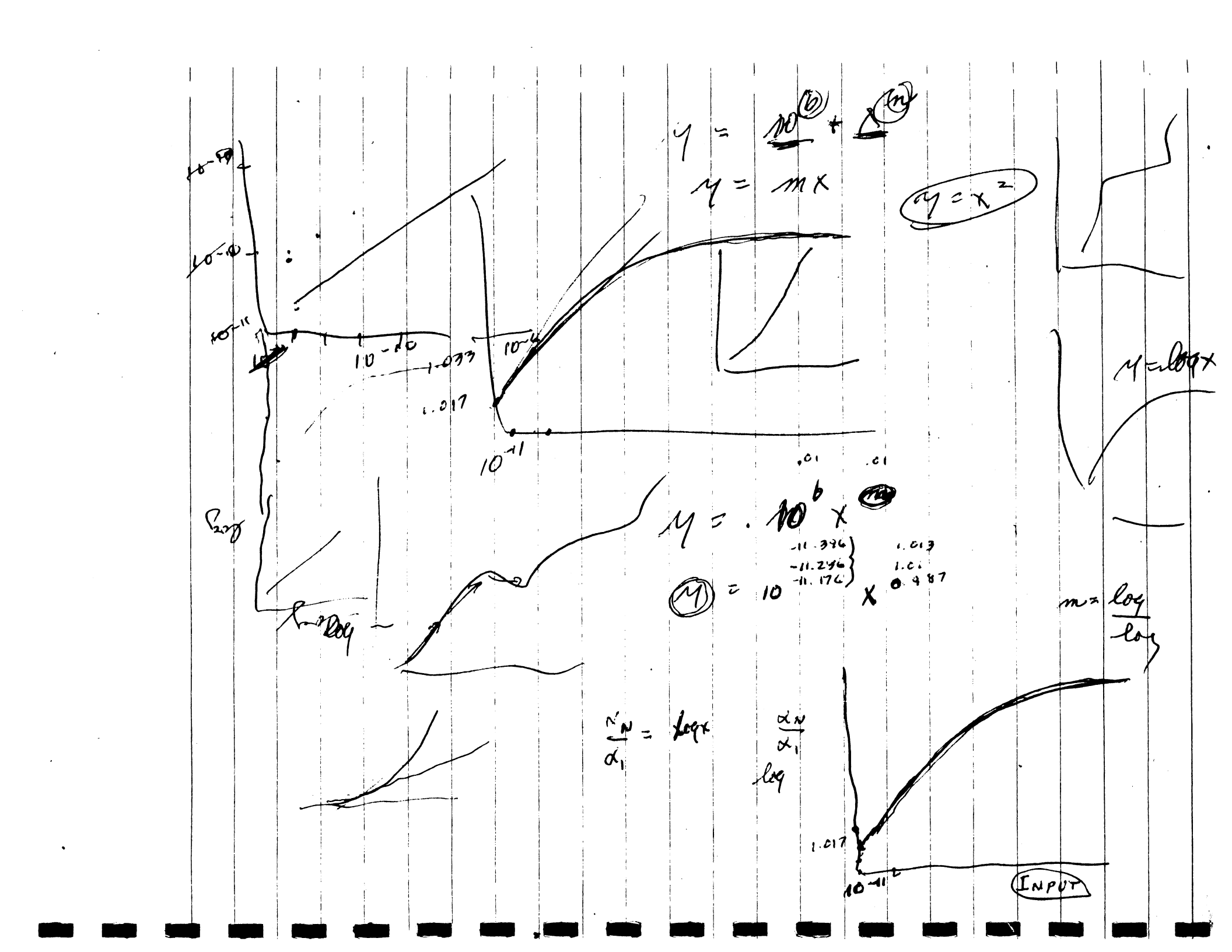
y = 10^b + m
y = mx
y = x^2
y = log x
y = . 10^b x
m = log / log
INPUT

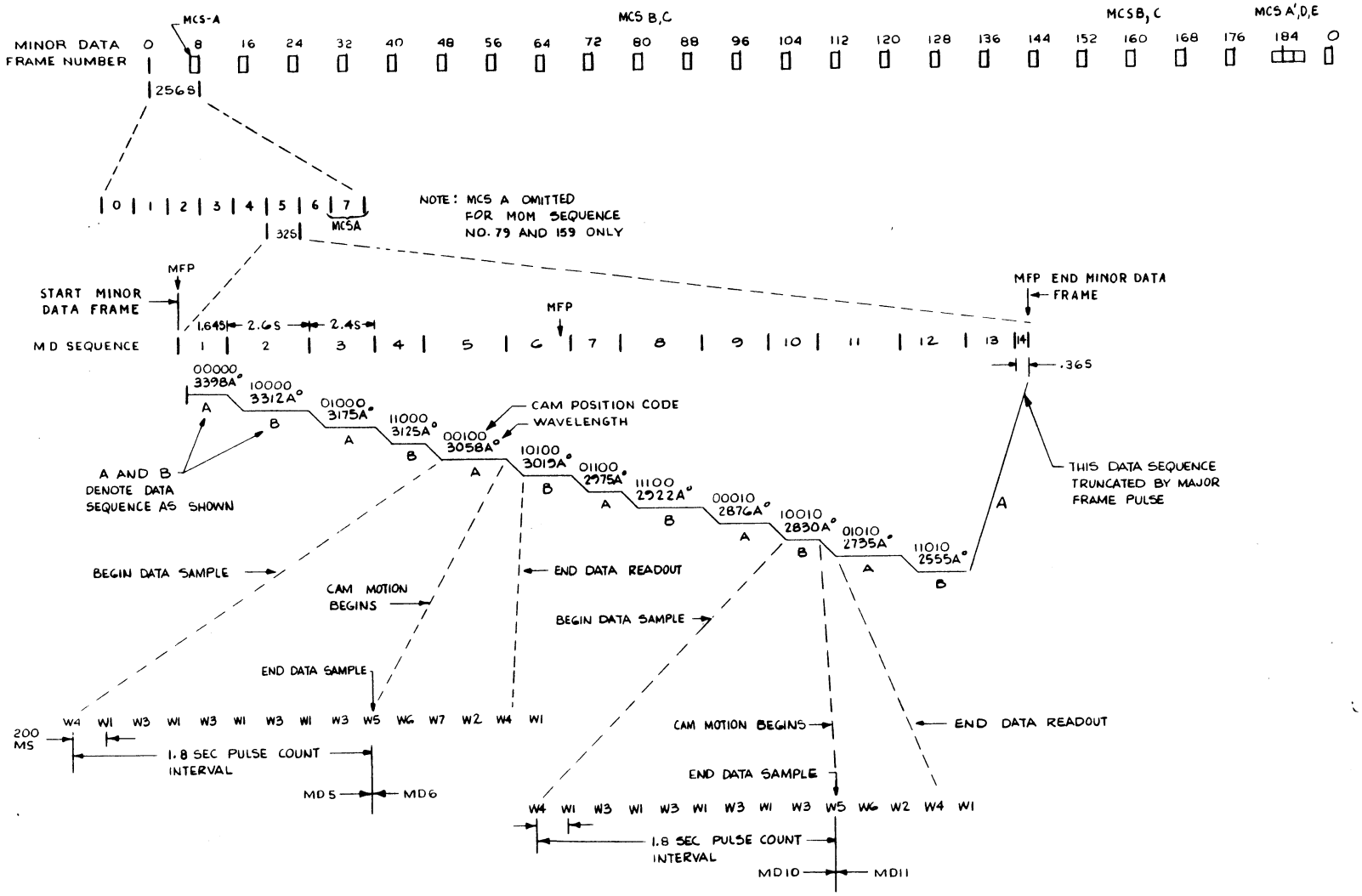

Figure 2-2. Data Format

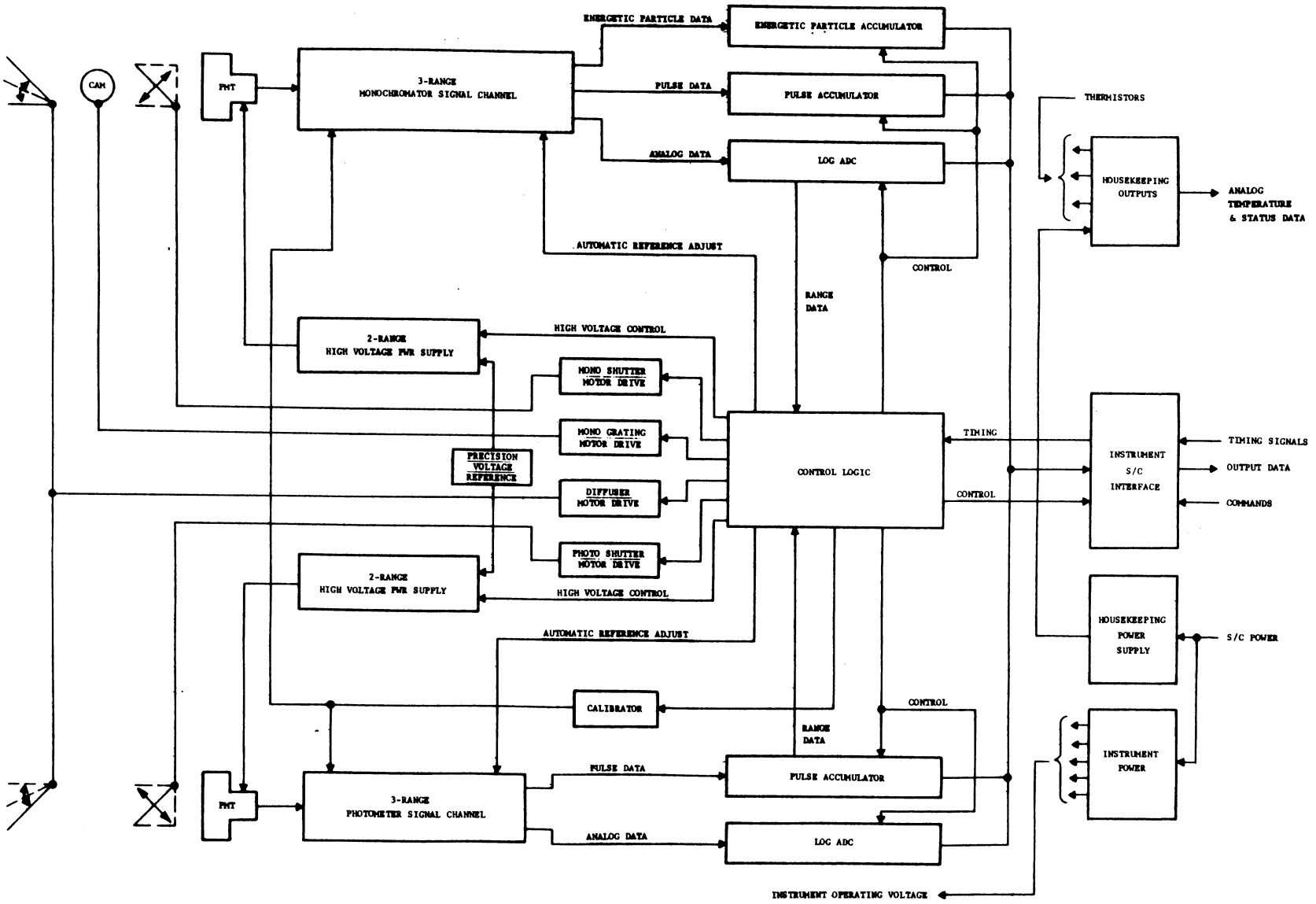

Figure 2-1. BUV Instrument, Simplified Functional Block Diagram

format the data to a form acceptable to the VIP "Digital A" channel. In addition to the signal processing electronics, there are two switchable high voltage supplies, four motor drive circuit assemblies, various control logic, separate power supplies for the calibration lamp, main instrument, and housekeeping voltages, and the electronics which provides for the reception and performance of the various spacecraft commands.

2.1.3 Operational Sequence

The BUV "power-on" command initiates a 6144 second duration experiment cycle. This cycle is repeated until the power off command is received and consists of 24 BUV master data frames, each of which is subdivided into eight minor data frames of 32 seconds duration each. (Each of these BUV minor data frames equals two VIP major frames.)

Each BUV master data frame consists of seven minor data frames during which experimental data is collected, followed by a single minor data frame in which a calibration is performed. During the calibration frame, the electronics calibration is performed except during master data frames No. 11 and No. 21, where a photometric calibration replaces the electronic calibration. Also, during the 24th and 1st master data frames, a series of wavelength calibrations are performed in the monochromator only, consisting of a normal electronics calibration followed by a BUV minor data frame in which the primary wavelength calibration is performed, followed immediately after by a secondary wavelength calibration. The total experiment sequence then repeats.

2.1.4 Data Format (Figure 2-2)

The digital A format of each BUV minor data frame is identical. Since each VIP frame is 16 seconds duration, the BUV digital A format repeats every two VIP frames.

The BUV minor data frame consists of 12, 2.5 second intervals, each representing one grating position, followed by a two second interval during which the wavelength cam and grating return to the start position. During each of the 12 intervals, the grating dwells for two seconds at the particular wavelength positions; during which time four analog samples are taken from each channel at 200 millisecond intervals. During the remaining 1/2 second of each interval, the grating is stepped into the next position.

Due to timing considerations relating to the VIP sampling rates, the data format actually consists of three distinct sequences, six of one, six of another, and a third single sequence occurring during the cam retrace time just before the beginning of the next minor data frame.

2.1.5 Bench Test Unit

The bench test unit, shown in Figure 2-3, contains the equipment necessary to test and evaluate the performance of the BUV instrument. It provides a spacecraft simulator, a command and control unit, and several pieces of test equipment. Meters are also provided to monitor the BUV input voltage, input current, and the elapsed operating time of the instrument while undergoing bench test.

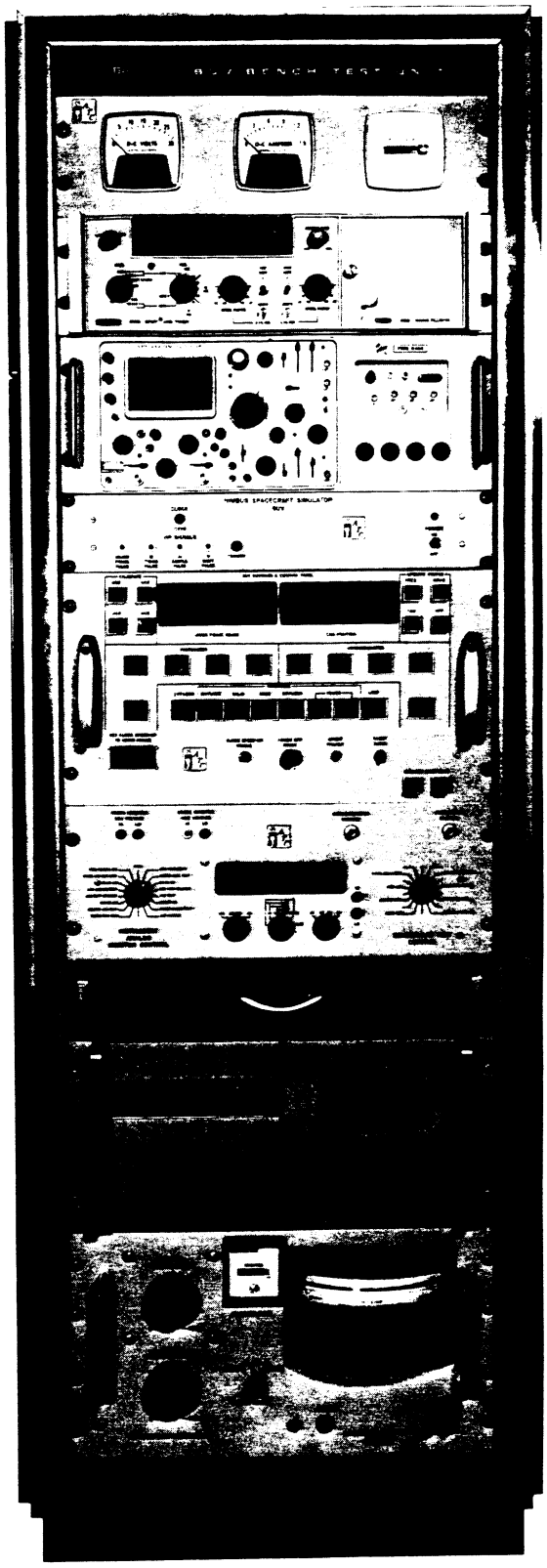

Figure 2-3. Bench Test Unit

The spacecraft simulator generates synchronization and clock signals identical to those provided to the BUV instrument by the VIP and command subsystem on the spacecraft.

The command and control unit provides the functions and displays necessary to obtain and reduce the scientific and engineering status data from the BUV instrument. It supplies the instrument with power, commands and timing signals and receives bi-level parallel and serial digital data from the instrument. The processing of data received from the instrument results in printer outputs or lamp displays.

The bench test unit also contains the digital printer, oscilloscope, Beckman counter and timer, a digital voltmeter, and an Eppley quartz-iodine calibration lamp supply.

2.2 SPECIFICATION SUMMARY

2.2.1 Optical Specifications

a. Wavelength repeatability: within ±0.2 Å on each wavelength step.

b. Wavelength steps:

Step No.	Angstroms (Å)	Step No.	Angstroms (Å)
0	3398	6	2975
1	3312	7	2922
2	3175	8	2876
3	3125	9	2830
4	3058	10	2735
5	3019	11	2555
Wavelength Calibration Steps:			
19	2522	23	2542
20	2527	24	2547
21	2532	25	2552
22	2537		

c. Bandwidth: 10 Å at center of wavelength scan.

d. Scan dwell time on each step: 2 seconds.

e. Transition time between successive steps: 0.5 seconds.

f. Wavelength uniformity along exit slit: 1.0 Å maximum.

g. Scattered light: less than 1 percent at all wavelengths.

h. Gratings: 2400 lines/mm.

i. Grating efficiency at blaze wavelength: 50% minimum.

j. Reflectivity of optical reflecting surfaces: 80% minimum from 2500 to 3400 Å.

k. Field of view: ~~0.44~~ 0.044 steradian.

l. Photometer: Transmission 3800 Å (Filter transmission measured within 1%, centered at 3800 Å, with 50 Å ±2 Å bandpass at half-power points).

m. Depolarizer: the monochromator is equipped with an optical depolarizer which reduces the residual polarization of the incident light to less than 5% over the range from 2555 Å to 3398 Å.

2.2.2 Electronic Specifications

a. Instrument shall have a sufficient dynamic range to accommodate moonlight backscatter radiation, sunlight backscatter radiation, and direct solar radiation on the diffuser plates.

b. Instrument shall operate continuously for one year using no greater than 15 watts of power.

c. Ripple - Instrument shall operate without degradation when 250 mV peak-to-peak ripple between 100 Hz and 1 MHz is superimposed on the dc supply voltage.

d. Overvoltage - Instrument shall operate at voltages between -20 and -35 volts and a temperature between -5° to +55°C.

e. Detector EMR Photomultiplier 541N-05M-14, Quantum Efficiency (min.) 21% at 4100 Å, Dark Current (max.) 10^{-11} amps (20°C, 10^6 gain).

f. High Voltage Power Supply - less than 3600 V. Less than 0.3 V peak-to-peak ripple. Voltage regulated to 0.2% from -5° to +55°C.

g. Electrometer Amplifiers - dc noise less than 5×10^{-13} amperes. Employ drift compensation. Linear.

h. Pulse Counter in parallel with analog channel. Design goal to measure 50 photons/second in the monochromator channel.

i. Measurement system for multiple counts produced by particulate radiation.

j. Calibration System - Instrument shall automatically calibrate with electronic current, electronic pulse rates, wavelength source, and photometric source.

k. Conductive Interference - The instrument shall not feed a voltage back to the power supply in excess of 10 mV peak-to-peak of a bandwidth from 100 Hz to 1 MHz.

l. Grounding - Instrument shall operate with a positive ground. Chassis ground shall be kept separate from either signal or power ground.

m. Transients - Instrument shall survive voltage transients of -40 V for up to 30 sec.

n. Interface with VIP system.

o Housekeeping. Measure analog voltages to ±0.5%. Measure temperatures to ±3°C.

2.2.3 Operating Parameters

The following tabulation shows the overall operating parameters of the BUV instrument in orbit:

Parameter	Monochromator	Photometer
Photomultiplier Tube Gain		
Low Voltage	1243	45.5
High Voltage	2.216×10^6	1.884×10^6
Electrometer Feedback		
10^7	1.0×10^7	1.0×10^7
2×10^9	1.876×10^9	1.870×10^9
3×10^{10}	3.047×10^{10}	3.050×10^{10}
Pulse Counting Dead Time	1.10×10^{-6} sec	1.33×10^{-6} sec
Cam Step Wavelengths (Å)		
3398	3400.26	N/A
3312	3313.85	N/A
3175	3177.23	N/A
3125	3126.90	N/A
3058	3060.03	N/A
3019	3021.34	N/A
2975	2977.27	N/A
2922	2923.69	N/A
2876	2877.85	N/A
2830	2831.85	N/A
2735	2737.93	N/A
2555	2558.24	N/A
2552		N/A
2547		N/A
2542		N/A
2537	2539.21	N/A
2532		N/A
2527		N/A
2522		N/A

SECTION III

OPTICS

3.1 DESIGN STUDY ANALYSIS

3.1.1 Preliminary Optical Design Investigations

Five basic monochromator optical layout designs were compared relative to the required performance characteristics. All had previously been used successfully in commercial and experimental spectrophotometers. The five optical layout designs considered were: (1) Littrow Monochromator, (2) Pfund Monochromator, (3) Czerny-Turner Monochromator, (4) Fastie-Ebert Monochromator, and (5) Rowland Circle Monochromator.

The best monochromator optical layout design for the Backscatter Ultraviolet (BUV) Instrument was selected by considering the following performance and structural features:

- Spectral radiant flux transfer from the entrance slit through the exit slit.
- Spectral dispersion.
- Spectral resolution by minimizing spectral image optical aberrations of the entrance slit at the exit slit.
- Spectral resolution by minimizing the mismatch between the curvature of the spectral image of the entrance slit at the exit slit and the exit slit itself.
- Wavelength stability as a function of the monochromator temperature and the mechanical stresses on and within it.

- o The ratio of wanted spectral radiant flux to unwanted (stray) radiant flux passing through the exit slit.
- o Optical and mechanical simplicity and reliability.

3.1.1.1 Spectral Radiant Flux Transfer

When the entrance slit of a monochromator is filled with the radiant flux from a uniform extended source, the spectral radiant flux passing through the exit slit having the same length and width as the entrance slit is:

$$W_\lambda = \frac{\pi B_\lambda (\Delta\lambda) A_s A_g \cos\phi T_\lambda}{F^2} \text{ (watts)} \quad (1)$$

where B_λ = the spectral radiance of source in watts/cm^2/micron-steradian.

$(\Delta\lambda)$ = the spectral half bandwidth in microns of the radiant flux passing through the exit slit.

A_s = the area of the entrance slit in cm^2. (The entrance and exit slits are assumed to have equal length and width.)

A_g = the ruled area of the grating or the face area of the prism in cm^2.

ϕ = the angle between the normal to the face of the grating and the incident or dispersed optical axis, whichever angle is larger.

T_λ = the transmittance of the monochromator from the entrance slit to the exit slit.

F = focal length of collimating mirror or mirrors in cm.

This equation shows that it is desirable for the monochromator to have high transmittance and have the slit area and the dispersive area as large as possible. The slit and dispersive areas are restricted in this monochromator for a number of reasons:

1. Increasing the slit area, A_S, by increasing slit width increases the spectral half bandwidth proportionately. The maximum slit width is determined by the maximum permissible spectral bandwidth. Wider slit widths do accrue for a given spectral bandwidth by increasing the focal length of the monochromator, by using a dispersive element with a high dispersion, or by using a double monochromator. The entrance and exit slit widths of a double monochromator are the sum of the slit widths that would be used for each single monochromator separately.
2. Increasing the slit length has varying effects in each of the five monochromator types. All monochromator designs except the Fastie-Ebert monochromator exhibit a changing curvature in the spectral image at the exit slit as a function of wavelength which often is sufficient to increase the spectral bandwidth. This is true whether the dispersive element is a prism or a grating. Such monochromators may use extra long slits for a single wavelength or over a short range of wavelengths.
3. Slit curvature mismatch is not the only problem with extra long slits. In all monochromator designs including the Fastie-Ebert monochromator the optical aberrations increase with an increase in slit length since the ends of the slit are a greater distance from the optical axis of the collimating mirror.
4. Slit length may also be restricted for a purely geometrical reason. The vertical area of use on a collimating mirror surface in transferring rays either from a slit to a dispersive surface, or vice versa, is approximately equal to the height of the dispersive surface

plus the height of the slit. Therefore, increasing slit height increases the size of the collimating mirror. For example, the height of the zone of use on a collimating mirror surface for a two inch high dispersive surface and a one inch high slit is three inches.

5. The maximum dispersive area, A_g, is limited for the same geometrical reason. That is, the height of dispersive surface plus the slit height determine the height of the collimating mirror.

6. The maximum dispersive area, A_g, may also be restricted to a maximum A_g/F^2 ratio. The approximate numerical aperture of the monochromator is equal to $1/2\ \sqrt{A_g/F^2}$, and as this term increases the optical aberrations in the spectral image increase at greater than proportional rate. The nature of the optical aberrations in the spectral images of the five monochromator types are quite different as a function of the numerical aperture of the monochromator.

3.1.1.2 Spectral Dispersion

The equations for the linear spectral dispersion at the exit slit of a Littrow monochromator are relatively simple for both prisms and gratings, since it is assumed that the entrance and exit slits have nearly the same location, and the angles of incidence and dispersion are equal. The spectral dispersion for monochromator designs with large angular separation between the entrance and exit slit are still of the same relative magnitude.

For a grating Littrow monochromator:

$$M\lambda = a\ (\sin i + \sin \theta)\ \text{(micron)} \qquad (2)$$

where M = grating order

λ = wavelength in microns

a = groove spacing in microns

$= \frac{1000}{k}$, where k = grooves/mm

i = angle of incidence

θ = angle of dispersion

and $\theta = i$ for rays with a wavelength of λ.

To find the monochromator dispersion, let angle i remain constant.

$$M d\lambda = a \cos\theta \; d\theta \quad \text{(micron)}$$

but: $\theta \simeq i$

so:
$$d\theta = \frac{M}{a \cos i} d\lambda \tag{3}$$

The linear dispersion at the exit slit is then:

$$ds = F \, d\theta \quad \text{(mm)} \tag{4}$$

Where F = focal length of the collimating mirror in mm, and finally,

$$ds = \frac{MF}{a \cos i} d\lambda \text{ (mm)} \tag{5}$$

The performance characteristics of a Littrow monochromator with a 250 mm focal length and a grating with 2400 grooves/mm are given in Table 3-1. Columns (7), (8), and (9) list the values of ds for spectral bandwidths of 0.2Å, 10Å, and 50Å, respectively. If this monochromator were free of optical aberrations, the entrance and exit slits would have the same widths as the ds values for the same spectral half bandwidths. For example, if the entrance and exit slit

1	2	3	4	5	6	7	8	9
Wavelength λ (microns)	$\sin i = \frac{M\lambda}{2a}$	angle i	cos i	$\frac{d\theta}{d\lambda} = \frac{M}{a \cos i}$ radians/micron	$\frac{d\theta}{d\lambda}$ radians/angstrom	$dS = F\left(\frac{d\theta}{d\lambda}\right)\Delta\lambda$ (mm)		
						$\Delta\lambda = 0.2$ Å	$\Delta\lambda = 10$ Å	$\Delta\lambda = 50$ Å
.25	.30	17° 27.465'	.95394	2.520	.000252	.0126	.620	3.15
.26	.312	18° 10.785'	.95008	2.530	.000253	.01265	.633	3.16
.27	.324	18° 54.296'	.94606	2.540	.000254	.0127	.635	3.175
.28	.336	19° 38.000'	.94186	2.550	.000255	.01275	.637	3.19
.29	.348	20° 21.893'	.93749	2.560	.000256	.01280	.640	3.20
.30	.360	21° 6.000'	.93295	2.572	.0002572	.01286	.643	3.217
.31	.372	21° 50.333'	.92823	2.586	.0002586	.01292	.647	3.235
.32	.384	22° 34.890'	.92333	2.600	.000260	.01299	.650	3.25
.33	.396	23° 19.704'	.91825	2.617	.0002617	.01307	.654	3.27
.34	.408	24° 4.770'	.91298	2.634	.0002634	.01316	.658	3.29

Table 3-1. Performance Characteristics of a Littrow Monochromator with a 250 mm Focal Length and a Grating with 2400 grooves/mm.

widths of this monochromator are fixed at 0.63 mm, then it passes 10Å at 2500Å, but only 9.6Å at 3400Å. Now letting i = θ in equation (2):

$$M\lambda = 2a \sin i \quad \text{(micron)}$$

$$\text{and,} \quad \sin i = \frac{M}{2a} \tag{6}$$

Values of incident angle i are listed in column (3) of Table 3-1, which shows the angular orientation of the grating and angle the grating must be rotated through a given wavelength range.

When a reflecting prism is used as the dispersive element in the Littrow monochromator:

$$\sin i = N \sin P \tag{7}$$

where: i = angle of incidence

N = index of refraction of prism material

P = prism angle

and for a small change in N

$$di = \frac{\sin P}{\cos i} dN \tag{8}$$

Equation (8) assumes the prism rotates to maintain the incident and dispersed angles constant. If, however, angle i is held constant and only the angle of dispersion θ is allowed to change, its value is double the value of di of equation (8) so

$$d\theta = \frac{2 \sin P}{\cos i} dN \tag{9}$$

and multiplying by $\frac{d\lambda}{d\lambda}$

$$d\theta = \frac{2 \sin P}{\cos i} \left(\frac{dN}{d\lambda}\right) d\lambda \qquad (10)$$

and finally,

$$ds = \frac{2F \sin P}{\cos i} \left(\frac{dN}{d\lambda}\right) d\lambda \quad (mm) \qquad (11)$$

Table 3-2 shows the performance characteristics of a prism Littrow monochromator with a 250 mm focal length and a fused silica reflecting prism with a prism angle of 36°. Column (4) lists values of i and columns (8), (9), and (10) list the ds values for spectral bandwidths of 0.2Å, 10Å, and 50Å, respectively. The ds value is 3.6 times greater at 2500Å than at 3400Å and the ds value at 2500Å for the grating is 1.75 times greater than the ds value for the prism at the same wavelength. The grating monochromator has 1.75 times greater spectral radiant flux than the prism monochromator at 2500Å.

If a transmitting prism is used with a Littrow mirror the ds value can be doubled. Such a prism monochromator matches the grating monochromator in energy transfer at 2500Å. However, the prism monochromator still will require cam controlled slit widths as a function of wavelength to maintain a reasonably constant spectral resolution.

When two identical monochromators are used in series, their dispersions are additive and the entrance and exit slits may have twice the slit width of one monochromator, and the values for ds in Tables 3-1 and 3-2 are doubled.

3.1.1.3 Effect of Optical Aberrations on Resolution

In the Littrow, Pfund, Czerny-Turner, and Fastie-Ebert Monochromators, the

1	2	3	4	5	6	7	8	9	10	11	12	13	14
Wavelength λ (microns)	Index of Refraction N	sin i = N sin P where P = 36°	angle i	cos i	$\frac{dN}{d\lambda}$ / Å	$\frac{di}{d\lambda} = \frac{2 \sin P}{\cos i} \frac{dN}{d\lambda}$ Radians/Å	$dS = F\left(\frac{di}{d\lambda}\right)\Delta\lambda$ (mm)			$\frac{dN}{dT} \times 10^6/°C$	$\frac{di}{dT} = \frac{2 \sin P}{\cos i}\left(\frac{dN}{dT}\right)$ (Radians/°C)	$dS_T = F\left(\frac{di}{dT}\right)_{(mm)} \Delta T, \Delta T = 1°C$	ΔT equivalent to wave-error of $\Delta\lambda$ = 0.2 Å (Column (8)/(13))
							$\Delta\lambda$ = 0.2 Å	$\Delta\lambda$ = 10 Å	$\Delta\lambda$ = 50 Å				
.25	1.5077	.886	62° 23'	.4635	.000057	.000145	.0073	.363	1.81	12.0	.0000304	.0076	.96°C
.26	1.5024	.883	62° 00'	.4695	.000049	.000122	.0061	.305	1.52	11.8	.0000296	.0074	.83°C
.27	1.4980	.880	61° 39'	.4749	.000042	.000106	.0053	.265	1.32	11.6	.0000288	.0072	.74°C
.28	1.4942	.878	61° 24'	.4786	.000038	.000093	.0047	.235	1.16	11.4	.0000281	.0070	.67°C
.29	1.4908	.876	61° 10'	.4823	.000033	.000082	.0042	.205	1.02	11.2	.0000274	.0068	.62°C
.30	1.4878	.874	60° 58'	.4853	.000029	.000072	.0036	.180	.90	11.0	.0000268	.0067	.54°C
.31	1.4851	.873	60° 48'	.4879	.000026	.000063	.0031	.157	.79	10.9	.0000263	.0066	.47°C
.32	1.4827	.872	60° 39'	.4901	.000023	.000055	.0028	.137	.69	10.8	.0000259	.0065	.43°C
.33	1.4805	.870	60° 30'	.4924	.000020	.000048	.0024	.120	.60	10.7	.0000255	.0064	.38°C
.34	1.4787	.869	60° 21'	.4948	.000017	.000041	.0021	.103	.51	10.6	.0000252	.0063	.33°C

Table 3-2. Performance Characteristics of a Prism Littrow Monochromator with a 250 mm Focal Length and a Fused Silica Reflecting Prism with Prism Angle of 36°

entrance slit is imaged at the exit slit with unit magnification. The spectral dispersion of this image is generally considered the major factor in determining the spectral half-bandwidth of the monochromator. This is true for large slit widths; but when the slit widths are very narrow, the optical aberrations in the spectral image at the exit slit may determine the real bandwidth of the monochromator. The half energy width at the exit slit due to the optical aberrations in the spectral image for an infinitely narrow entrance slit defines the minimum spectral half bandwidth capabilities of a monochromator.

The magnitude of these optical aberrations is a function of (1) the monochromator optical layout, (2) the Ag/F^2 ratio, (3) the slit length, (4) the quality of the dispersive elements and the mirrors, and (5) the locating accuracy of functional components. In most monochromator designs, prisms, and gratings may be interchanged as the dispersive element, with a relatively small change in the magnitude of the optical aberrations. The slit curvatures are quite different, however, for the prism and grating.

To compare the performance of the five different monochromator optical layouts under consideration assume that the monochromator to be used in the Backscatter Ultraviolet Instrument has an $\sqrt{Ag/F^2}$ ratio of .2, a focal length F of 250 mm, and a slit height of 25 mm.

The preliminary ray trace analysis showed that the Fastie-Ebert monochromator optical layout exhibited a total aberration spread in the spectral image which varies depending on slit height from 16 percent to 29 percent of the slit width required for 10Å resolution. Substantially, the same magnitude of aberration spread should exist along the exit slit for all the required

wavelengths. The optical aberration spread in the spectral image of a Czerny-Turner or Pfund monochromator is less than for the Fastie-Ebert. The optical aberrations produced by the Littrow monochromator are greater than for the Fastie-Ebert when a spherical collimating mirror is used, but can be less when a paraboloid collimating mirror is used.

A Fery prism has the same spectral dispersion as a Littrow prism for the same prism angle. The optical aberration spread in the spectral image of the Fery prism or concave grating monochromator is greater than for the Littrow monochromator using a spherical collimating mirror.

3.1.1.4 Effect of Slit Curvature

All of the monochromators except the Fastie-Ebert Monochromator have exit slit curvature mismatch with the spectral image as a function of wavelength. The wavelength range from 2500Å to 3400Å is not great for a monochromator and slit curvature may not become a real problem in any of the monochromator designs, unless the slits have excessive length. A ray trace study was performed (paragraph 3.1.3) on the entrance and exit slits to determine spectral resolution and spectral image characteristics.

3.1.1.5 Wavelength Accuracy and Stability

The wavelength accuracy of a monochromator depends on a number of considerations:

1. A knowledge of the grating spacing when a grating is used or the prism angle and the prism material index refraction versus wavelength, when a prism is used as a dispersive element.

2. The accuracy of the wavelength cam, the accuracy of its location relative to the axis of the dispersive element, and the accuracy of the length of the wavelength arm.
3. The accuracy of the focal length of the monochromator.
4. The accuracy in the location of the entrance and exit slits.

Wavelength stability is a function of the following:

1. Locational stability of the collimating mirrors and other plane mirrors, the grating or prism, wavelength cam, and the entrance and exit slits.
2. The effect of temperature on the grating groove spacing or on the prism index of refraction.
3. The changes in the dimensions of the structure and the monochromator's functional elements as a function of temperature.

Most of the factors listed above have the same effect on the accuracy and stability of wavelength, whether the dispersive element is a prism or a grating, and each of these factors were considered in the selection of a final monochromator. The selection of a grating vs. prism was based largely on the following considerations:

The groove spacing of the grating, as given by the manufacturer, is generally quite accurate, better than 1 part in 10,000 and this information can be used directly in the calculation of the wavelength cam.

Consider next the change in groove spacing as a function of temperature. The wavelength error at the exit slit of a grating monochromator, due to a change

in the temperature of the grating, may be derived by differentiating equation (2) relative to groove spacing a.

$$d\lambda = \frac{(\sin i + \sin \theta)}{M} da \text{ (micron)} \tag{12}$$

and combining with equation (2)

$$d\lambda = \frac{\lambda}{a} da \text{ (micron)} \tag{13}$$

and for a change in temperature dT

$$d\lambda = \frac{\lambda}{a} \left(\frac{da}{dT}\right) dT \text{ (micron)} \tag{14}$$

where $\left(\frac{da}{dT}\right)$ is the change of groove spacing for a small change in temperature. A grating is usually replicated on a thick pyrex substrate, and the expansion of the grating is equal to the expansion of the pyrex. The coefficient of thermal expansion of pyrex is equal to 3.2×10^{-6} per degree centigrade. Then,

$$\frac{da}{dT} = ka \text{ (mm/°C)} \tag{15}$$

where k = coefficient of thermal expansion of the substrate

and finally:

$$d\lambda = k\lambda \, dT \text{ (microns)} \tag{16}$$

To illustrate, a grating used at $\lambda = .25$ microns and subjected to a temperature change of $dT = 5°C$ causes a wavelength shift of

$$\begin{aligned} d\lambda &= k\lambda \, dT \\ &= 3.2 \times 10^{-6} \times .25 \times 5 \\ &= 4 \times 10^{-6} \text{ microns} \\ &= 0.04\text{Å} \end{aligned}$$

This is five times smaller than the wavelength accuracy tolerances. If a large temperature range is encountered, a fused quartz substrate can be used since its thermal coefficient of expansion is six times lower at .55 x 10^{-6}/°C.

Uniform temperature changes of a prism change its size and index of refraction but do not change its prism angle. The change in the wavelength passing through the exit slit of a Littrow prism monochromator is only a function of the change in index of refraction. Multiply equation (9) by $\left(\frac{dT}{dT}\right)$ and

$$d\theta = \frac{2 \sin P}{\cos i} \left(\frac{dN}{dT}\right) dT$$

The linear spectral shift at the exit slit is then

$$ds_T = \frac{2F \sin P}{\cos i} \left(\frac{dN}{dT}\right) dT \text{ (mm)} \qquad (17)$$

A fused quartz prism has $\left(\frac{dN}{dT}\right)$ values ranging from 10.5 x 10^{-6}/°C to 12 x 10^{-6}/°C in the 0.34 to 0.25 micron wavelength range. These values are listed in column (11) of Table 3-2.*

Column (13) of Table 3-2 lists the wavelength error produced by a prism temperature change of 1°C. Column (14) lists the prism temperature change which produces a wavelength error equal to the maximum allowable wavelength error of 0.2Å; Column (8) is divided by column (13). The maximum allowable prism temperature change, therefore, is only 0.33°C at 3400Å.

---

* "Interspecimen Comparison of Refractive Index of Fused Silica," I. H. Malitson, Journal of the Optical Society of America, Volume 55, Number 10, October 1965, Pages 1205-1209.

3.1.1.6 Stray Light

Stray Light is the generally accepted term to describe the total radiant flux of all unwanted wavelengths which pass through the exit slit of a monochromator. The factors which effect the level of this stray light are the following:

1. A field lens may be located at the entrance slit to image an optical stop which is mounted in object space within the dispersive area of the dispersive element. This insures that all rays entering the monochromator from object space fall within a dispersive area.

   However, the Backscatter Ultraviolet Instrument monochromator must use a depolarizer at the entrance slit. The depolarizer is a light scatterer, so a field lens cannot be used at the entrance slit.

2. A field lens may be located at the exit slit of the monochromator to image the dispersive area onto an optical stop in front of the photo detector. This stop matches the size of the image of the dispersive area. Therefore, rays arising from outside the dispersive area cannot directly reach the photodetector. Such a field lens for the detector often produces a remarkable reduction in the stray light received by the detector.

3. In a monochromator with field lens control at both the entrance and exit slit, there is still a high level of stray light which arises primarily from two different optical mechanisms.

   a. Direct "white light" scattering from the dispersive element

      In a monochromator it is assumed that the dispersive element

angularly separates the various wavelengths by some mathematical function. However, this is not completely true. The microscopic surface texture of prisms and gratings, internal imperfections in prisms, and dust and foreign material on the dispersive surface scatter a certain percentage of the incident radiant flux directly through the exit slit without the process of dispersion. This form of stray light is at least ten times greater in a grating monochromator than in a prism monochromator, since the prism can be given a very fine surface polish.

b. Indirect "white light" and spectral scattering from the dispersive element and from other mirrors in the monochromator.

The monochromator volume can be thought of as comparable to a black integrating sphere. The walls of a monochromator are generally illuminated by many decades more radiant flux than that which passes through the exit slit. This includes the direct scattering of the input radiant flux from imperfect mirror surfaces and the Fresnel reflection from the prism face or the zero order reflection of the grating. However, usually the major source of radiant flux in the monochromator is the spectral radiant flux in the portion of the spectral image which does not pass through the exit slit. In a monochromator used over broad wavelength range, the magnitude of this radiant flux is often 10^6 to 10^7 times greater than the radiant flux passing through the exit slit.

The radiant flux density within the volume of the monochromator becomes quite high even if the walls are painted black and special baffles are used to trap concentrations of radiant flux.

The only mechanism by which a portion of this high internal radiant flux can reach the photodetector is for a percentage of it to be scattered from the dispersive surface and the mirrors into the same optical paths of the wanted spectral band and hence through the exit slit. A common experience is that of seeing dusty collimating mirrors raise the stray light level of a monochromator 100 times by this mechanism.

4. In those monochromators where the exit slit is located at the side of the dispersive element such as in the Fastie-Ebert monochromator, the primary spectral image is not only spread across the exit slit but also across the face of the dispersive element. Those wavelengths which fall on the dispersive element are redispersed and a certain bandwidth of these unwanted wavelengths passes through the exit slit. The spacing of the entrance and exit slits and the method of use of the grating or prism determine the wavelength make-up of the secondary spectra.

5. Baffles are often used improperly in a monochromator. They should be used to trap high concentrations of radiant flux within the monochromator. Too often they are used to define the ray boundaries within the monochromator. When used in this way, they may be optically visible to the photodetector due to the diffractive scattering from

their edges in the front direction. They appear as extra slits which are at incorrect geometric locations compared to the entrance slit. Therefore, they produce unwanted wavelengths, relatively near the wanted wavelength, which pass through the exit slit. They cannot be eliminated by any means short of a field lens at the exit slit and an optical stop before the photodetector.

3.1.2 Selection of the Final Monochromator Design

3.1.2.1 Performance Considerations

The performance characteristics of five monochromator optical layouts using either a prism or grating as the dispersive element previously discussed were considered to determine the optimal monochromator design for the BUV Instrument. Tables 3-1 and 3-2 show the linear dispersion at the exit slit as a function of wavelength for a grating and a prism, and show the grating has much better dispersion over the required wavelength range, and much less dispersion change as a function of wavelength than the prism.

A grating on a pyrex substrate produces 15 times less wavelength error due to a temperature change than a fused silica prism at 3400Å. The prism produces a wavelength error equal to the wavelength tolerance for a change in its temperature of 0.33°C. For the Backscatter Ultraviolet Instrument application, the grating definitely was the best dispersive element to use.

Single grating monochromators have high stray-light levels, so it was decided to use a double-grating monochromator. The double-grating monochromator has twice the linear dispersion listed in columns (7), (8), and (9) of Table 3-1, and the entrance and exit slit widths will be twice the ds values listed in column (8) for a 10Å bandwidth and in column (9) for a 50Å bandwidth.

3.1.2.2 Monochromator Optical Layout Selection

The choice of monochromator optical layout was then selected from between the Littrow, Pfund, Czerny-Turner, and the Fastie-Ebert.

The double Littrow monochromator required an expensive paraboloid collimating mirror to match the other three monochromators in image quality. The entrance and exit slits also had to be optically near each other which could complicate a double-monochromator layout, and the location of auxiliary external optics.

The double Pfund monochromator required four spherical collimating mirrors and four flat mirrors which were too many mirrors for this application.

The double Czerny-Turner monochromator required four spherical collimating mirrors which is also too many. Double Czerny-Turner monochromators have, however, been built using only two spherical mirrors by having each spherical mirror serve as a collimating mirror for each monochromator by properly folding the optical layout.

The double Fastie-Ebert monochromator has acceptable image quality and requires only two spherical collimating mirrors regardless of how the two monochromators are mated. With all the data obtained from investigating the various designs and performing ray-trace studies, the Fastie-Ebert monochromator using two identical gratings was the optimal design and the one selected for the BUV Instrument.

3.1.2.3 Final Monochromator System

Each monochromator of the double Fastie-Ebert design uses a single spherical collimating mirror. The entrance and exit slits are on a common circle which

encircles the grating (Figure 3-1). Each point on this circle is imaged by the monochromator on the opposite side of the same circle (180° away) for all wavelengths. The entrance slit is imaged on the exit slit with unit magnification. The focal length of the monochromator is 250 mm. The height of both the entrance and exit slits is 25 mm.

Several ways were used to reduce the stray light in the final BUV Instrument. One is the double monochromator design chosen. The dispersed radiant flux passes from the first into the second monochromator through the intermediate slit. This slit is only slightly larger than the image of the entrance slit formed at the intermediate slit. The second monochromator and intermediate slit effectively reduce the indirect "white light" scattering in the second monochromator.

Another means of reducing stray light is the field lens located at the exit slit of the second monochromator which images the dispersive area of the grating in the second monochromator onto an optical stop in front of the photodetector. This stop matches the size of the image of the dispersive area. Therefore, rays arising from outside the dispersive area cannot directly reach the photodetector.

All optical elements, slits, gratings, collimating mirrors, and transfer prisms are supported by a single compact casting giving maximum rigidity, heat transfer efficiency, and minimum weight.

The double monochromator of Figure 3-2 places the first monochromator on top of the second in such a way that the two identical gratings are fixed to a common bearing axis with identical angular orientation.

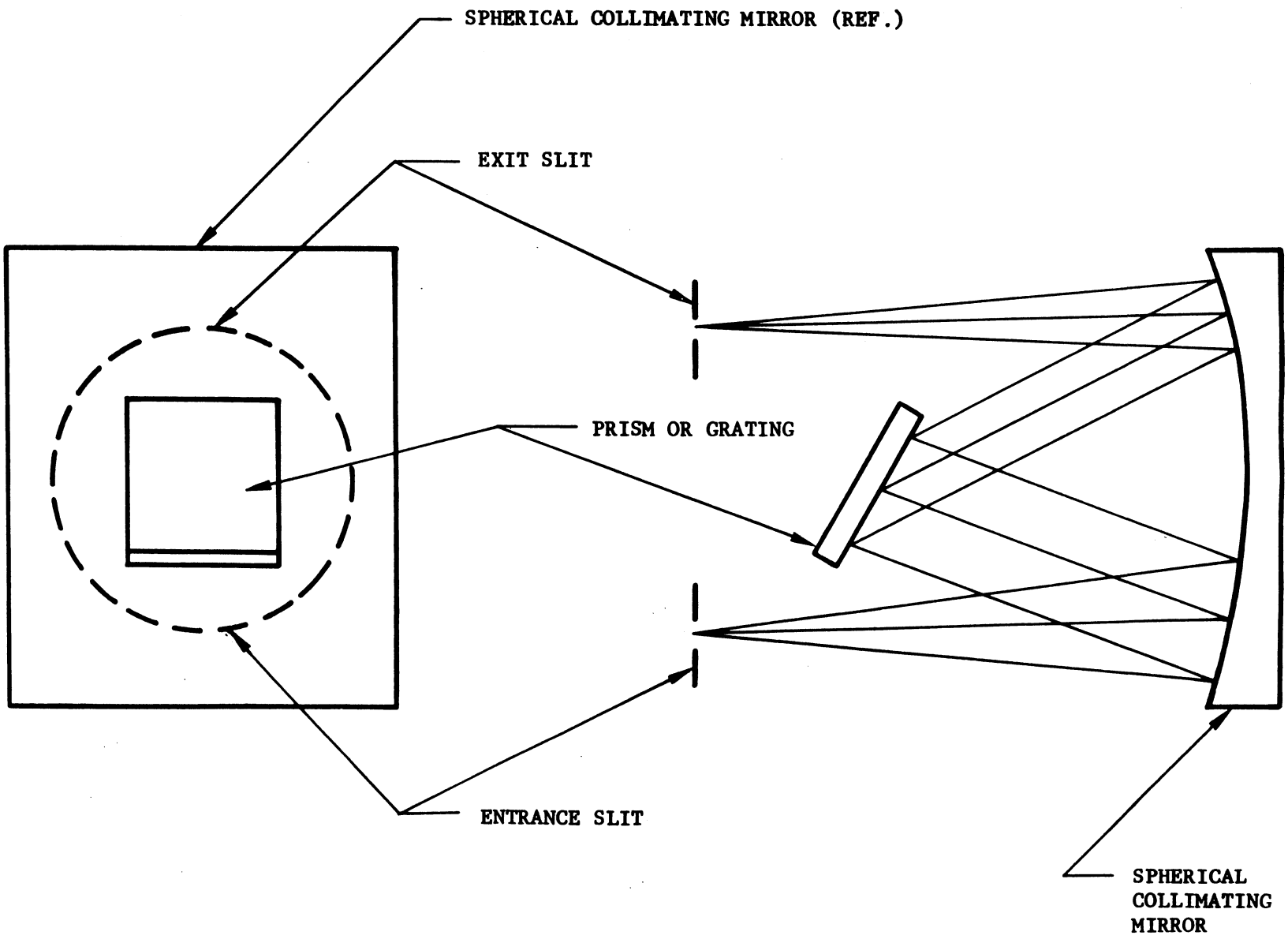

Figure 3-1. Fastie-Ebert Monochromator

The entrance slit is mounted immediately above the exit slit in the same plane, both slits are mounted on a common slit plate. Two transfer prisms are used to divert the optical path through the intermediate slit. The volume required by this double monochromator structure is 11 x 6 x 7 inches.

The imaging characteristics are shown in Figure 3-3. An image of the earth and the photomultiplier aperture are traced through the optical system. The aperture opening falls well within the dispersing surface of the second grating, with the aperture (grating) defining the f/5 field-of-view.

3.1.3 Ray-Trace Studies

3.1.3.1 Computer Programs

A highly developed computer ray-trace program was used with the IBM 360 computer to precisely determine the optical and mechanical parameters of the BUV double Fastie-Ebert monochromator. The ray-trace program is exact with no approximations. Line equations represent the light rays, and surface equations define the optical surfaces, and each optical surface is in a separate axis system. Each axis system may have any linear or angular orientation to the previous axis system. The rays may have any orientation.

The standard available surfaces in the ray-trace program are the plane, sphere, ellipsoid, paraboloid, hyperboloid, cylinder, cone, and toroid. The standard ray-trace program provides that at each surface the incident rays may be transmitted, reflected, refracted, or diffracted.

The standard printout, at each surface for each ray gives:

1. The exact distance the ray traveled from the previous surface.

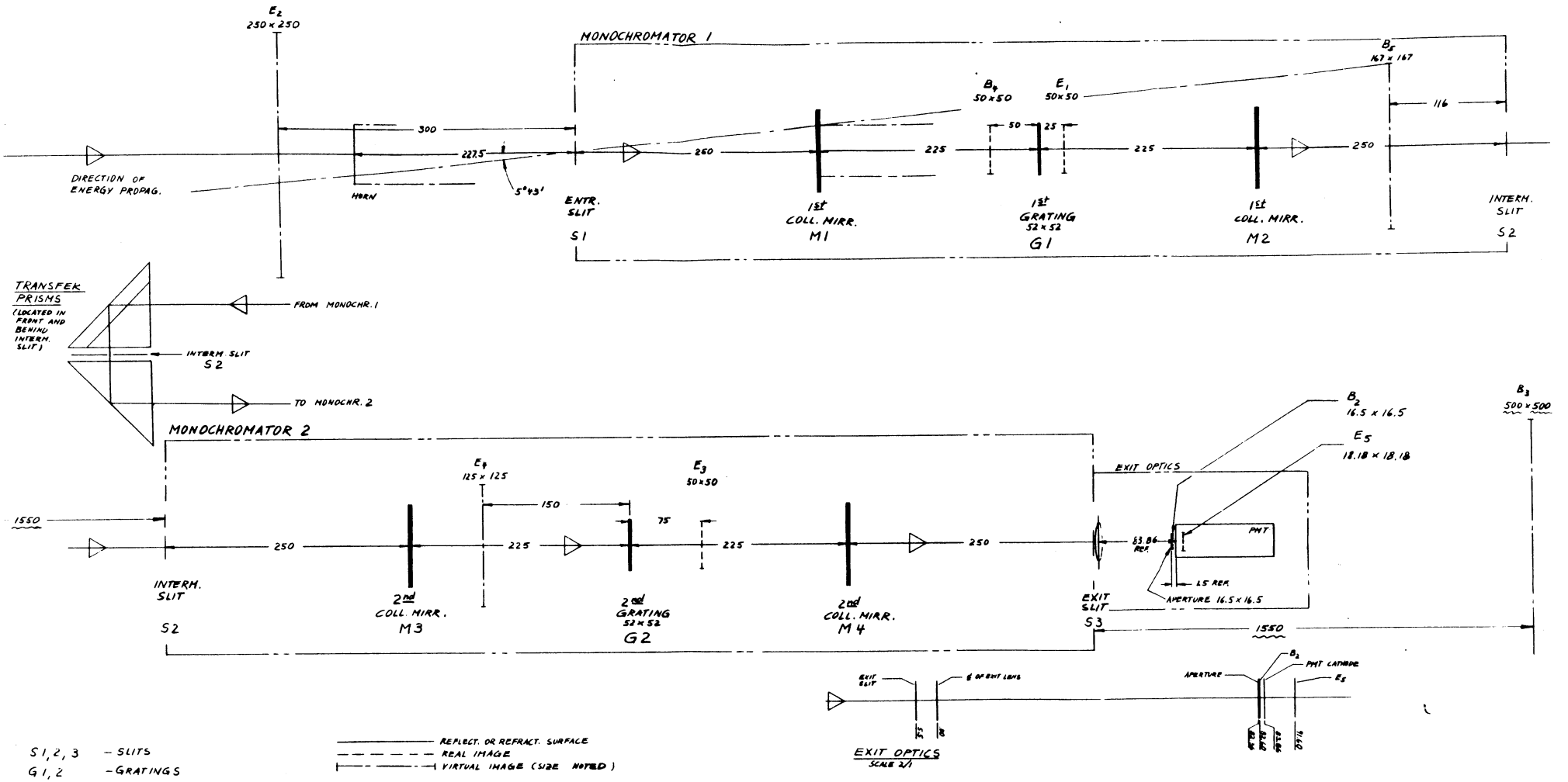

Figure 3-3. BUV Monochromator Imaging Characteristics (Horizontal Beam)

2. The X, Y, Z coordinates of the ray intercept with the surface in the axis system of the surface.
3. The three direction cosines for the ray as it leaves the surface after being transmitted, reflected, refracted, or diffracted.

Several valuable subroutines are available in the program.

1. Ray control cards are computed and punched for a family of rays which start from any single point and intercept any single surface in either a circular or rectangular uniform array. The physical dimensions of the circular or rectangular array and the number of rays in the array are input data.

   This subroutine is often used to generate families of rays which start from points on the entrance slit of a monochromator and which uniformally fill the dispersive area of a grating. Different ray families must be generated for several angular orientations of the grating which represent different wavelengths. The point image spread is analyzed by spot diagrams in the vicinity of the exit slit to define the characteristics of the exit slit aberration function. This exit slit aberration function adds to the spectral linear dispersion of the monochromator and defines the real half bandwidth of the monochromator.

2. A second subroutine ascribes a number to each ray in a family of rays generated in the above subroutine. Then at any chosen surface the actual ray numbers are printed out grouped with the other ray numbers which are in the same small incremental coordinate range. This

analysis may be made for the X, Y and Z coordinates and the three direction cosines. This subroutine is generally more valuable than a spot diagram since the ray numbers of major error producing rays are indicated and their location is accurately defined on every surface by the ray trace, so remedial action can be properly evaluated.

3. A third subroutine provides completely general equations for determining the location of a prism or grating axis system relative to the preceding and following axis systems. These equations determine a prism or grating axis system transformation as a function of wavelength.

4. Index of refraction equations are also available for the determination of the index of refraction of prism materials at any desired wavelength.

3.1.3.2 Parameter Definition

The ray-trace program described was used to optimize the BUV monochromator design and define all optical and mechanical parameters of the monochromator with a dimensional accuracy of 10^{-7} inches (1/100 fringe of visible light). Some of the analyses performed were as follows:

1. Determination of the physical location of all optical elements for the best focus.
2. Determination of the zone used by all rays on each surface.
3. Determination of the design of field lenses at the entrance of exit slit and the location of optical stops at the image of the dispersive surface in entrance or exit space for stray-light control.

4. The ray trace of unwanted rays reflected from dispersive surfaces so methods can be planned for trapping them.
5. Determination of the nature of the unwanted second pass spectral image at the exit slit.
6. Determination of the optical aberrations in the spectral image, and the focusing range over which there is little change in the magnitude or effect of the aberrations on the resolution of the monochromator.
7. Determination of the true spectral image curvature as a function of wavelength so the physical curvatures of the entrance and exit can be planned.
8. Development of optical surface maps similar to contour maps which delineate zones on an optical surface of the monochromator which contribute the same magnitude of optical aberration in the spectral image. Such aberration contour maps are helpful in indicating improved shapes for that optical surface or methods of hand working the optical surface to maximize the monochromator image quality. The contour maps may be generated for any optical surface in the monochromator.

The aberration contour map also indicates the shadow pattern that is seen to form over the surface of the dispersive element when very narrow entrance and exit slits are used with the wavelength set for the edge of a narrow spectral emission band. This type of shadow analysis can be used to focus a monochromator, or to determine that the monochromator is in proper focus.

9. Determination of those rays from an object which are actually accepted by the monochromator. In this analysis, the families of rays from the entrance slit which define the boundaries of the dispersive area are the true characteristic rays of the monochromator. By ray tracing backward with these same ray families from the entrance slit through object space optics to the object, one obtains a better understanding of how the object is viewed spectrally by the monochromator. This is a better procedure than designing object space optics to merely illuminate the entrance slit.

3.1.4 Result of a Comparative Spectral Image Ray-Trace Analysis of Monochromator Configurations

A complete ray-trace analysis of the spectral images in the vicinity of the intermediate and exit slits was performed for the following monochromator configurations:

1. The Double Fastie-Ebert Monochromator with double dispersion which uses quartz prisms to form, in effect, a corner prism about the intermediate slit. This was used in the BUV Instrument.
2. A Double Fastie-Ebert Monochromator with zero dispersion at the exit slit using only two right-angle mirrors about the intermediate slit.

These monochromator configurations have identical dimensions except for the relative locations of the intermediate slit transfer optics. An identical ray-trace image analysis was performed for each monochromator using the following two procedures:

1. 625 Rays were traced from each of three starting locations of the entrance slit, namely, the center, y = 0; y = 6.25; and the top of the entrance slit, y = 12.5. (The magnitude of the optical aberrations for rays starting from y = -6.25 and y = -12.5 are the same as those starting from y = 6.25 and y = 12.5, respectively.) The image analysis was performed for both 2500Å and 3400Å at the geometrical ray intersections between each family of 625 rays and a series of parallel planes in the vicinity of both the intermediate and exit slits.

   The effective linear half bandwidths of these geometrical intersections, which are defined as the minimum dimension in the direction of dispersion which contains 75 percent of the 625 rays (469 ray intersections) were determined. Graphs were then plotted for each monochromator configuration to define spectral resolution as a function of the image location along the optical axis.

2. 81 Rays were traced from the same three starting points and the same two wavelengths in (1) above. Spot diagrams were plotted showing the intersections of each 81 ray family with the successive image planes.

3.1.4.1 625 Ray Analysis

Figure 3-4 shows the spectral resolution capabilities in the vicinity of the exit slit for the double dispersive double Fastie-Ebert Monochromator using the two quartz prisms. The best spectral resolution is represented by the minima of each curve. The ordinate scale for Figure 3-4 is linear half-bandwidth

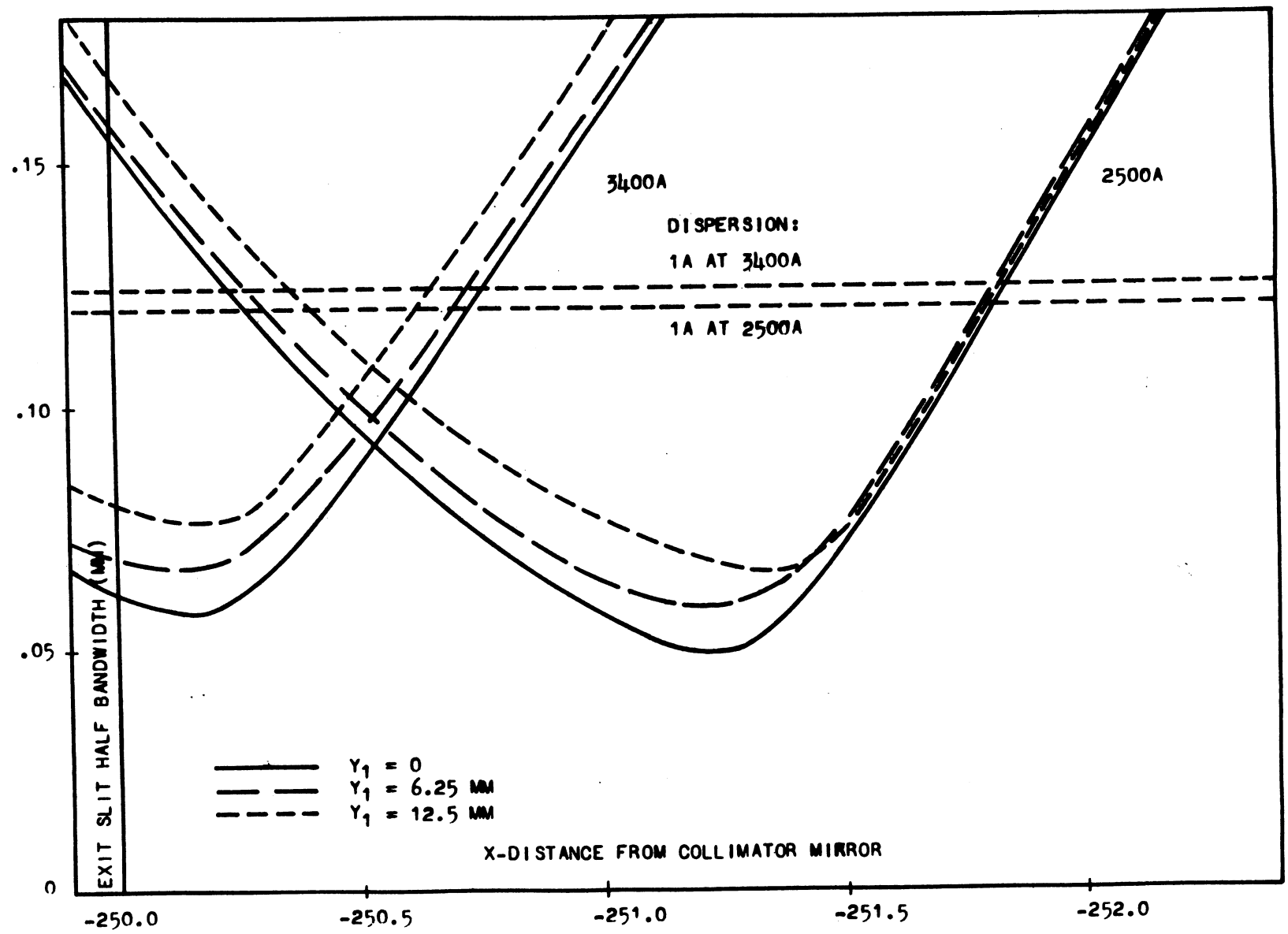

Figure 3-4. Double Ebert Mono-F/5 250 mm Fl, 2400 1/mm Grating - Double Prism

in mm, and represents the minimum width within which 75 percent of the rays fall. The two horizontal lines at 0.12 mm and 0.125 mm illustrate the linear dispersion of the monochromator for 1Å at 2500Å and 3400Å, respectively. The best resolution for y = 0, 6.25 mm, and 12.5 mm occurs at different image planes. Also, the shorter wavelengths are focused further along the optical axis because of their longer optical path in the two prisms.

Figure 3-5 demonstrates how the resolution of this monochromator was improved and optimized by bending the exit slit surface such that the best spectral resolution occurs simultaneously along the full slit height. The graph has been constructed by bending the exit slit surface from a plane such that the y = ±6.25 mm and y = ±12.5 mm locations on the exit slit are 0.17 mm and 0.72 mm, respectively, further along the optical axis than the y = 0 location. The best overall focus for all wavelengths between 2500Å and 3400Å is obtained when the y = 0 point on the exit slit is located at -250.53 mm. For this exit slit location nearly all image half bandwidths are less than 0.10 mm which is equivalent to a spectral half bandwidth of 0.83Å at 2500Å or 0.80Å at 3400Å.

Figure 3-6 shows the resolution capabilities of the double dispersive Double Ebert Monochromator with corner mirrors, and these are nearly identical to those for the double dispersive Double Ebert Monochromator with two prisms except for the different focal locations along the optical axis as a function of wavelength.

The spectral resolution capabilities of the zero dispersive Double Ebert Monochromator are shown in Figure 3-7. This spectral resolution is equivalent to that of the two double dispersive Double Ebert Monochromators when the rays

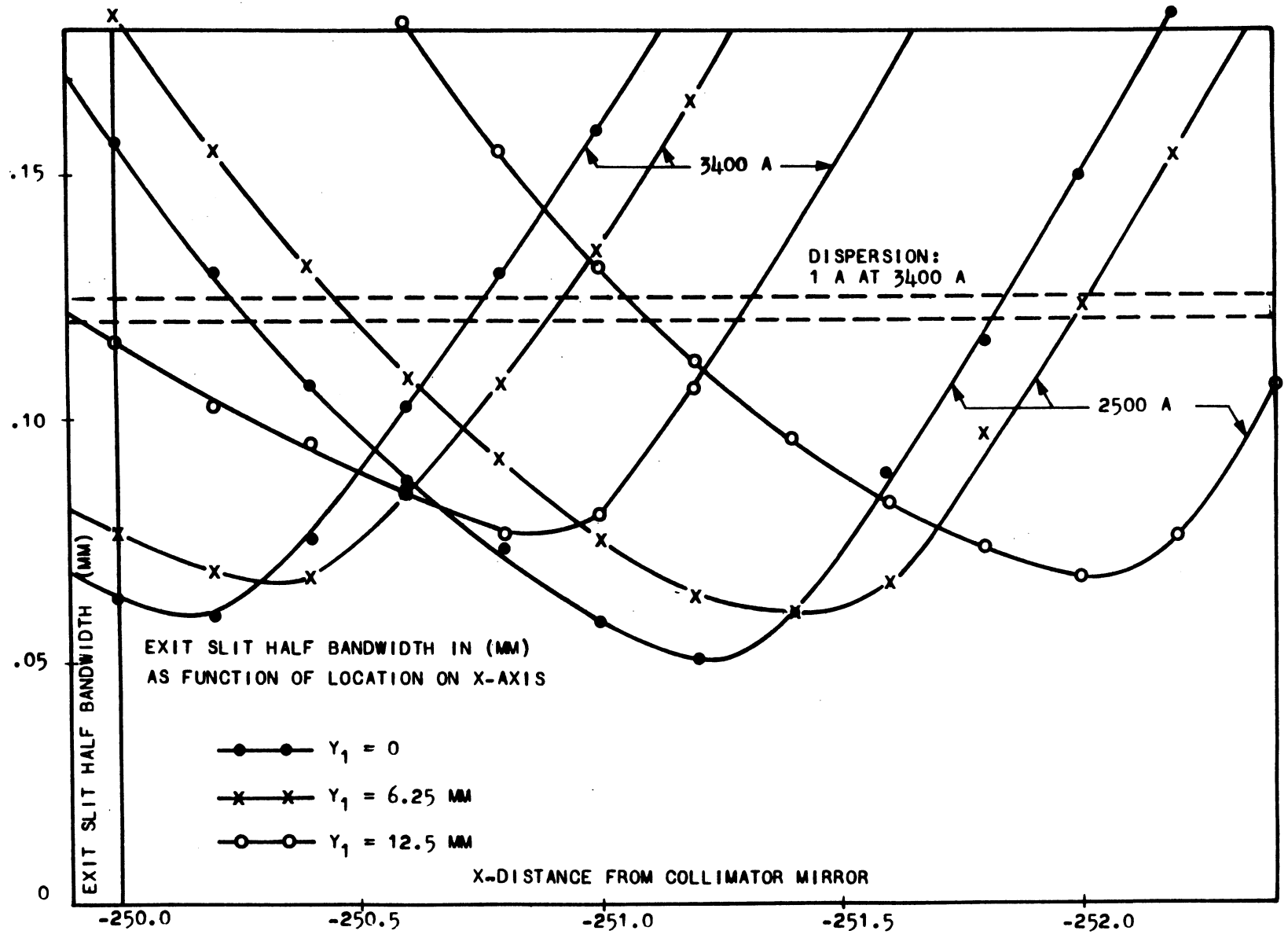

Figure 3-5. Double Ebert Mono - F/5 250 mm Fl,
2400 1/mm Grating - Double Prism

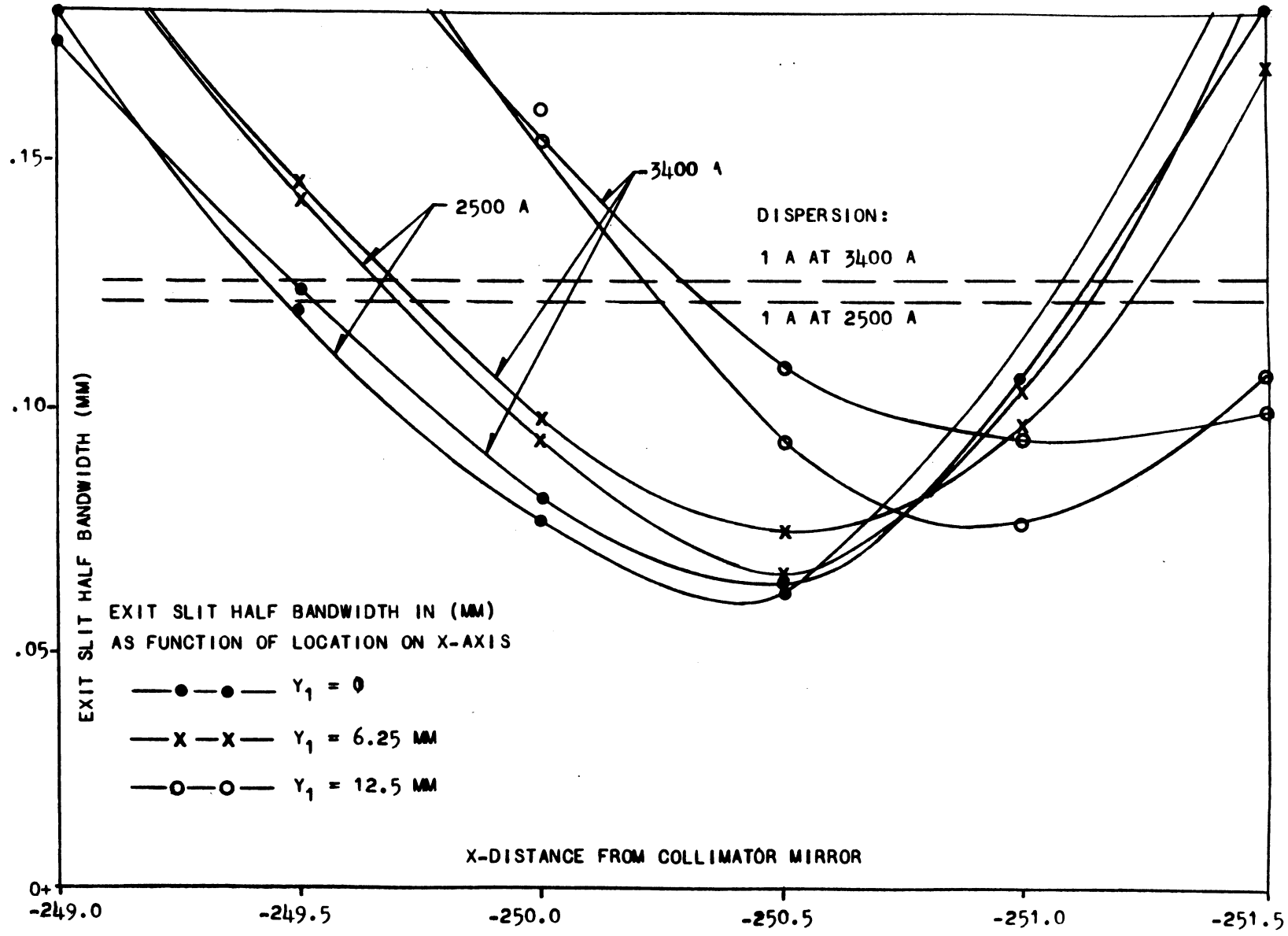

Figure 3-6. Double Ebert Mono - F/5 250 mm Fl.
2400 1/mm Grating - Corner Mirror

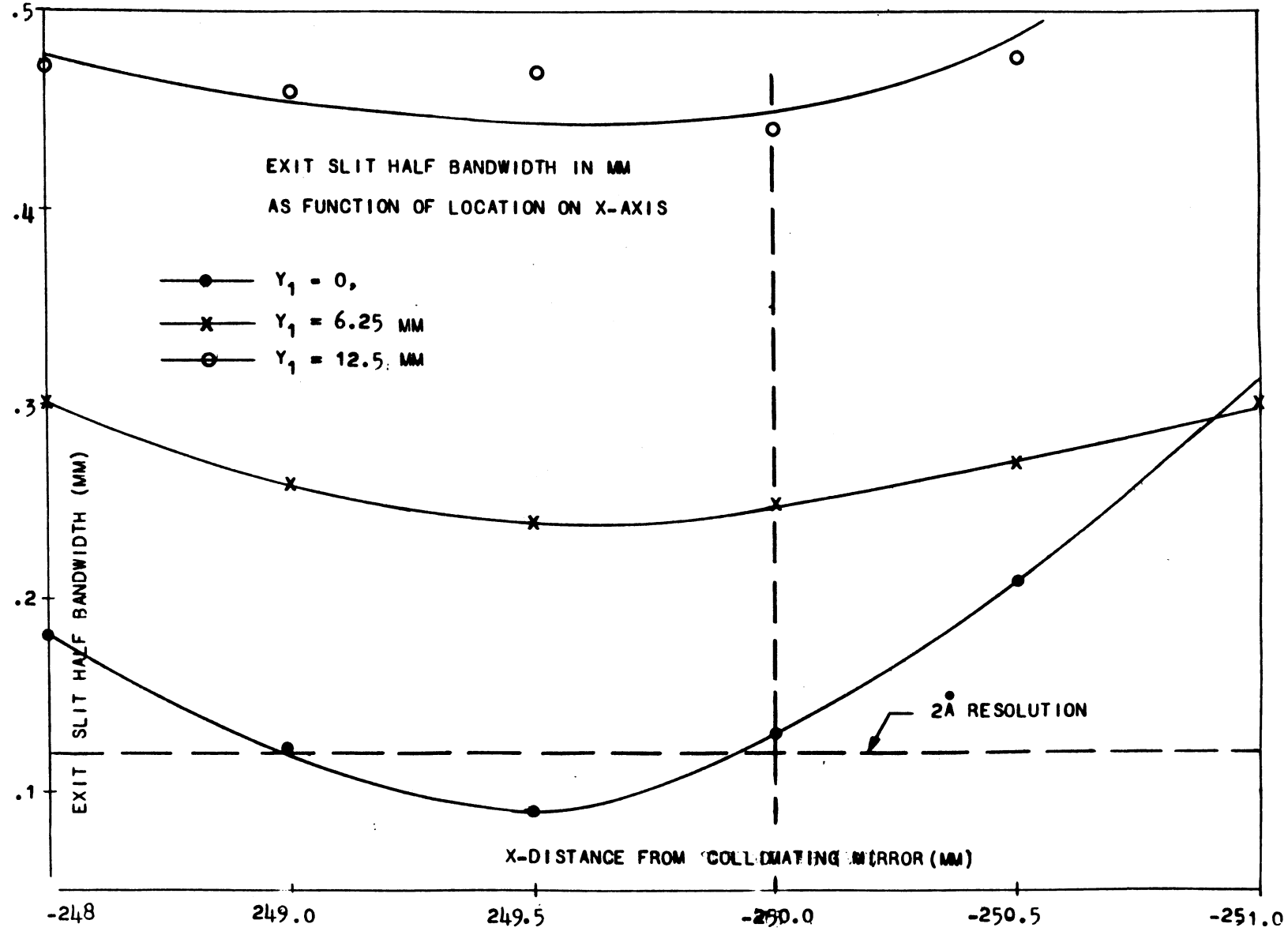

Figure 3-7. Double Ebert Mono - F/5 - 250 mm Fl
2400 l/mm Grating - Two Mirror

start from y = 0. However, for y = ±6.25 mm and y = ±12.5 mm the resolution of this monochromator is considerably poorer than the other two. This is because the optical distortion created in the second monochromator adds to the distortion of the first monochromator, whereas it subtracts in the case of the two double dispersive monochromators.

3.1.4.2 Ray Spot Diagram Analysis

Figures 3-8 through 3-16 are nine selected spot diagrams which demonstrate the relative spectral image characteristics of these monochromator configurations. Each spot diagram shows the geometrical intercepts on a specific plane, normal to the optical axis, for all 81 rays which commenced from a common starting point at the entrance slit.

Figures 3-8, 3-9, and 3-10 are spot diagrams at the intermediate slit for entrance slit starting locations of y = 0, 6.25 mm, and 12.5 mm, respectively. The length of each half axis measured from the origin of its axis system is .5 mm.

These particular spot diagrams are for the double dispersive Double Ebert Monochromator with corner mirrors, however, the image shapes and dimensions are substantially the same at the intermediate slit of the monochromator configurations. The lateral offset of the centroid of the spot diagram at large y-values is the so-called slit curvature effect. The image distortion develops for $y > 0$.

Figures 3-11, 3-12, and 3-13 are spot diagrams at the exit slit of the double dispersive Double Ebert Monochromator with corner mirrors for the same entrance

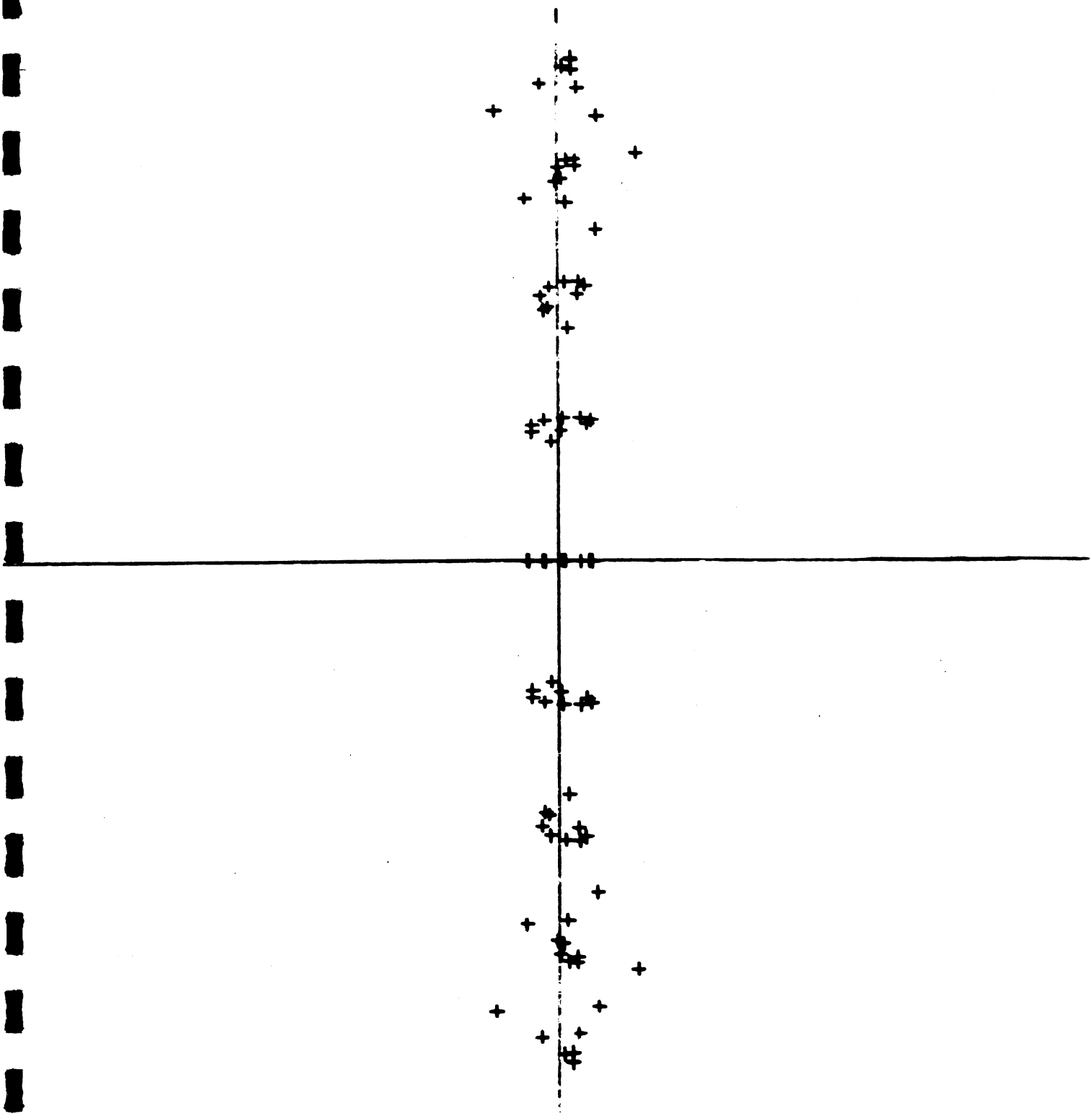

FIGURE 3-8.

81 RAY SPOT DIAGRAM AT INTERMEDIATE SLIT FOR Y = 0

DOUBLE EBERT MONO-F/5-250MM FL-2400 L/MM GRATING-CORNER MIRROR

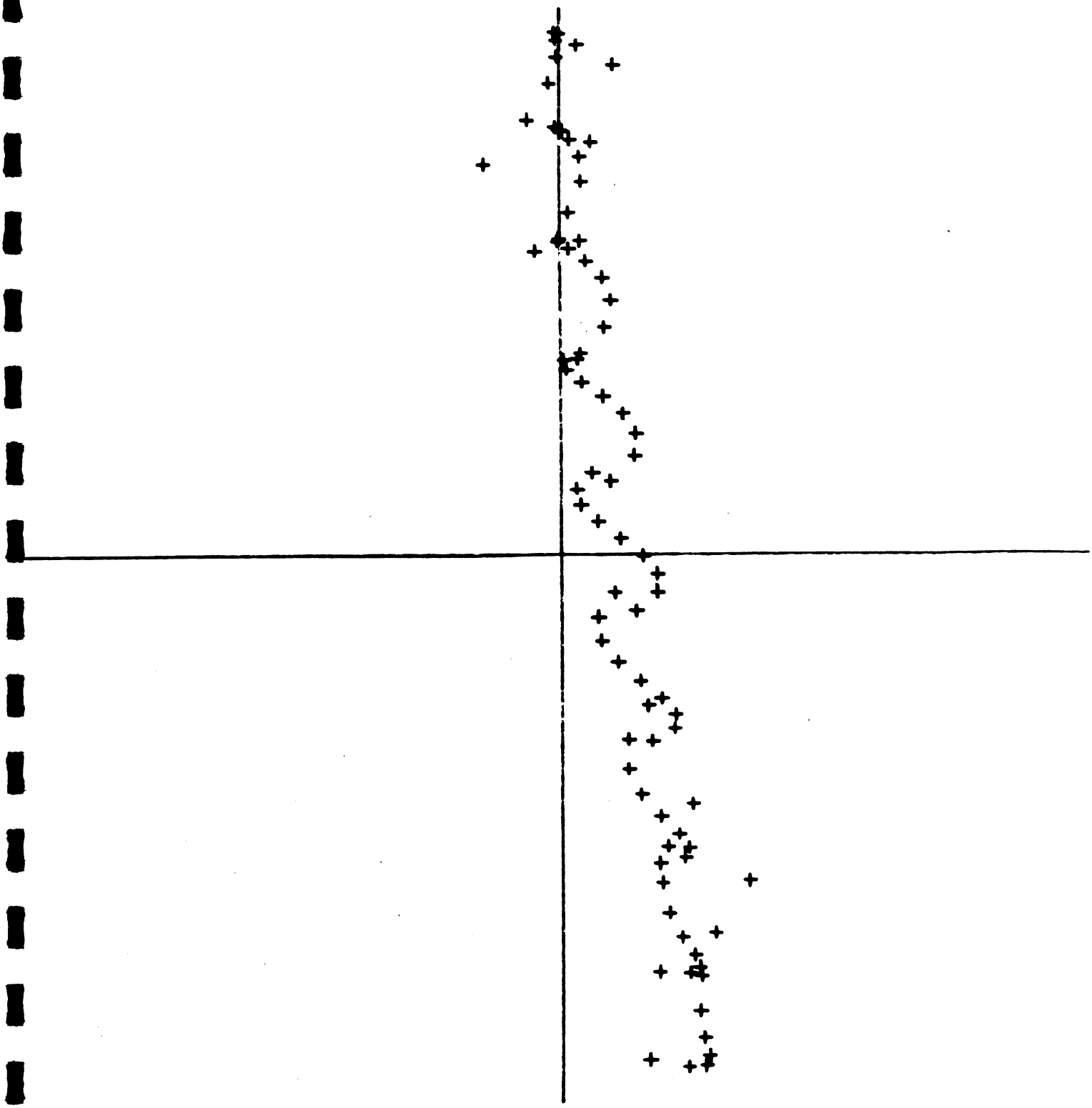

FIGURE 3-9.

81 RAY SPOT DIAGRAM AT INTERMEDIATE SLIT FOR Y = 6.25 MM

DOUBLE EBERT MONO-F/5-250MM FL-2400 L/MM GRATING-CORNER MIRROR

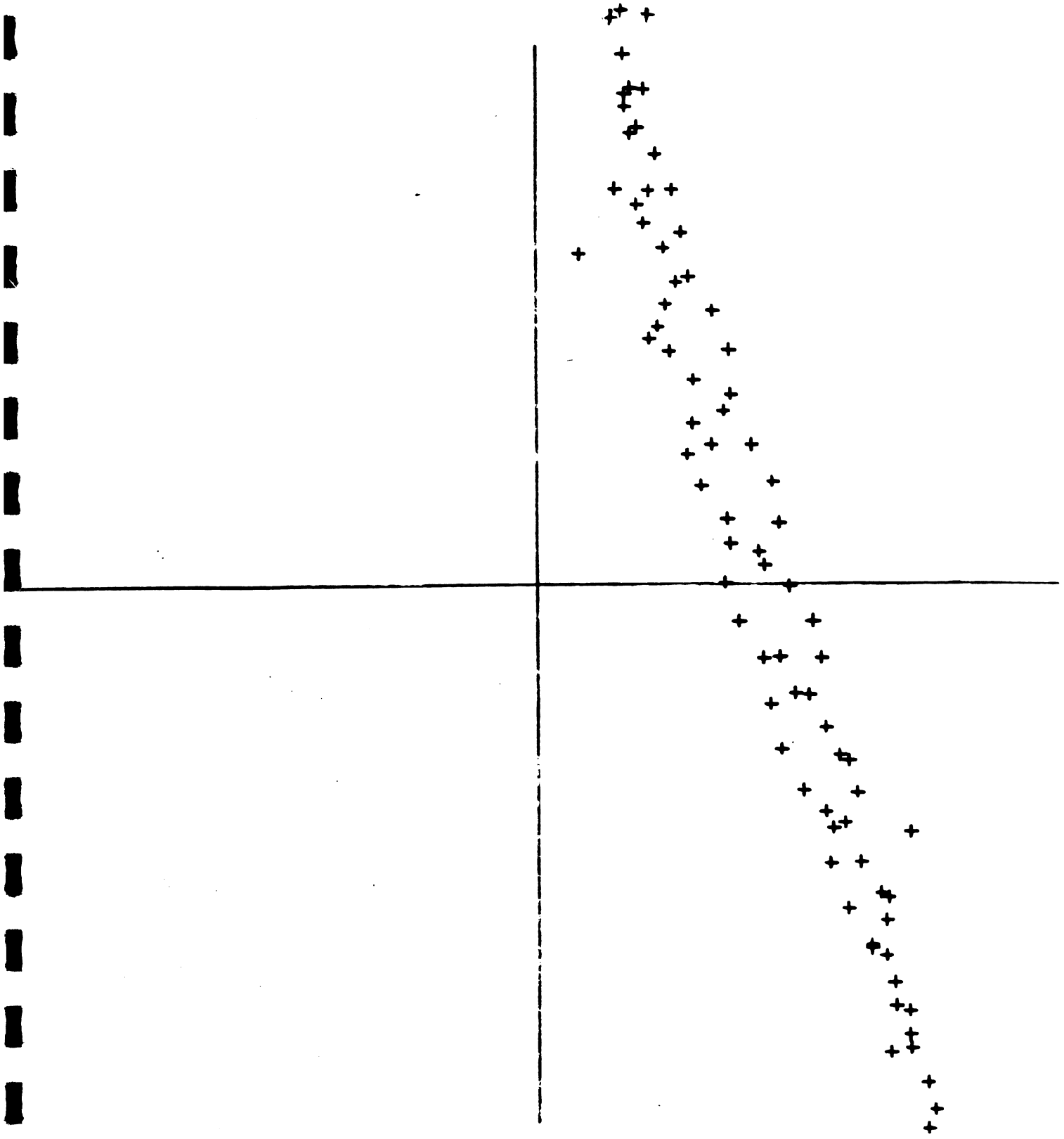

FIGURE 3-10.

81 RAY SPOT DIAGRAM AT INTERMEDIATE SLIT FOR Y = 12.5 MM

DOUBLE EBERT MONO-F/5-250MM FL-2400 L/MM GRATING-CORNER MIRROR

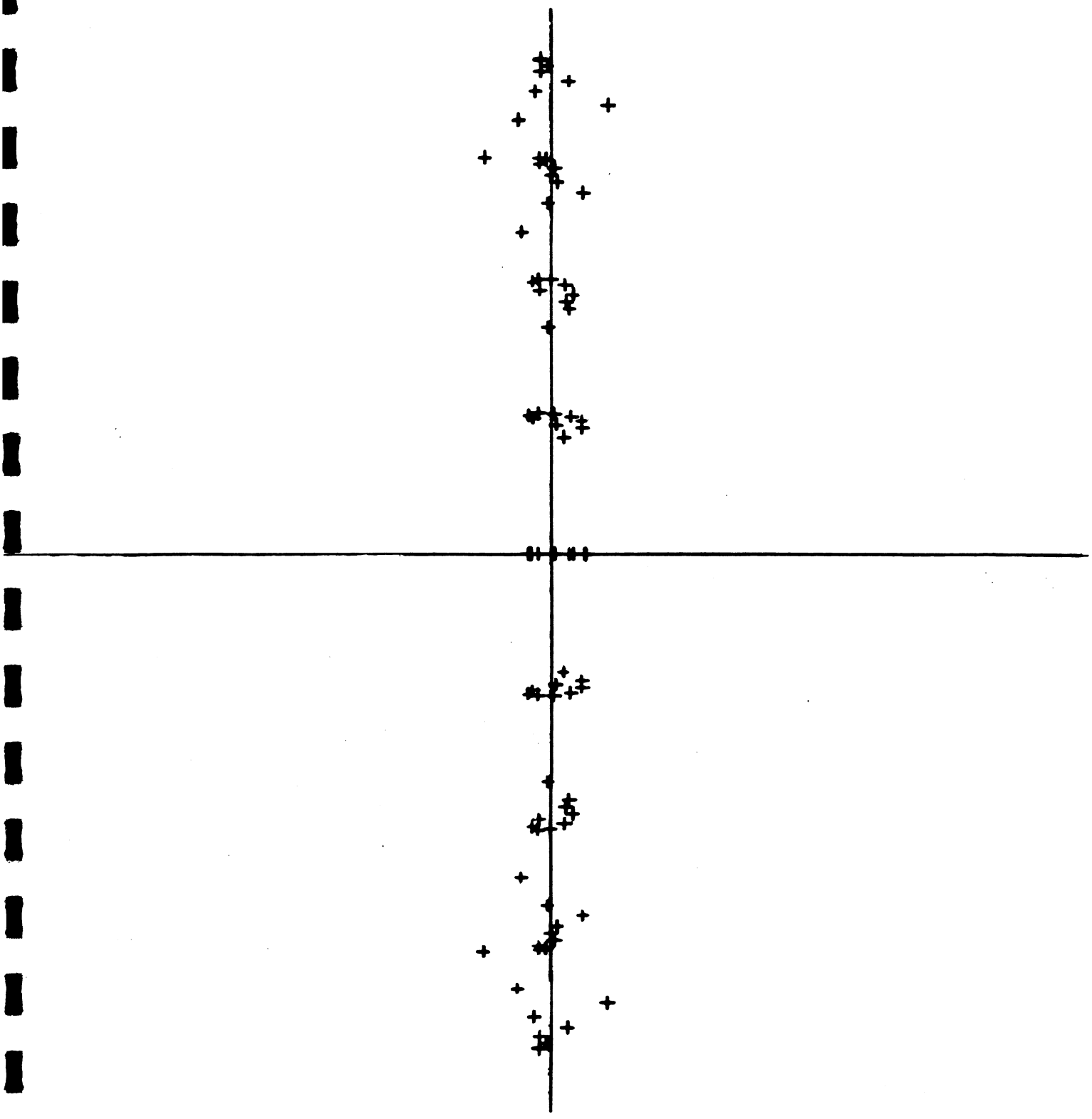

FIGURE 3-11.

81 RAY SPOT DIAGRAM AT EXIT SLIT FOR Y = 0

DOUBLE EBERT MONO-F/5-250MM FL -2400 L/MM GRATING-CORNER MIRROR

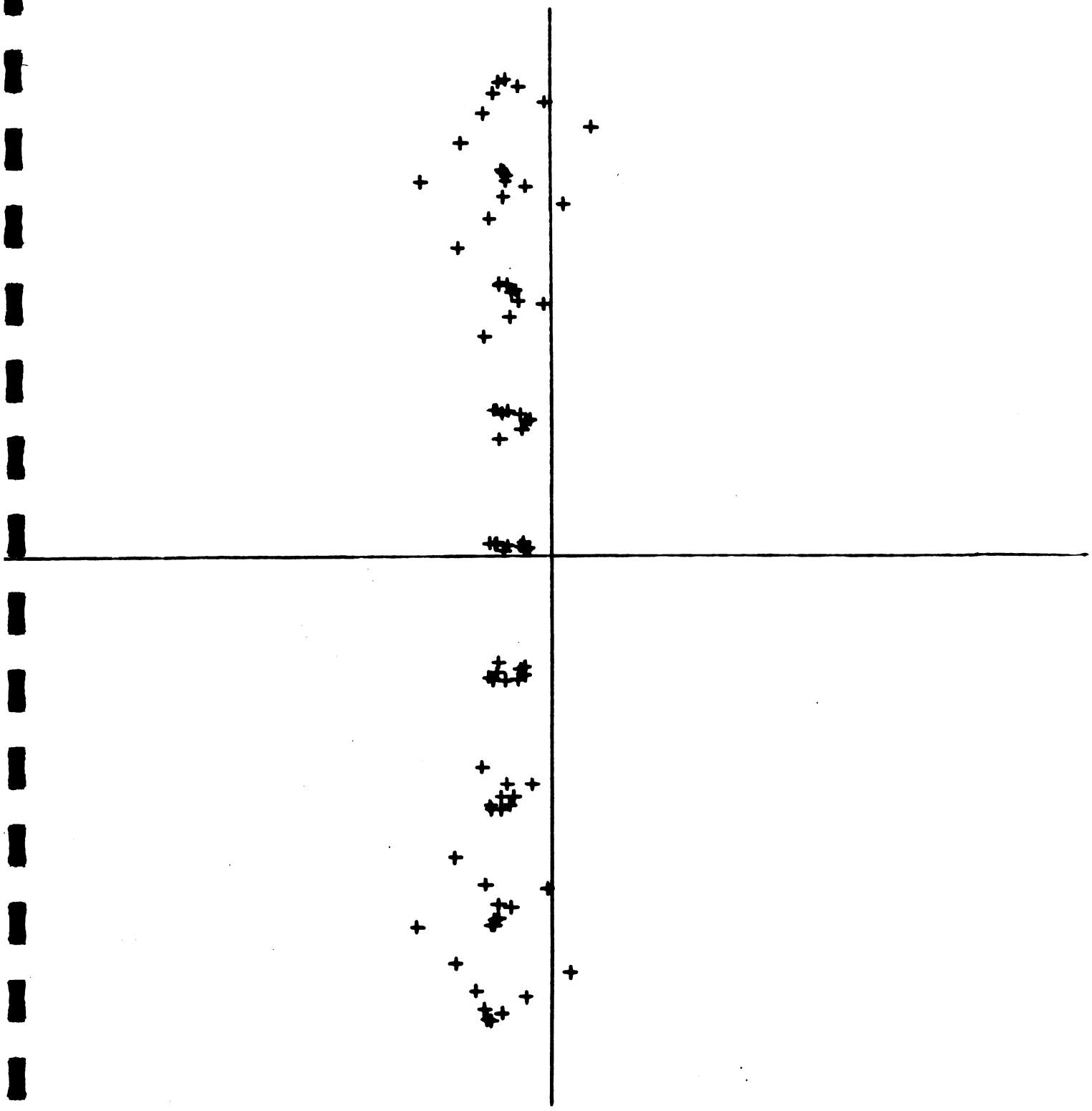

FIGURE 3-12.

81 RAY SPOT DIAGRAM AT EXIT SLIT FOR Y = 6.25 MM

DOUBLE EBERT MONO-F/5-250MM FL-2400 L/MM GRATING - CORNER MIRROR

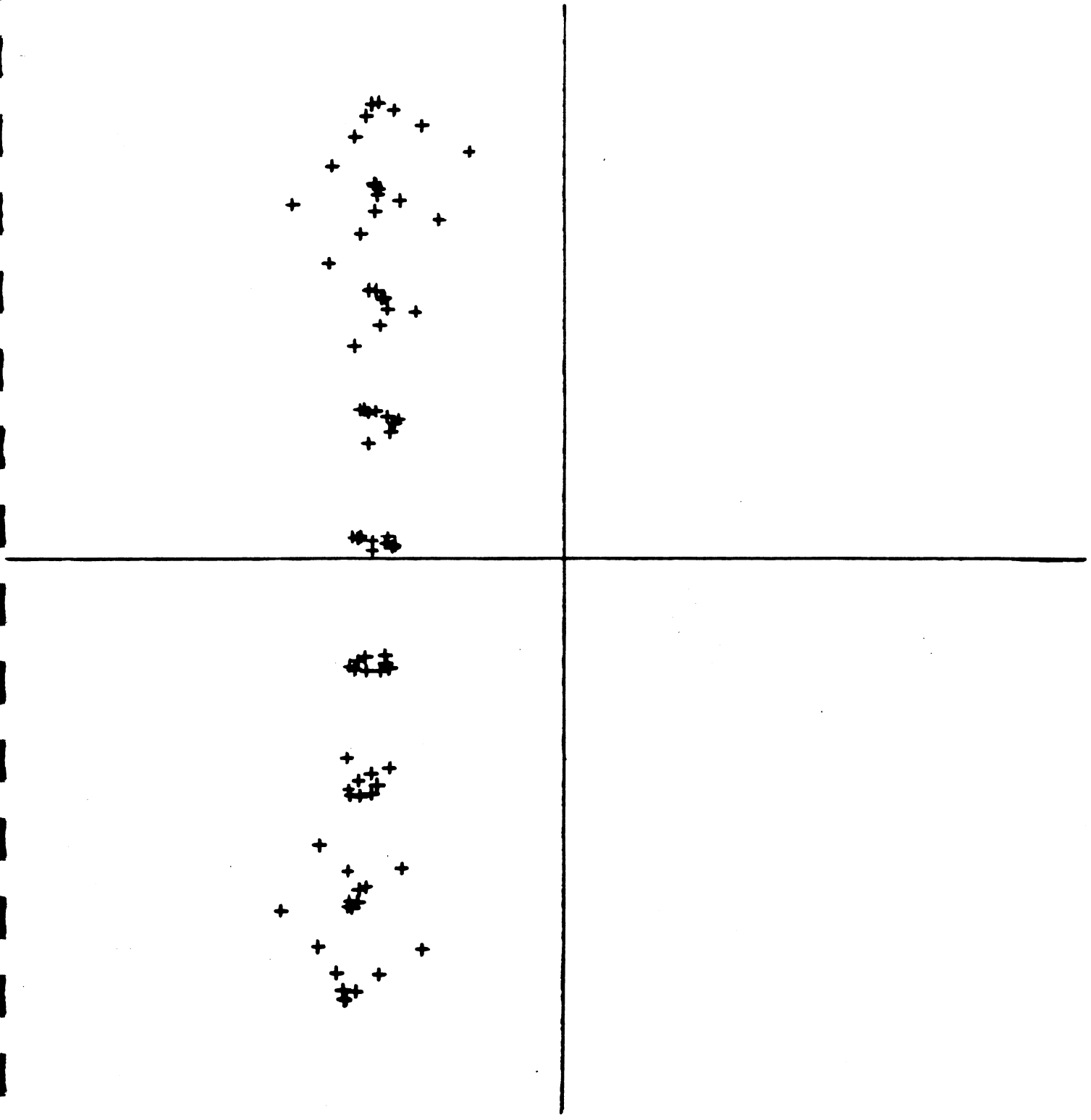

FIGURE 3-13.

81 RAY SPOT DIAGRAM AT EXIT SLIT FOR Y = 12.5 MM

DOUBLE EBERT MONO-F/5-250MM FL-2400 L/MM GRATING-CORNER MIRROR

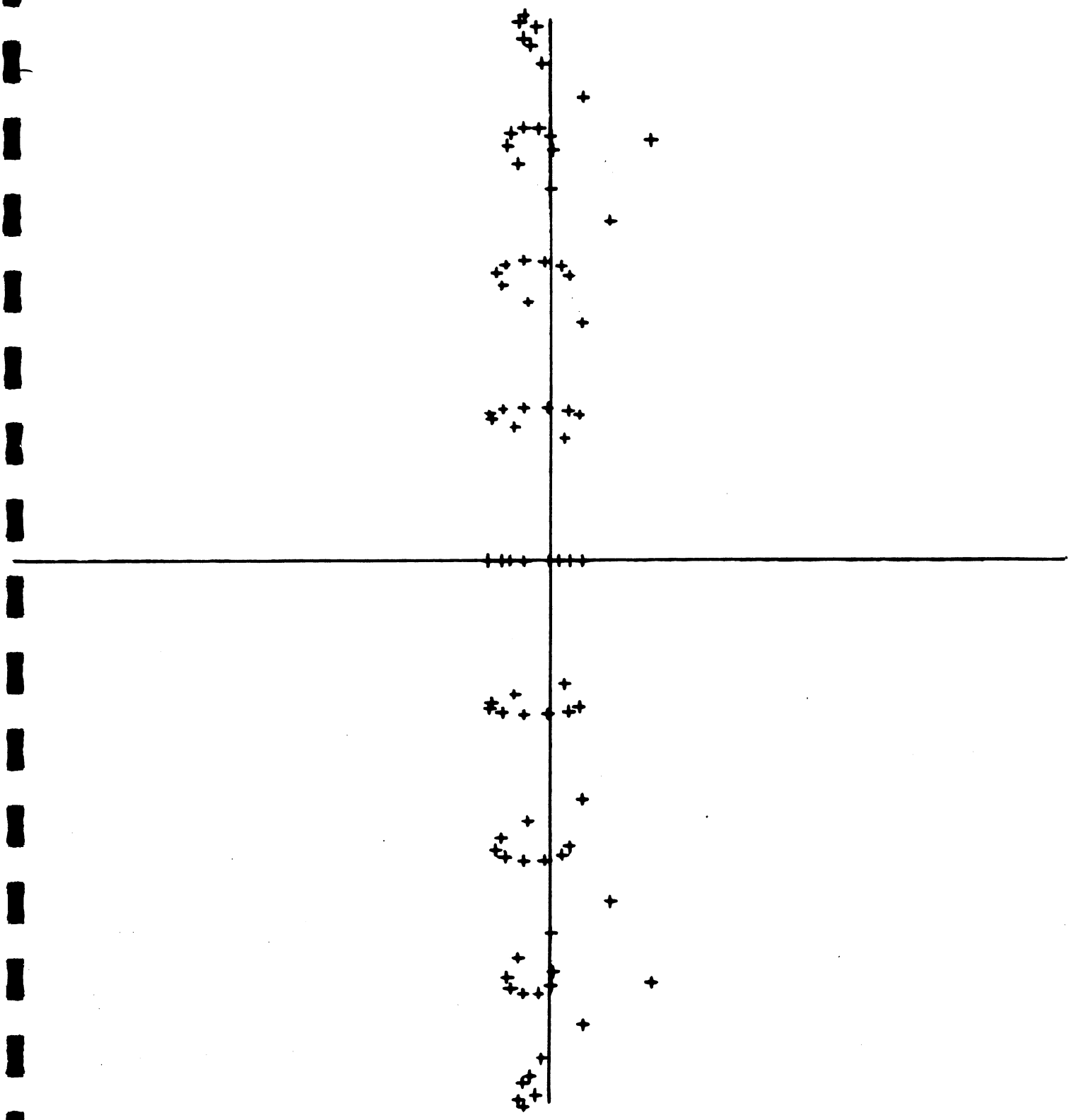

FIGURE 3-14.

81 RAY SPOT DIAGRAM AT EXIT SLIT FOR Y = 0

DOUBLE EBERT MONO-F/5-250MM FL-2400 L/MM GRATING-TWO MIRROR

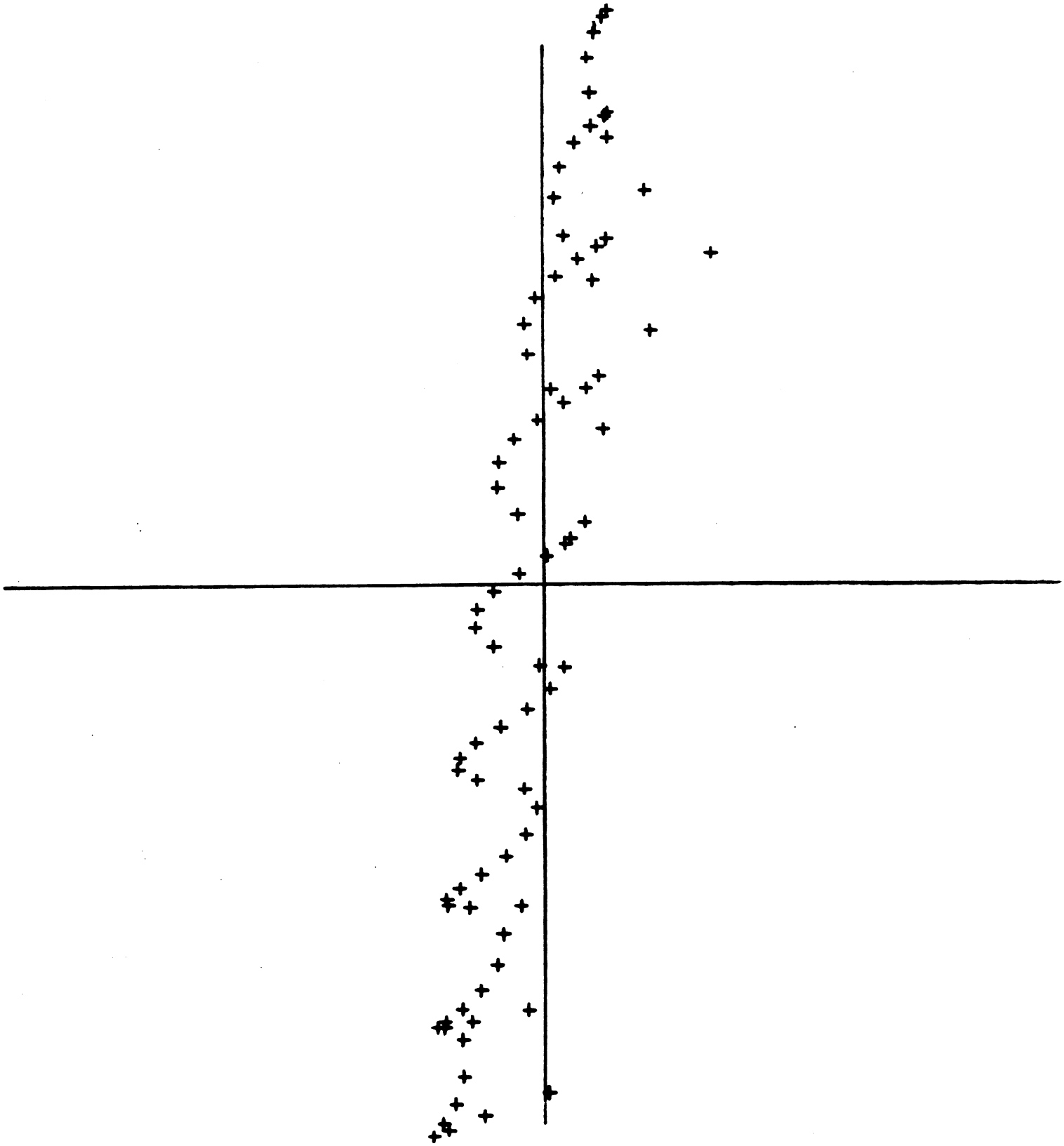

FIGURE 3-15.

81 RAY SPOT DIAGRAM AT EXIT SLIT FOR Y = 6.25 MM

DOUBLE EBERT MONO-F/5-250MM FL-2400 L/MM GRATING-TWO MIRROR

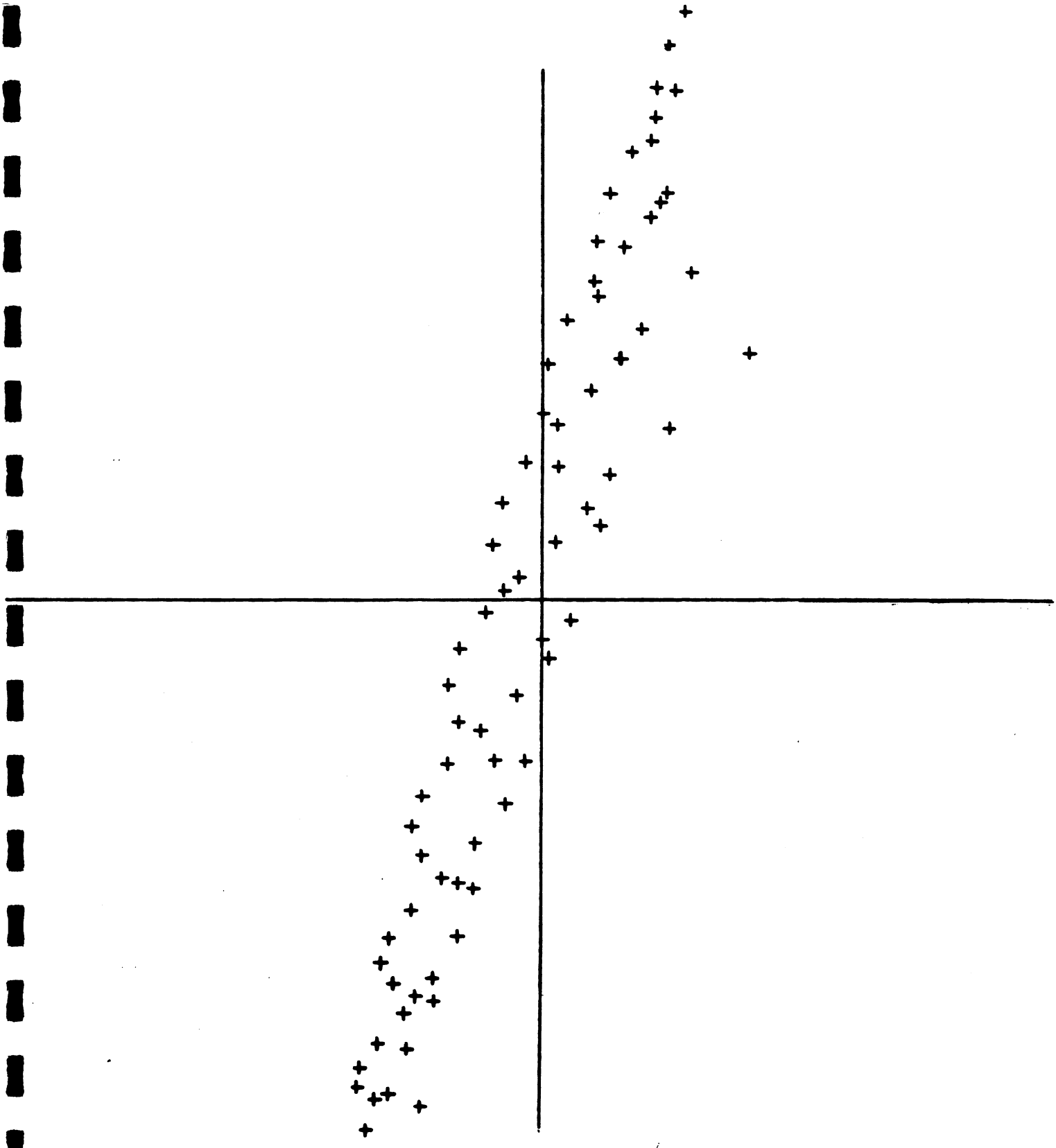

FIGURE 3-16.

81 RAY SPOT DIAGRAM AT EXIT SLIT FOR Y = 12.5 MM

DOUBLE EBERT MONO-F/5-250MM FL-2400 L/MM GRATING-TWO MIRROR

slit starting locations of y = 0, 6.25 mm, and 12.5 mm, respectively. The length of each half axis measured from the origin of its axis system is now 1.0 mm. The shape and dimensions of these patterns are nearly identical to those that were obtained for the double dispersive Double Ebert Monochromator with quartz prisms. The two double dispersive monochromators cancel the distortion which exists at the intermediate slit, and the resultant spectral images at the exit slit are remarkably consistent in shape and size for the full height of the slit. The spectral resolution capabilities of the double dispersive Double Ebert Monochromator are actually better than the Single Ebert Monochromator for tall slits.

Figures 3-14, 3-15, and 3-16 are spot diagrams at the exit slit of the zero dispersive Double Ebert Monochromator, for entrance slit starting points of y = 0, 6.25 mm, and 12.5 mm, respectively. The length of each half axis is again 1.0 mm. These spot diagrams are twice size duplicates of the intermediate slit images. The effective half bandwidth of the spot diagrams increase rapidly with the y-value. It should also be noted that the slit curvature offset exhibited at the intermediate slit, disappears at the exit slit of this particular monochromator, which is a characteristic of a zero dispersive double monochromator.

3.1.4.3 Entrance Optics for the BUV Photometer

An optical system consisting of two quartz lenses was designed to transfer those light rays entering the entrance slit of the photometer to the photomultiplier cathode. This imaging system has been made slightly complicated because of small size of the beam switching mirror, so two lenses have been required.

3.1.4.4 Exit Slit Curvature

The entrance slit of the BUV double monochromator is straight. Therefore, the exit slit must have that curvature which optimizes wavelength accuracy and spectral bandwidth. The physical curvature of the exit slit has been computed so as to match the optical image curvature for a wavelength of 2975 Å which is approximately midway between 2500Å and 3400Å.

The correct shape of the exit slit was determined by ray tracing a group of rays that are parallel to the axial ray from starting points on the entrance slit at 1 mm intervals of height.

3.2 OPTICAL TESTS AND RESULTS

3.2.1 Transmission Efficiency

To establish the effect of the different reflections and absorption losses in the BUV, transmission efficiency measurements were performed. The test set up is shown in Figure 3-17. A ratio measurement was attempted to establish the transmission percentage by comparing the results of a measurement taken when the photomultiplier was mounted directly behind the exit slit, vs. a measurement taken when the energy was directed onto the photomultiplier mounted behind the entrance slit (Figure 3-17). Since the photomultiplier could not be mounted directly behind the entrance slit in the second measurement, the energy was directed out of the monochromator with a special focusing mirror (Figure 3-17). The image obtained on the photomultiplier face plate was approximately .4 x .4 inches and resembled the size of image in the standard position configuration. A Beckman 2260 mercury lamp was used as the source. The spectrum isolation was accomplished with a DU Prism monochromator. The prism

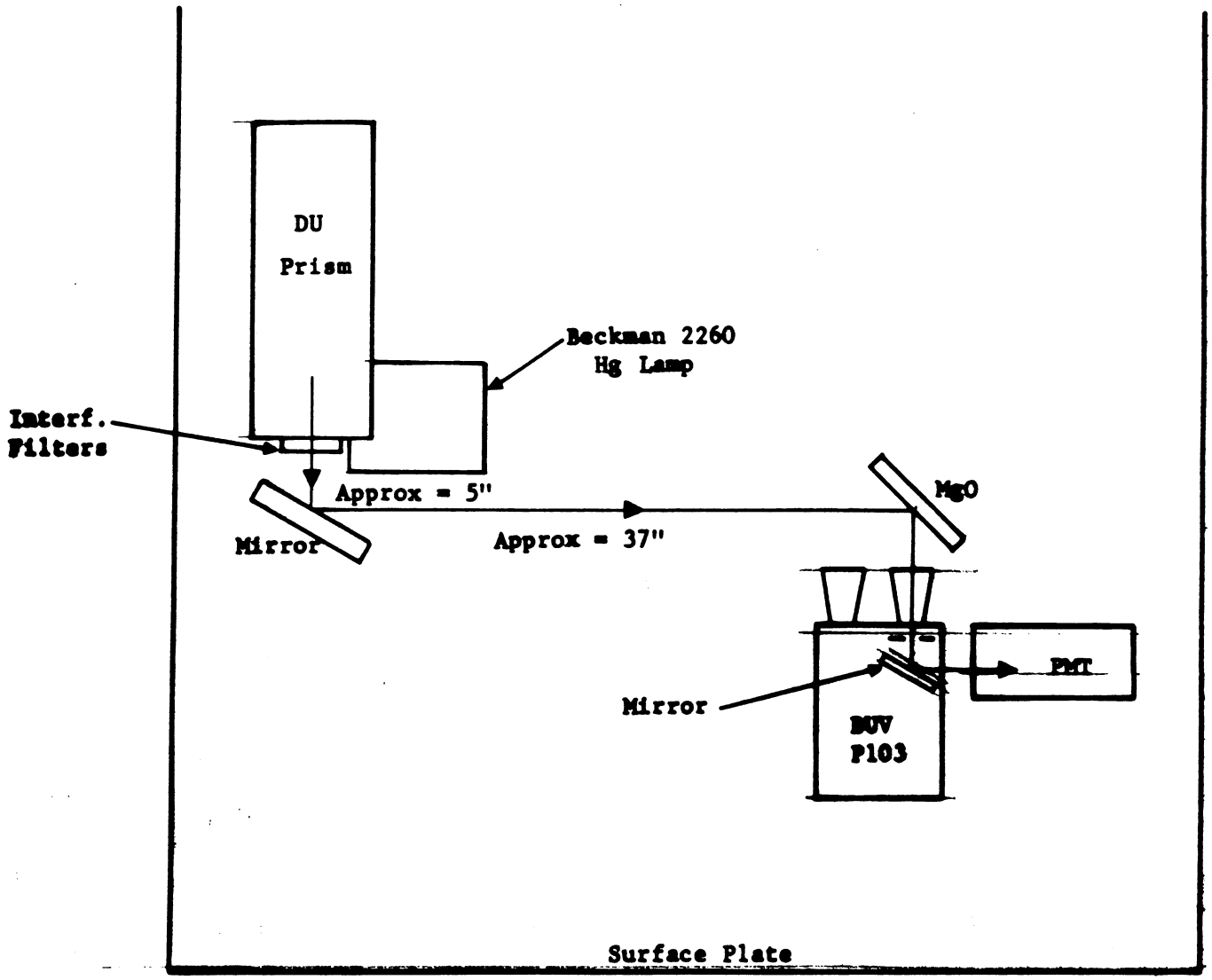

Figure 3-17. Transmission Efficiency Test Setup

monochromator was chosen to give the least amount of stray light in the wavelength region of interest. Further isolation was accomplished with interference filters which were mounted directly in front of the exit slit of the monochromator. The slit of the DU prism monochromator was adjusted in all cases to pass the equivalent BUV bandwidth of 10 angstroms.

A scan of the transmission bandwidths of the filters used for the measurements is shown in Figure 3-18. The setting on the micrometer corresponded to a mercury emission line. The center wavelength of the interference filters vs. the mercury emission line are also shown in Figure 3-18. The MgO plate placed directly in front of the BUV monochromator horn was over filled with the energy from the DU prism monochromator, in such a way that the BUV field of view was always filled with energy. In all measurements, the auxiliary slit was closed and the data was obtained in the sequence shown.

Transmission efficiency was the most difficult measurement to make on the BUV instrument. The measurements were taken without and with the depolarizers installed. The results, shown in Tables 3-3 and 3-4 under percent transmission, were inconclusive in respect to the percentage of transmission efficiency obtained. It was estimated that approximately 15 percent transmission could be obtained; however, this could never be verified with the transmission measurements. It was extremely difficult to exclude all the stray light in the "No Monochromator" measurements, especially with the high voltage settings employed. The ratio measurement between "No Monochromator" and the energy going through the "Two Monochromators", however, revealed that the slope of the curve of the data obtained was correct as predicted. This slope is mainly

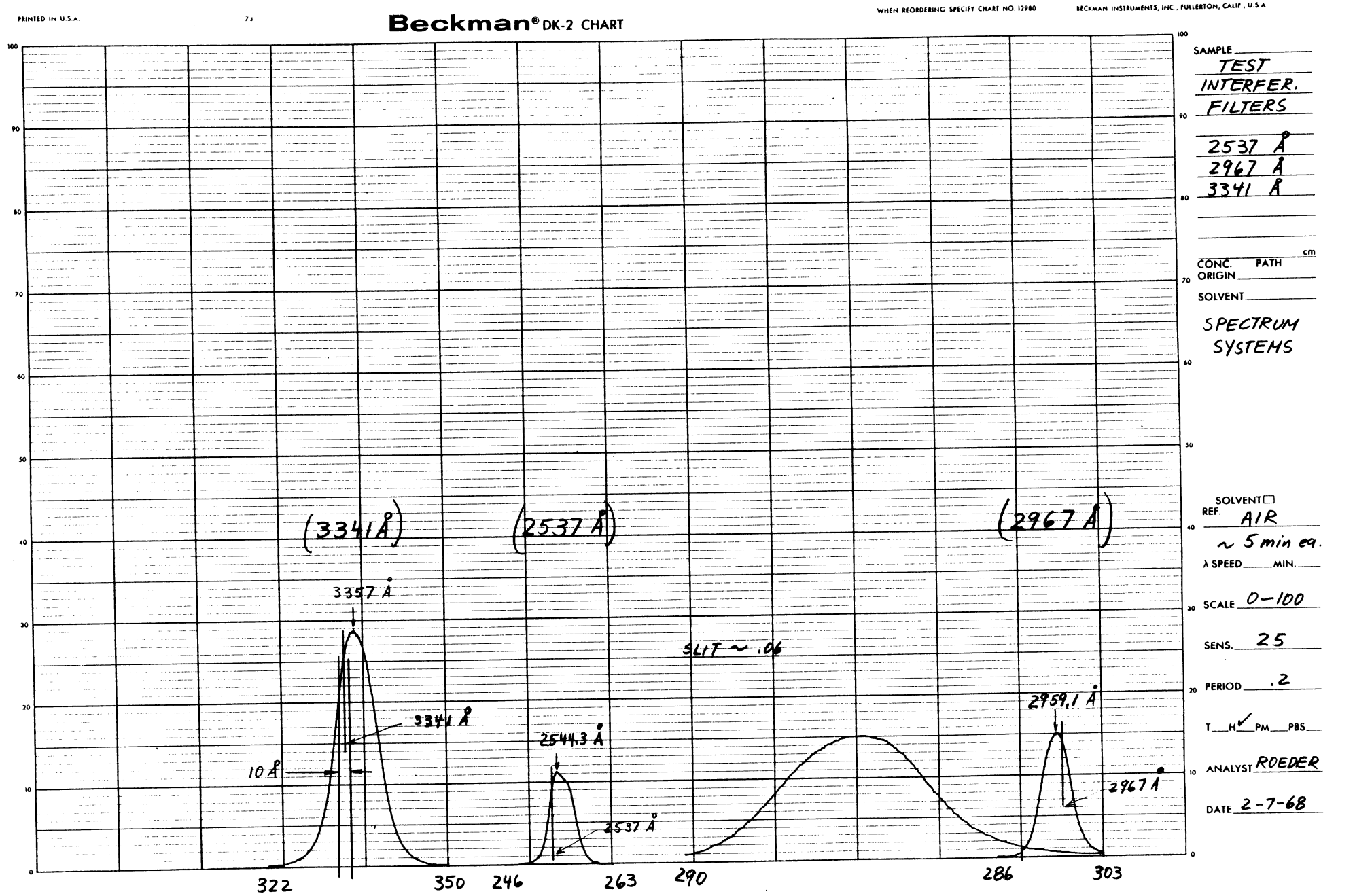

Figure 3-18. DK-2 Transmission Bandwidth Scan of Filter Used for Measurements

	Wavelength (Angstroms)	Micrometer Setting	Slit Width (mm)	Keithley Amperes	i_d (Amperes)	Percent Transmission
Through Two Monochromators	2537	0.0648	0.4	2.1×10^{-10}	0.62×10^{-10}	10.6
	2967	0.3864	0.25	7.8×10^{-10}	0.64×10^{-10}	5.18
	3341	0.6741	0.15	1.15×10^{-10}	0.70×10^{-10}	0.0765
No Monochromator	2537	-	0.4	0.17×10^{-8}	3×10^{-10}	
	2967	-	0.25	1.22×10^{-8}	2.8×10^{-10}	
	3341	-	0.15	0.62×10^{-8}	3×10^{-10}	

Notes:

1. Auxiliary Slit Closed
2. Used #2260 Beckman Hg Lamp, and #12313 PMT - 3200 V

Table 3-3. BUV Transmission Efficiency; P103 Instrument

	Wavelength (Angstroms)	Micrometer Setting	Width (mm)	Keithley Amperes	i_d (Amperes)	Percent Transmission
Through Two Monochromators	2537	.0586	0.4	1.95×10^{-10}	1.30×10^{-10}	5.8
	2967	.3788	0.25	4.1×10^{-10}	1.30×10^{-10}	3.2
	3341	.6662	0.15	1.38×10^{-10}	1.30×10^{-10}	0.0019
No Monochromator	2537	-	0.4	1.35×10^{-9}	2.35×10^{-10}	
	2967	-	0.25	$.89 \times 10^{-8}$	2.65×10^{-10}	
	3341	-	0.15	4.5×10^{-9}	2.45×10^{-10}	

Notes:

1. Auxiliary Slit Closed
2. Used #2260 Beckman Hg Lamp, and #12313 PMT - 3200 V

Table 3-4. BUV Transmission Efficiency, F104 Instrument

influenced by the blaze wavelength of the grating and the first monochromator collimating mirror which was coated favoring the shorter wavelength as shown in Figure 3-19. The measurements for transmission efficiency were performed to verify the percentage transmission calculated from reflection and absorption losses. The data obtained in this measurement, however, was inconclusive. So much depended on the set up and the stray light that the data obtained was essentially disregarded.

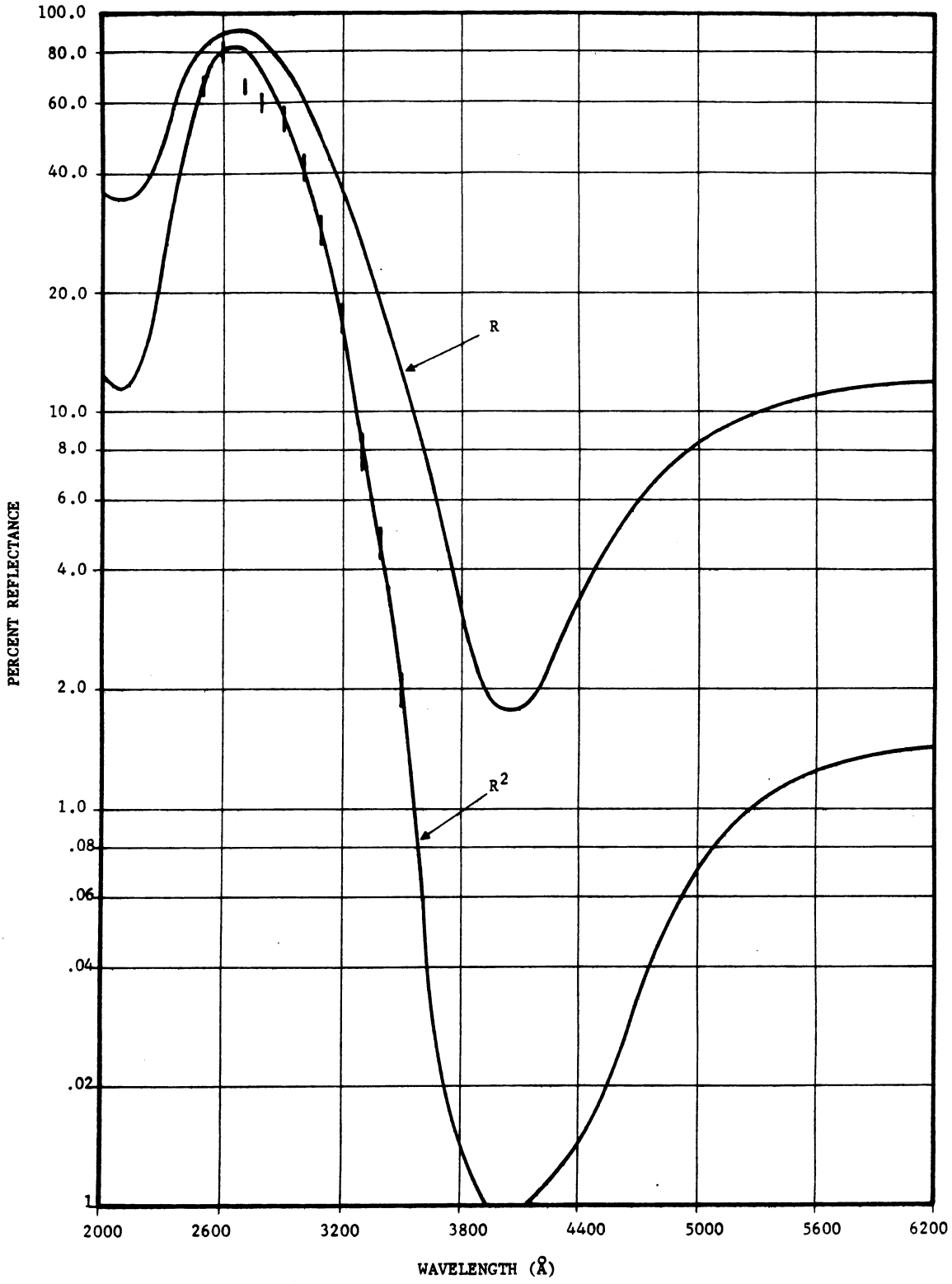

Figure 3-19. BUV First Monochromator Collimating Mirror Percent of Energy Reflectance Vs. Wavelength

3.2.2 Optical Alignment

Optical alignment of the BUV Instrument was verified using several methods. The most effective and the one discussed in this paragraph is the photographic method. With this method, the alignment of the images at the intermediate and exit slit were measured and compared to the slit openings. Refer to Beckman Report No. PR-2475-10, paragraph 2.4, for additional information. Optical alignment is also verified by compliance of the actual wavelength steps with the nominal design wavelength steps (paragraph 7.2.2).

3.2.2.1 Slit Image Photographs, Exit and Intermediate Slit, Monochromator

These photographs are used to verify the following optical properties of the Instrument:

(a) Alignment of optical elements
(b) Wavelength uniformity along the exit slit
(c) Positions of entrance, exit, and intermediate slits
(d) Proper image curvature
(e) Alignment of internal Hg wavelength calibration lamp

The Instrument is installed in the optical test fixture using the MgO plate. A piece of Kodak Spectrum Analysis No. 3 film is mounted at the exit slit. BUV shutters or entrance horns are closed. A PEN RAY Mercury Light Pencil is used as a source and allowed to stabilize. With the micrometer screw, the cam follower arm is set to the known position of a mercury spectrum line.

The film is exposed by allowing the light from the diffuser plate to enter the BUV. The film is developed and enlarged, if necessary, to make the required analyses.

To compare the image of the entrance slit to the exit slit, the exit slit is back-lighted through a diffuser (such as opal glass) to superimpose the image of the exit slit on the spectral image of the entrance slit. This test is performed for the following mercury lines: 2537 Å, 2967 Å, and 3341 Å.

The procedure is then repeated for photographs of the intermediate slit to verify that the energy passes unobstructed from the first into the second monochromator.

Exit Slit	P103 Instrument	F104 Instrument
2537	P-72, P-101	F-69, F-72
2967	P-92	F-76
3341	P-79	F-77
Intermediate Slit		
2537	P-80	F-74

The bright image on all the photographs shows the image of the energy at the intermediate slit plane and the exit slit plane. For contrast, the back-lighted slit appears less bright. To measure or verify alignment of the images vs. the slit, the images in some photographs are off-set a certain distance from the slit outline.

3.2.2.2 Alignment of Internal Hg Lamp, Monochromator

To check the alignment of the internal Hg wavelength calibration lamp, a piece of Kodak Spectrum Analysis No. 3 film is mounted at the exit slit.

A micrometer screw is used to set the cam follower arm to the known position of a mercury line. The micrometer settings for the internal Hg lamp differ by about 3 Å from the positions of the Hg lines in paragraph 3.2.2.1 due to the offset of the calibration lamp opening with respect to the main slit.

The internal Hg lamp is lighted and the film exposed. This test is performed for the 2537 Å Hg line.

To compare the image of the entrance slit to the exit slit, the exit slit is back-lighted through a diffuser (such as opal glass) to superimpose the image of the exit slit on the spectral image of the entrance slit.

BUV P72

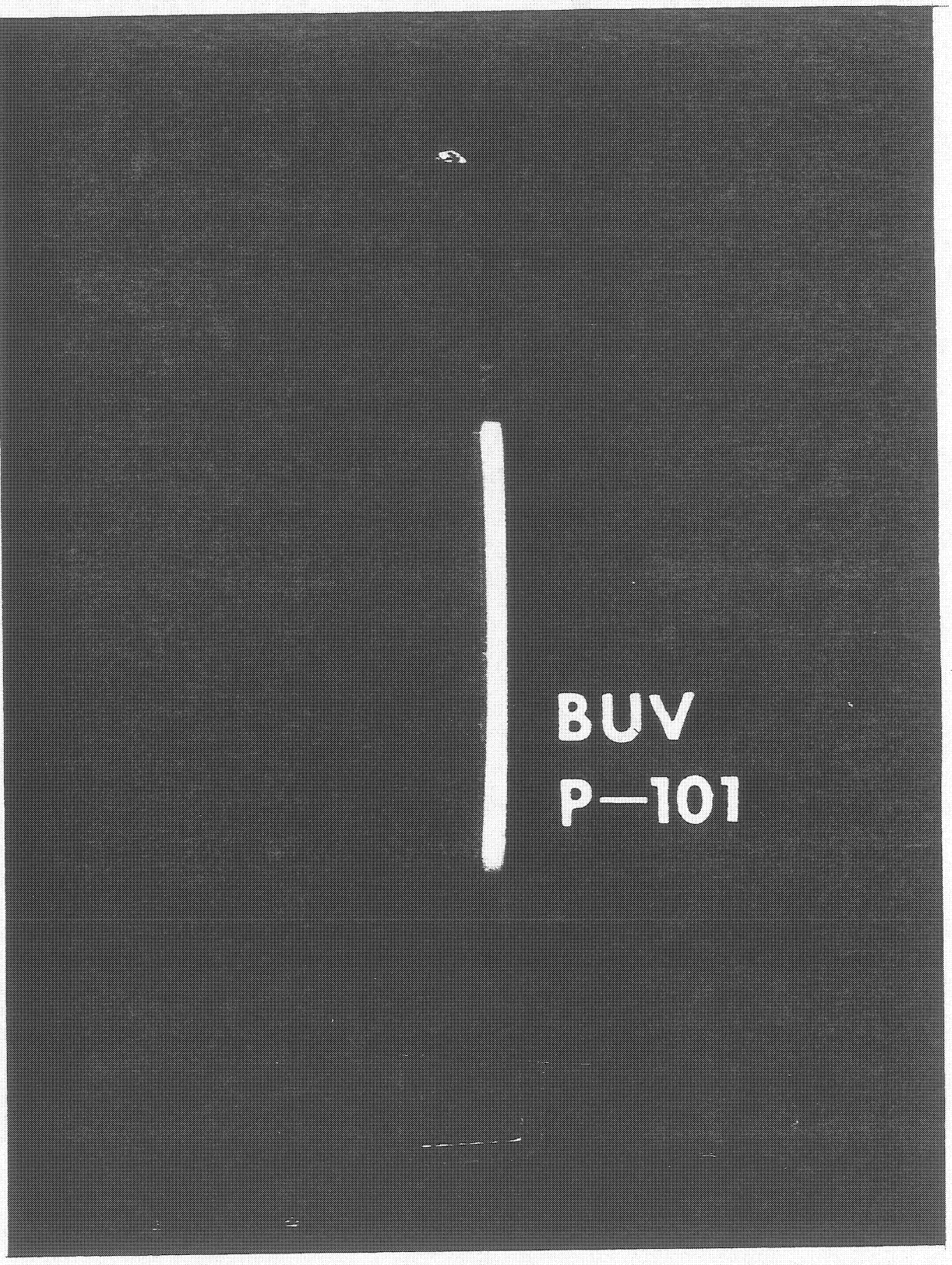
BUV
P—101

BUV
P92

BUV P79

BUV F69

BUV F72

BUV F76

BUV F77

BUV P80

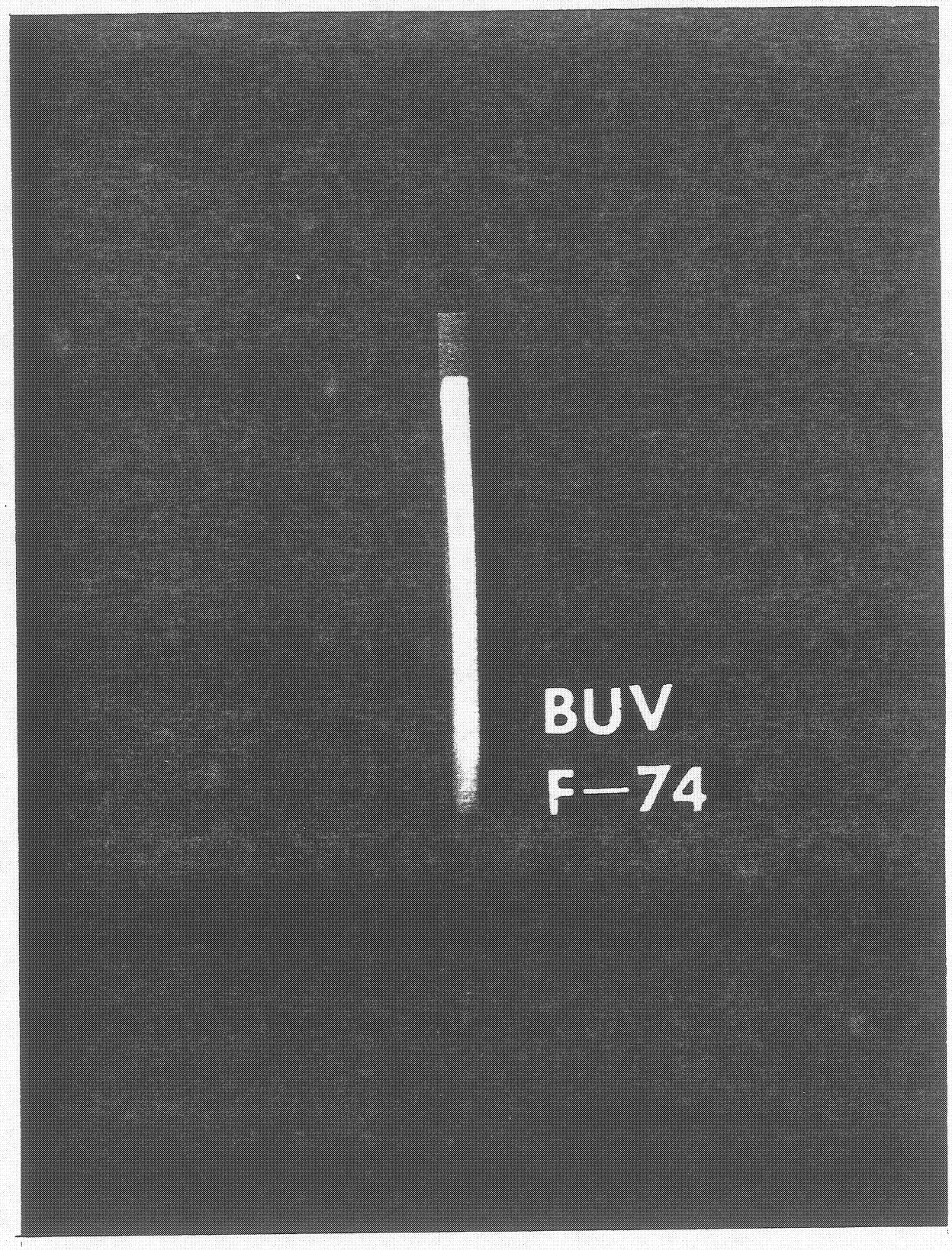
BUV
F—74

BUV P98

BUV
FS3

BUV P97

BUV F54

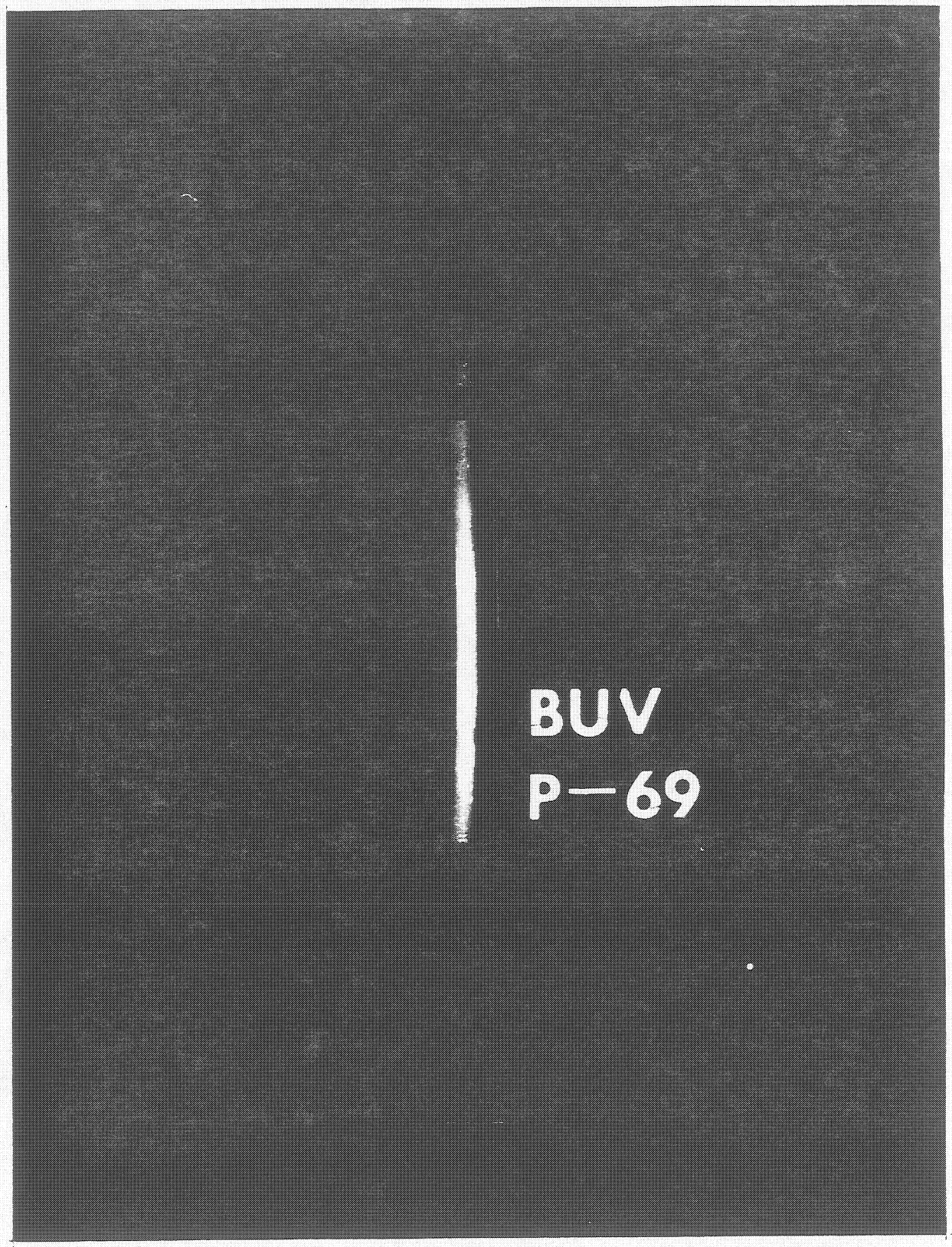
BUV
P—69

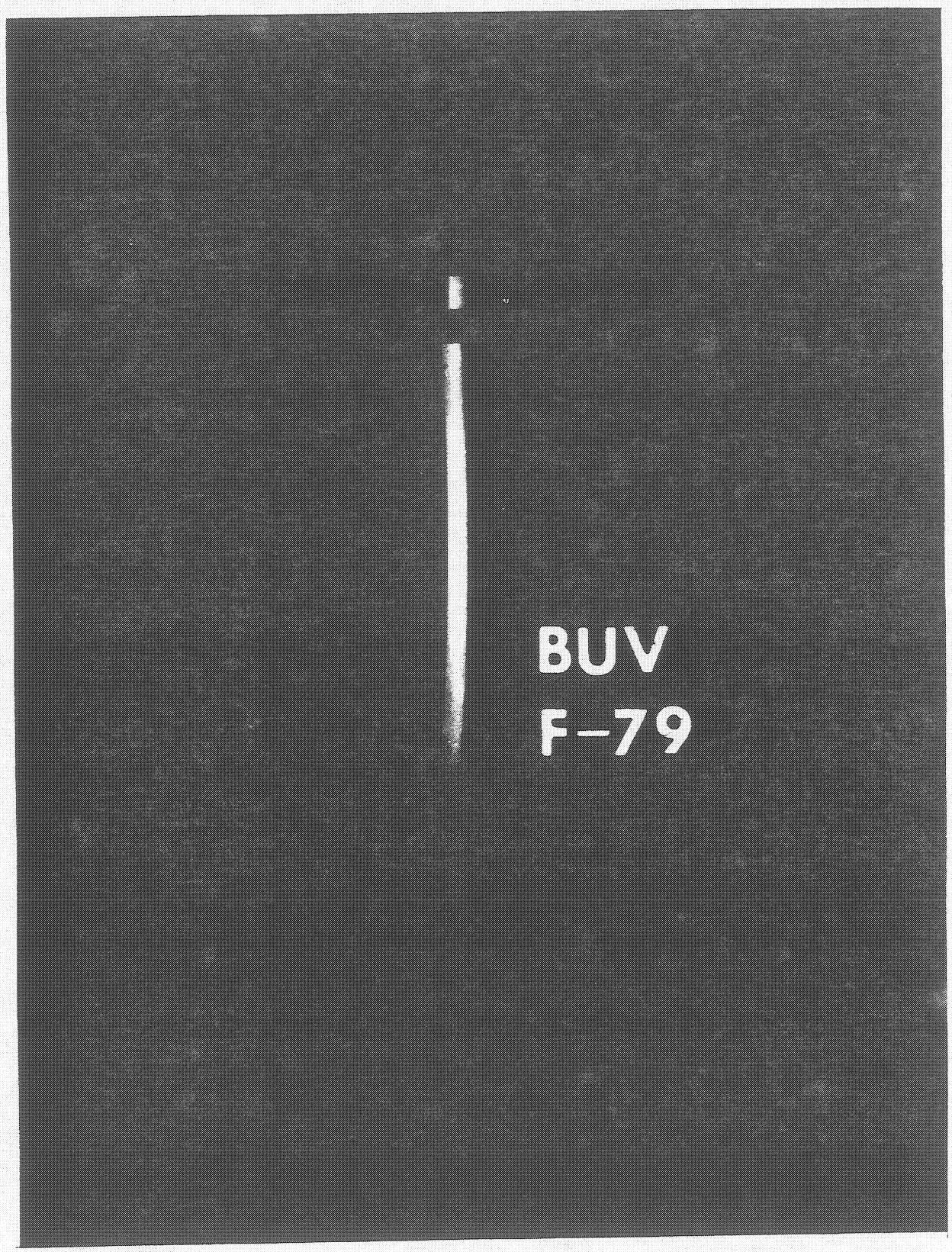
BUV
F-79

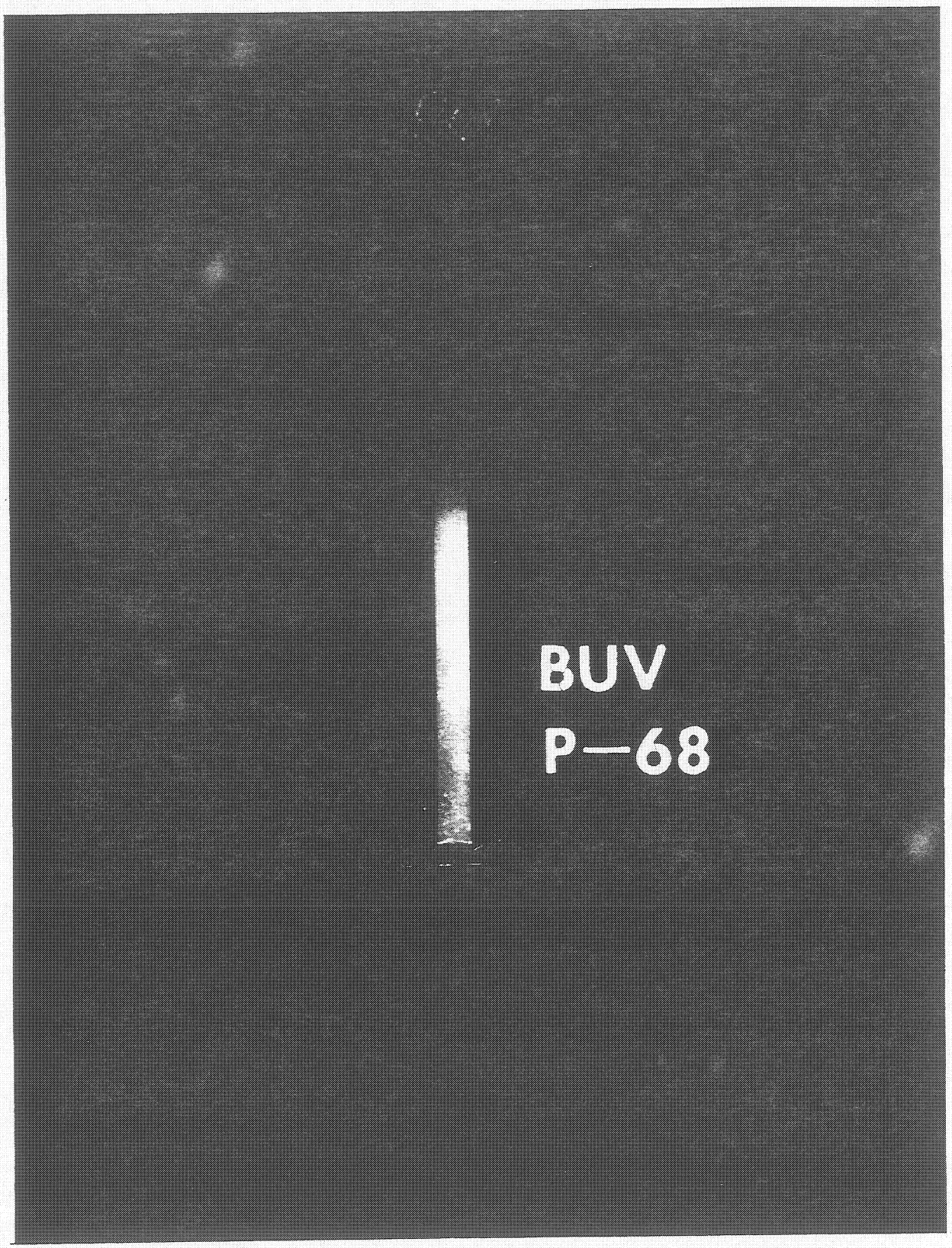
BUV
P—68

BUV F81

Exit Slit	P103 Instrument	F104 Instrument
2537 Å	P-98	F-53
Intermediate Slit		
2537 Å	P-97	F-54

In pictures P-80 and P-97, the intermediate slit is very effective in allowing the energy from the entrance slit and from the auxiliary slit to pass without obstruction. All energy outside this image is successfully rejected (reflected and absorbed). The same is true for pictures F-74 and F-54. The cubed shape image of the auxillary slit is due to optical aberration.

3.2.2.3 Alignment of Internal Photometric Source, Monochromator

To check the alignment of the internal monochromator photometric calibration source the wavelength micrometer is set to the peak emission wavelength for the phosphor. The entrance shutter is rotated to the photometric calibration position and a piece of Spectrum Analysis No. 3 film is mounted and exposed at the exit slit and intermediate slit. The slits are then diffusely back-lighted to superimpose the slit image on the spectral slit image.

	P103 Instrument	F104 Instrument
Exit Slit	P-69	F-79
Intermediate Slit	P-68	F-81

The rather wide image of the photometric source as depicted in pictures F81 and P68 is the reflection of the metal mirror intercepting the energy from the photometric source.

3.2.2.4 Alignment of Photomultiplier Aperture, Monochromator

A piece of Kodak Spectrum Analysis No. 3 film is mounted between the PMT aperture mask and the monochromator exit lens. The grating arm is set to the known position of a mercury line using a micrometer screw. A PEN RAY Mercury Light Pencil is used as a source. The lamp is allowed to stabilize before the film is exposed.

Pictures are taken in front and behind the aperture. Back-lighting is not possible in this configuration.

To check the relative size of the aperture opening with respect to the grating image on the film, the outline of the opening is superimposed on the pictures.

	P103 Instrument	F104 Instrument
In front of aperture	P-25	F-62
Behind aperture	P-26	F-60

3.2.2.5 Alignment of Internal Photometric Source, Photometer

To check the alignment of the photometer internal photometric calibration source, a piece of Spectrum Analysis No. 3 film is placed in front of the PMT cathode aperture, the shutter rotated to the photometric calibration position, and the film exposed. It is not possible to back-light the film in this configuration.

The film size conforms to the outside diameter of the photomultiplier tube; the orientation of the image on the film, therefore, serves as alignment verification.

	P103 Instrument	F104 Instrument
At PMT cathode	P-105	F-80

3.2.2.6 Alignment of Photometer

To check the alignment of the photometer, a piece of Spectrum Analysis No. 3 film is placed behind the aperture. With the field-of-view filled by an MgO diffuser plate, the film is exposed by illuminating the plate.

This procedure is repeated with the film mounted in front of the photomultiplier cathode.

The film sizes conform to the outside diameters of photomultiplier and aperture.

BUV
P—25

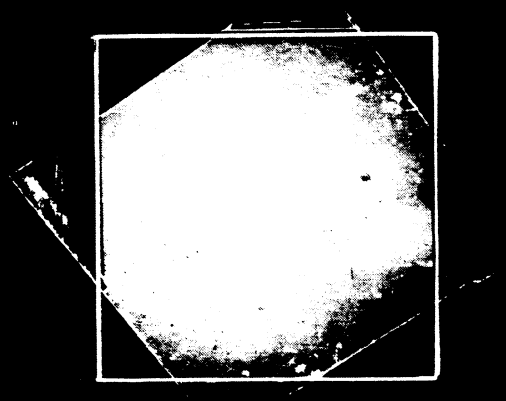

BUV
F—62

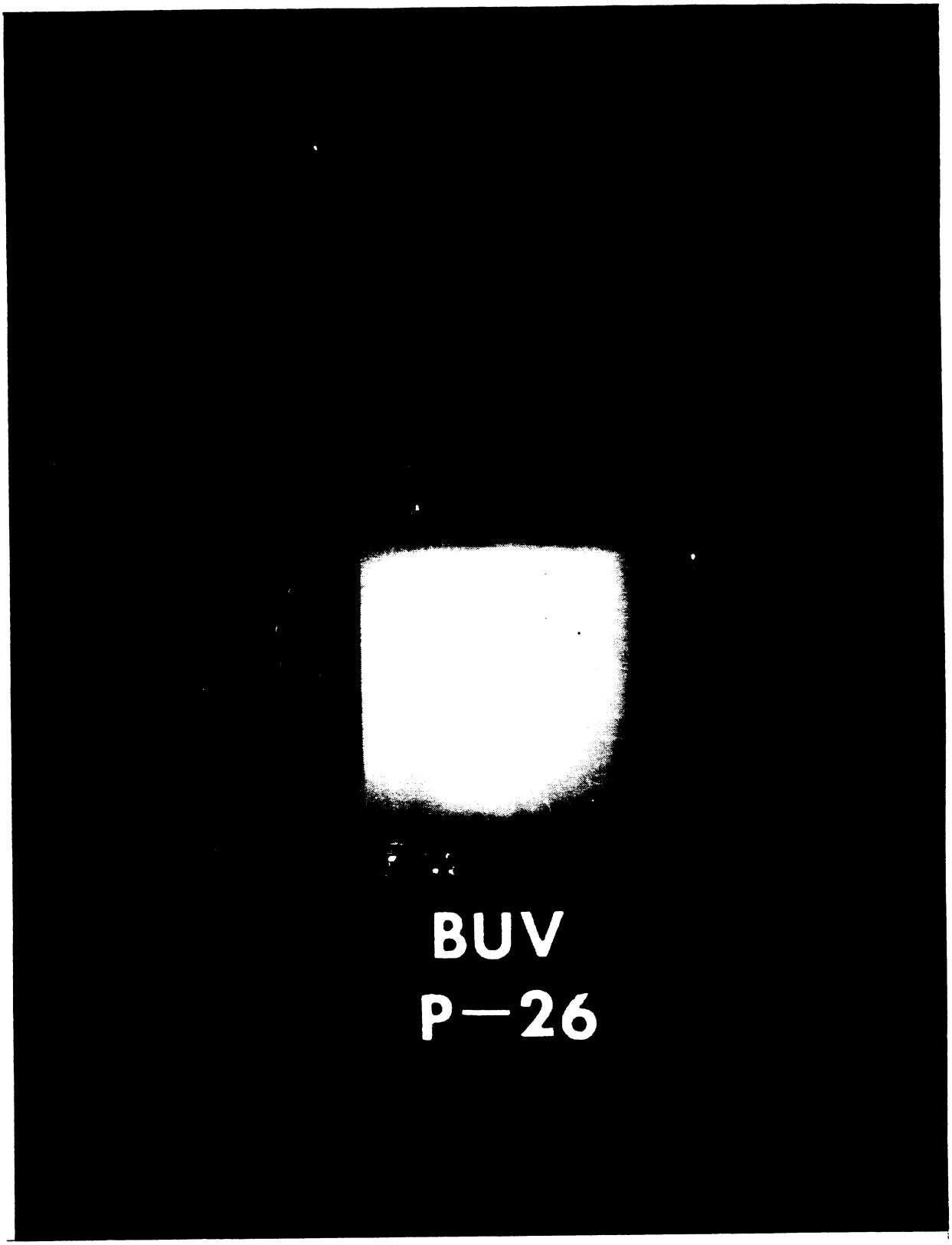
BUV
P—26

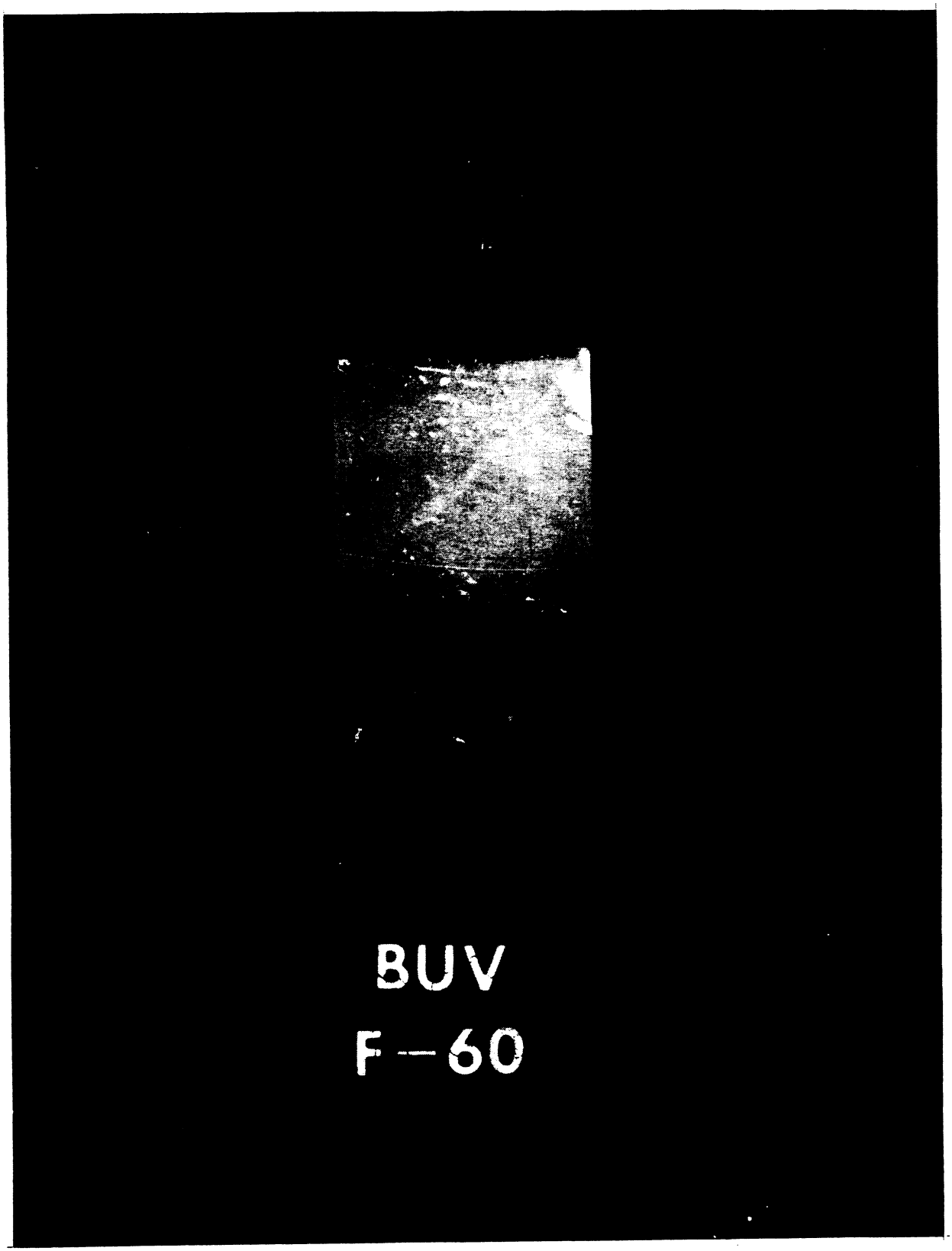
BUV
F-60

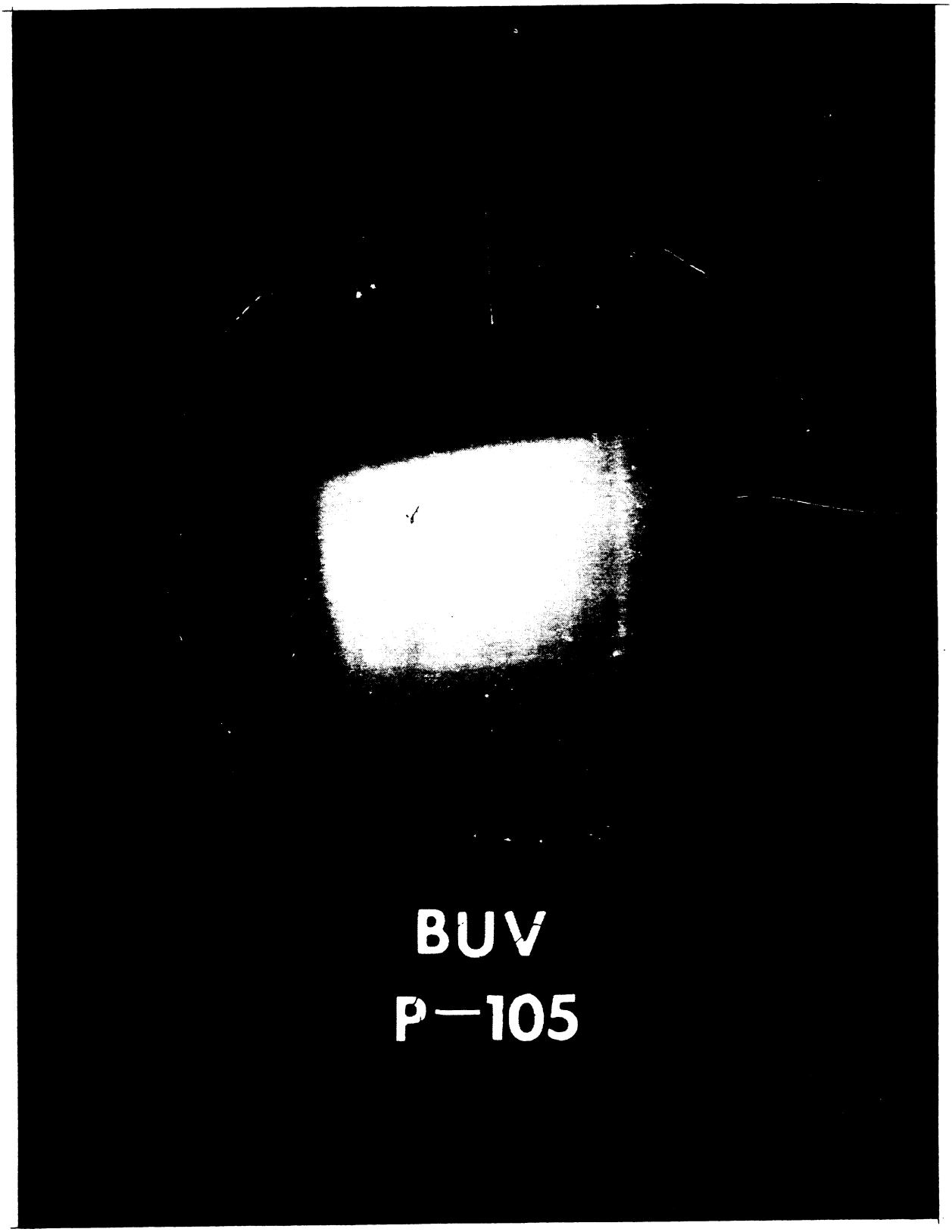
BUV
P—105

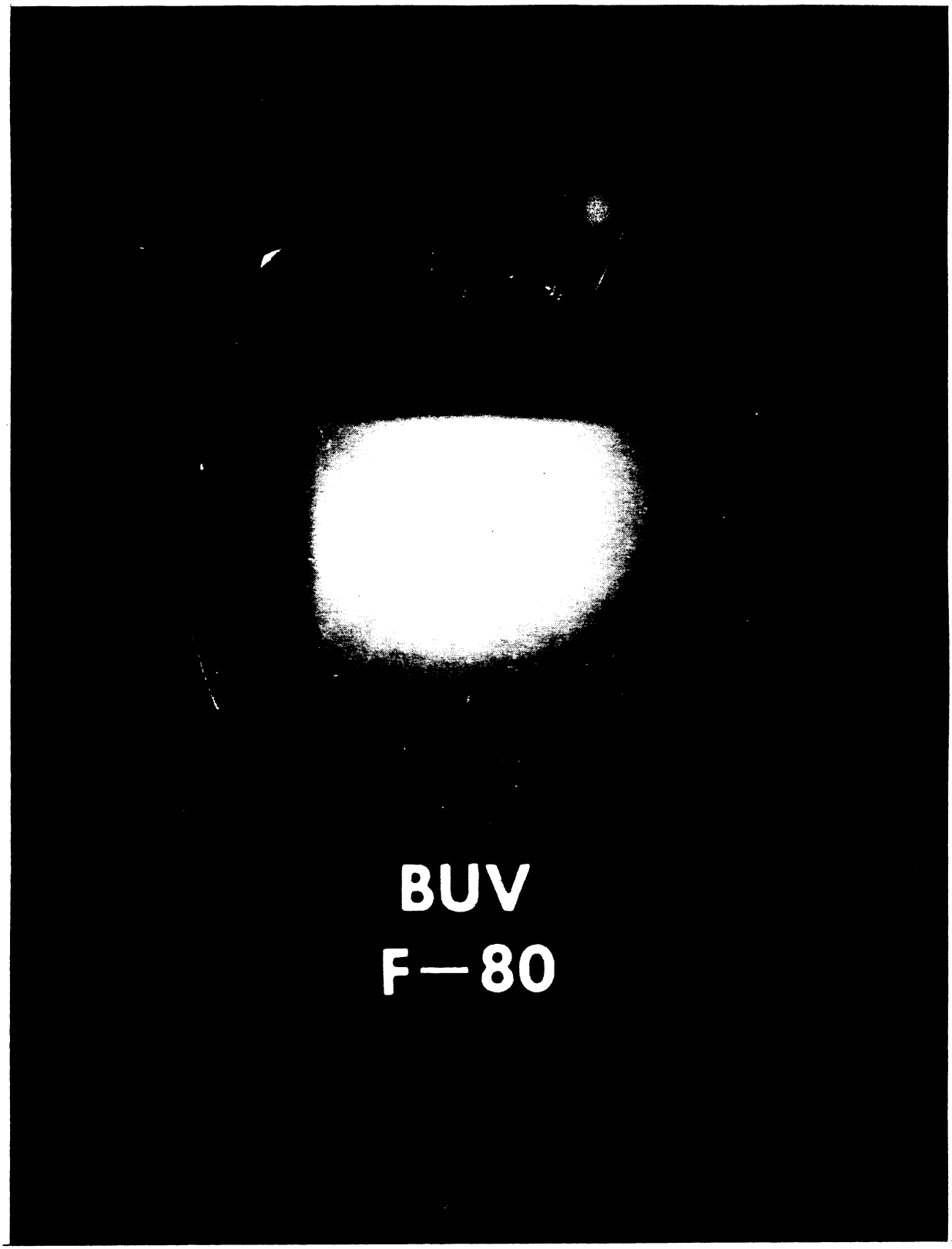
BUV
F—80

The orientation of the image on the film serves as alignment verification.

	P103 Instrument	F104 Instrument
At PMT cathode	P-65	F-84
At aperture	P-66	F-86

3.2.2.7 Wavelength Transfer Function

This test verifies the following:

(a) Uniformity of slit function versus wavelength at mercury lines
(b) Bandwidth of the instrument at mercury lines
(c) Repeatability of wavelength versus grating arm position
(d) Resolution of Instrument
(e) Focus

The Instrument is installed in an optical test fixture. A PEN RAY Mercury Light Pencil is installed at the light source position on the test fixture and allowed to stabilize. The photomultiplier tube is connected either to a high voltage power supply and electrometer, or to the BUV Electronic Subsystem.

A micrometer screw is used to move the grating arm. The selected mercury spectrum line is scanned manually, taking enough data points to plot relative PMT output versus λ through the following mercury lines: 2537 Å, 2967 Å, and 3341 Å (Figures 3-20 through 3-23).

The mercury spectrum is scanned by driving the micrometer screw with a synchronous motor and the electrometer output is recorded on a strip-chart recorder. The gain of the electrometer is adjusted to give full-scale deflection. These tests are performed for the 2967 Å and 3341 Å lines (Figures 3-24 through 3-27).

The scans of the mercury lines using a synchronous motor are part of a procedure to test the Instrument performance during environmental testing.

Table 3-5 is an example of the results obtained on the bandwidth changes. The straightness of the sides of the scanned slit function is an indication of alignment and focusing quality.

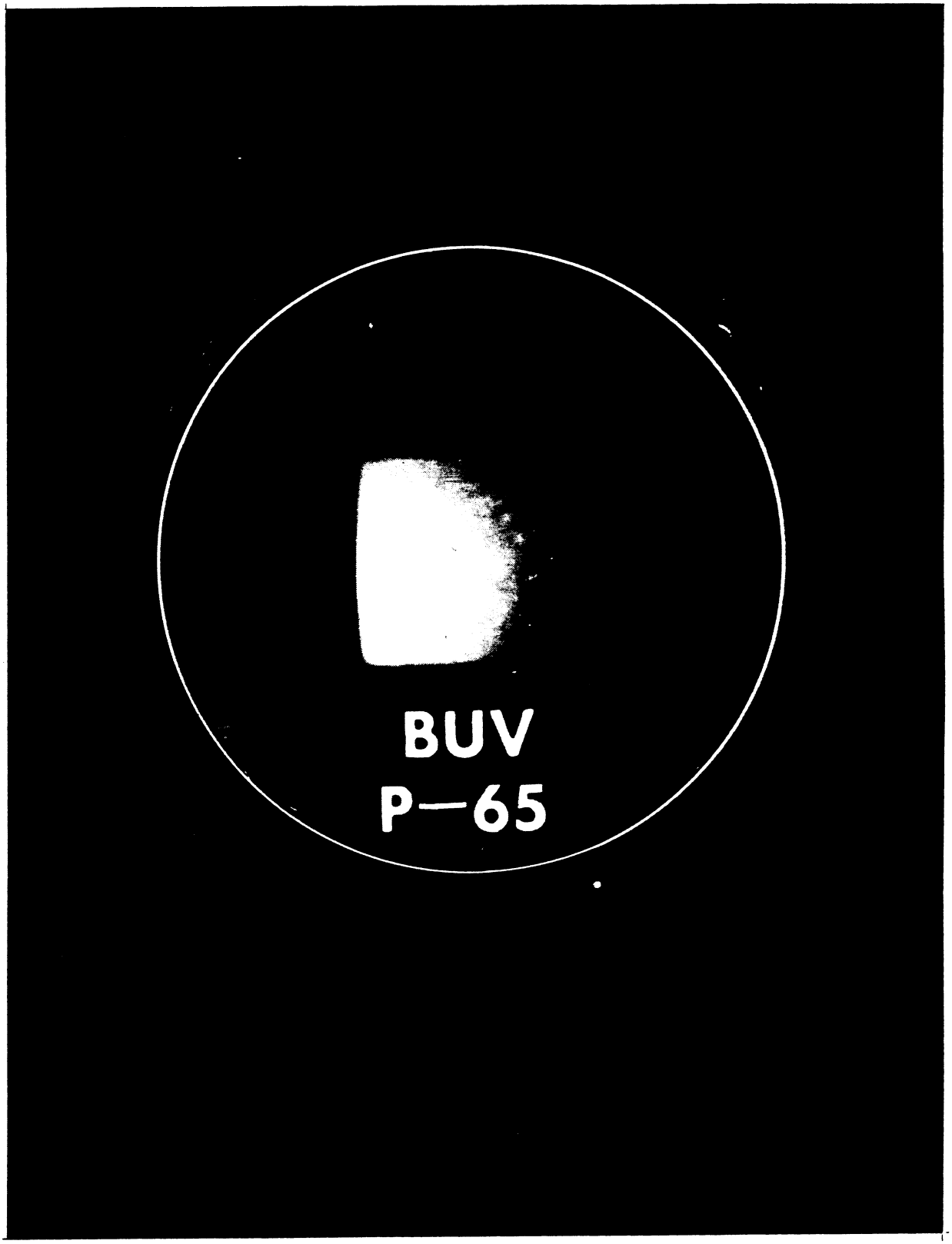
BUV
P—65

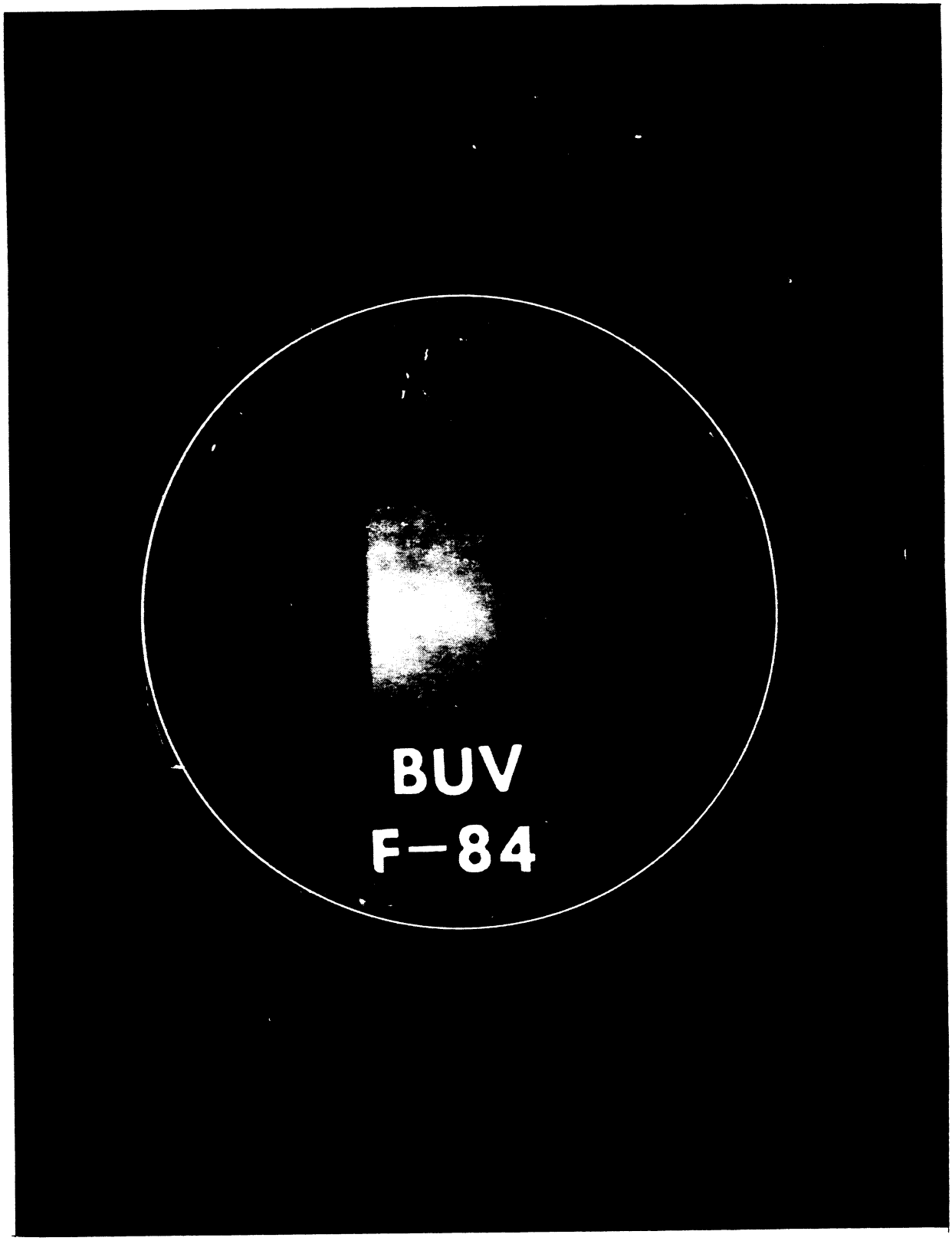
BUV
F-84

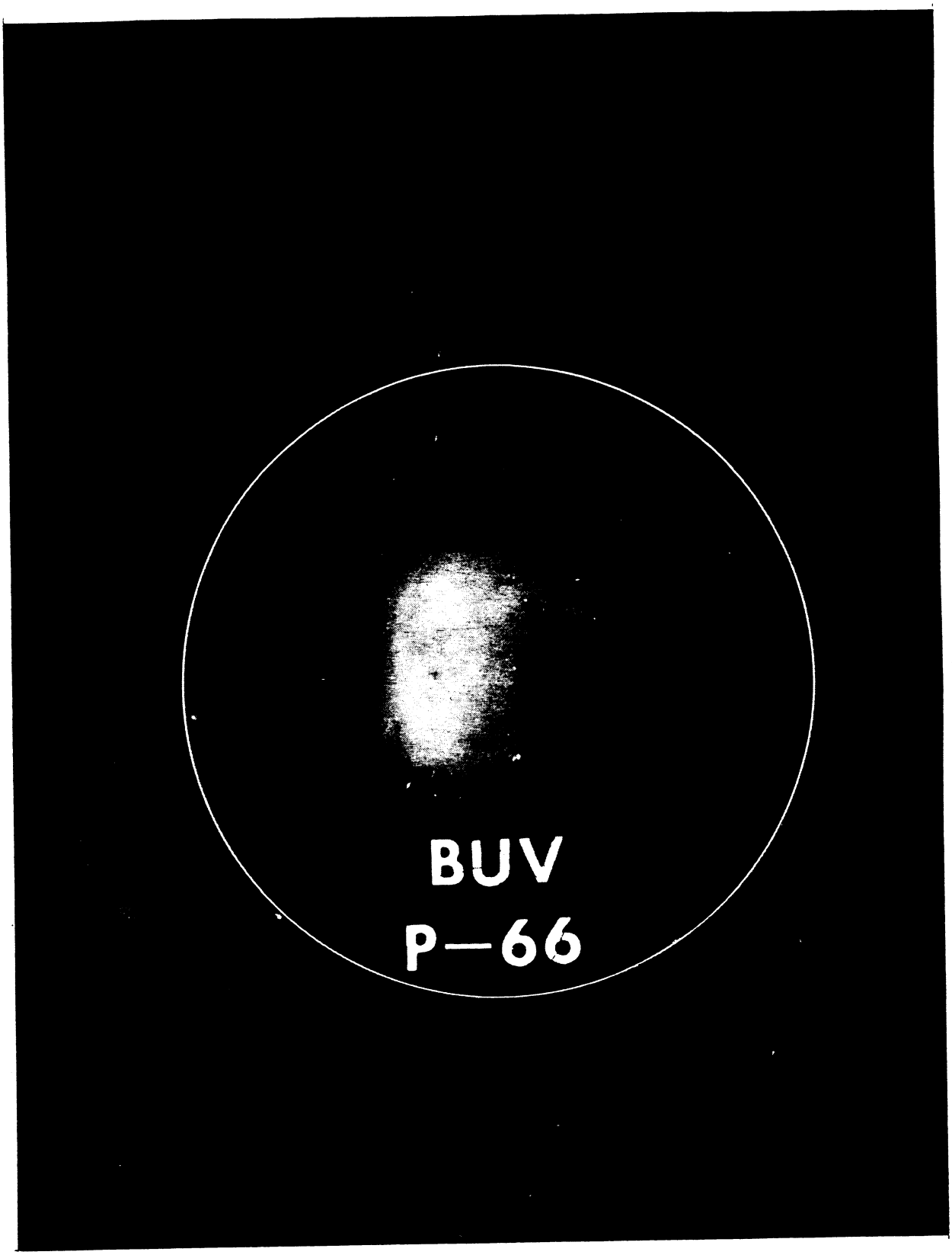
BUV
P—66

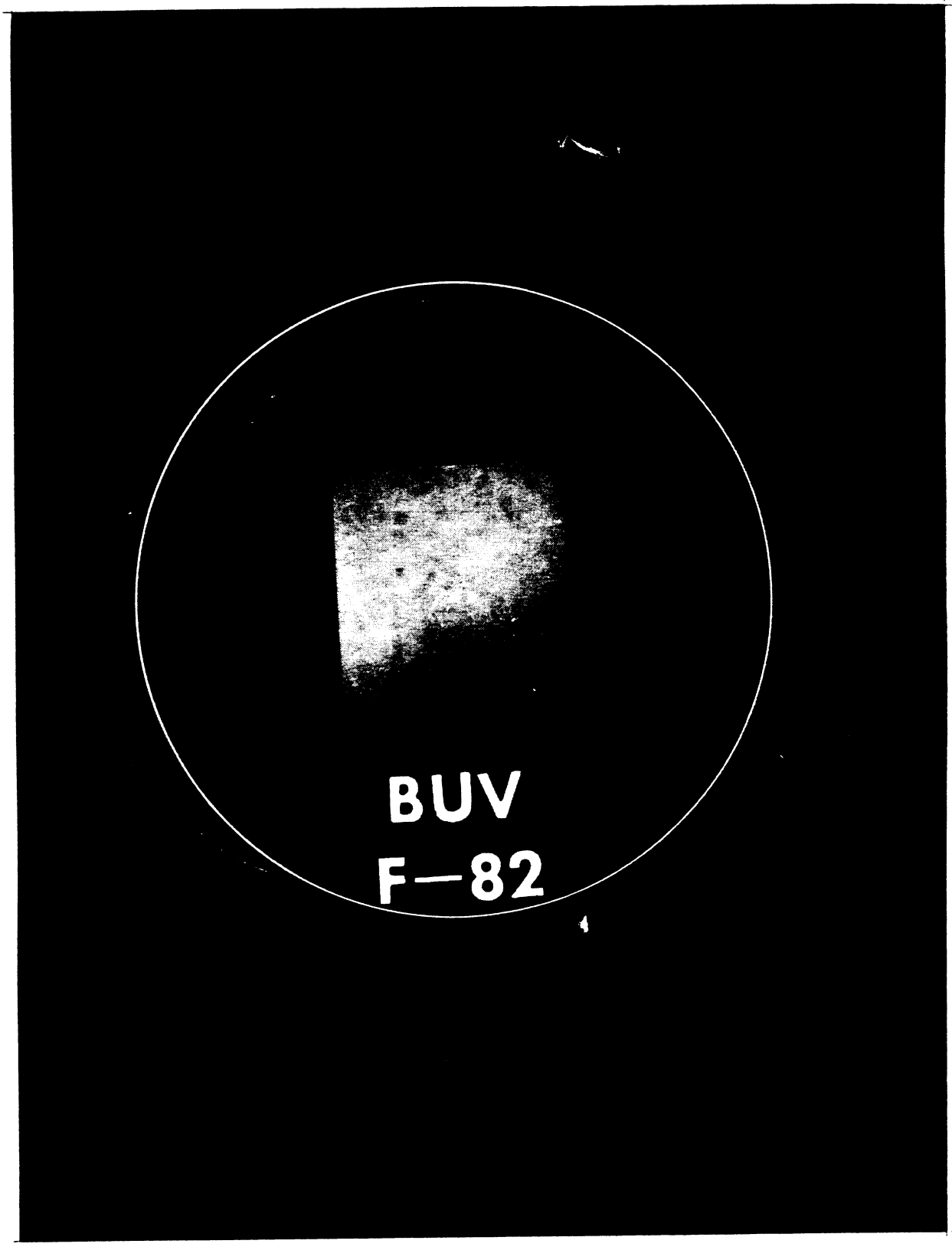
BUV
F—82

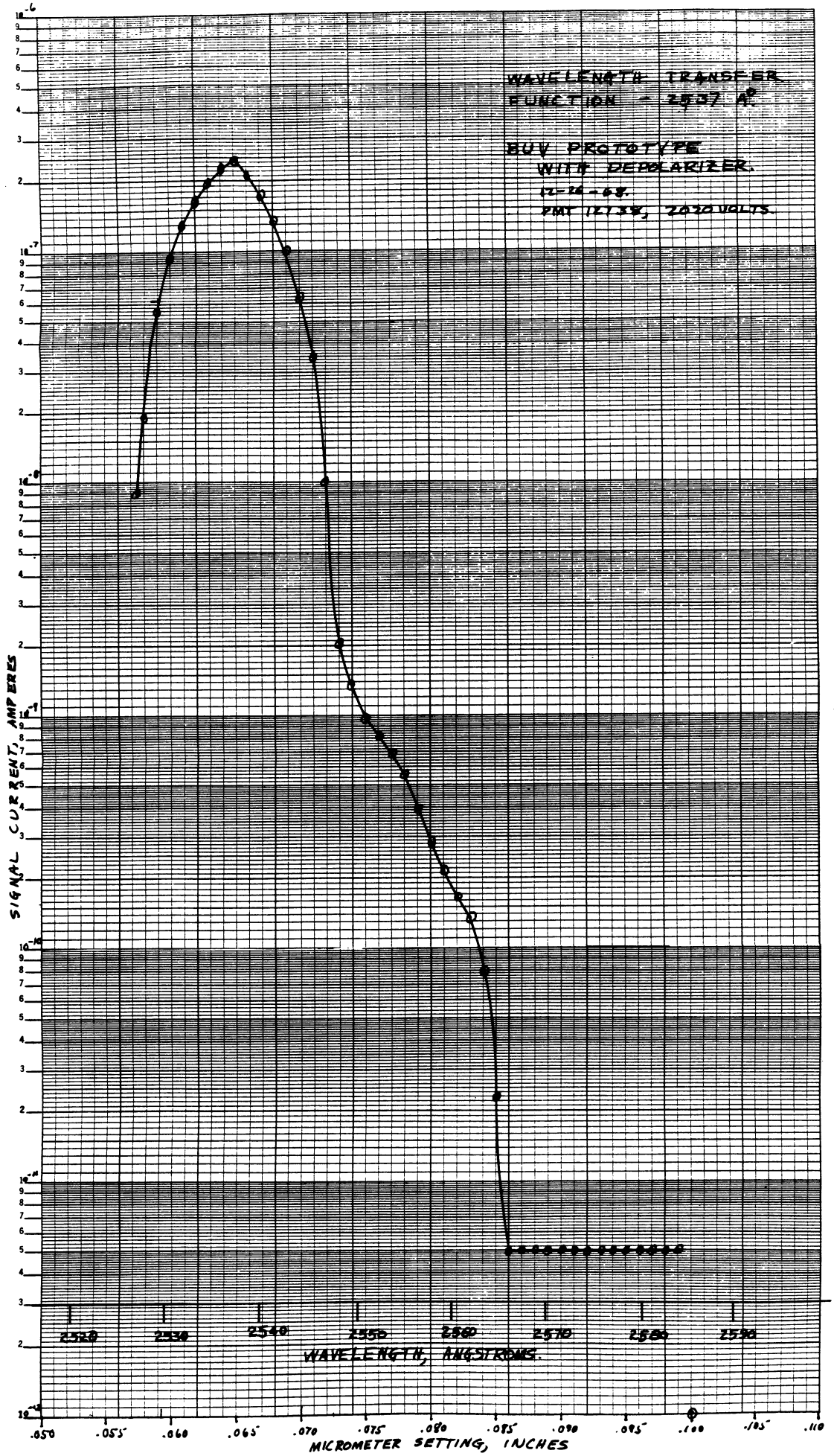

Figure 3-20. Wavelength Transfer Function 2537 Å, P103 Instrument

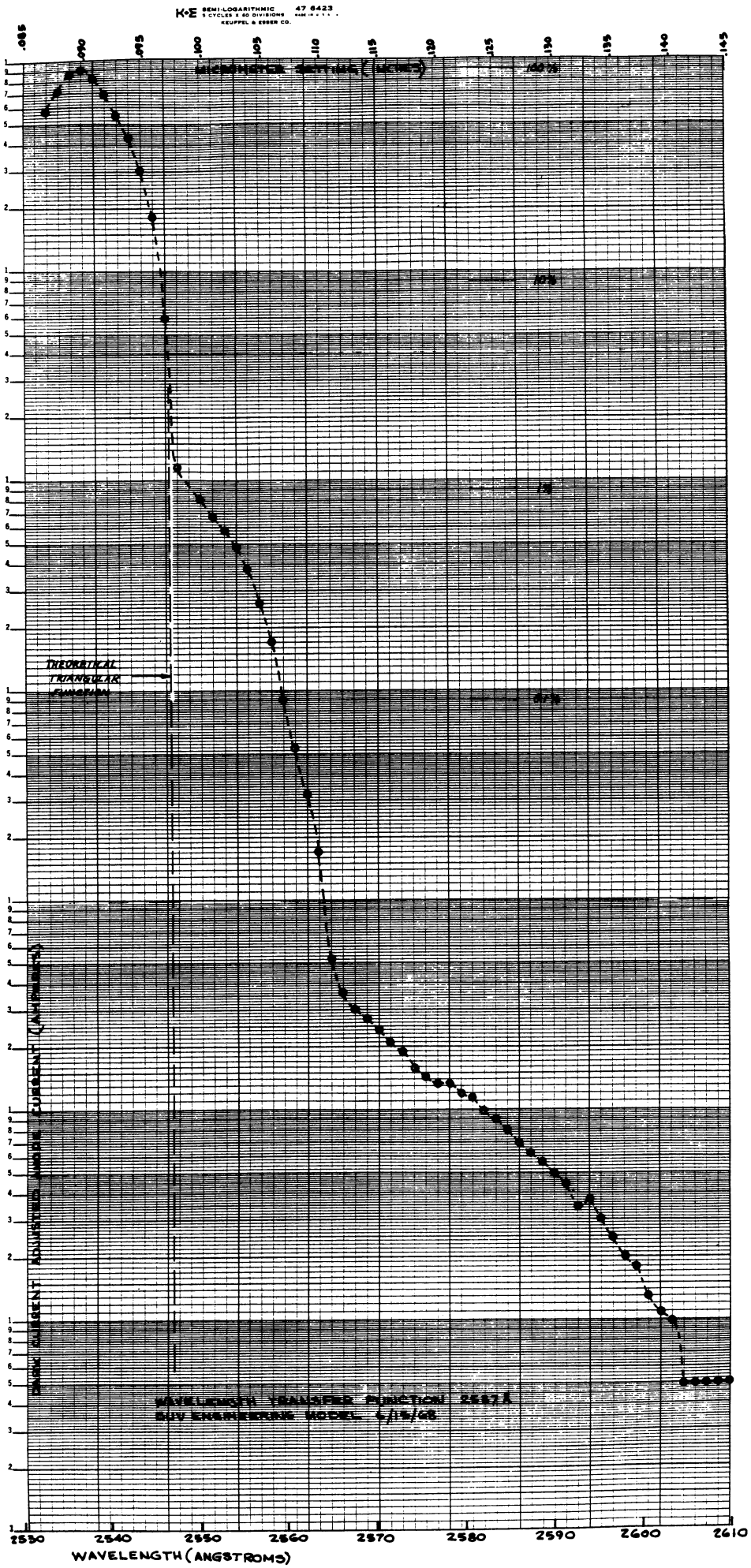

Figure 3-21. Wavelength Transfer Function 2537 Å, Engineering Model

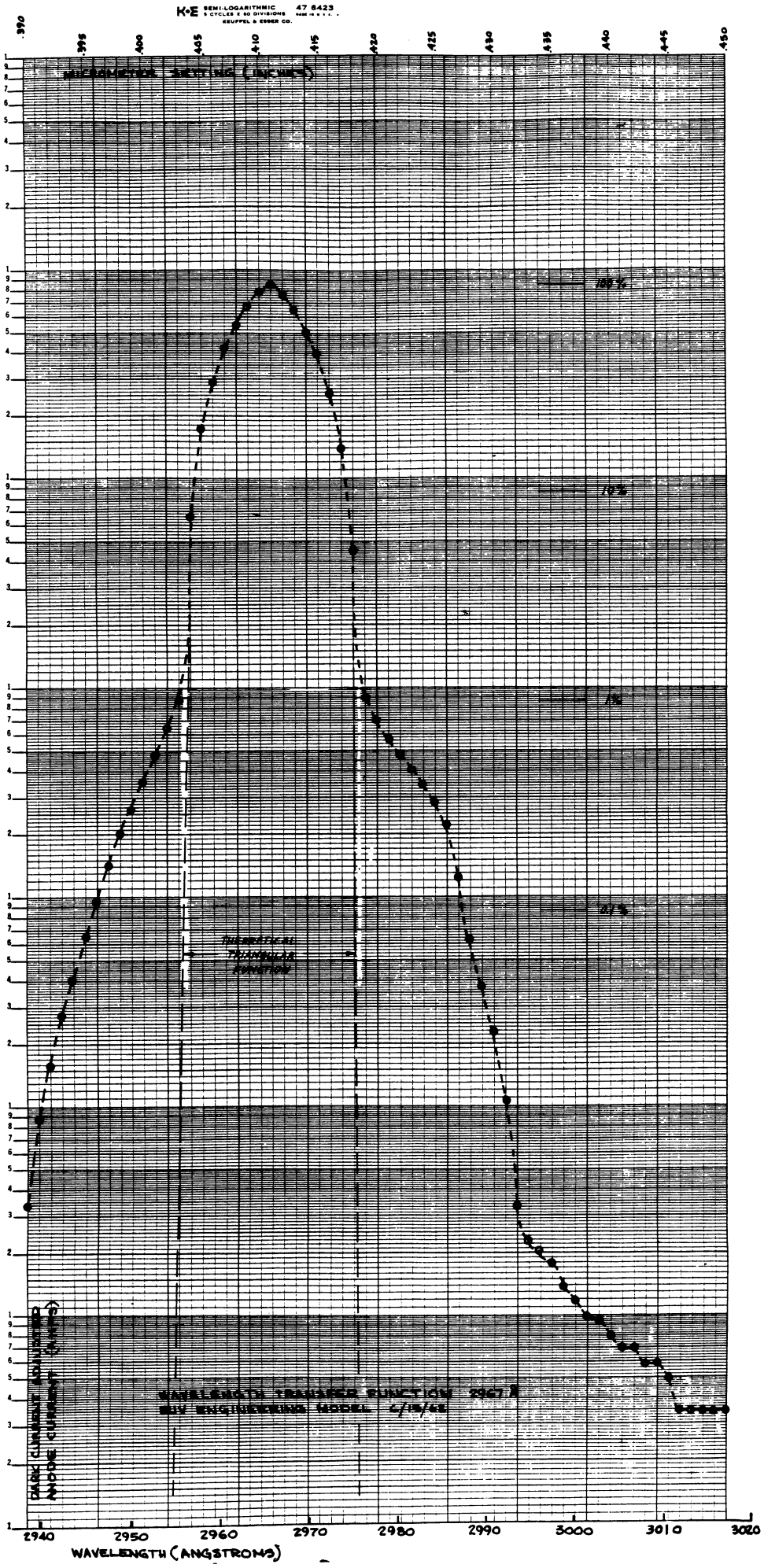

Figure 3-22. Wavelength Transfer Function 2967 Å, Engineering Model

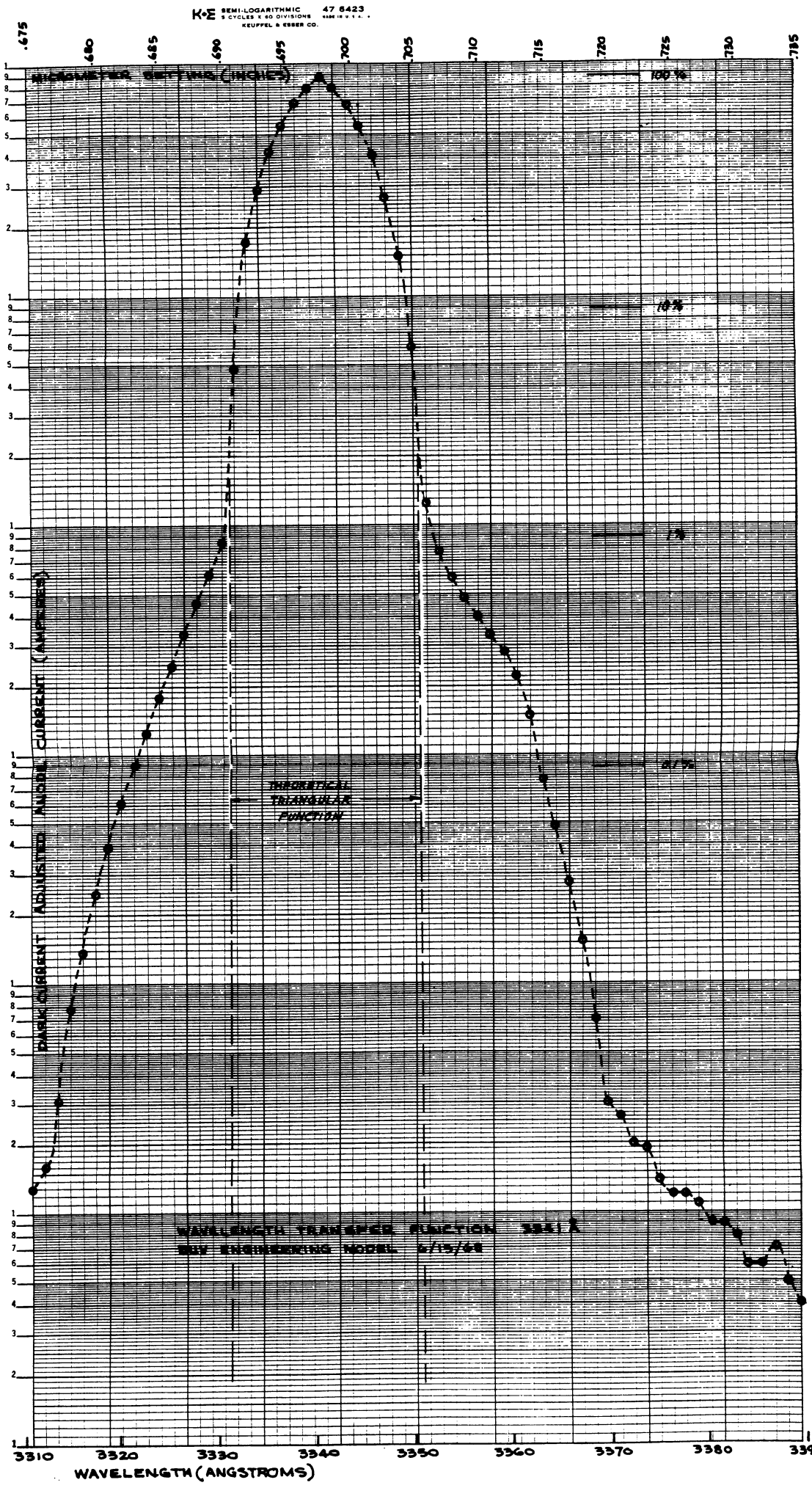

Figure 3-23. Wavelength Transfer Function 3341 Å, Engineering Model

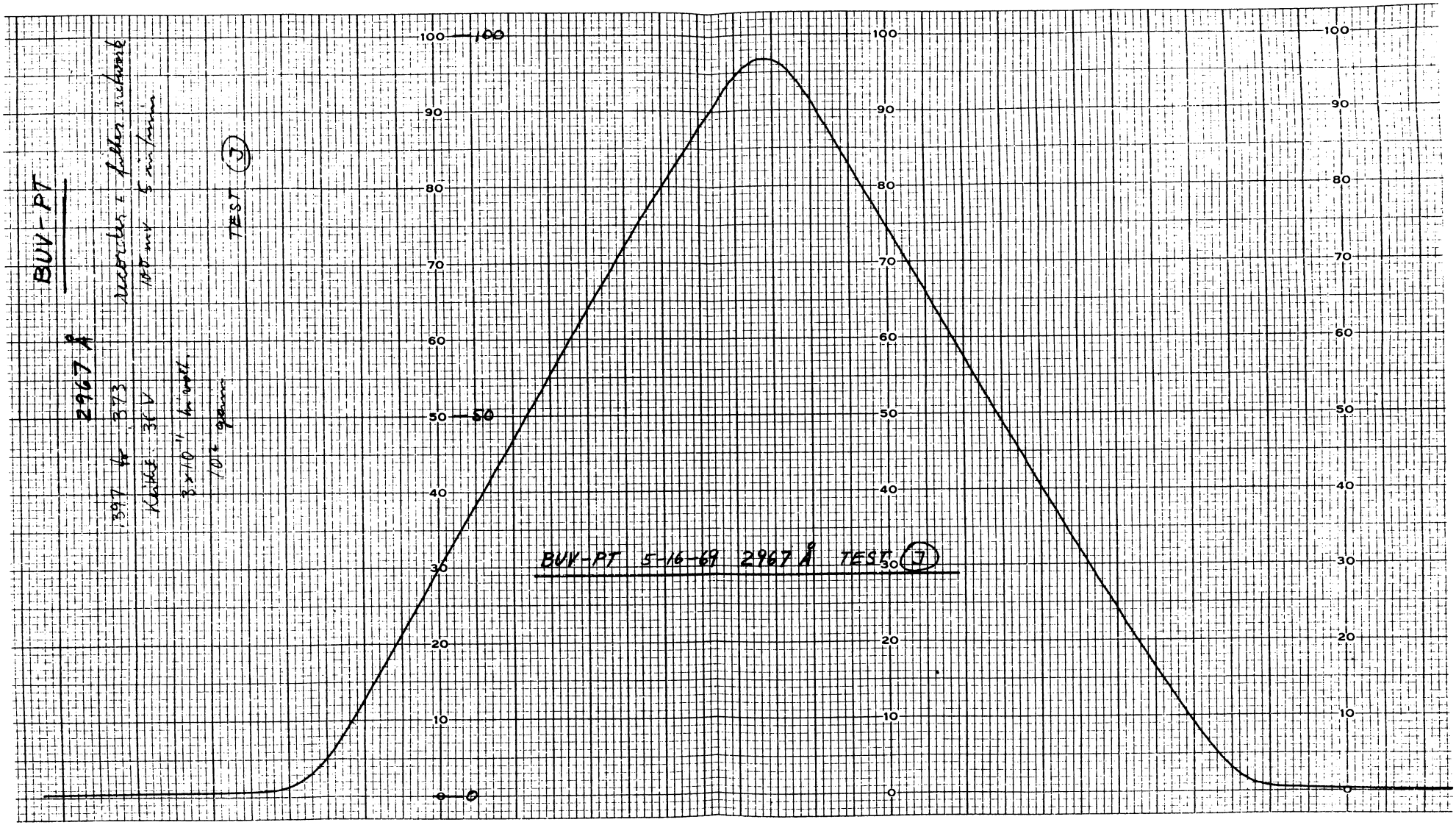

Figure 3-24. Slit Transfer Function 2967Å
Scan I, P103 Instrument

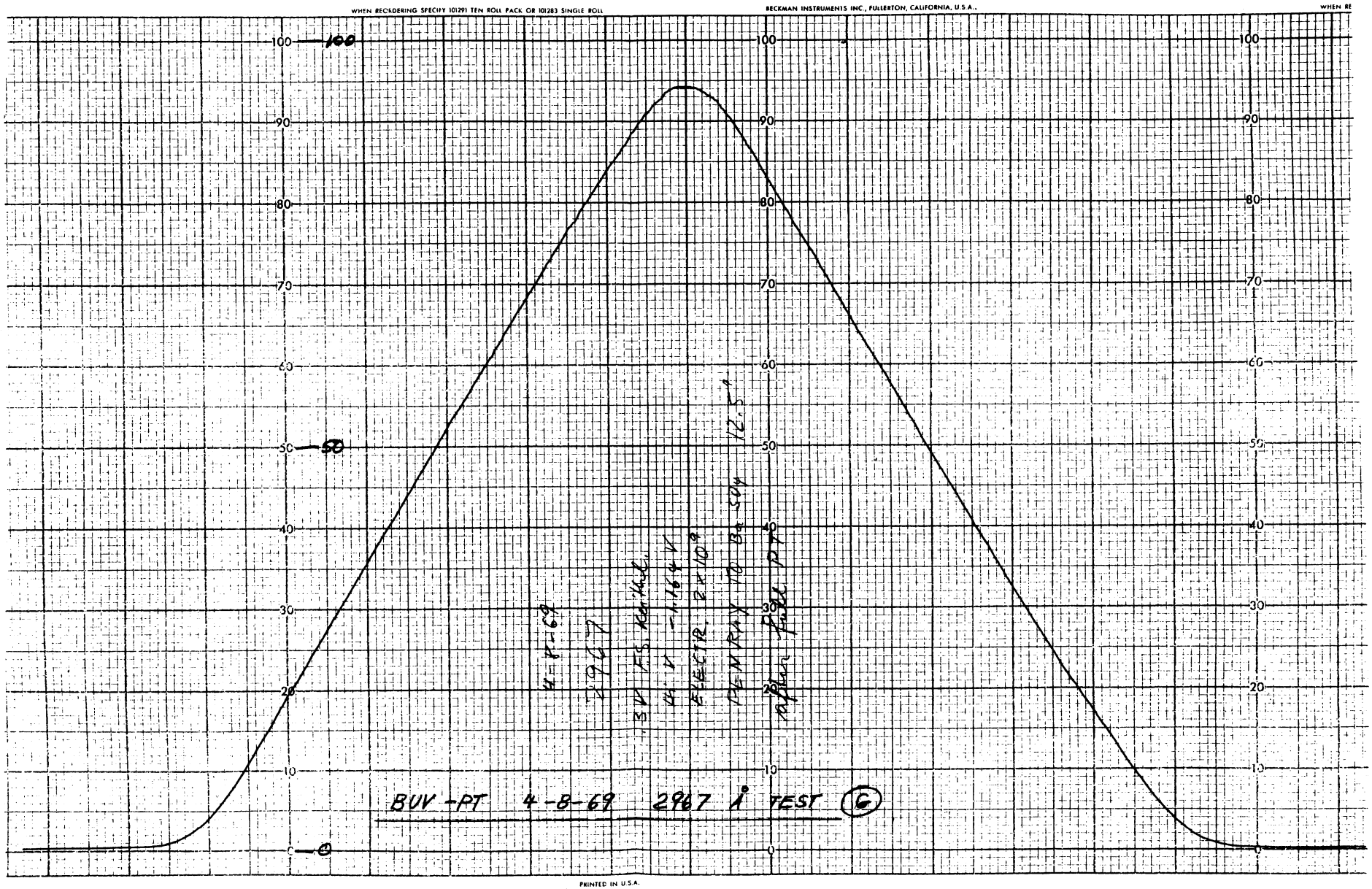

Figure 3-25. Slit Transfer Function 2967 Å
Scan G, P103 Instrument

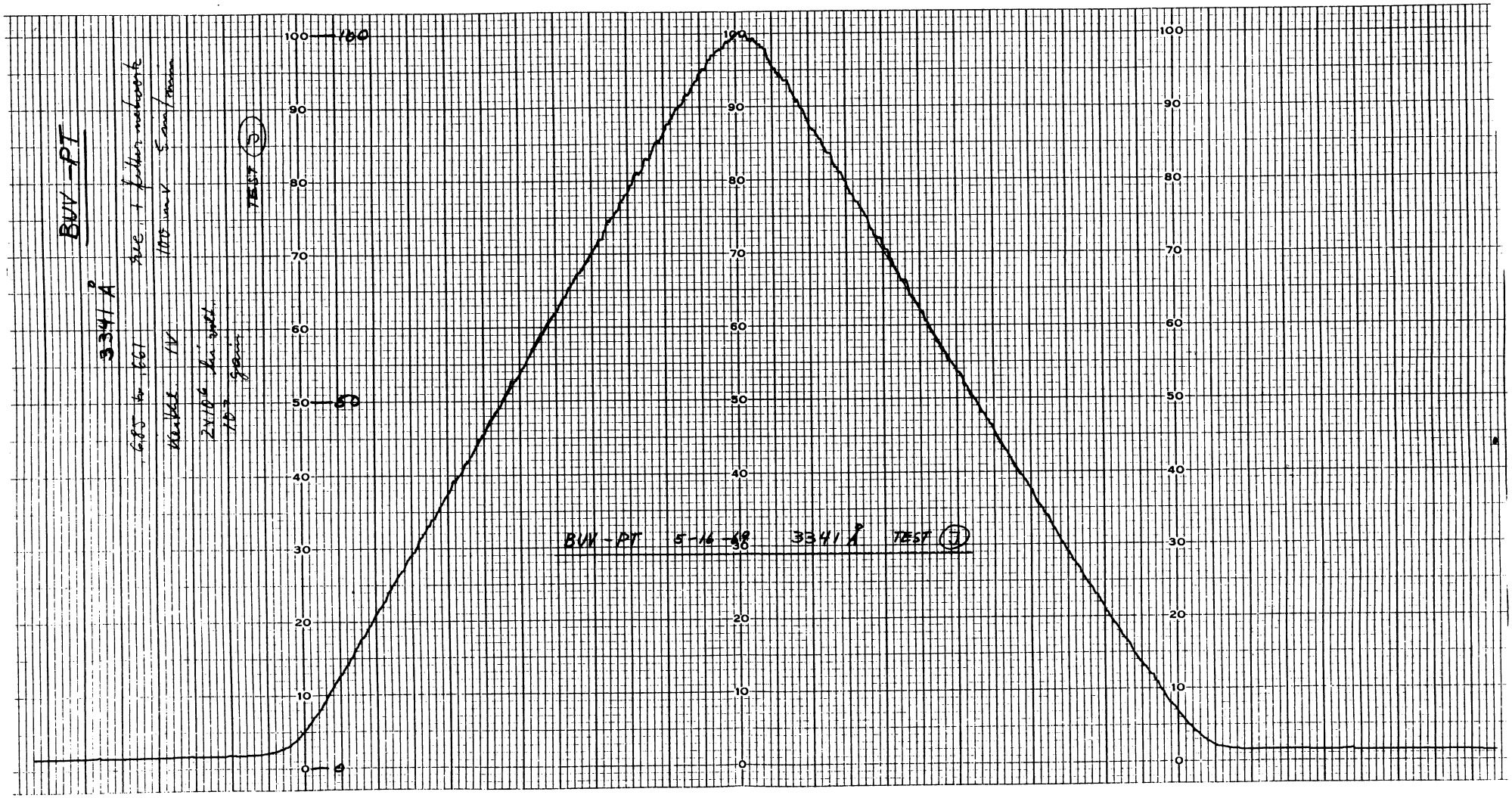

Figure 3-26. Slit Transfer Function 3341 Å
Scan J, P103 Instrument

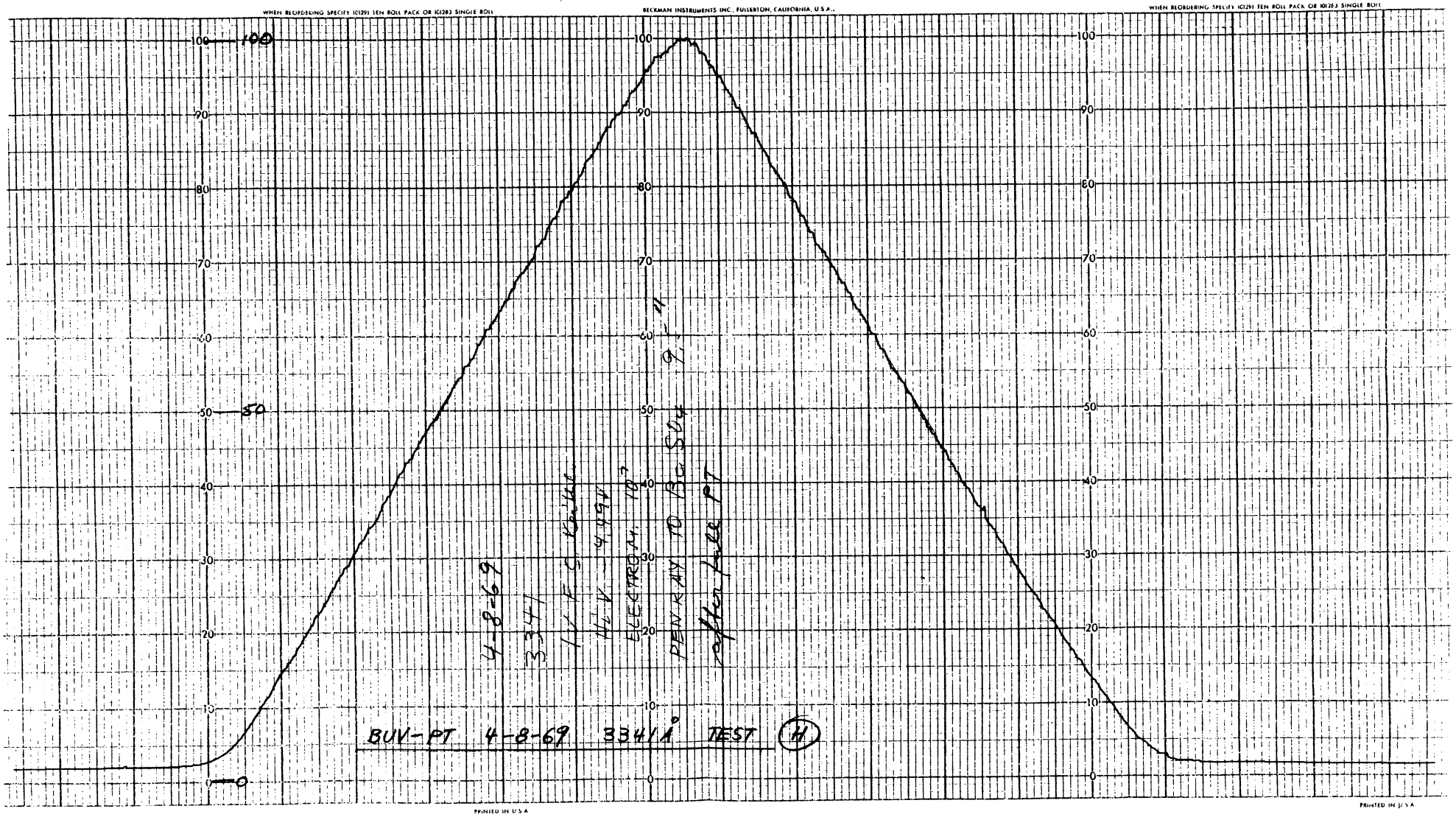

Figure 3-27. Slit Transfer Function 3341 Å
Scan H, P103 Instrument

Wavelength (Angstroms)	2-3-69 After Survey Test	2-22-69 After Full PT Test	3-28-69 After Disassembly for Wavelength Shift Parallel Clean Mirror	4-8-69 After Full PT Test Before TV Test	5-16-69 After All Environmental Tests Before Accept. Tests	
	Germicidal Lamp	Germicidal Lamp	Pen Ray	Filter Netw.Rec. Pen Ray - BTU	Filter Netw.Rec. Pen Ray - BTU	
3341	Å(HBW) 6.7" 10.65	Å(HBW) 6.46" 10.27	6.70 F Å(HBW) 6.66 G 10.60 6.67 H	Å(HBW) 6.36 10.11 6.33	Å(HBW) 6.57 10.44 6.54	MAX CHANGE 5.2%
	Scan B	Scan D	Scan F	Scan H	Scan J	
2967	6.55" 10.41	6.42" 10.20	6.47 B 6.44 C 10.28 6.46 I 6.48 J	6.42 10.20 6.43	6.47 6.45 10.25	MAX CHANGE 2.18%
	Scan A	Scan C	Scan E	Scan G	Scan I	
2537	6.44" 10.22	6.64" 10.56	6.53 E 6.37 K 6.38 L	6.46 6.35	⁄	NOT VALID LINE NOT STABLE
TEST	Ⓔ	Ⓕ	Ⓖ	Ⓗ	Ⓙ	

Table 3-5. Slit Functions--P103 Instrument

3.2.2.8 Instrument Performance During Environmental Testing

The environmental testing of the BUV Instrument poses the potential danger of performance degradation through shifting of optical parts, contamination through outgassing, and others.

A group of tests were performed, utilizing the BTU equipment, before and after each individual environmental test, such as vibration, acceleration, and thermal vacuum.

Tables 3-6, 3-7, and 3-8 are examples of a typical checkout procedure for the F103 Instrument.

The test data was evaluated for performance, degradation, and corrective action where required.

During the thermal vacuum tests, outgassing in the chamber was checked with transmission scans on fused silica windows. Scans were obtained both before and after irradiation exposure.

3.2.3 Field-of-View

The fields-of-view of the BUV Instrument are 0.044 steradian. The fields are matched in size and location so that both the spectrometer and photometer view the same area.

A method for checking the field-of-view is shown in Figure 3-28. The Instrument, with baffles and depolarizer in place, is mounted on the rotary test fixture table as shown in Figure 3-28 (A). A light source (quartz-iodine lamp) is placed on the optical axis OA_M of the monochromator at a distance R such that $R > (\frac{D}{2} \times 10^3)$, where D is the largest dimension of the emitting area of the light source. The Instrument is rotated about the horizontal axis WH and monochromator signal readings and angular position measurements are recorded across the field-of-view.

The complete procedure is repeated for three different wavelength settings of the monochromator. The source is then moved vertically until it lies along

MAY 15 1969

TEST (3)

TABLE 3-6. TYPICAL MONOCHROMATOR CHECKOUT PROCEDURE

BUV - FM MONOCHROMATOR

PMT # 12735

Optical tests performed after every vibration run.

Tests performed:

By: H. REID H. ROEDER

Date: 5-14-69 HR: 15th
5-15-69

The tests listed below were performed to check optical alignment after the following vibration tests:

Before vibration, after elect. integration.

The following tests have to be performed:

(1)	External Hg lines (use pen ray) vs. microm.	5-15-69	Check ✓
(2)	Internal Hg lines vs. micrometer	5-15-69	Check ✓
(3)	Cam steps vs. micrometer	5-15-69	Check ✓
(4)	Slit function (recorder)	5-15-69	Check ✓
5)	Pictures at exit slit		Check
6)	Pictures at interm. slit		Check
7)	Stray Light tests (Q.I. Lamp)		Check
8)	Depolarizer Tests		Check
(9)	Internal phosphor source	5-15-69	Check ✓
(10)	Radiant Sensitivity with Q.I. lamp SEE TAPE	5-14-69	Check ✓
11)	Field of view		Check

HR:yd
2/25/69

MAY 15 1969

3 PAGES

BUV - FM MONO

PMT # 12735

PMT # 12735
2×10^6 fw v.
10^7 elects.
*

TABLE 3-7. TYPICAL MONOCHROMATOR DATA RECORD

Hg LINES Å	BUV-FM ORIGINAL MICROM. SETTING OF: 1-13-67	EXT. Hg LINES (PEN RAY) new	INTERNAL Hg LINES new		BUV-FM ORIGINAL CAM STEPS VS. MICROM. CF: 1-[illegible]-67	NEW CAM STEPS VS. MICROM. new	STRAY LIGHT @ I. 50 AM PMT 2X10⁶ GAIN	INTERNAL PHOSPHOR SOURCE KEITHL. → STEPS	VOLTS
		1)							
3341	.6663	.6647		00	3378 .7093	.7101		.709	.003 *
3131 3125 >	.5036	.5024		01	3312 .6419	.6416		.642	.004 *
	.4202	.4188		02	3175 .536	.5357		.536	.008
2967	.3790	.3779		03	3125 .4475	.4471		.498	.012
	.3476			04	3058 .4464	.4464		.446	.024
	.3235	.3223		05	3019 .4168	.4166		.417	.029
	.2963		too weak	06	2975 .3837	.3835		.384	.031
	.2723			07	2922 .3437	.3434		.344	.027
	.2561			08	2876 .3[illegible]	.3090		.309	.016
	.2186	.2173		09	2830 .2741	.2747		.275	.007
	.1786			10	2735 .2041	.2039		.204	.003 *
	.1444	.1430		11	2555 .0713	.0710		.071	.003 *
2537	.0587	.0575		18				ii	
				19	2522 .05	.0497			
				20	2527 .6536	.0535			
				21	2532 .0574	.0571			
			.0601	22	2537 .061	.0608			
				23	2542 .0646	.0644			
				24	2547 .0683	.0681			
				25	2552 .0118	.0716			

MAY 1 5 1969

TABLE 3-8. TYPICAL PHOTOMETER CHECKOUT PROCEDURE

BUV - FM PHOTOMETER

PMT # 12739

Optical tests performed after every vibration run.

Tests performed:

By: H. REID

Date: 5-14-69 HR: 15TH

The tests listed below were performed to check optical alignment after the following vibration tests:

_____

_____

The following tests have to be performed:

1) Radiant sensitivity with Q.I. lamp RTU TYPE 5-14-69 Check ✓

2) Internal phosphor source _____ Check

3) Field of view _____ Check

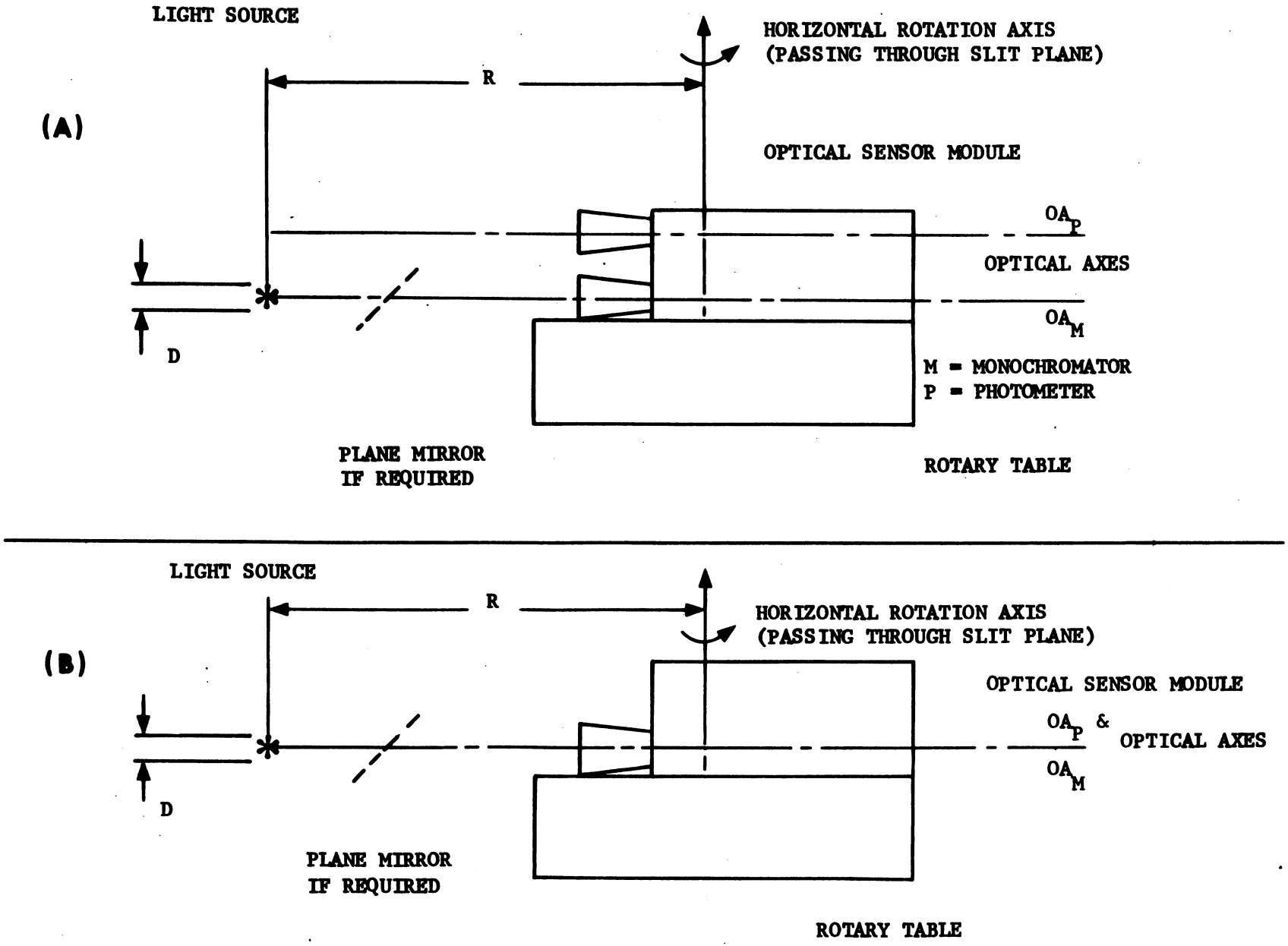

Figure 3-28. Field-of-View, Test Set-up

OA_P and the entire procedure is again repeated and the output signals of the photometer are recorded. The Sensor Module is then mounted on the rotary table as shown in Figure 3-28 (B), and all of the foregoing procedures repeated.

Figures 3-29 and 3-30 depict the match obtained for the P103 and F104 Instruments. To correct for mismatch, the aperture in the photometer usually is corrected, enlarged, or made smaller, since the grating defines the field-of-view for the spectrometer. The baffles do not define the field-of-view. They have approximately 0.050 clearance on each side.

For the final alignment of field-of-view aperture in the photometer, tests were conducted to scan through the center and through the two sides of the opening, as shown in Figures 3-31 and 3-32. The depicted square waves, Figures 3-33 through 3-41, show the final opening of the aperture with respect to the monochromator field-of-view. While the fields-of-view of the F104 Instrument are matched to ±3 percent, the fields-of-view of the P103 Instrument are not as well aligned. The square waves depicting the field-of-view in the F104 Instrument are taken through the center of the aperture opening in the photometer. The measurements taken at the sides of the aperture openings show that there is no significant difference between these and the ones taken through the center of the apertures.

3.2.4 Stray Light

The BUV Instrument is designed to have less than one percent of stray light throughout the wavelength region 2500 to 3400 Å. A measurement of stray light is the ratio of signal-to-scattered-light:

$$R = \frac{\text{anode current at 2555 Å - dark current}}{\text{anode current at 3398 Å - dark current}}$$

Two methods are used to obtain this ratio. For both methods, the Instrument is installed in the test fixture as shown in Figure 3-42. The wavelength is varied by using the micrometer screw.

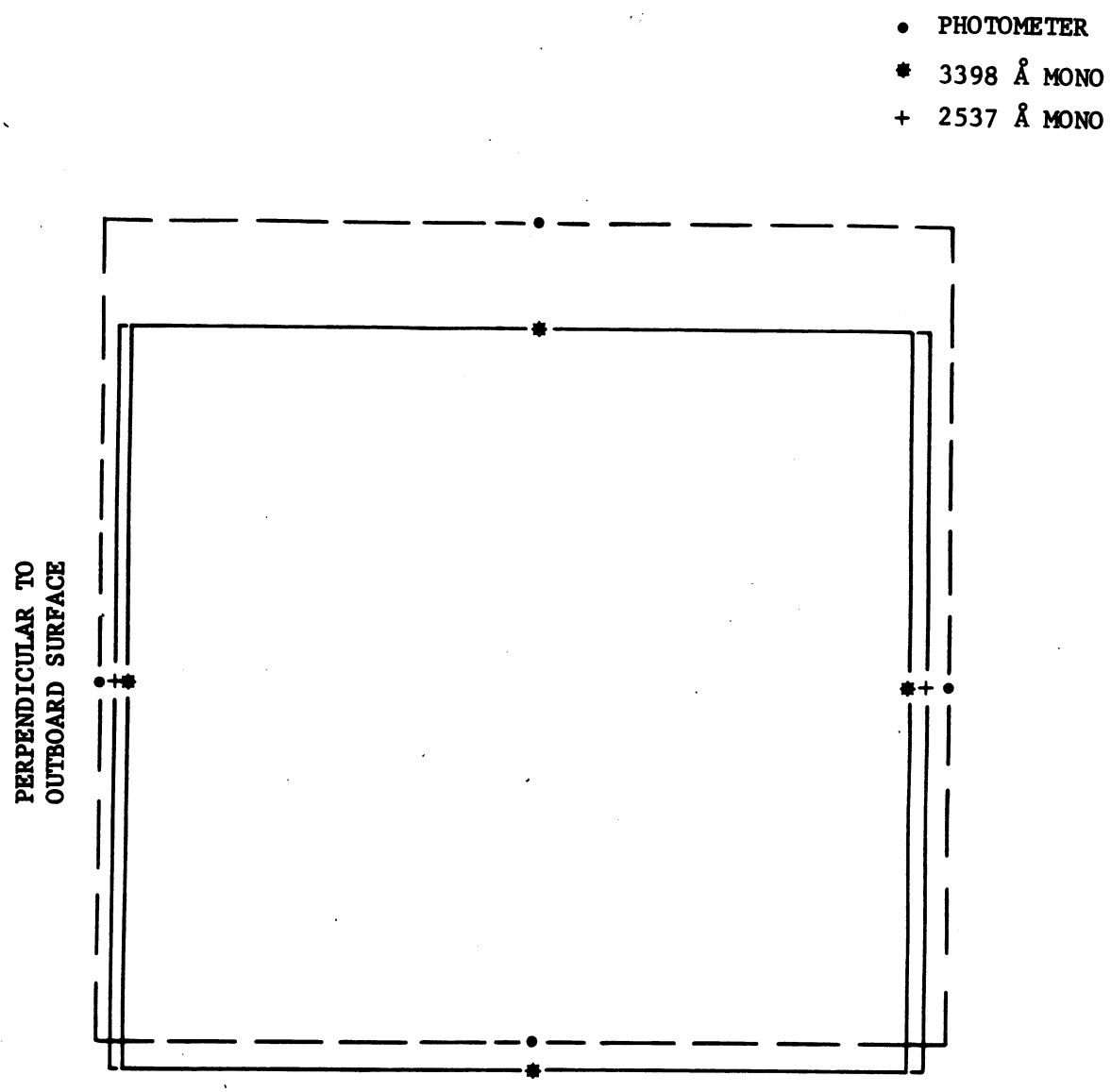

Figure 3-29. Field-of-View (P103 Instrument)

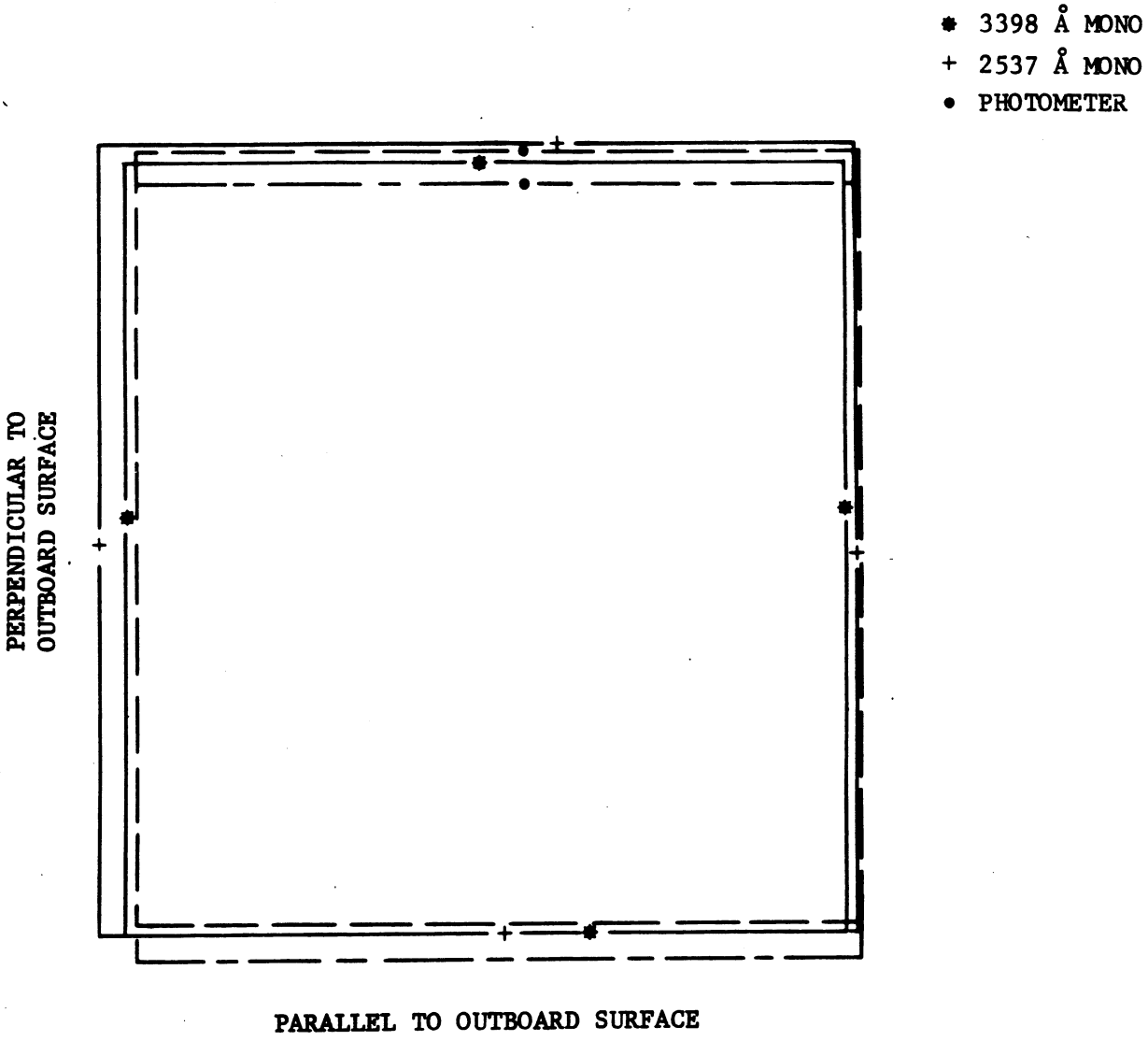

Figure 3-30. Field-of-View (F104 Instrument)

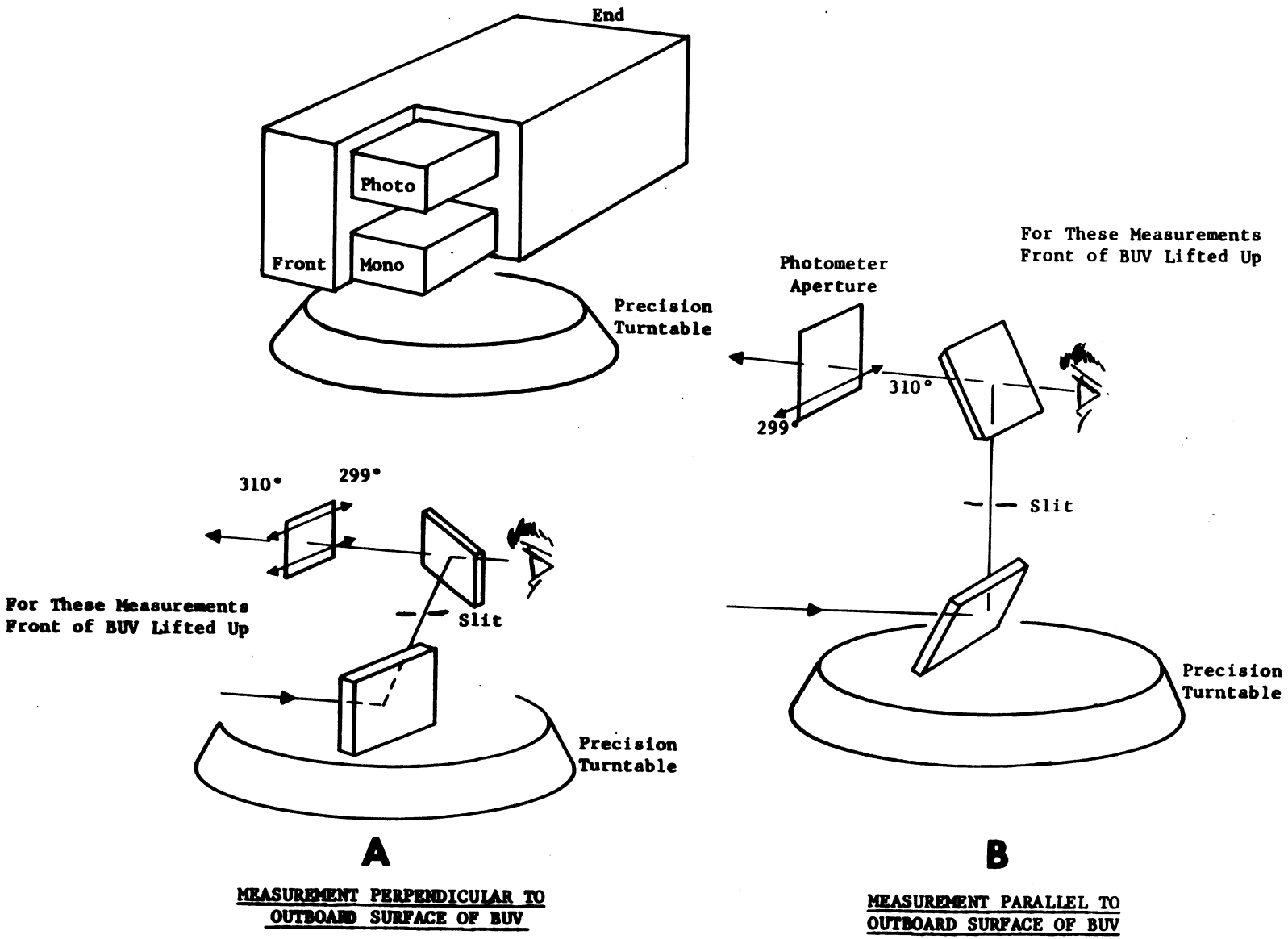

Figure 3-31. Orientation of BUV for Field-of-View Measurements Perpendicular and Parallel to Outboard Surface of BUV

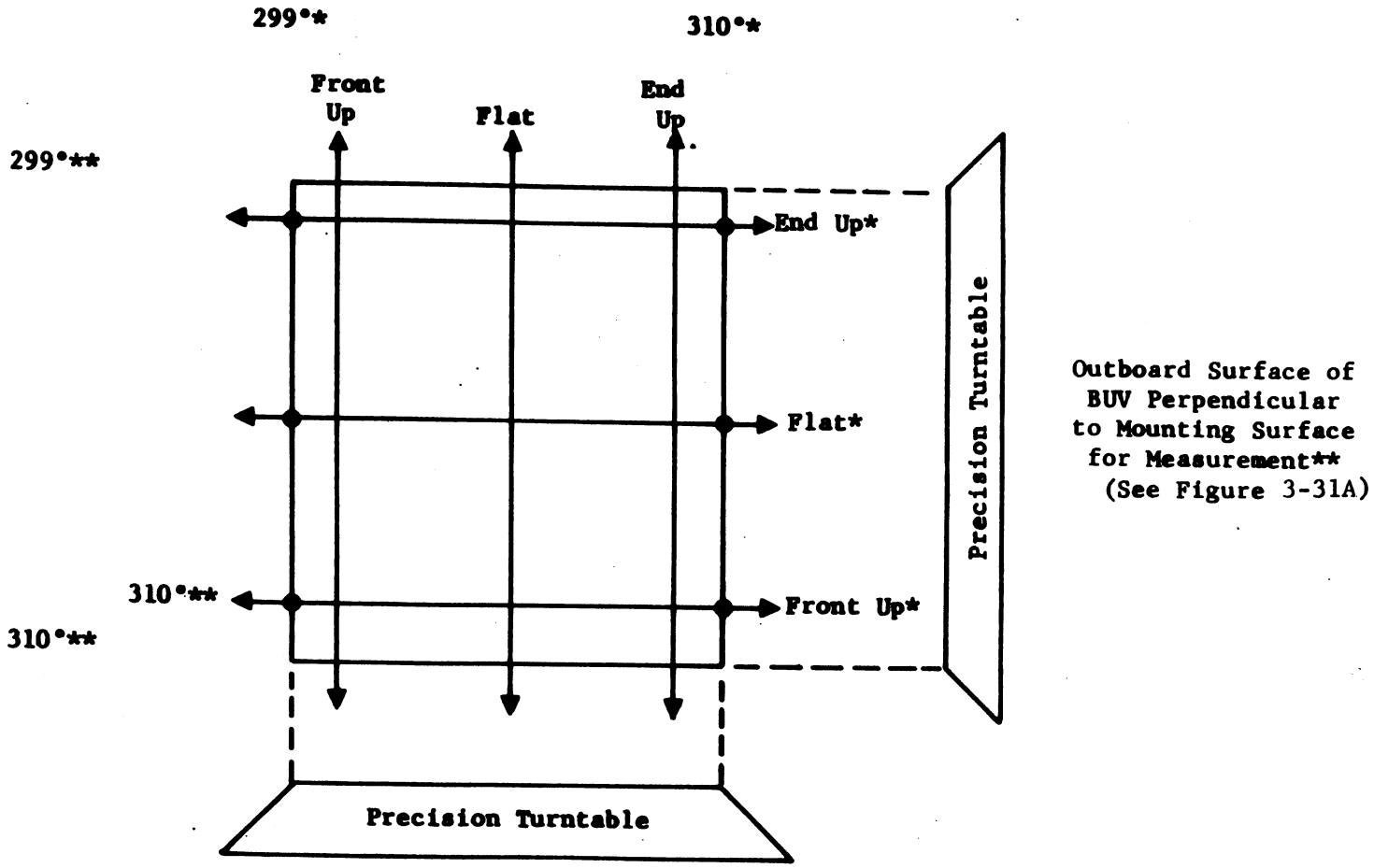

Figure 3-32. Traversal of Photometer Aperture for Field-of-View Measurements with BUV Outboard Surface Perpendicular and Parallel to Mounting Surface

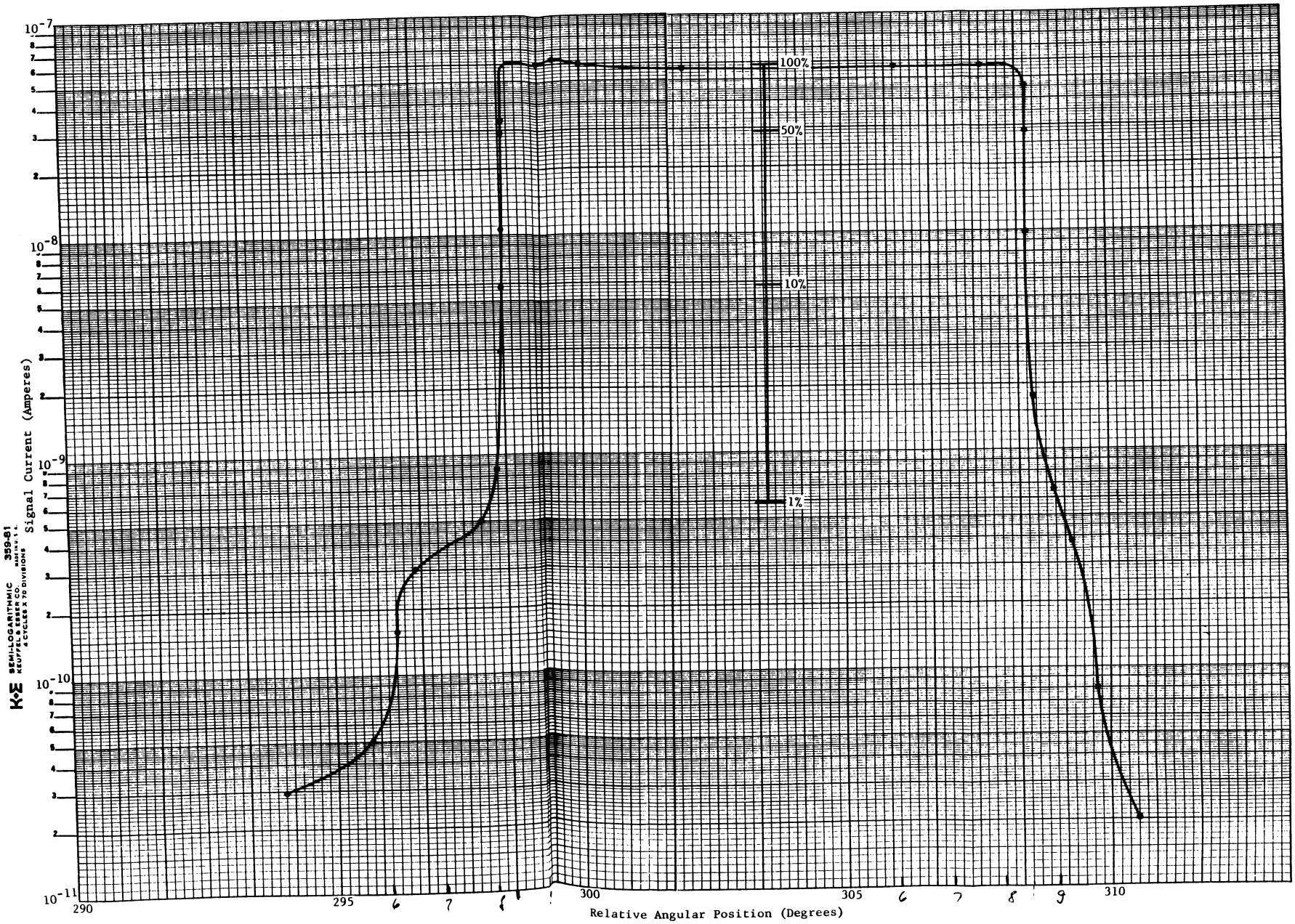

Figure 3-33. Monochromator Field-of-View at 3398 Å - Parallel to Outboard Surface (F104 Instrument)

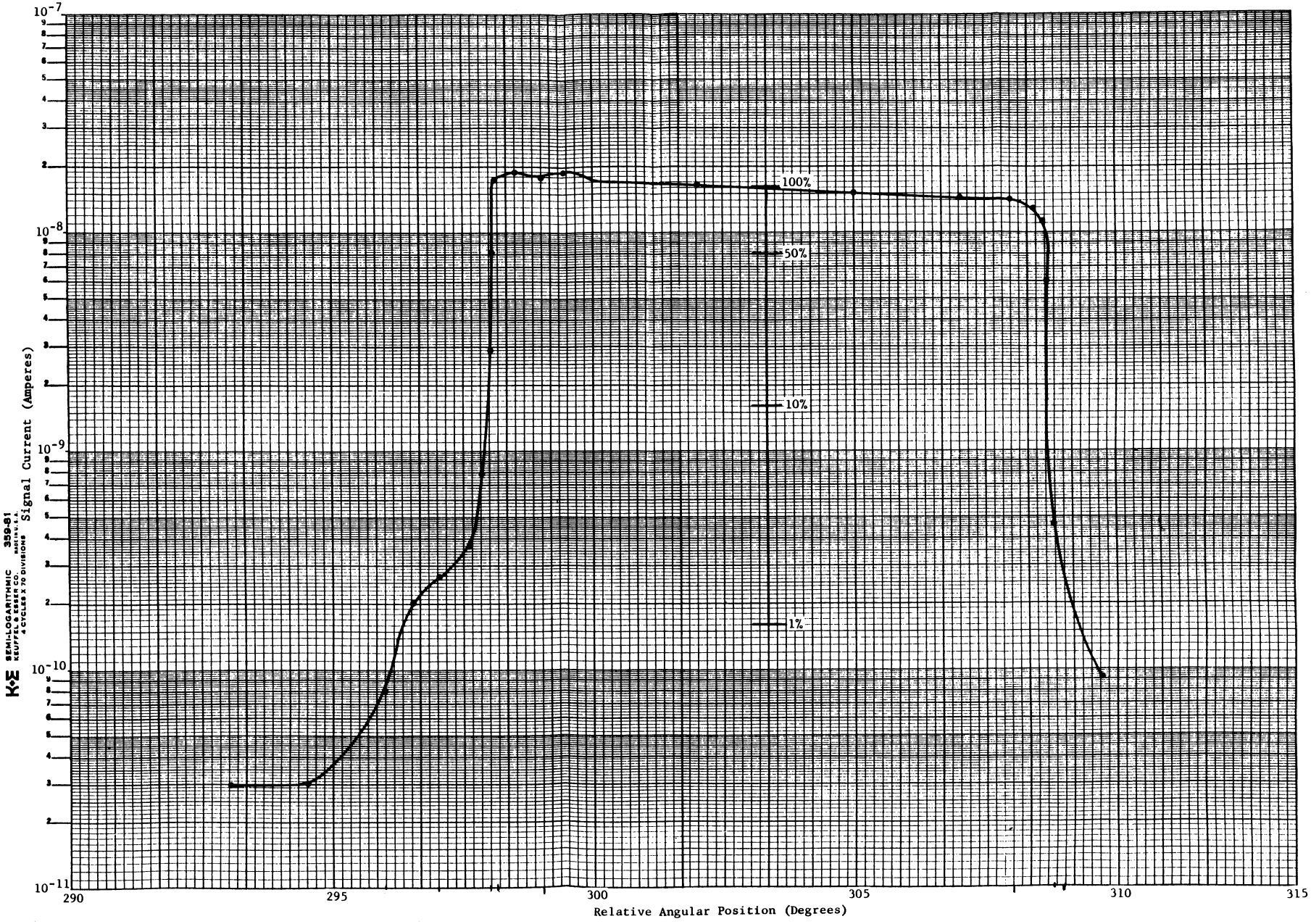

Figure 3-34. Monochromator Field-of-View at 2537 Å - Parallel to Outboard Surface (F104 Instrument)

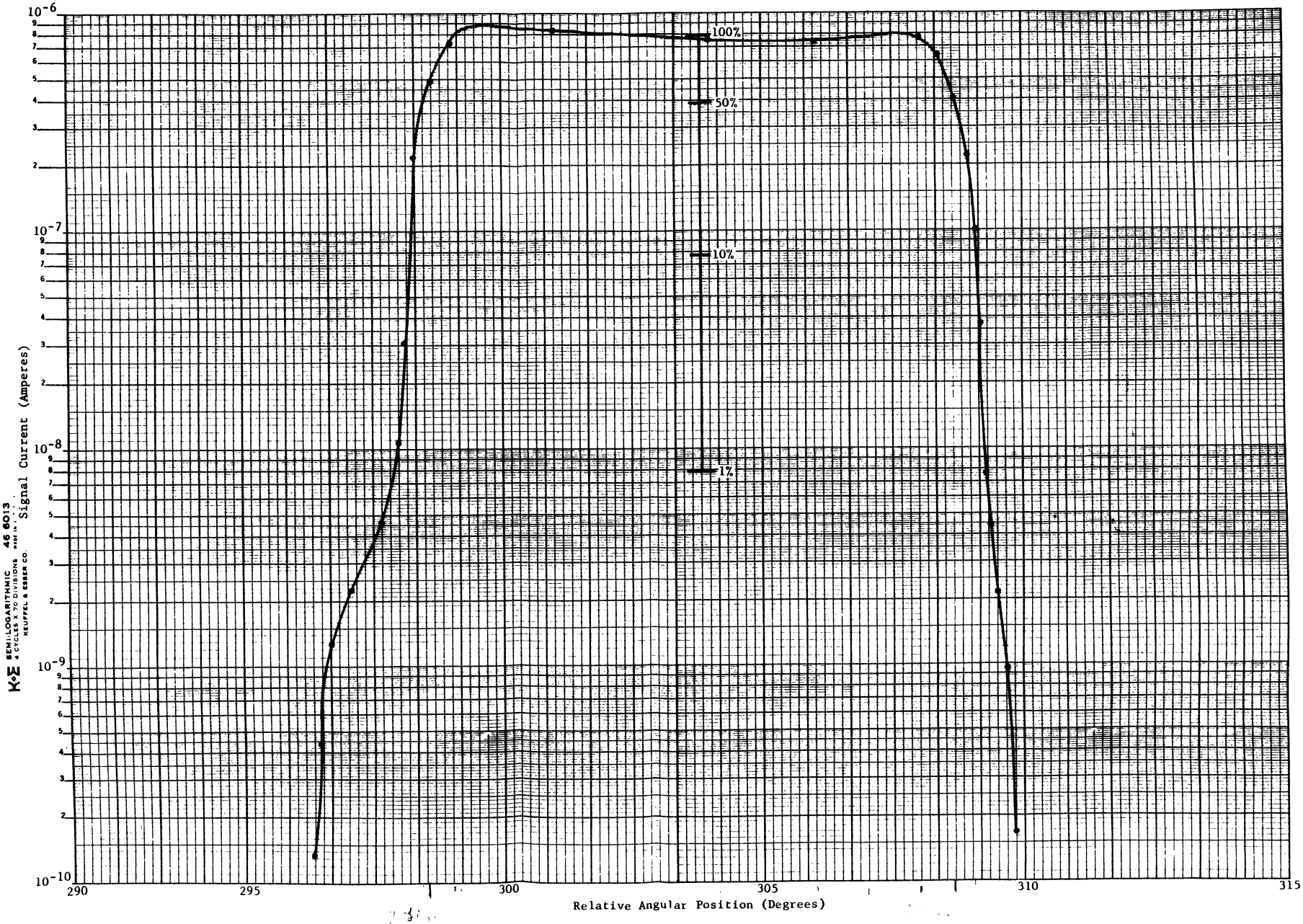

Figure 3-35. Photometer Field-of-View Parallel to Outboard Surface (F104 Instrument)

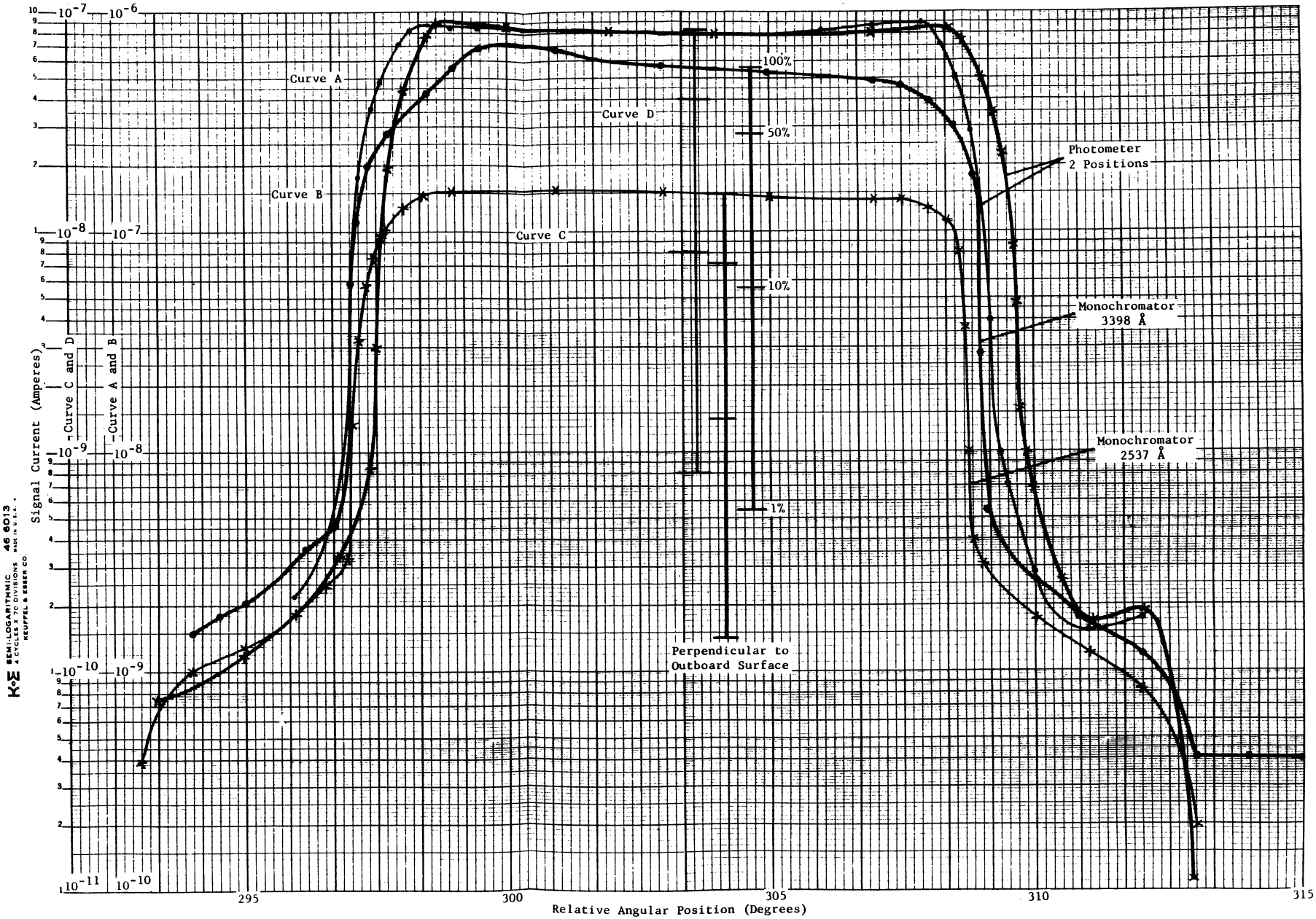

Figure 3-36. Field-of-View - Perpendicular to Outboard Surface (F104 Instrument)

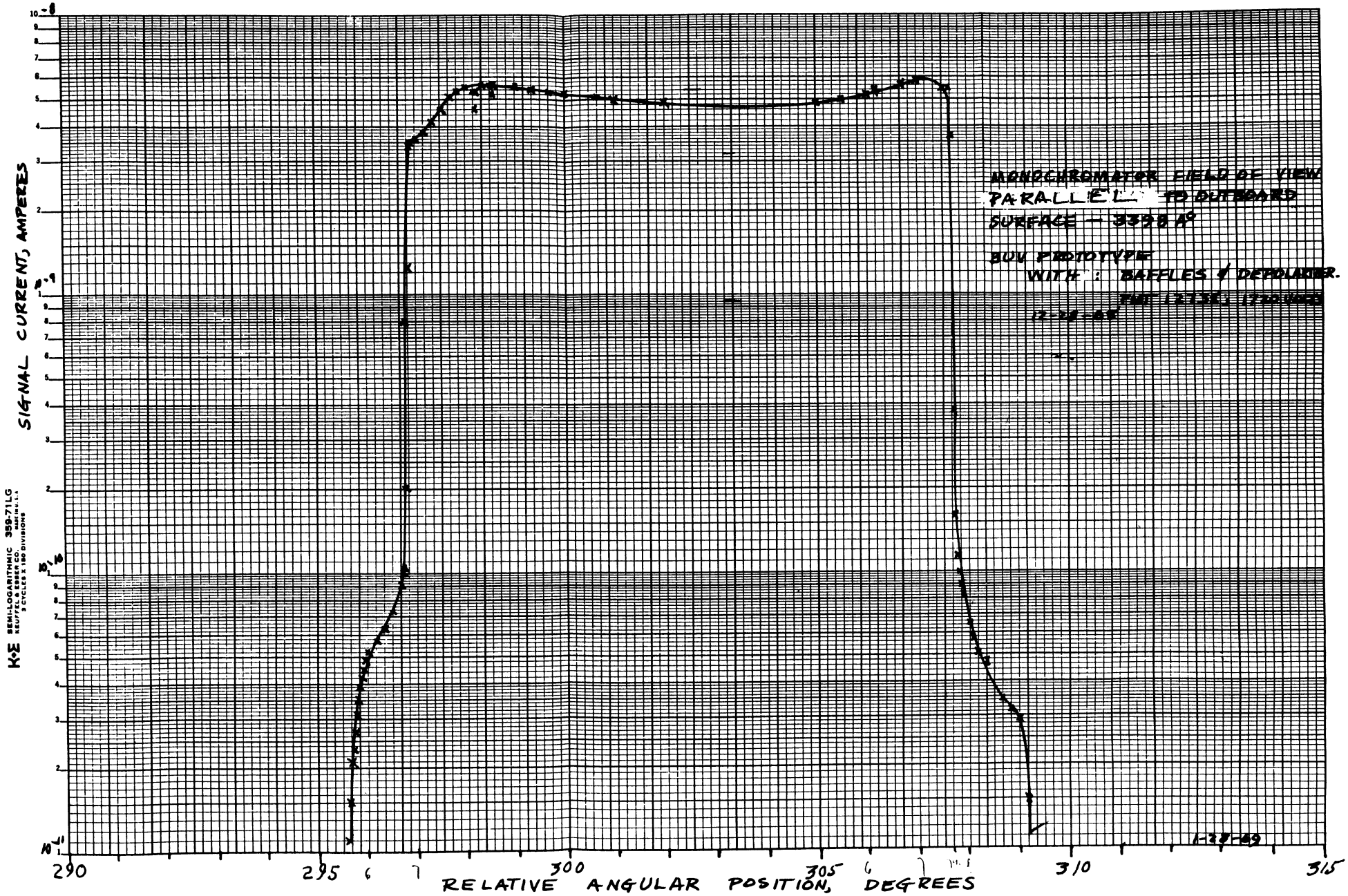

Figure 3-37. Monochromator Field-of-View at 3398 Å - Parallel to Outboard Surface (P103 Instrument)

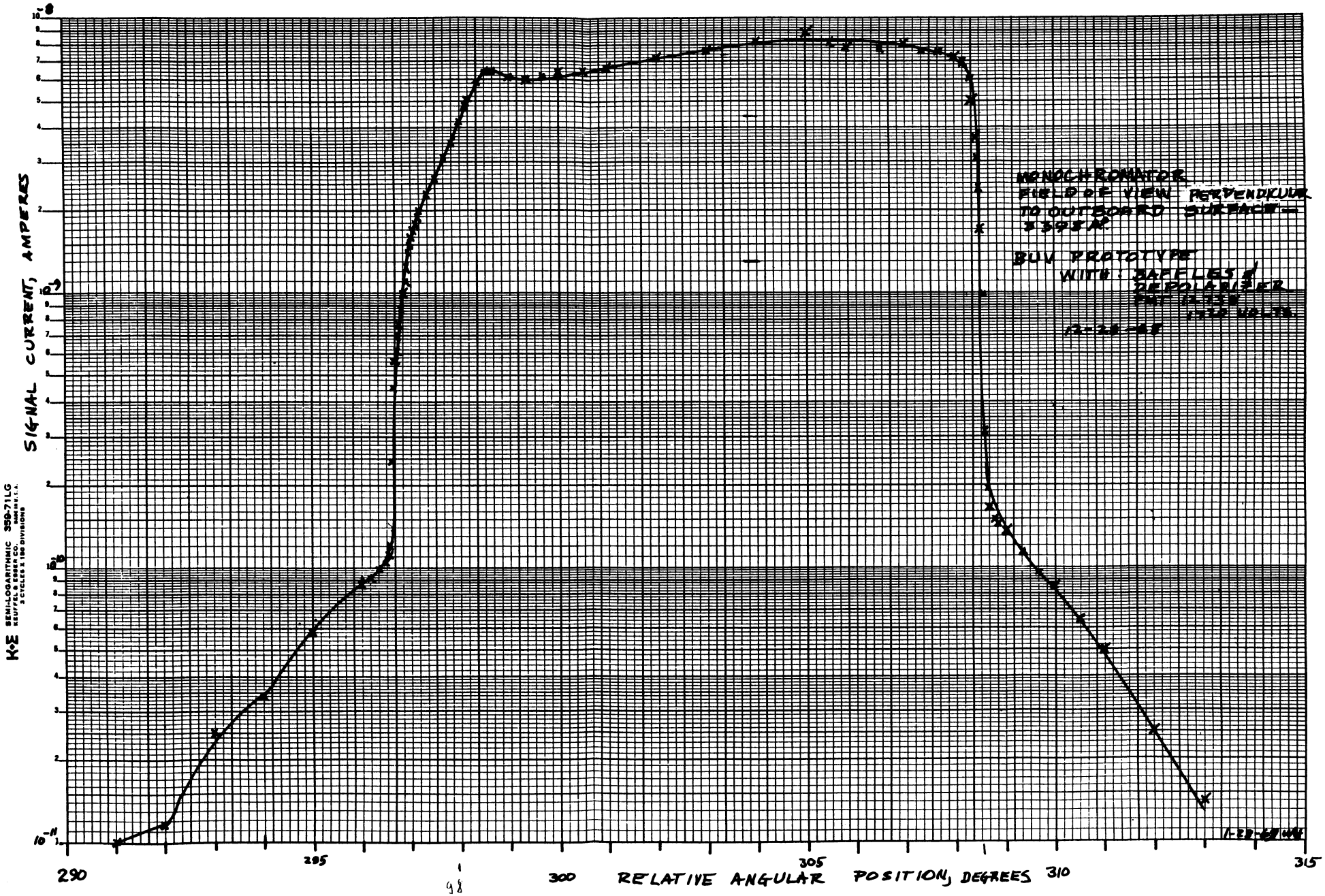

Figure 3-38. Monochromator Field-of-View at 3398 Å - Perpendicular to Outboard Surface (P103 Instrument)

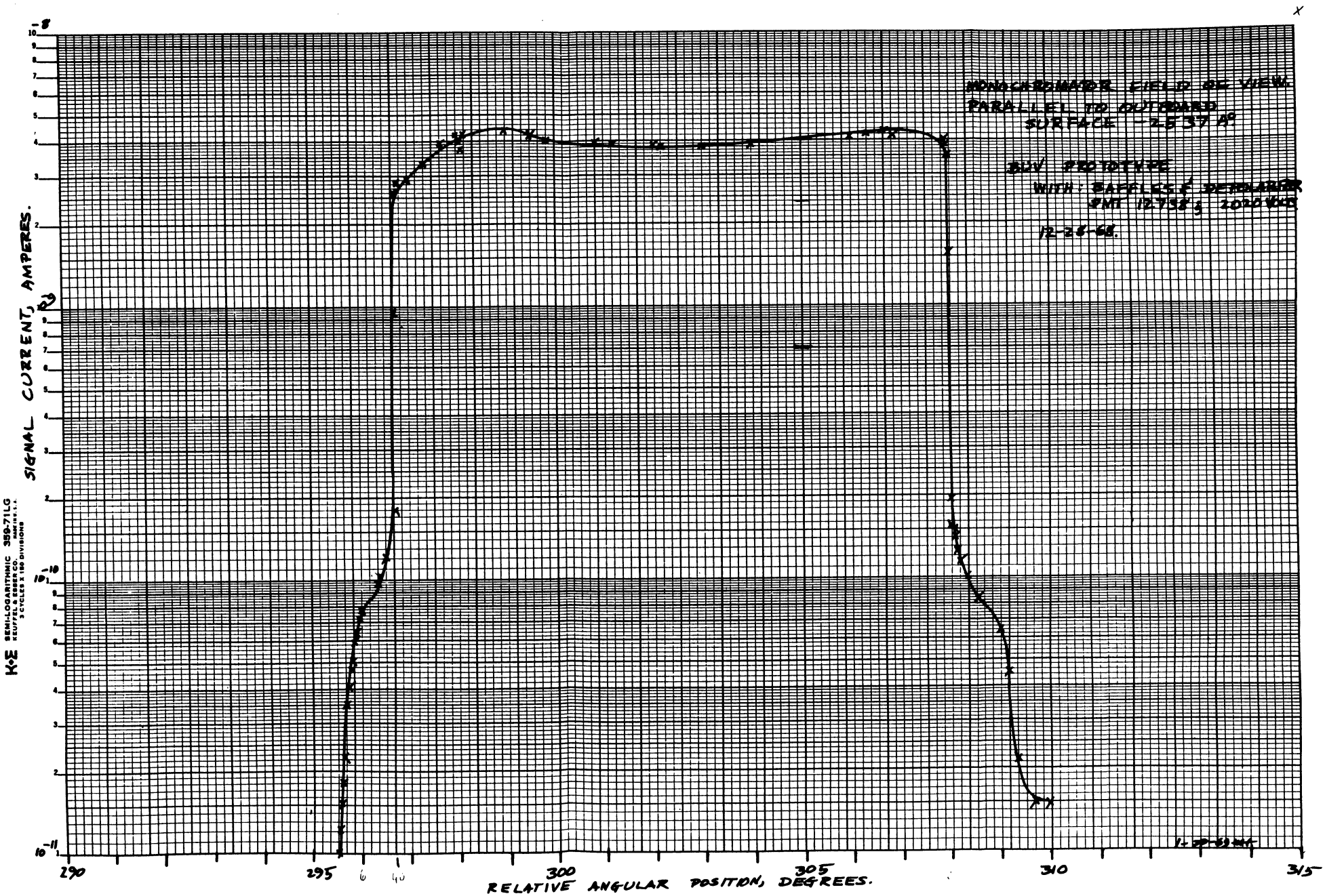

Figure 3-39. Monochromator Field-of-View at 2537 Å - Parallel to Outboard Surface (P103 Instrument)

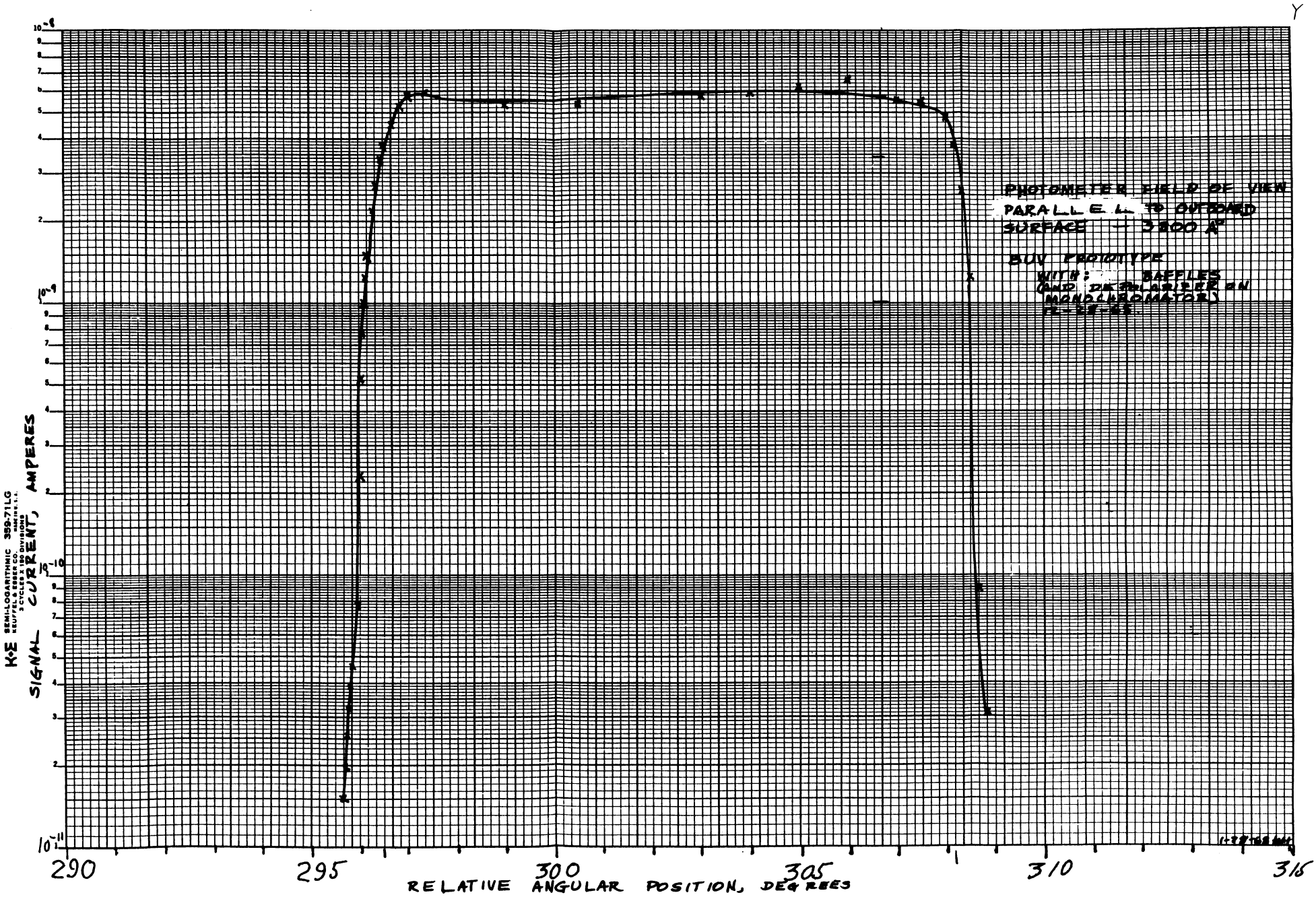

Figure 3-40. Photometer Field-of-View at 3800 Å - Parallel to Outboard Surface (P103 Instrument)

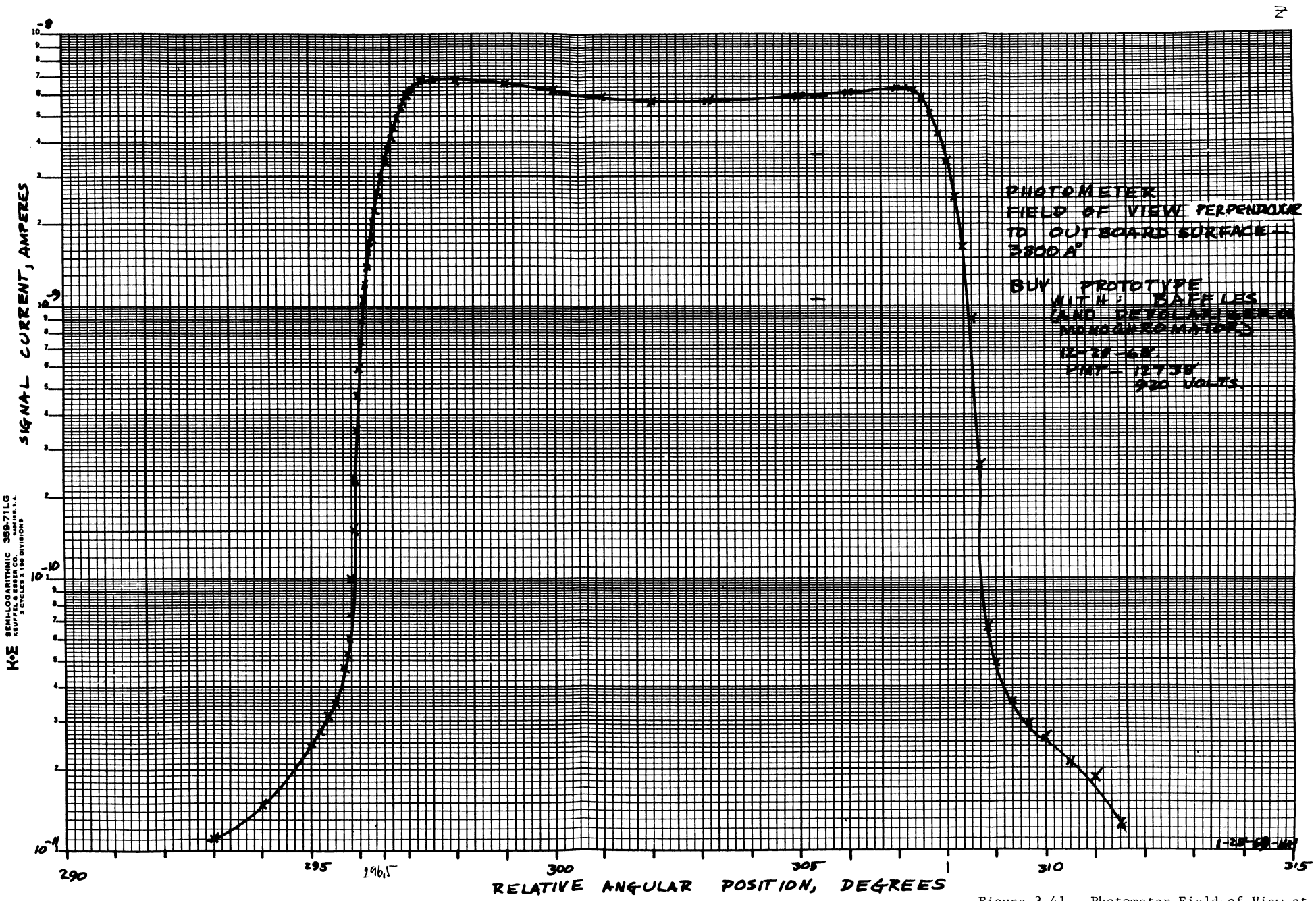

Figure 3-41. Photometer Field-of-View at 3800 Å - Perpendicular to Outboard Surface (P103 Instrument)

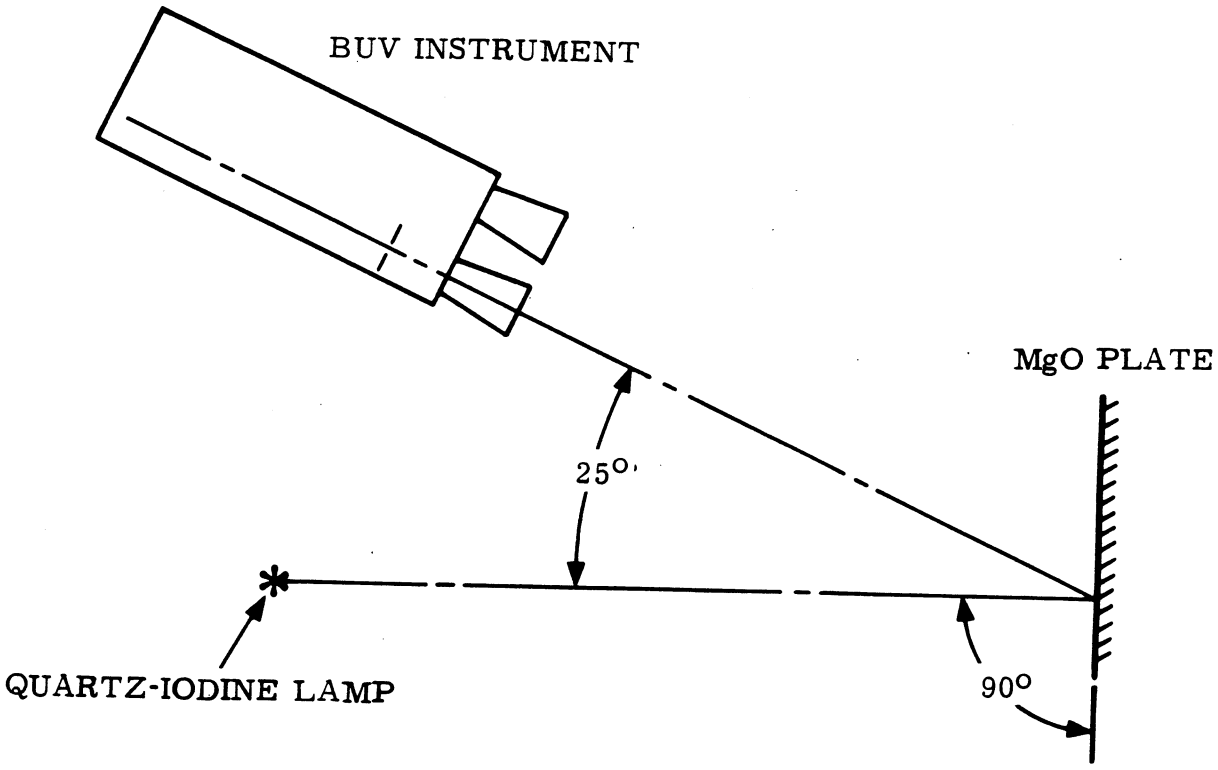

Figure 3-42. BUV Test Fixture

For the first method, the Instrument is transported outside during clear daylight hours. The sun is used as the light source. The fixture is positioned so that direct sunlight impinges perpendicularly on the MgO diffuser plate. The grating arm is set to 3398 Å and the dynode voltage is adjusted so that the anode current measures about 0.9 μA. The arm is then positioned to each wavelength step and the current recorded. The shutters are closed next, to measure the dark current. The BUV Instrument is then removed from the test fixture and aimed directly toward the zenith sky (not the sun) and the measurements again recorded.

In the second method, a 1000 W quartz-iodine lamp is employed as the excitation light source. The setup is identical to that shown in Figure 3-42. Again, the dynode voltage is adjusted for an anode current of approximately 0.9 μA at 3398 Å. A lucite plate is then inserted directly in front of the baffle and the anode current measured for the wavelength steps.

The stray light in the photometer is measured in a similar fashion. With the Instrument viewing the MgO plate, the photomultiplier current is measured with a Corning 3-69 filter in front of the baffle. The filter is then removed and measurement is repeated.

The following graphs show the results obtained with P103 and F104:

Figure 3-43	P103 Instrument	MgO Plate
Figure 3-44	P103 Instrument	Zenith Sky
Figure 3-45	F104 Instrument	MgO Plate
Figure 3-46	F104 Instrument	Zenith Sky

The calculated ratios for the different measurements are as follows:

	MgO Plate	Zenith Sky	Photometer
P103 Instrument	2.82×10^{-6}	1.2×10^{-6}	0.54% (3-69 Filter)
F104 Instrument	1.17×10^{-5}	1.11×10^{-6}	0.32% (3-69 Filter)

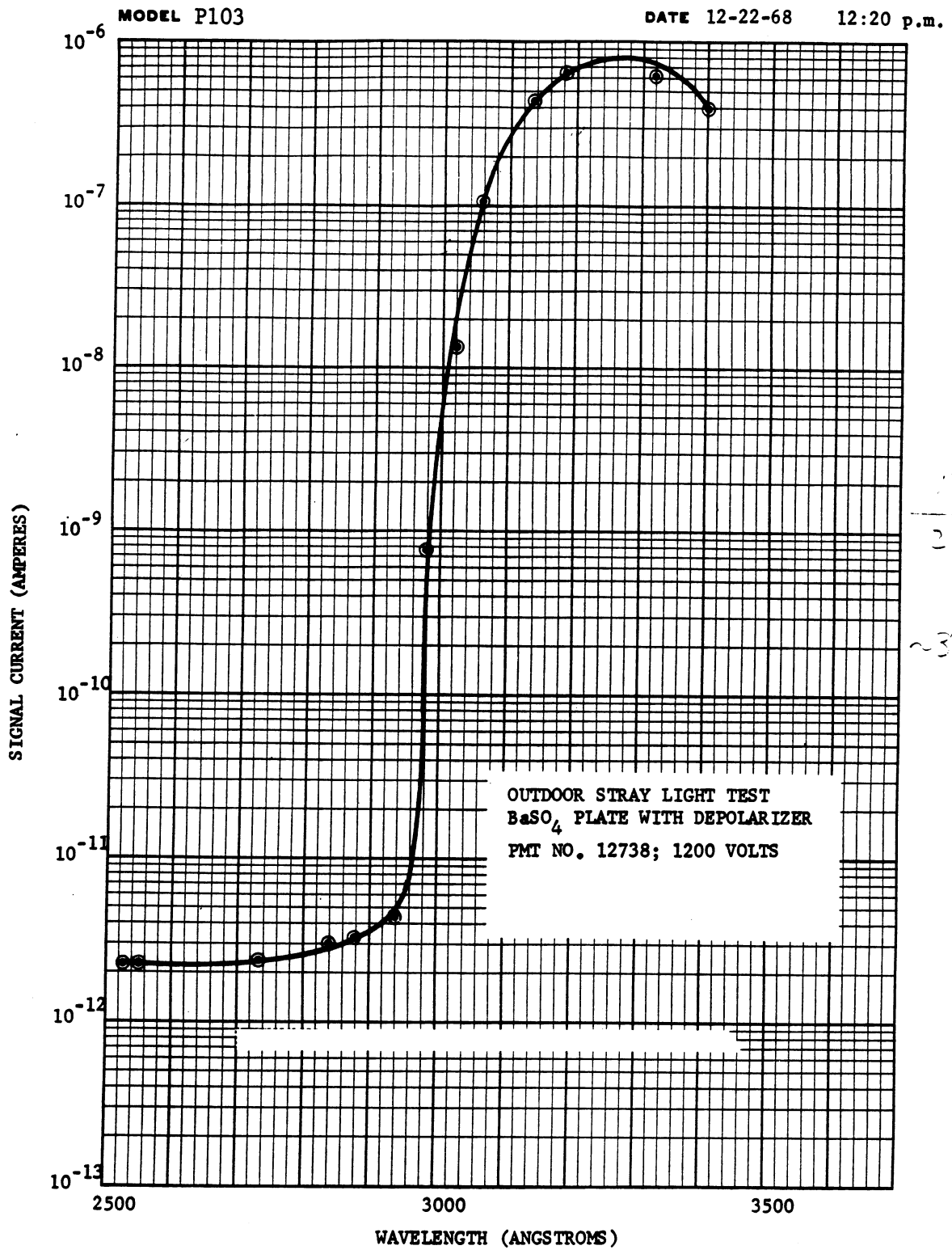

Figure 3-43. P103 Instrument - MgO Plate

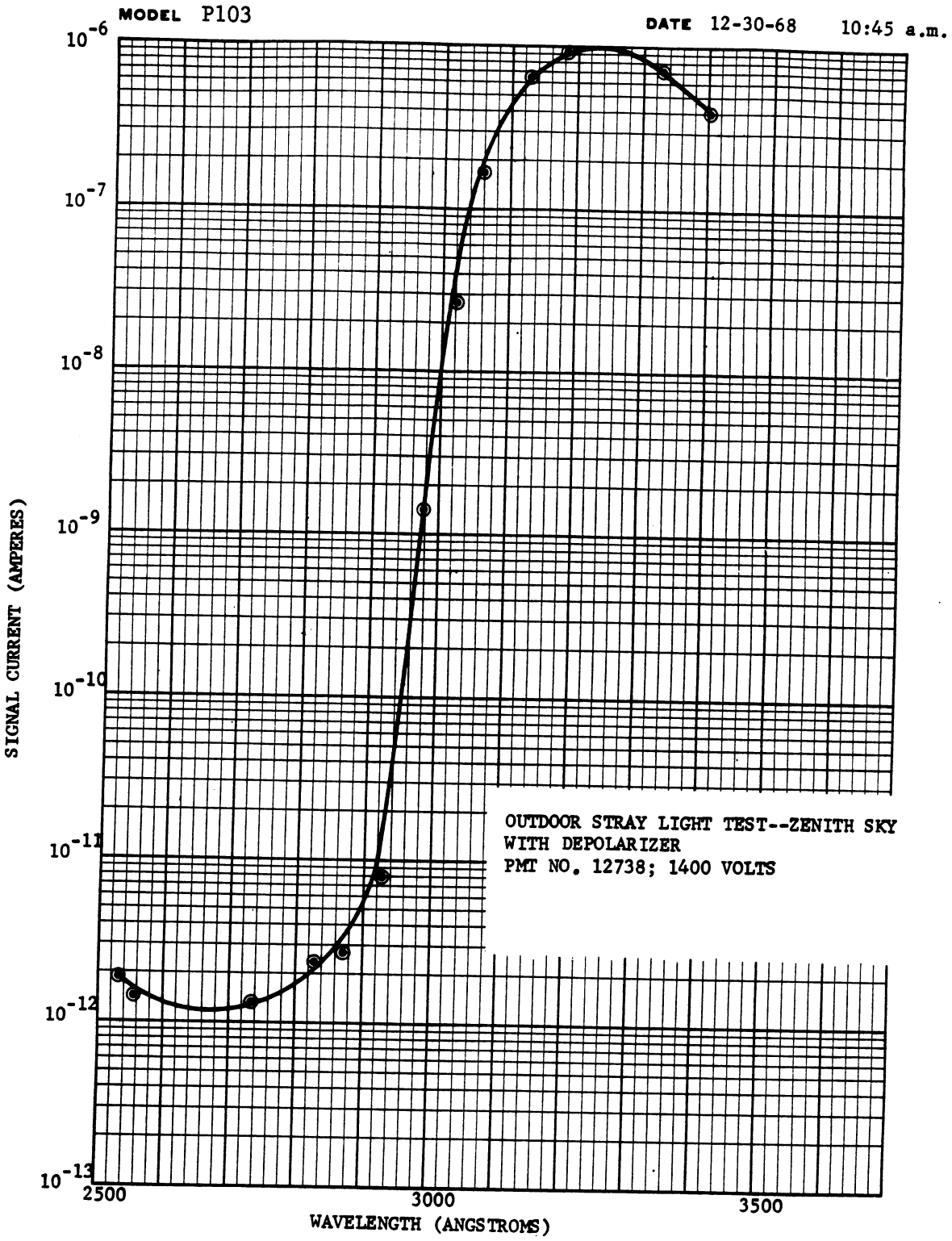

Figure 3-44. P103 Instrument--Zenith Sky

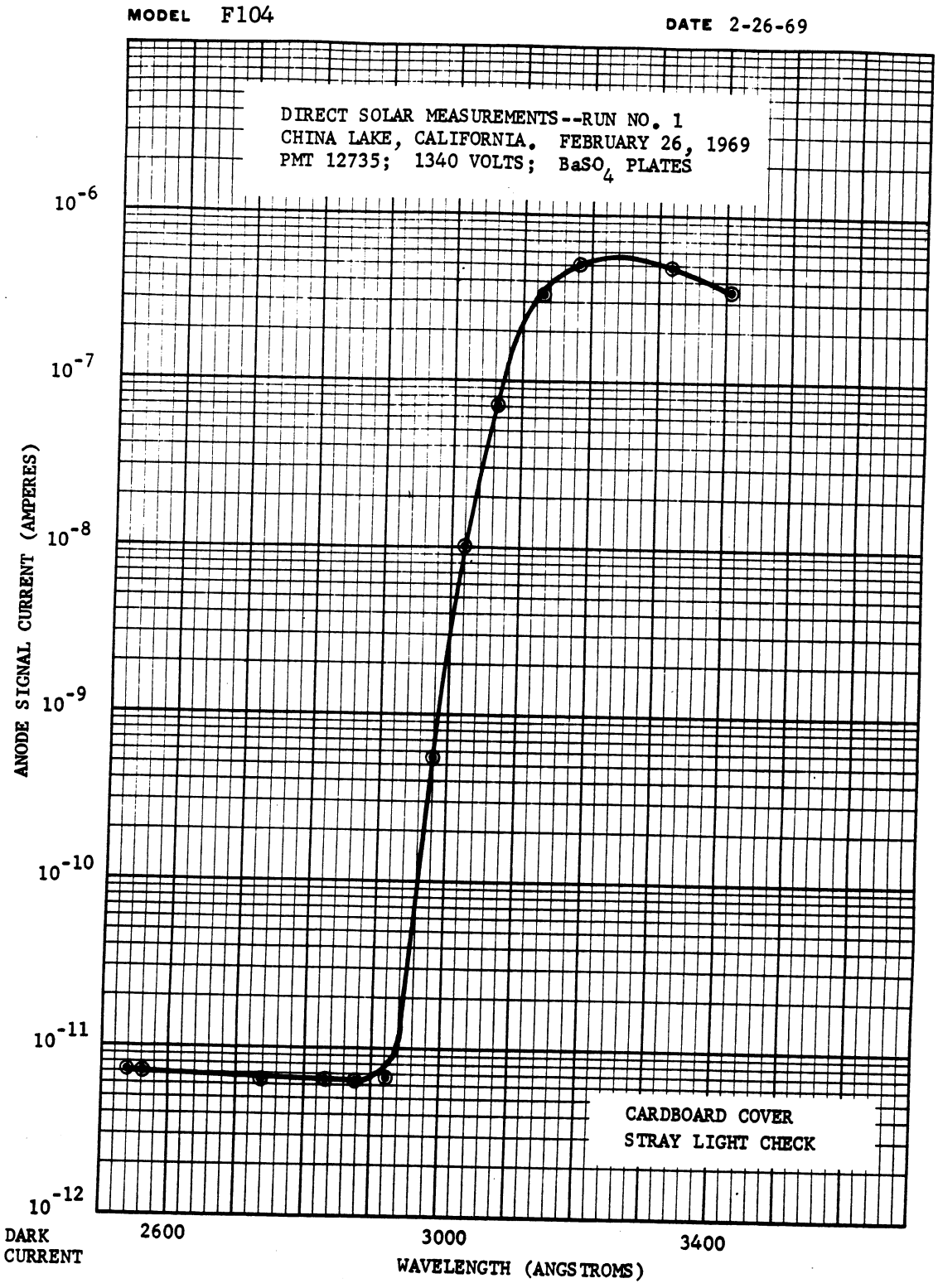

Figure 3-45. F104 Instrument--MgO Plate

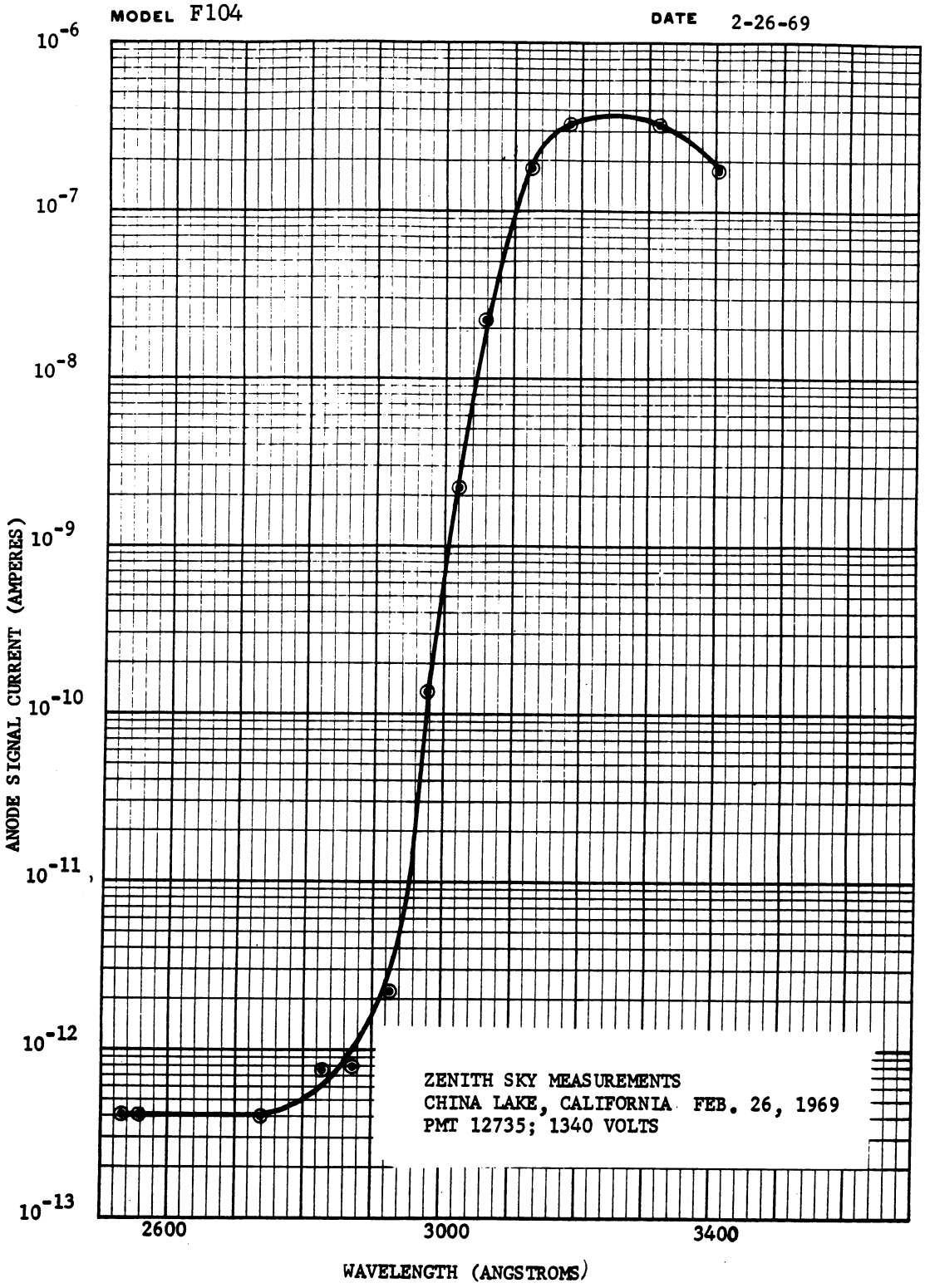

Figure 3-46. F104 Instrument--Zenith Sky

During the acceptance tests of the F104 Instrument on 7-29 to 8-1-69, the stray light increased significantly. The stray-light ratio of 4×10^{-6} observed on February 19, 1969, had increased to 2×10^{-5} as observed on 8-1-69. This is an increase by a factor of five.

The focusing of the sun as a source was used to discover the stray-light leaks. Three actual leaks were discovered. The origins are unknown, although it is speculated that they were created by environmental testing. The first light leak was over the cover of the collimating mirrors where they join the casting. This very small leak was not corrected because the entire instrument would be completely covered in the bay of the NIMBUS.

With all shutters closed, monochromator and photometer, the instrument had a second light leak from the photometer entrance to the monochromator photomultiplier when the concentrated beam of light was directed into the photometer entrance (Figure 3-47). The increase in stray light is higher when the intense beam is directed against a 45° mirror along the edge where the mirror is resting against the casting. At this point, the pulse count increased to 6,000 where a maximum of 60 counts should be expected.

The third source of stray light was observed (with all shutters closed) around the mounting of the monochromator horn at the joint with the casting (Figure 3-48). With the intense beam focused along the edge as shown or directed against the plastic switch mount, the stray-light count was approximately 200 where 60 is desired. It was speculated that the P103 Instrument also could have the same stray-light increase. When the P103 was returned from General Electric, this was verified. A solution was found by mounting an additional stray-light shield into the photometer opening. The stray-light shield (P/N 148530) was installed as shown in Figure 3-49. The additional stray light shield was installed with HYSOL epoxy. The installation of the additional light shield resulted in the decrease of the stray light in the F104 Instrument to approximately 6×10^{-6}. This is the signal ratio of 2555 Å over 3175 Å. Table 3-9 shows the results of the stray-light-shield installation on the P103 Instrument.

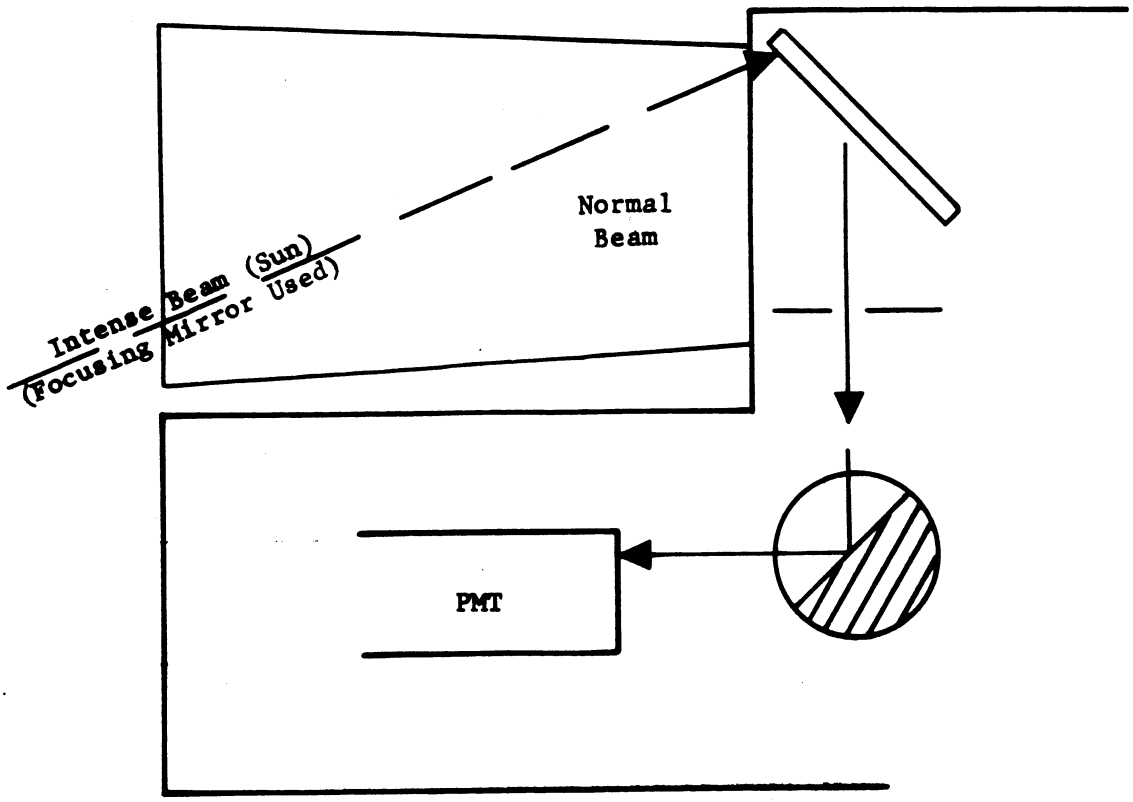

Figure 3-47. Concentrated Beam of Light Directed into Photometer

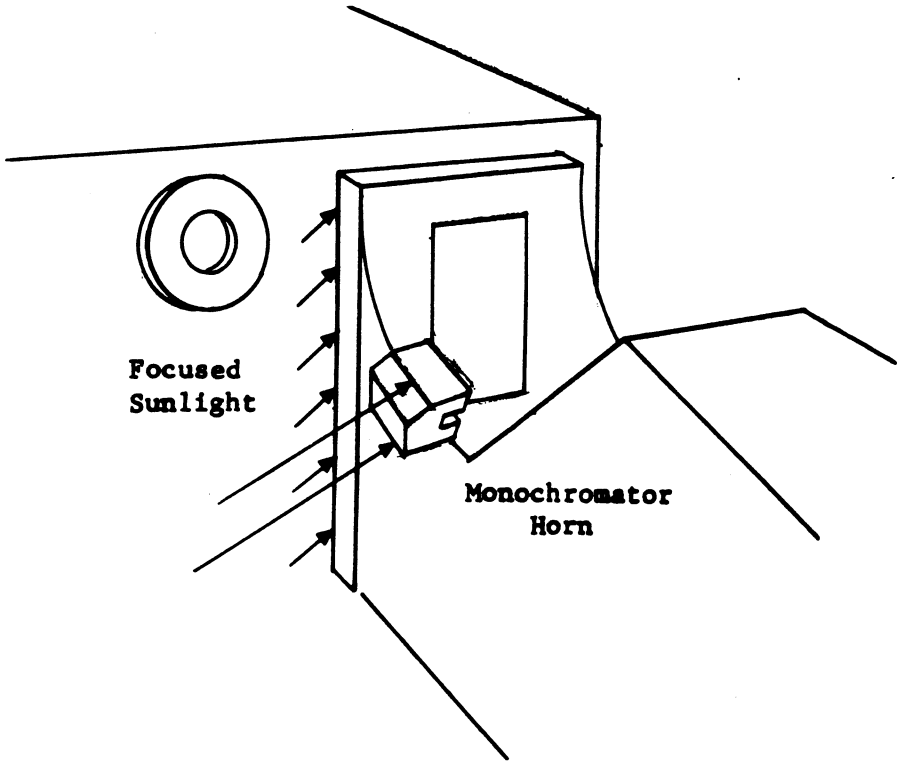

Figure 3-48. Focused Sunlight Directed into Monochromator Horn

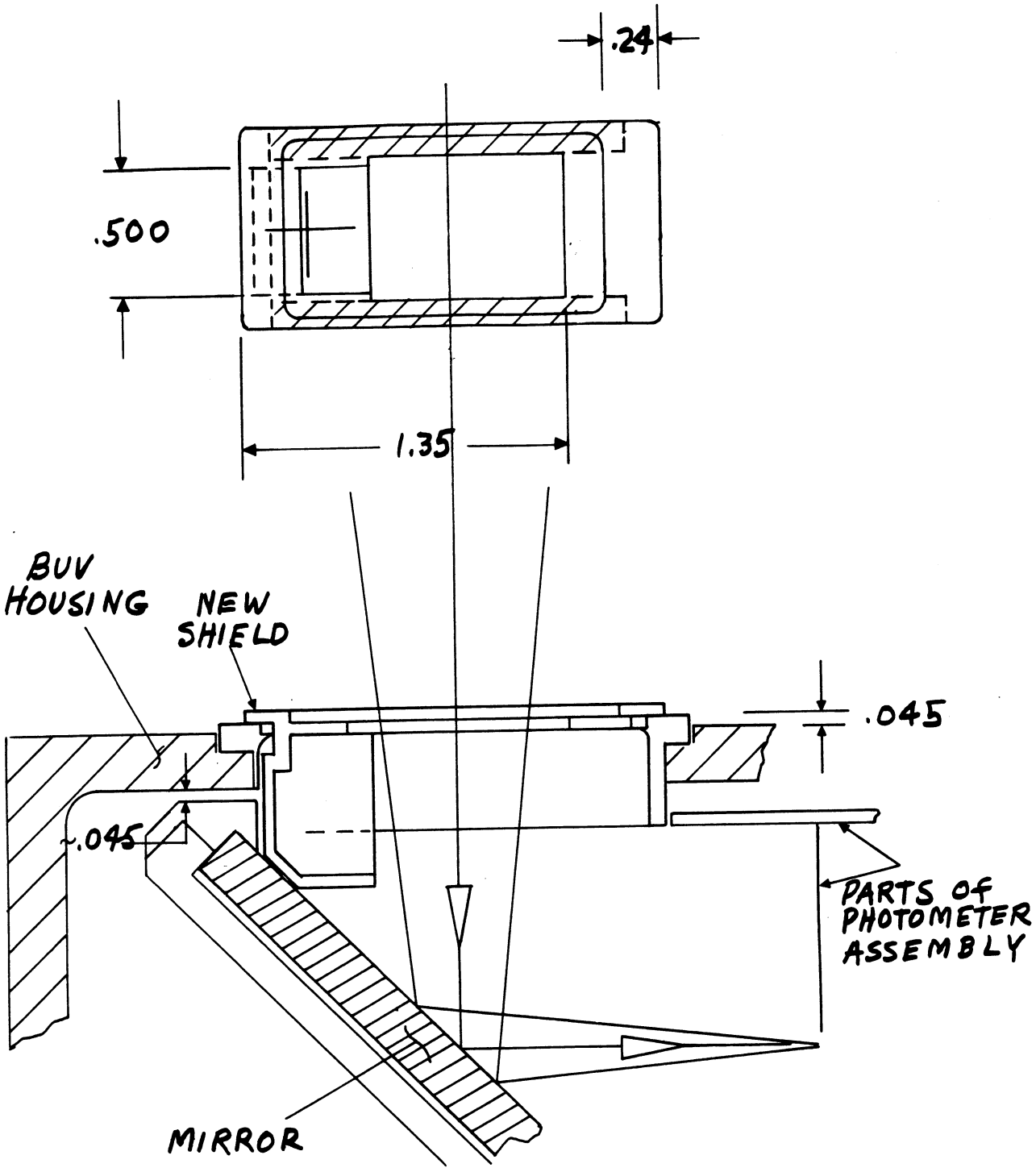

Figure 3-49. Installation of Additional Stray-Light Shield

Tests for stray light were performed before and after installation of the addit. stray-light shield in the photometer for prevention of crosstalk	9-16-69 No Addit. Shield	Time; Bright Sunny; Addit. Shield Epoxy Before	9-19-69 Counts Per Second Envir.	Time; Bright Sunny; Addit. Shield Tape	9-18-69 Counts Per Second	Time; Bright Sunny; Addit. Shield Epoxy After	9-22-69 Counts Per Second Envir.	
1) Id; all shutters closed; horns covered; diff. retract.		13:32 13:34	127.3 143.6	14:45 14:49	214.5 236.3	10:33 10:35	106.0 121.3	In Shade 1A in Sun
2) Diff. depl.; all shutters closed; sun on both $BaSO_4$ plates		13:36	166.8	14:51	251.7	10:38	130.3	
3) Diff. depl.; all shutters closed; sun on mono $BaSO_4$ plate, photom. covered		13:38	172.5	14:53	242.2	10:40	123.1	
4) Diff. depl; all shutters closed; sun focused in photom Mirror Edge	~80,000	13:39	181.4	14:54	254.5	10:42	147.6	
4A) Sun. foc. on mirror center		13:40	209.4	14:56	261.6	10:43	146.3	4A
5) Id; shutters open or closed; horns covered; diff. retr.		13:43	199.9	15:09	327.5	10:44	172.7	
6) Diff. depl; shutters open; 2555 Å (11); sun on both $BaSO_4$		13:45	1715.7	15:11	1388.6	10:48	1639	
7) Diff. depl; shutters open; 2555 Å; sun on mono $BaSO_4$ only photom. covered		13:46	1716.0	15:13	1236.0	10:49	1596	
8) Id; cond. see 5)		13:47	269.3	15:15	332.0	10:51	225.6	
9) Scan of λ range on both channels; $BaSO_4$ plates		13:51	8.0×10^{-6}	15:19	9.5×10^{-6}	10:53	9.3×10^{-6}	
10) Scan of λ range on mono channel; $BaSO_4$ plate; photom covered		13:53	7.45×10^{-6}	15:20	9.9×10^{-6}	10:55	9.17×10^{-6}	

Table 3-9 (1 of 2). Results of Stray Light Shield Installation

Tests for stray light were performed before and after installation of the addit. stray-light shield in the photometer for prevention of crosstalk	9-16-69 No Addit. Shield	Time; Bright Sunny; Addit. Shield Epoxy Before	9-19-69 Counts Per Second Envir.	Time; Bright Sunny; Addit. Shield Tape	9-18-69 Counts Per Second	Time; Bright Sunny; Addit. Shield Epoxy After	9-22-69 Counts Per Second Envir.
11) Id; cond. see 5)		13:55	513.9	15:21	483.7	10:57	504.7
12) Id; shutters closed; instru. pointed at Zenith sky; horns covered; diff. retr.		13:58	869.45			11:00	602.0
13) Scan of λ range on both chan. of Zenith sky		14:00 1.69×10^{-6}				11:01 1.46×10^{-6}	
14) Scan of λ range on mono chan. of Zenith sky; photom covered		14:01 2.494×10^{-6}				11:02 2.22×10^{-6}	
15) Id; cond. see 12)		14:02	814.5			11:03	699.1
16) Id; all shutters closed; horns covered; direct sun		14:07	347.9			11:10	242.8
17) All shutters closed; both borns open; direct sun			339.8			11:13	261.4
18) All shutters closed; photom. horn covered; direct sun		14:10	343.1			11:15	254.2

Table 3-9 (2 of 2). Results of Stray Light Shield Installation

3.2.5 Monochromator Grating

The gratings used in the BUV Instrument are Bausch & Lomb high-quality reflection gratings, 58 x 58 x 10-mm thick. The ruled area is 52 x 52 mm. The gratings are ruled 2400 grooves/mm with a blaze wavelength at 2400 Å, or 16° 44'.

The replicas are deposited on a special substrate manufactured from SUPRASIL fused silica. Selection of the gratings for first and second monochromators was predicated on high efficiency, low polarization sensitivity, and low scattering. The two gratings of a BUV Instrument are mounted on a common grating holder. Blaze arrows of both gratings point towards the intermediate slit. The gratings are lapped into position on 4 bases in the four corners of the grating. The bases support the back of the grating, while spring clips press against the grating front surface.

The gratings are aligned parallel and perpendicular to each other and to the rotary axis of the holder to better than 1/2 min of arc. While the common grating holder may be removed from the Instrument if necessary, the individual grating cannot be taken out of the mount without loss of alignment.

The following gratings are installed in the P103 and F104 Instruments:

	1st Mono	2nd Mono
P103 Instrument	1132-9-5	1132-13-1
F104 Instrument	1132-10-1	1132-10-2

The data for the selection of the gratings for the individual instruments and monochromators was obtained on a special test fixture which was constructed for this purpose. A sketch of this test fixture is shown in Figure 3-50. Additional sketches show the orientation of the gratings in the first and second monochromators (Figures 3-51 through 3-54).

After the data was obtained, the desired values were calculated and a readout for the various categories which determine the selection of the gratings was obtained. The gratings were selected for Relative Spectral Efficiency, Relative Efficiency, Absolute Grating Efficiency, and scattering. A tabulation

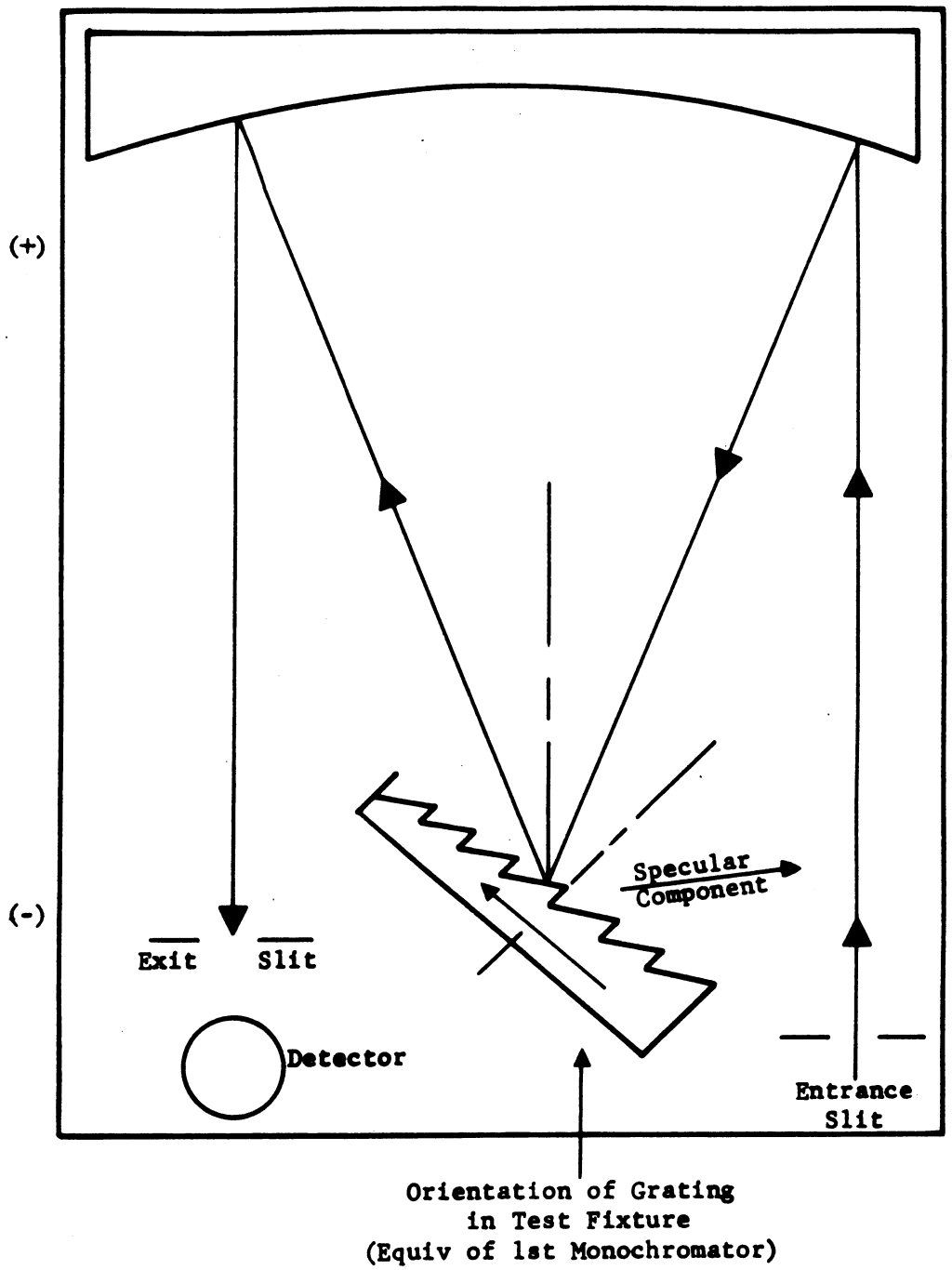

Figure 3-50. Orientation of Grating in Test Fixture (Equivalent of First Monochromator

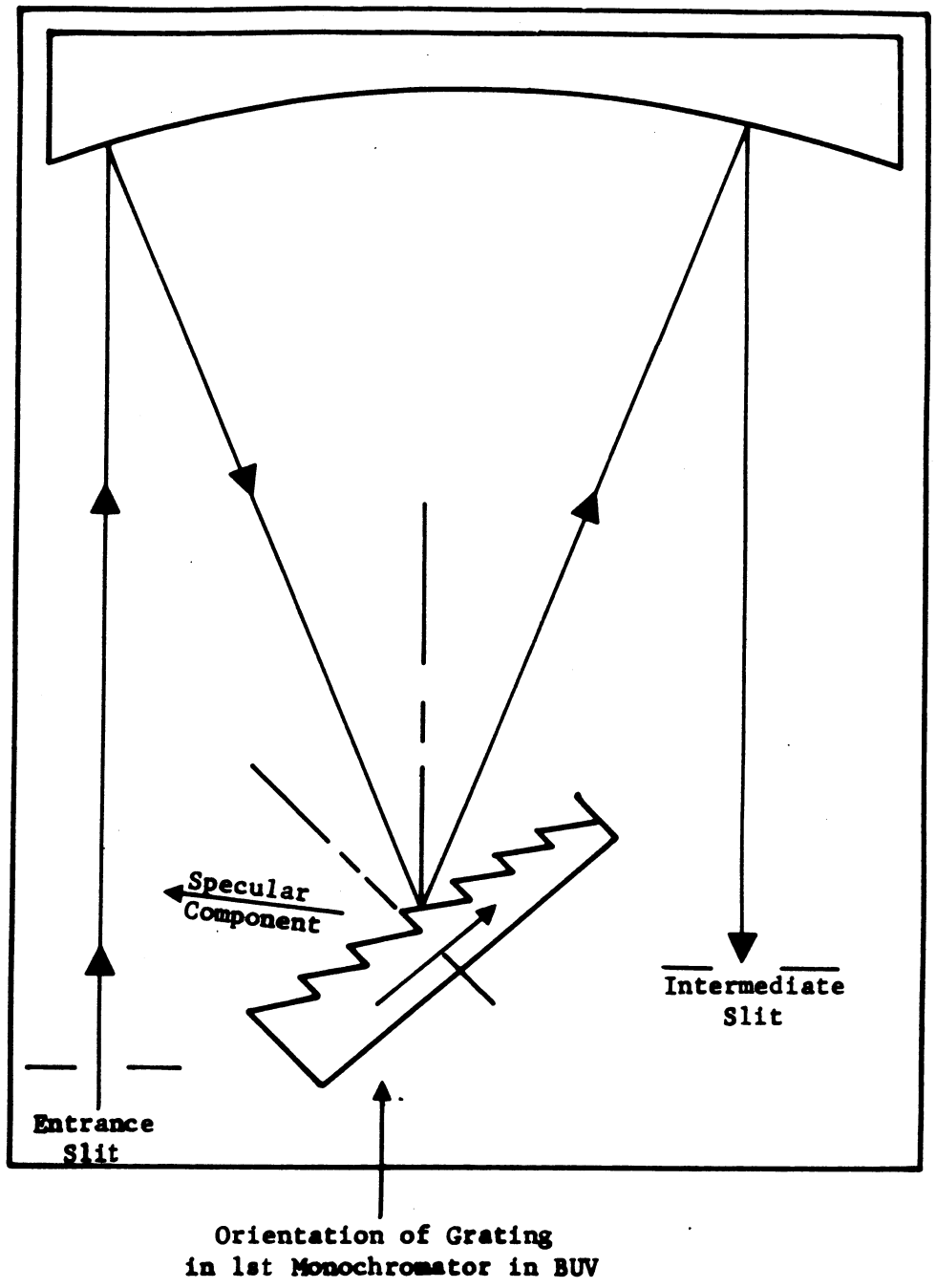

Figure 3-51. Orientation of Grating in BUV First Monochromator

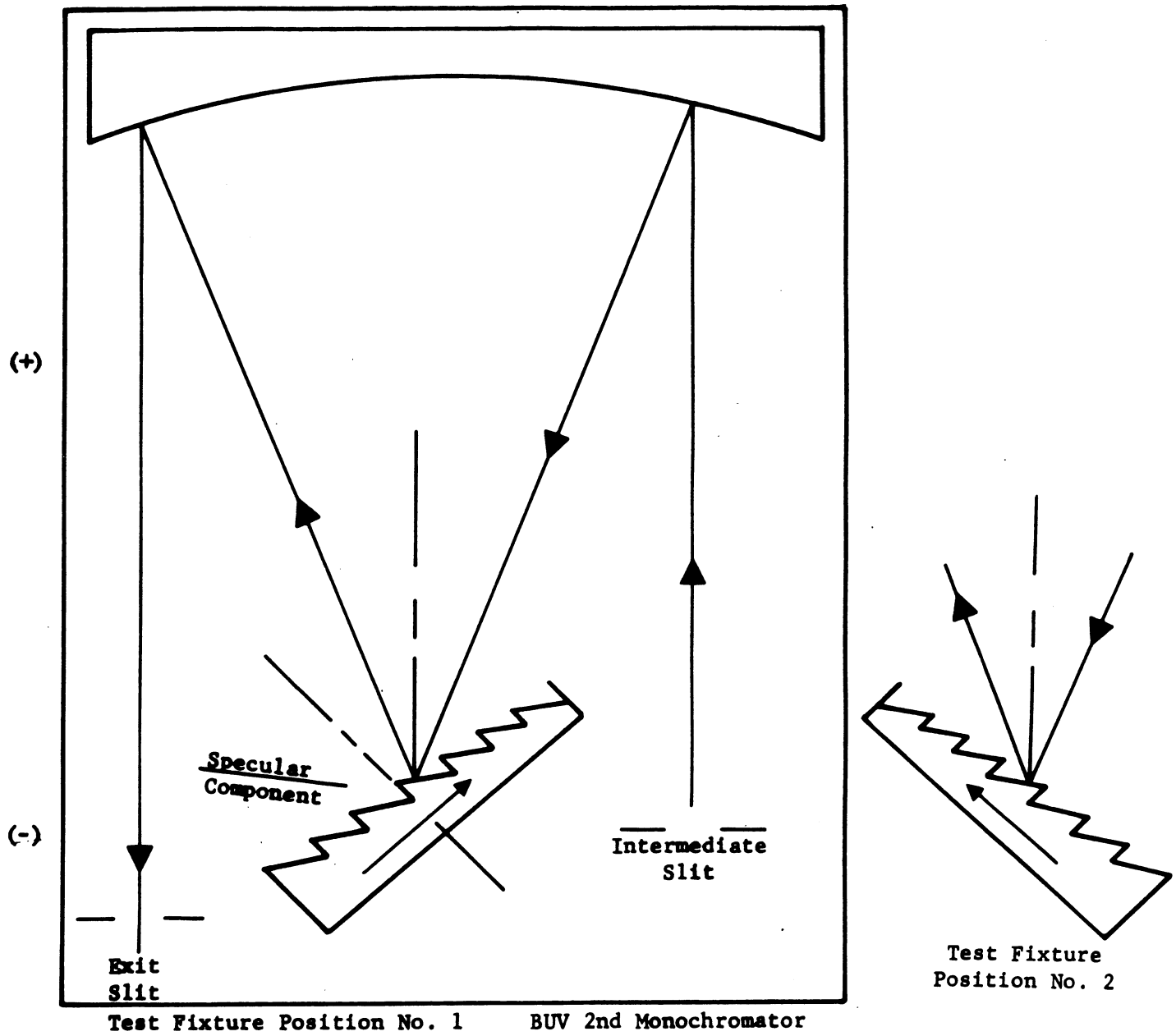

Figure 3-52. BUV and Test Fixture--Second Monochromator

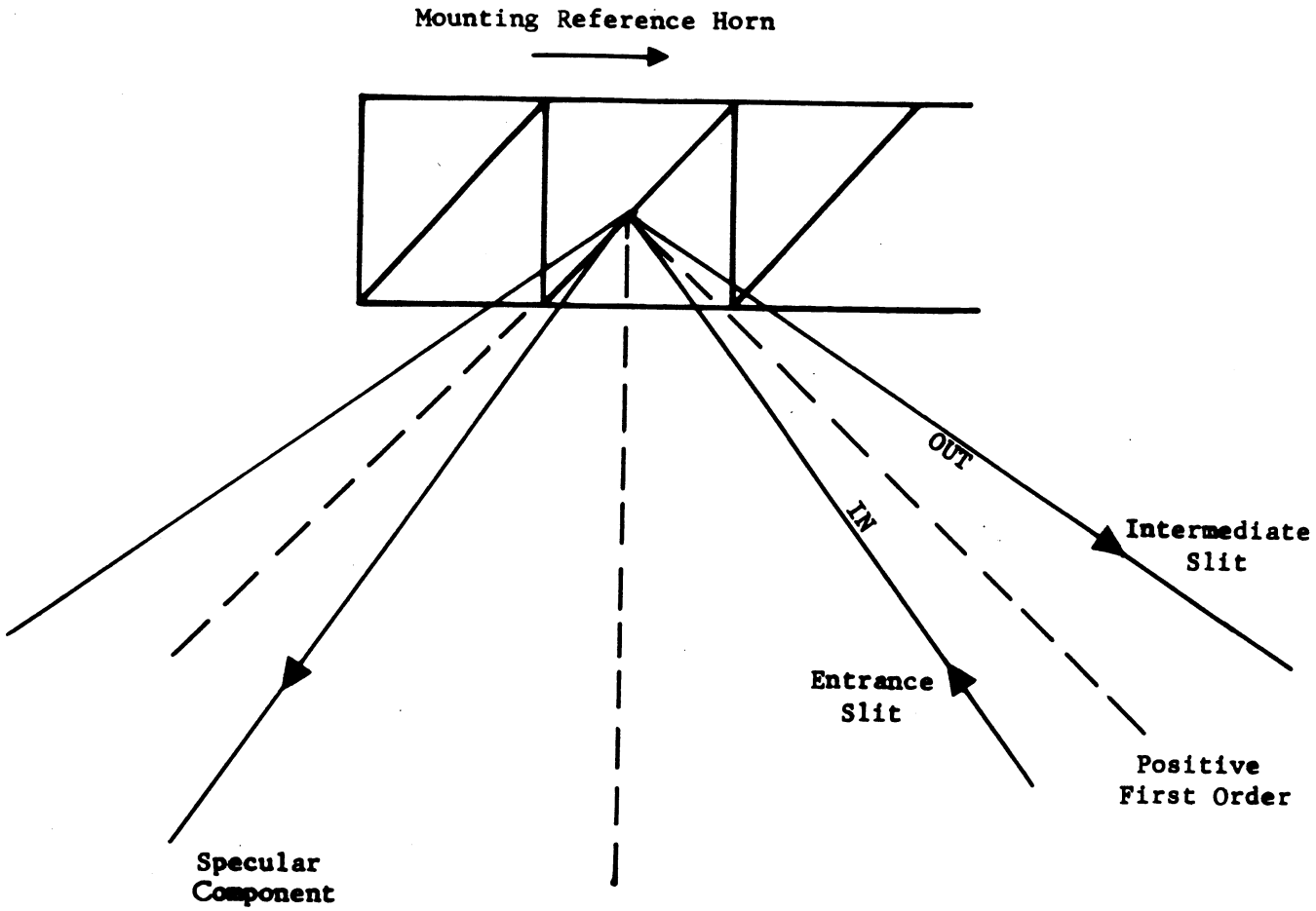

Figure 3-53. First Monochromator Blaze Orientation

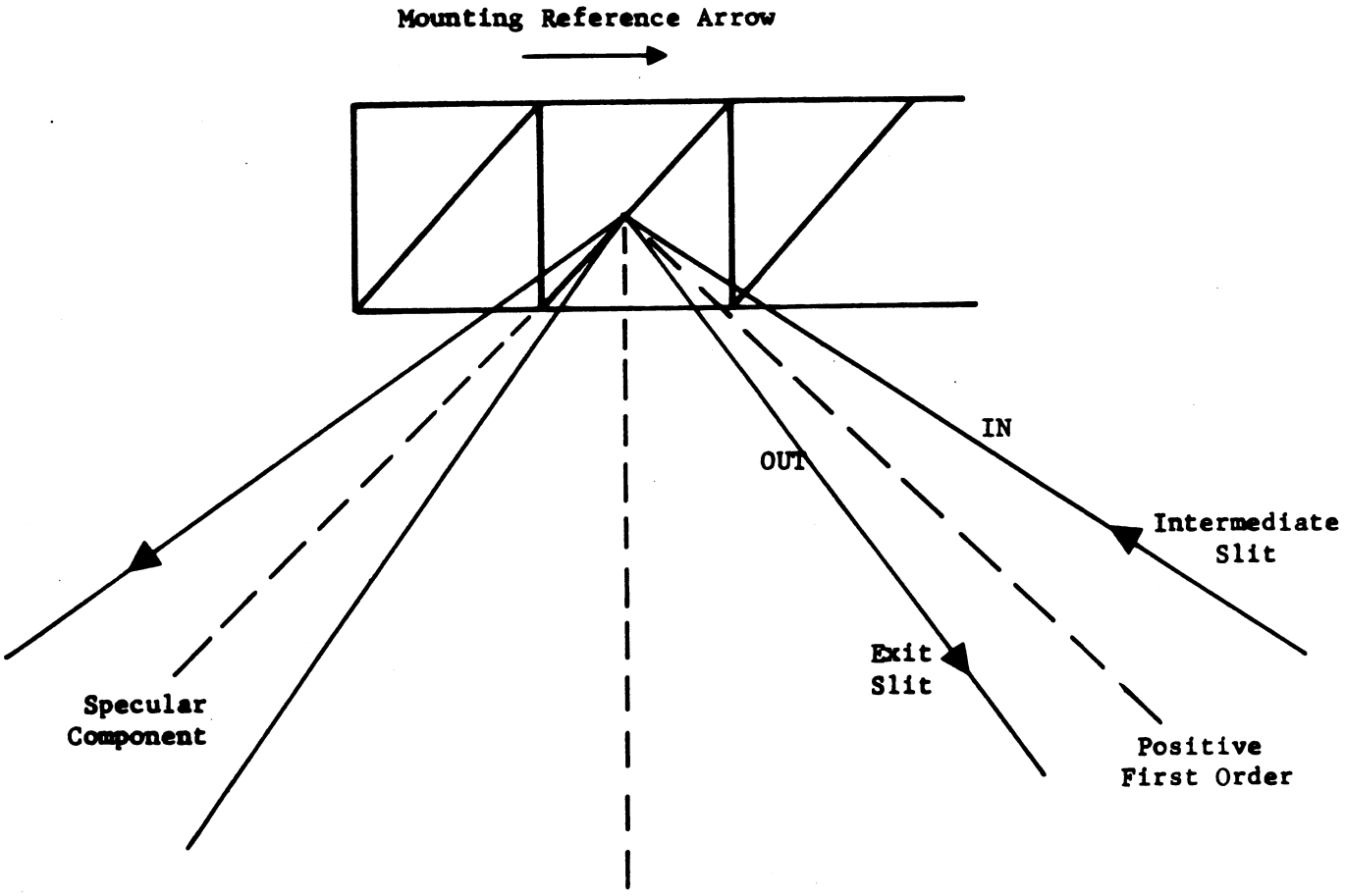

Figure 3-54. Second Monochromator Blaze Orientation

with the explanation for the various selection criteria is shown in Table 3-10. A computer was used in the selection of gratings. The calculations obtained in the computer runs were graded from 1 to 6, with the lower numbers being the superior results (Table 3-11).

A tabulation with the graded results of the gratings is shown in Figure 3-55. The grating for the first and second monochromators was primarily selected for superior scattering characteristics.

3.2.6 Depolarizer

3.2.6.1 Summary

Because the BUV Instrument would exhibit selective sensitivity up to 65 percent to polarized light, called "Polarization Sensitivity", the use of a depolarizer was deemed necessary to reduce this sensitivity to an acceptable level (5 percent or below). This sensitivity is summarized as follows:

	Polarization Sensitivity
Monochromator (without Depolarizer)	65%
Monochromator (with Depolarizer):	
P103 Instrument	5.2 ±0.5%
F104 Instrument	4.2 ±0.5%

The customary definition for Polarization Sensitivity is $\frac{Imax - Imin}{Imax + Imin}$, whereas the definition taken for these measurements is $\frac{Imax-Imin}{Imax}$. This definition offers a more stringent approach than the customary definition which is based on average fluctuation and signal strengths.

The results of measurements of BUV instrument polarization characteristics show that the maximum transmittance axis is oriented 90° to the entrance slit on both the P103 and F104 instruments. In general, the Polarization Sensitivity for the F104 instrument is between 3.7 and 4.7 percent at all wavelengths. For the P103 instrument it is between 4.7 and 5.7 percent, with the possible exception of

	Relative Spectral Efficiency **	Relative Efficiency ***	Absolute Scattering Efficiency ****		Average Total of **)***)****	Average Absolute Only ****)	Final Placement of Gratings	Scattering Grade *
	+	+	1)	2)				+
G2	6	1	1	2	1	1	FM 1st	2
G3	1	4	3	5	3	4	RES 1st	1
G4	3	3	2	3	2	2	PT 2nd	6
G5	4	6	6	6	6	6	PT 1st	3
G6	2	5	5	1	4	3	FM 2nd	4
G7	5	2	4	4	5	5	RES 2nd	5
							BASIS FOR SELECTION	
G2	2	5			3		FM 1st	1
G3	6	2			4		RES 1st	4
G4	4	1			2		PT 2nd	5
G5	3	6			5		PT 1st	6
G6	1	3			1		FM 2nd	2
G7	5	4			6		RES 2nd	3

Table 3-10. Grating Selection Criteria

06W2	1.75	2.42	3.5	21.0	7.25	61.8	6.1	.075	.075			
07W1	14.5	66.	28.	63.	13.	10.5	6.75	22.3	67.5	67.	67.	4.15
07W2	1.7	2.42	3.42	21.0	7.4	61.8	6.1	.075	.075			
3	07	07	07									

X Grating Relative Efficiency-Dark Current Adjusted-Perpendicular Polarization
" " " - " " " -Perpendicular Polarization
" " " - " " " -Parallel Polarization)
" " " - " " " -Unpolarized Light)
" " " -Relative Spectral Efficiency-Perpendicular Hg)
" " " - " " " -Perpendicular Hg)
" " " - " " " -Parallel Hg Spectrum
" " " - " " " -Parallel Hg Spectrum
" " " - " " " -Unpolarized Hg)
" " " - " " " -Unpolarized Hg)
" " " -Principal Transmittance Ratio
" " " - " " "
" " " -Relative Efficiency of Gratings-Perpendicular)
" " " - " " " -Perpendicular)
" " " - " " " -Parallel)
" " " - " " " -Parallel)
" " " - " " " -Unpolarized)
" " " - " " " -Unpolarized)

** a	b	***a	b	a	b	λ1 -λ9 + λ11-λ19-
2	6	3	1	4	2	6 1
5	16	1	3	5	4	
4	5	2	3	4	1	3
3	4	4	4	6	3	6
1	2	1	3	5	2	5
6	3	3	6	4	5	2

3 08 08 08

Grating Absolute Efficiency-Dark Current Adjusted-Perpendicular Polarization
" " " - " " " -Parallel Polarization
" " " - " " " -Without Polarization
" " " -Absolute Grating Efficiency-Perpendicular
" " " - " " " -Perpendicular
" " " - " " " -Parallel
" " " - " " " -Parallel
" " " - " " " -Without Polarization
" " " - " " " -Without Polarization
" " " -Principal Transmittance Ratio
" " " -Mean Polarized Efficiency:Unpolarized Efficiency

**** a	b	a	b	1/1+0+1 1/Mirror 1/1+0+1 1/Mirror 1/1+0+1 1/Mirror
1	2	1	3	3 4
3	4	4	5	2 3
2	3	5	1	1 6
5	6	6	6	6 5
6	5	1	5	2 4
4	6	4	2	2 3

X Scattering-Scaled & Dark Current Adjusted
" - " " " "
" -Grating Scattering (Times 10**5)
" - " " (Times 10**5)
" - " " Relative to Mirror (Times 10**-1)
" - " " " (Times 10**-1)

*				18°-25°+ 18°-25°- 18°-25°+ 18°-25°-
4	1	4	1	
5	6	5	6	
6	3	6	3	
2	4	2	4	
3	5	3	5	

B&L 35-53-06-15

b	a			18°-25°+
G1 2464-1-1-4 2400 1/min 3000 Å				
G2 1132-10-1 2400 1/min 2400 Å	1	2	1	2 1 2
G3 1132-12-2	4	1	1	4 1 4 1
G4 1132-13-1	5	6	5	6 5 6
G5 1132-9-5	6	3	6	3 6 3
G6 1132-10-2	2	4	2	4 2 4
G7 1132-12-3	3	5	3	5 3 5

NOTES:

* Choice of Gratings for Scattering
Lowest Scattering-Grade 1
Column a = 1st Monochromator
Column b = 2nd Monochromator

* Choice for 1st Mono
1 - Best

* Choice for 2nd Mono
1 - Best

Table 3-11. Summary of Computer Printout Selection Matrix

	Grating Serial No.
BUV - F104	
1st MONO	1132-10-1
2nd MONO	1132-10-2
BUV - P103	
1st MONO	1132-9-5
2nd MONO	1132-13-1
BUV - RES (Reserve)	
1st MONO	1132-12-2
2nd MONO	1132-12-3

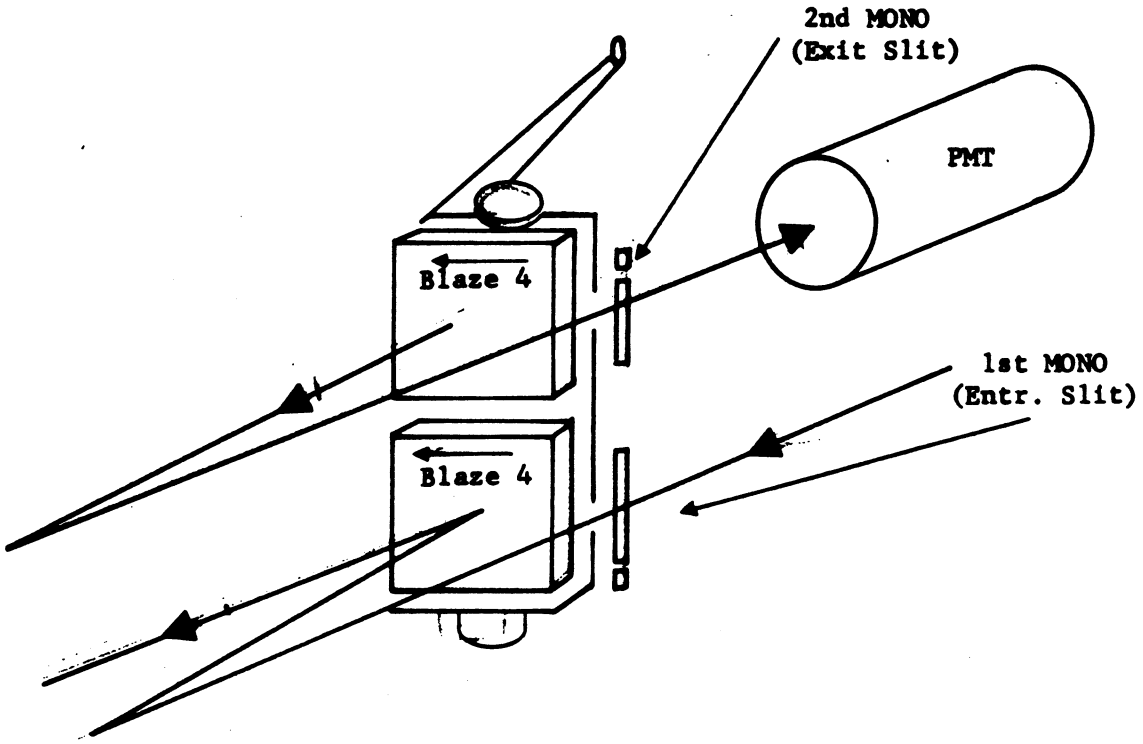

Figure 3-55. Grating Selection

2555 Å on the P103 instrument, which could be as large as 9.3 percent. The radiation from the $BaSO_4$ diffuser plate was on the order of 1.0 to 1.5 percent in the measurements just completed on the F104 instrument. This would correspond to a residual polarization of this radiation on the order of 0.5 to 0.75 percent. In some previous measurements, the radiation was polarized as much as 2.5 to 3 percent (1.3 to 1.5 percent residual polarization).

3.2.6.2 Description

The depolarizer consists of three parts: a 5-mm-thick sapphire shield and two calcite plates 6 and 3-mm thick. Orientation of the optical axis is very important in all three items. In the sapphire shield, the optical axis is oriented along the propagation direction of the incoming beam into the BUV. The optical axes of the calcite are perpendicular to the incoming beam. Figure 3-56 shows the critical angular relationship between the two calcite plates as well as the critical orientation of the optical axes. The thickness ratio between the 6- and the 3-mm calcite plates is held to 2.000 ±0.003.

Assembly of the complete depolarizer into the BUV Instrument is shown in Figure 3-57. The energy entering the Instrument passes in order through the sapphire, 6-mm calcite, and 3-mm calcite, before passing through the entrance slit. The individual components are separated by Teflon gaskets. Two springs apply equal pressure along the longitudinal axis of the total assembly.

3.2.6.3 Test Setup and Procedures

The apparatus used in the most recent measurements is shown in Figure 3-58. The quartz-iodine (Q-I) lamp is held in fixed relationship to the $BaSO_4$ plate by the lamp support rod. The lamp, rod, and base can be rotated together through 180° with their axis of relation colinear to the BUV monochromator axis. This angle of rotation, θ, is shown in the end view. Its relationship to the BUV slit is shown at the bottom of the sketch. Also, the inclination of the $BaSO_4$ plate to this optical axis and the lamp can be changed. This inclination angle, B, is shown in the side view.

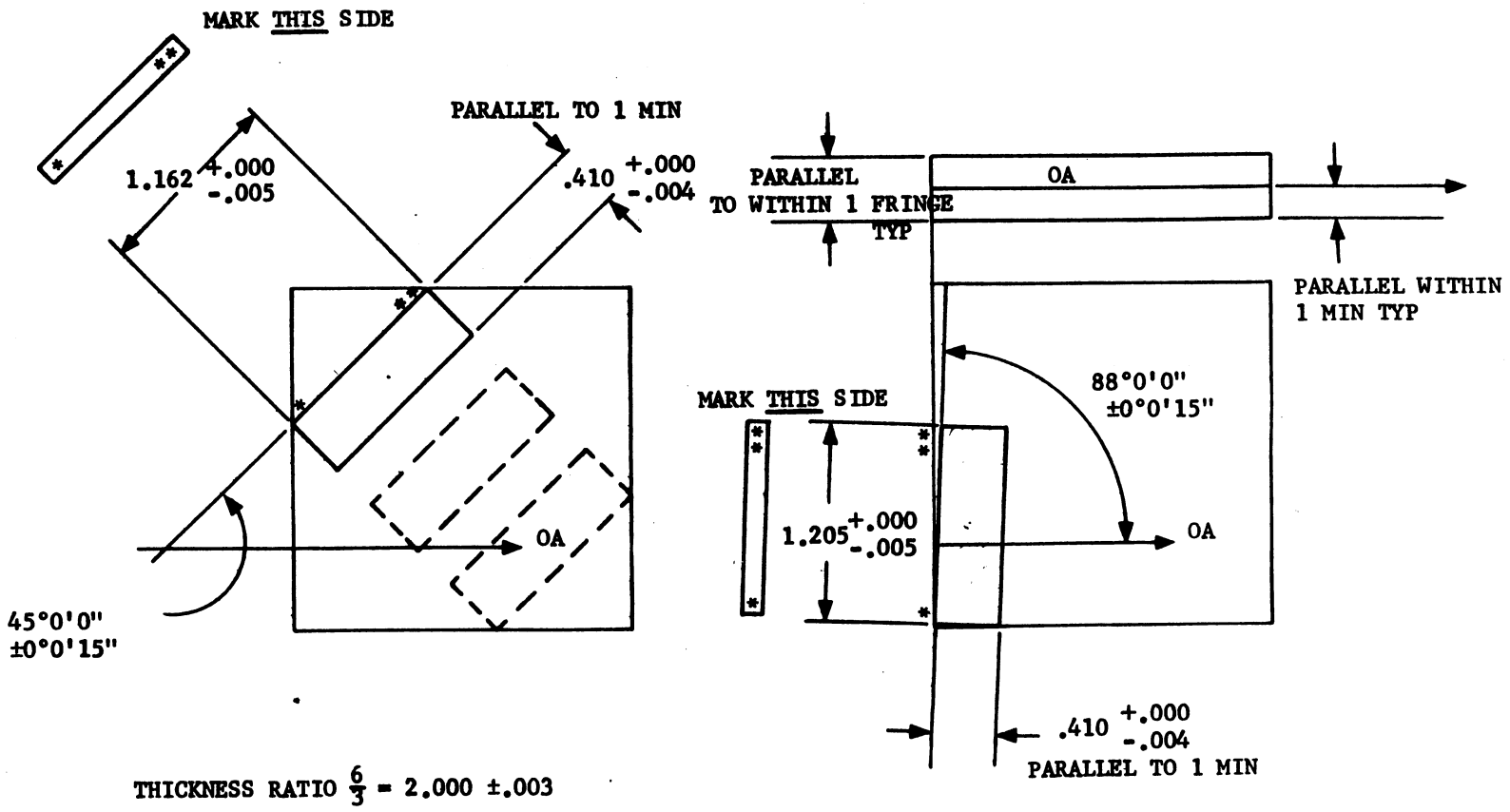

Figure 3-56. Calcite Depolarizer

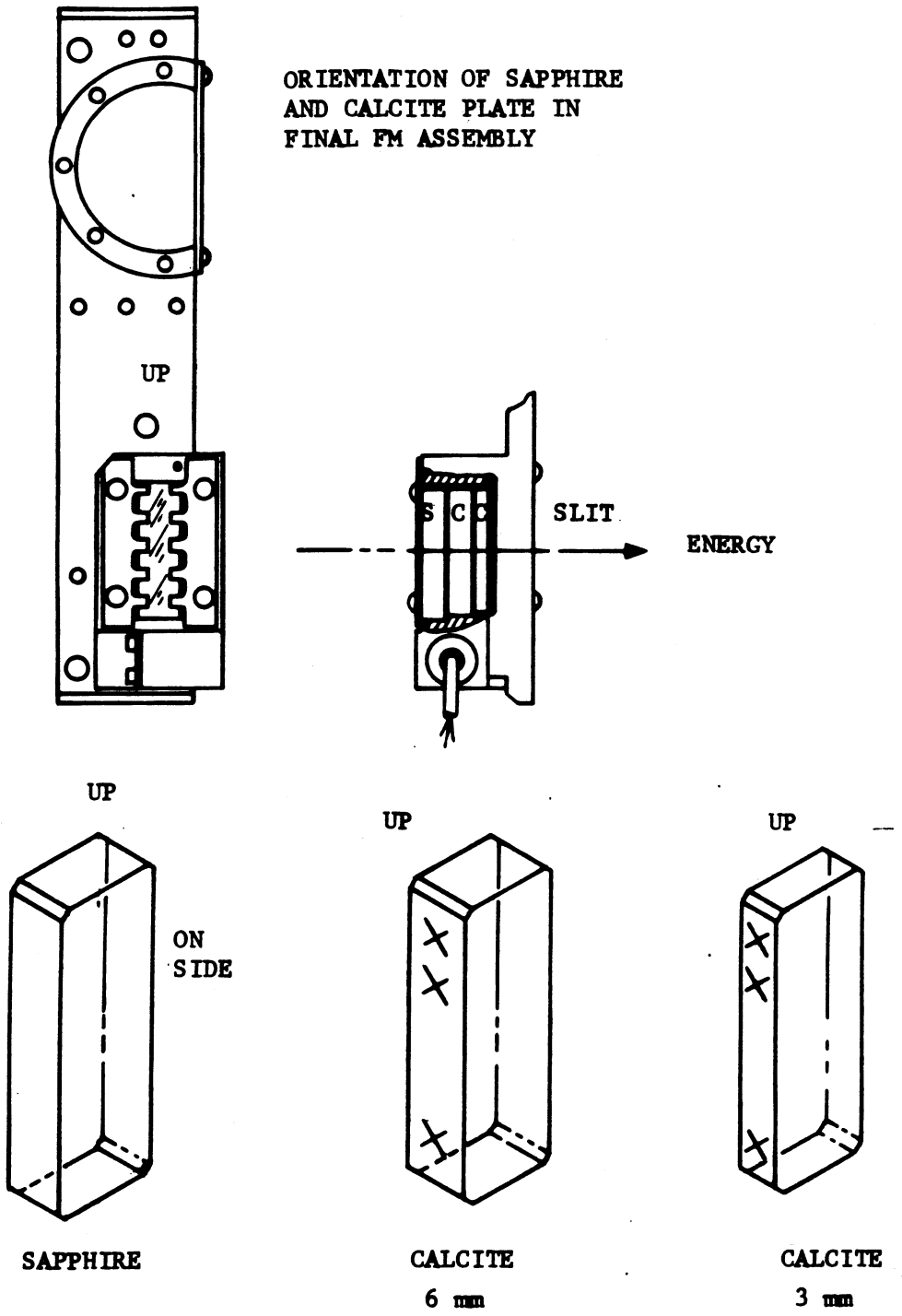

Figure 3-57. Assembly of the Complete Depolarizer into the BUV Instrument

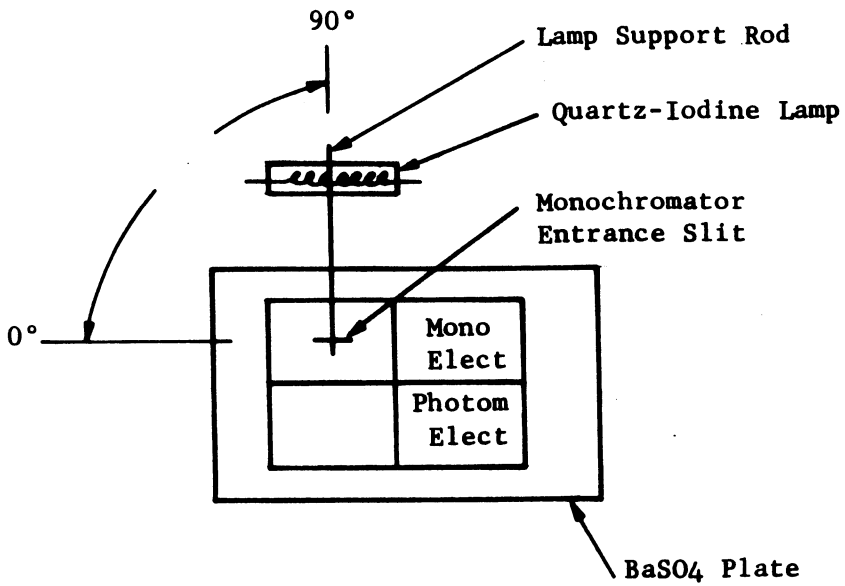

END VIEW

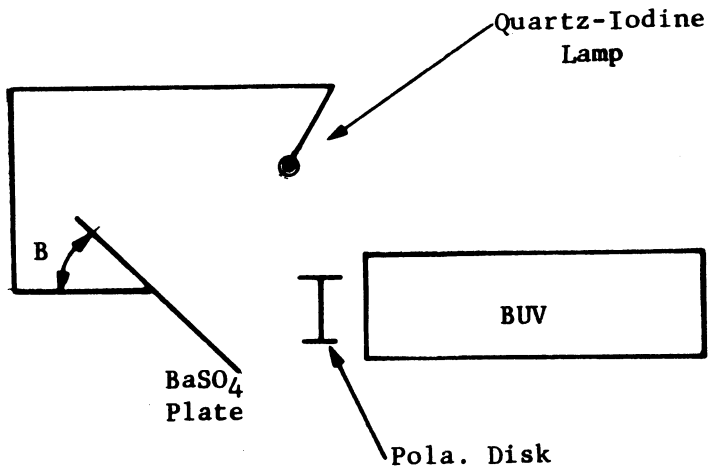

SIDE VIEW

EXPERIMENTAL EQUIPMENT LAYOUT

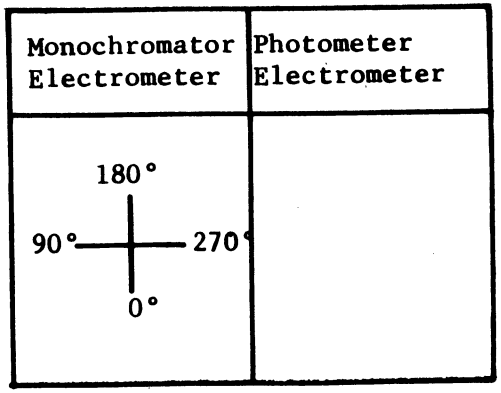

Sketch showing angular coordinate system used to measure orientation of pola. disk, $BaSO_4$ plate, lamp and support rod relative to BUV monochromator entrance slit.

Figure 3-58. Polarization Sensitivity Experimental Equipment Layout

The following procedure was used to make measurements and perform calculations to determine Polarization Sensitivity:

1. Rotate lamp plate and poladisk together and calculate Polarization Sensitivity = $\frac{Imax - Imin}{Imax}$.

2. Fix lamp plate with plane of incidence parallel to slit height, rotate poladisk and calculate Polarization Sensitivity, then with plane of incidence perpendicular to slit height, rotate poladisk. Again, calculate Polarization Sensitivity.

3. Because the above calculations include the effect of polarization of radiation from the $BaSO_4$ plate, averaging cancels this out, giving a true Polarization Sensitivity of the BUV Instrument.

3.2.6.4 Results and Conclusions from Testing P103

The Polarization Sensitivity of the P103 Instrument was obtained from the average of the measurements made at General Electric with the Instrument installed on the satellite, and the measurements made at Beckman after assembly, but prior to environmental testing. The former data was taken with a geometry which placed the maximum intensity axis of the radiation parallel to the maximum transmittance axis of the BUV, giving larger values of Polarization Sensitivity. The latter data was taken with the maximum intensity axis parallel to the minimum transmittance axis of the BUV. The average of these values gives the higher Polarization Sensitivity of the Instrument. Because of differences in the lamp-to-plate illumination geometry, particularly the plate angle B, the radiation from the plate at General Electric was less polarized than the radiation giving the lower values of Polarization Sensitivity. To compensate for the unequal effects of this source polarization on the measurements, the average of the two values was multiplied by a scale factor determined from a simulation of these geometries with the F104 Instrument. The results of these tests are summarized in Table 3-12 and Figure 3-59.

The values for the P103 Instrument probably represent an upper limit on the value of the Polarization Sensitivity. The scaled average is influenced strongly

Wavelength Step	*Plane of Perpendicular Slit 60° $BaSO_4$ (Percent)	Incidence Parallel Slit 45° $BaSO_4$ (Percent)	Average (Percent)	Scaled Average (Percent)
00	0.96	6.5	3.73	4.85
01	0.96	7.4	4.18	5.44
02	0.95	6.9	3.93	5.11
03	0.93	7.4	4.17	5.43
04	0.90	7.1	4.00	5.20
05	0.87	7.4	4.14	5.38
06	0.80	6.3	3.55	4.61
07	0.67	7.4	4.04	5.25
08	0.52	7.1	3.81	4.95
09	0.57	8.4	4.49	5.84
10	1.00	7.6	4.30	5.59
11	4.75	9.7	7.23	9.40

Final measurement 12-30-68

Plane of Incidence Perpendicular to Slit.

Wavelength (Angstroms)	Sensitivity (Percent)
3400	1.08
3385	0.852
3250	0.943
3120	0.926
2990	0.859
2855	0.532
2721	1.03
2590	3.18
2537	5.85

*NOTE: Last data for plane of incidence perpendicular to slit was taken 12-30-68, using micrometer wavelength drive.

Data used to calculate the average was interpolated graphically from this data. (Figure 3-60).

Table 3-12. Polarization Sensitivity, Manual and Lock-in Data--Two Different Geometries (P103)

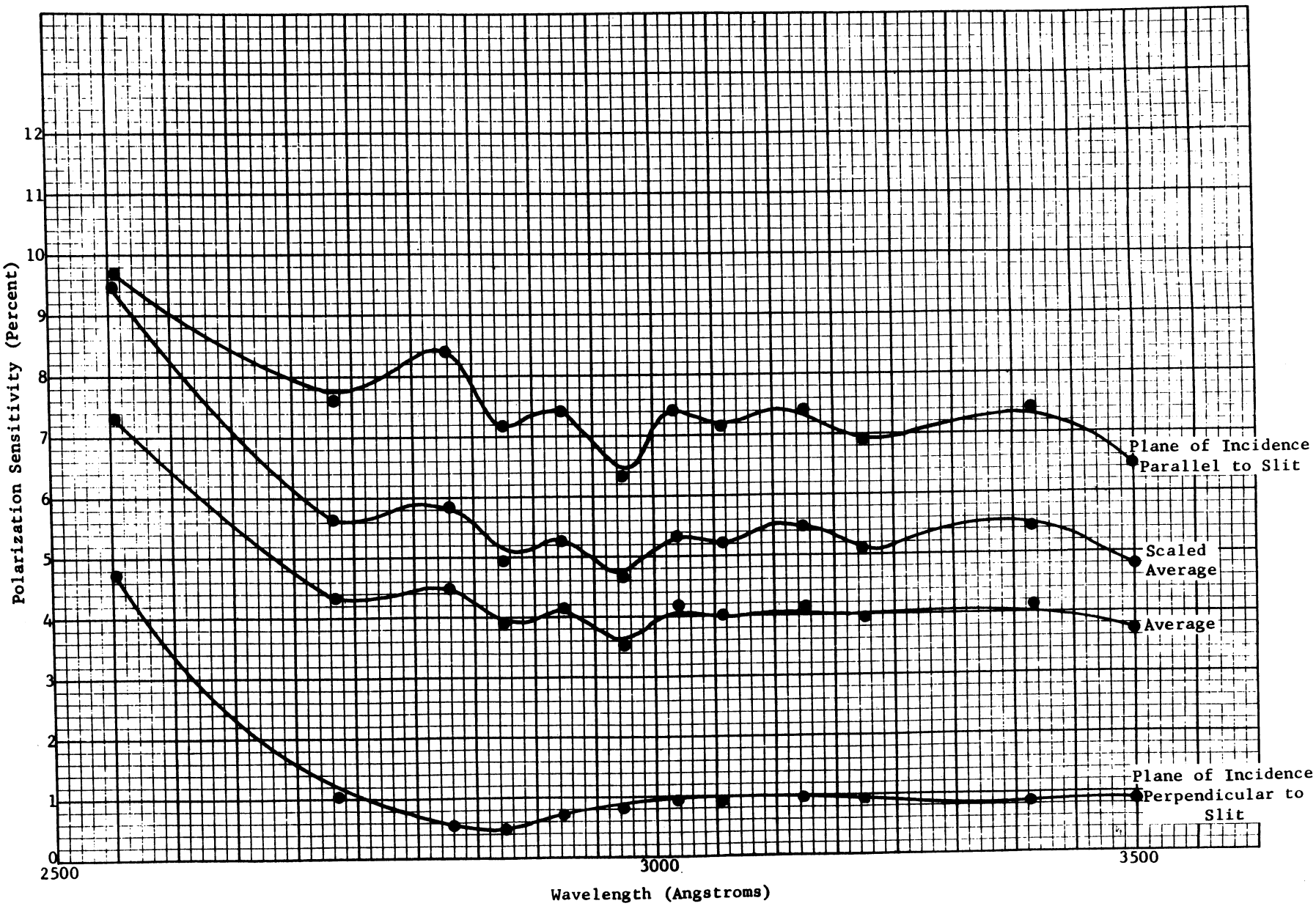

Figure 3-59. Polarization Sensitivity (P103 Instrument)

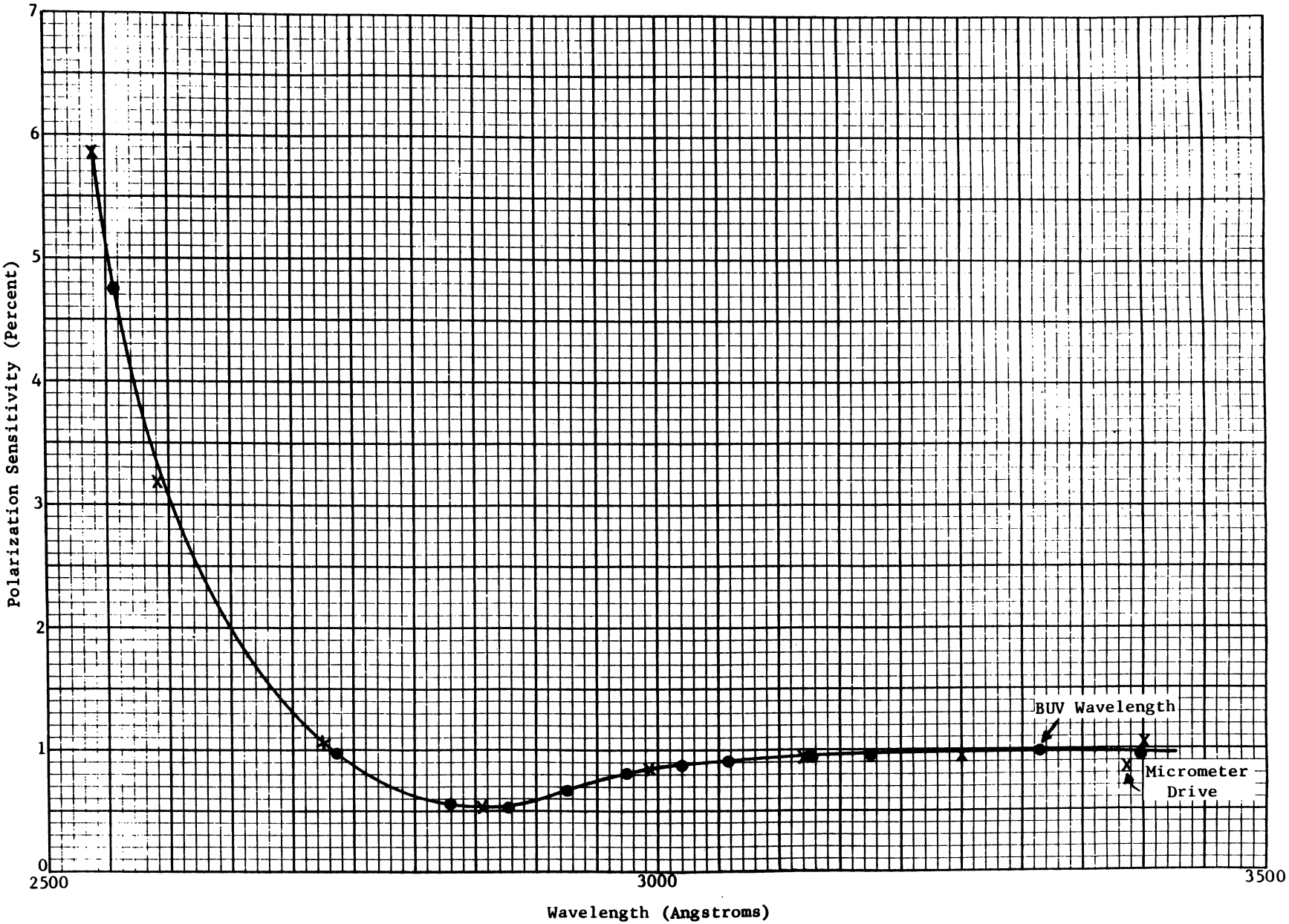

Figure 3-60. Polarization Sensitivity Interpolation Graph (P103 Instrument)

by the higher results where the worst case of these data, rather than an average, were used. This would give the highest values of Polarization Sensitivity which could be as much as 30 percent too high.

Because the measurements with the plane of incidence perpendicular to the slit were made just after assembly and prior to environmental testing, and wavelength was varied with the micrometer instead of the wavelength cam, the Polarization Sensitivity of the P103 Instrument was interpolated as shown in Figure 3-60.

3.2.6.5 Results and Conclusions from Testing F104

A summary of the results of the May 1970 tests on the F104 Instrument is given in Table 3-13 and Figures 3-61 and 3-62. Under each type of test (except the manual checks and the manual average), there are two columns of results labelled 0°-90° and 90°-180°. These headings indicate that the maximum and minimum were taken from the 0° and 90° data points, while 90° to 180° indicates the maximum and minimum were taken from the 90° and 180° data. Because the 90° data point is common to both calculations and the 0° and 180° positions should be fully equivalent, results of the two calculations ideally should be identical. The extent to which these columns of results differ is a measure of the lack of repeatability or systematic errors present in the system.

In general, there is good agreement between the BUV Polarization Sensitivity results taken by rotating the lamp-plate-poladisk combination and the results of averaging the manual data for the two different lamp-plate orientations. The 0°-90° rotating source results are higher than the results of the 90°-180° measurements and the manual measurements. In a very detailed and careful check of the illumination uniformity at wavelength step 04, some slight evidence of a systematic nonuniformity in the 0°-90° measurements was found which tends to cause a degree of mistrust in this angular region.

There is a fairly large relative scatter among the data and results of the $BaSO_4$ radiation polarization measurements. The magnitude of the differences which are used in the calculations is about the same as the fluctuations which occur in reading each individual data point. Thus, a scatter about this large

Wavelength Step	Rotating Polarized Source		Manual Average		Manual Checks $BaSO_4$ Plate Orientation		
	0°-90°	90°-180°	0°-90°	90°-180°	0°	90°	180°
0	4.90	3.43	3.57	4.38	3.57	3.57	5.19
1	4.57	3.55	4.29	4.43	5.45	3.12	5.74
2	4.67	4.00	4.53	4.24	5.66	3.39	5.08
3	4.82	4.43	4.37	4.28	5.50	3.23	5.33
4	4.94	4.29	4.39	4.59	5.34	3.43	5.74
5	4.44	3.90	4.00	4.29	4.63	3.37	5.21
6	4.30	4.02	4.08	4.25	5.28	2.87	5.63
7	3.85	3.69	3.83	3.65	5.65	2.00	5.29
8	4.47	3.35	4.05	4.04	5.15	2.95	5.12
9	3.64	3.44	4.21	4.18	5.02	3.39	4.97
10	3.88	3.88	4.59	4.61	5.45	3.73	5.49
11	3.48	3.25	3.65	4.16	4.26	3.03	5.28

Wavelength Step	$BaSO_4$ Radiation Polarization* *Not Residual Polarization				Illumination Uniformity	
	Poladisk 0°		Poladisk 90°		No Poladisk	
	0°-90°	90°-180°	0°-90°	90°-180°	0°-90°	90°-180°
0	0.992	0.992	0.714	0.239	0.256	1.54
1	1.67	1.30	0.179	0.714	0.595	0.557
2	1.33	1.03	0.849	1.55	0.561	0.347
3	1.01	2.89	0.693	0.703	-	5.07
4	1.01	1.01	1.11	1.66	0.752	0.552
5	1.19	1.19	1.00	1.42	0.709	0.380
6	1.11	1.11	1.37	1.82	0.610	2.70
7	1.06	0.176	1.52	2.01	0.202	0.202
8	1.57	1.18	1.13	1.32	0.318	0.287
9	1.33	1.33	1.70	-0.852	0.000	0.106
10	0.331	0.331	1.89	1.89	-0.191	0.000
11	-1.83	-0.731	3.74	2.07	0.189	1.70

Table 3-13. Polarization Sensitivity Summary of Results, F104 (Expressed in Percent)

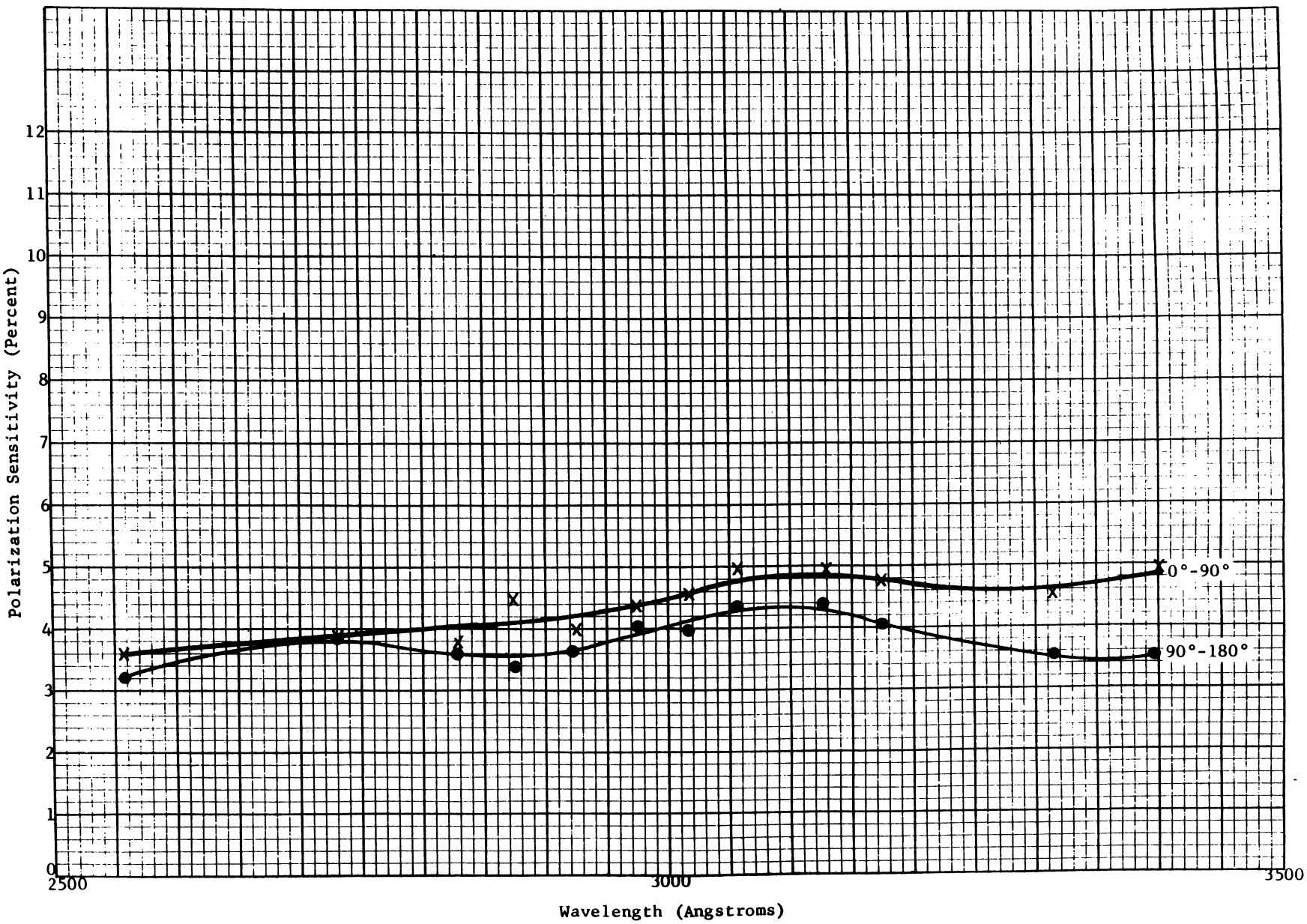

Figure 3-61. Polarization Sensitivity with Rotating Polarized Light Source (F104 Instrument)

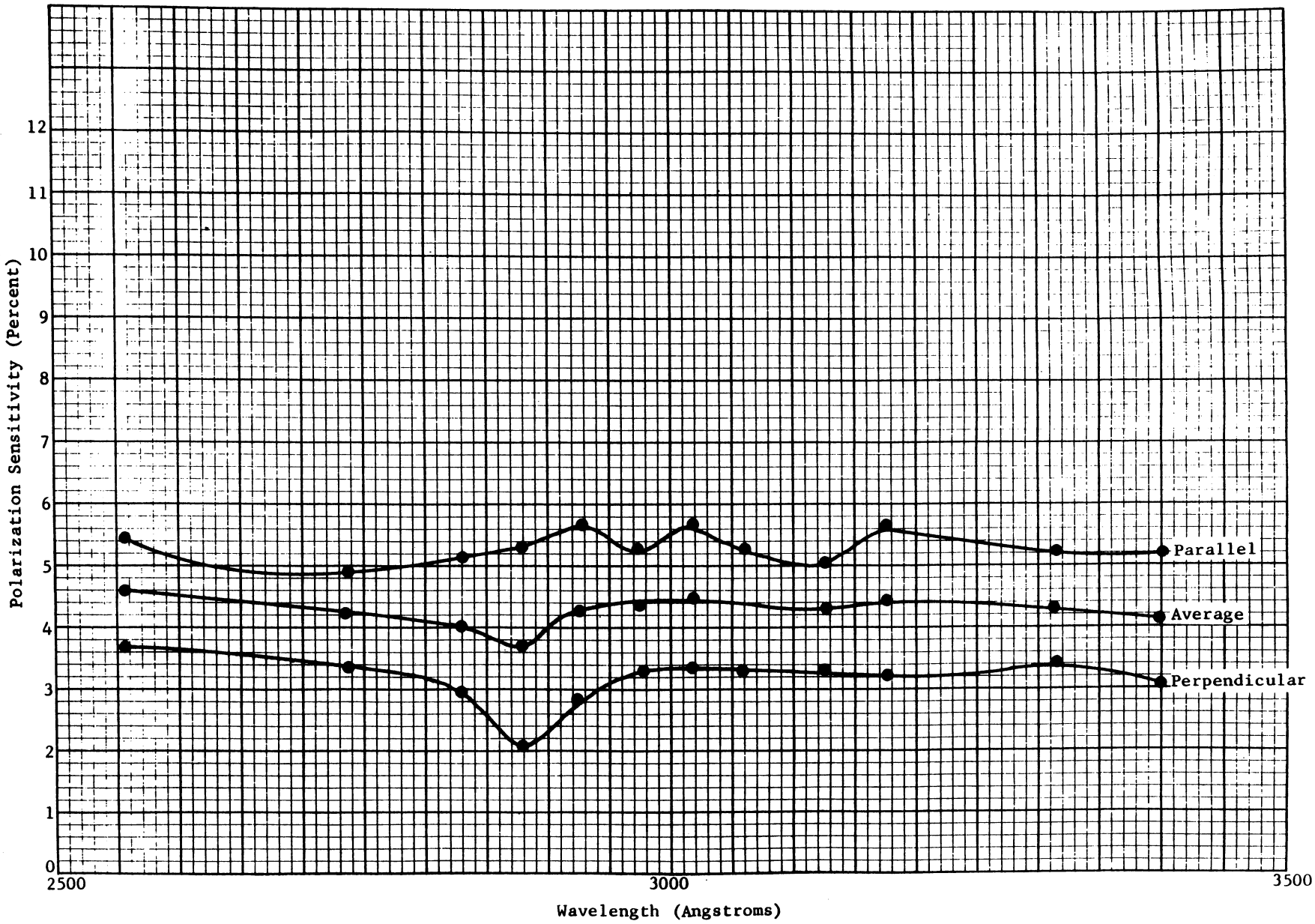

Figure 3-62. Polarization Sensitivity--Manual Poladisk Rotation (F104 Instrument)

would be expected in the results, and accordingly, most of the scatter is attributed to noise. The scatter is somewhat smaller at the center of the spectral internal than at the ends where the signal is smaller and the relative fluctuations are larger.

For simple internal consistency, the percentage polarization of the radiation is also determined by, $\frac{Imax - Imin}{Imax}$, in the same manner as the Polarization Sensitivity of the BUV. This also facilitates direct comparison of the characteristics of the radiation and of the Instrument. Because the radiation is almost completely depolarized, the more conventional measure of residual polarization is very nearly one-half the percentage polarization tabulated in the results.

Comparison of the averages of the manual checks with the results obtained with the lamp, plate, and polarizer rotated together shows good agreement between the methods. A further consistency check can be obtained by taking one-half the difference between the manual results for the two lamp-plate orientations which should be the polarization of the radiation from the $BaSO_4$ plate and comparing this to the values measured directly. Again, the agreement is good.

In general, the measurements were carefully made. The largest signals are obtained at the center of the wavelength region, and even here the signal will fluctuate about 1 percent due to noise. At larger and shorter wavelengths, the noise fluctuations may approach 3 percent. These fluctuations are on the order of the signal variations expected from rotating the source or polarizer. To insure good accuracy, each reading was taken as a visual average over a period of a minute or so of monitoring the signal level and its fluctuations. The monitoring was done only after allowing the lamp to equilibrate at each new orientation. No dark current correction was applied since dark current never amounted to more than 0.1 percent of the signal.

This multiplicative scale factor for P103 was determined empirically from measurements made on the corresponding F104 geometry (see Table 3-14 and Figure 3-63.) Additional measurements on the F104 Instrument values which were felt to be more reliable, and the single scale factor which adjusted the

Wavelength Step	60° Plate Filament Parallel to Slit (Percent)	45° Plate Filament Perpendicular to Slit (Percent)	Average (Percent)	Scaled Average (Percent)
00	0.63	4.18	2.41	3.13
01	0.72	4.24	2.48	3.22
02	0.97	5.01	2.99	3.89
03	1.19	4.89	3.04	3.95
04	1.19	5.31	3.25	4.24
05	1.12	5.53	3.33	4.33
06	1.03	5.36	3.20	4.16
07	1.09	5.27	3.18	4.14
08	0.96	5.37	3.17	4.13
09	0.98	5.41	3.20	4.16
10	0.98	5.70	3.34	4.34
11	1.78	6.99	4.43	5.75

Table 3-14. Polarization Sensitivity Summary of Results, F104 (Expressed in Percent)

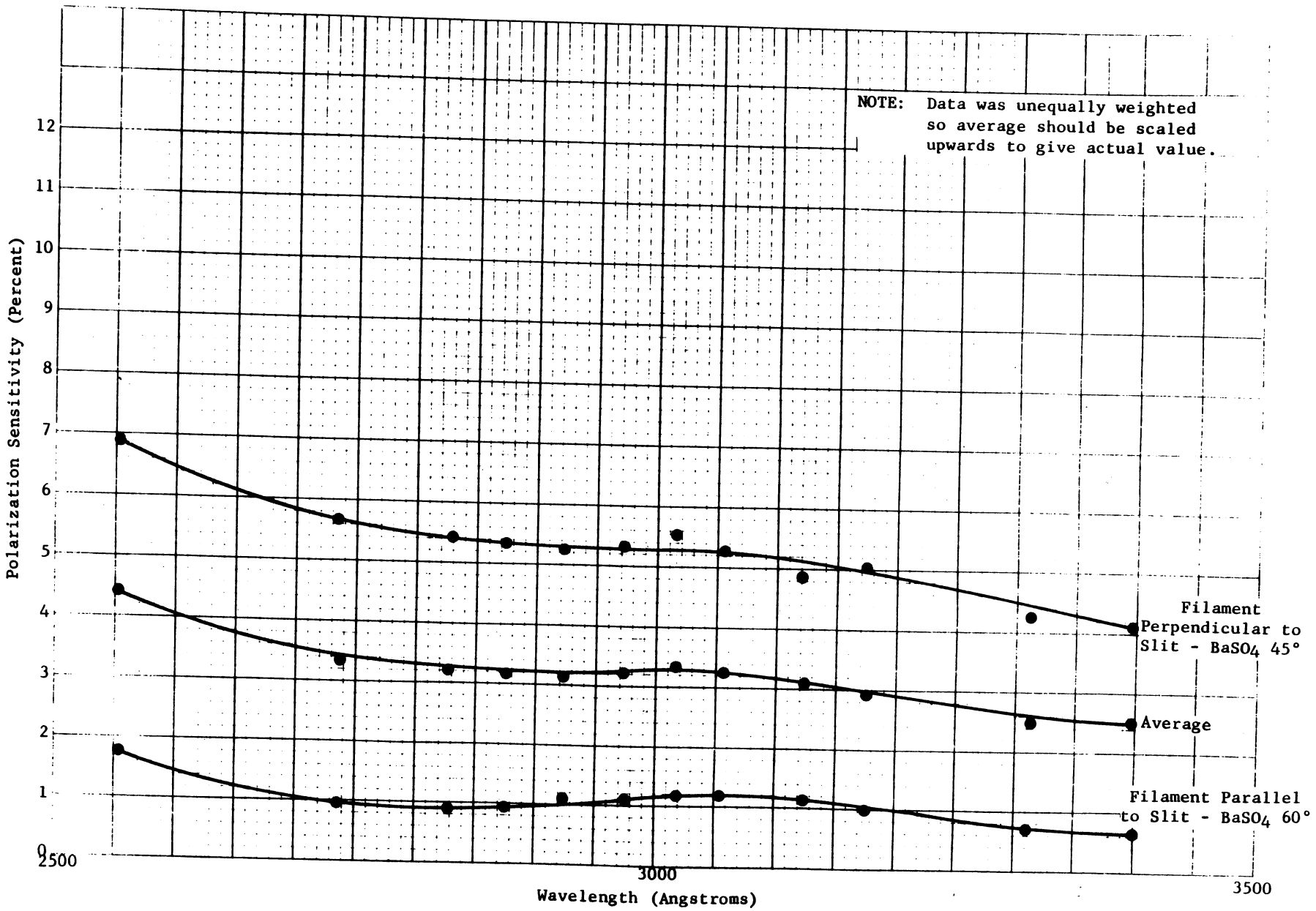

Figure 3-63. Polarization Sensitivity--Manual Data and Average (F104 Instrument)

unequally weighted data to give a best fit to the better data was determined. This scale factor was then applied to the P103 data to give the final value of the Polarization Sensitivity.

3.2.7 Filters

This section covers the interference filter employed in the photometer of the BUV. It was first contemplated to use a first-order interference filter and color glass filter blocking to isolate the 3800 Å wavelength for the photometer. However, none of the color glasses investigated withstood radiation exposure without degradation. The color glasses investigated are shown in Figures 3-64 and 3-65, before irradiation, and Figure 3-66 after irradiation, and the damage can easily be seen.

It was then anticipated to use color glass doped with cerium oxide. The transmission scans of the samples obtained are shown in Figures 3-67 and 3-68, before irradiation, and Figure 3-69, after irradiation. Again, this solution had to be abandoned due to the degradation of the transmission of the color glasses when exposed to irradiation.

A filter using first- and second-order interference stacks centered around the 3800 Å wavelength and deposited on the same substrate proved to be the final solution. The substrates were manufactured from SUPRASIL I, and after the interference stacks were deposited a cover glass of the same material was cemented onto the filter. The cement used resisted degradation due to irradiation and solarization exposure. This is verified in the scan from Figures 3-70 and 3-71.

Four of the interference filters were exposed to irradiation and solarization. The scans before and after these exposures are shown in Figures 3-72 through 3-76. Practically no degradation in the transmission was experienced. The sideband rejection of the filter was specified from 7500 Å to 1400 Å. The short wavelength transmission could be disregarded due to the absorption of the cement used while the long wavelength rejection specified at 3,000 to 1 was met, as shown in the scan in Figure 3-77. The filters used for installation in the P103 monochromator were not subjected to irradiation and solarization,

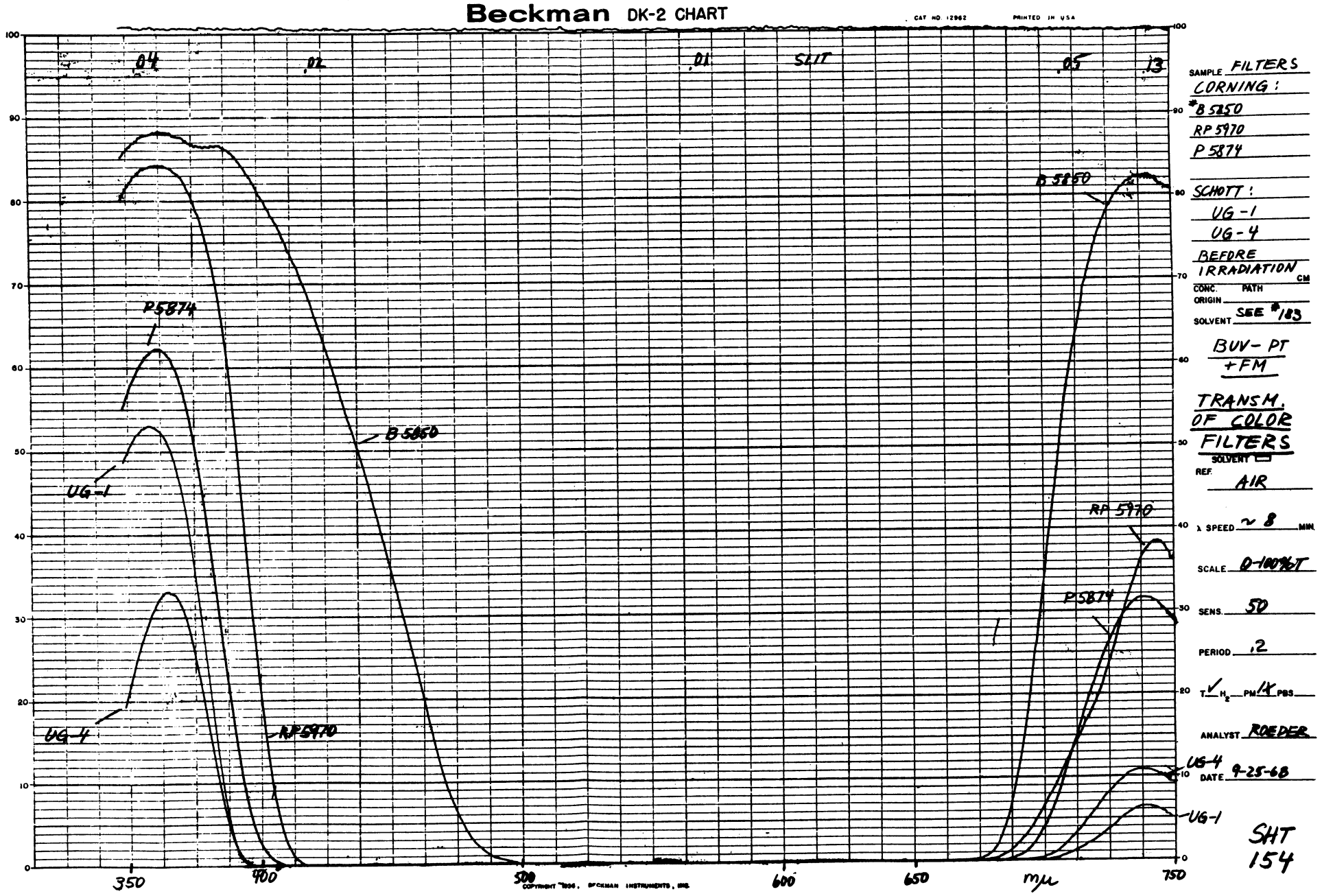

Figure 3-64. Percent Transmission of Corning Filters (Before Irradiation) (1 of 2)

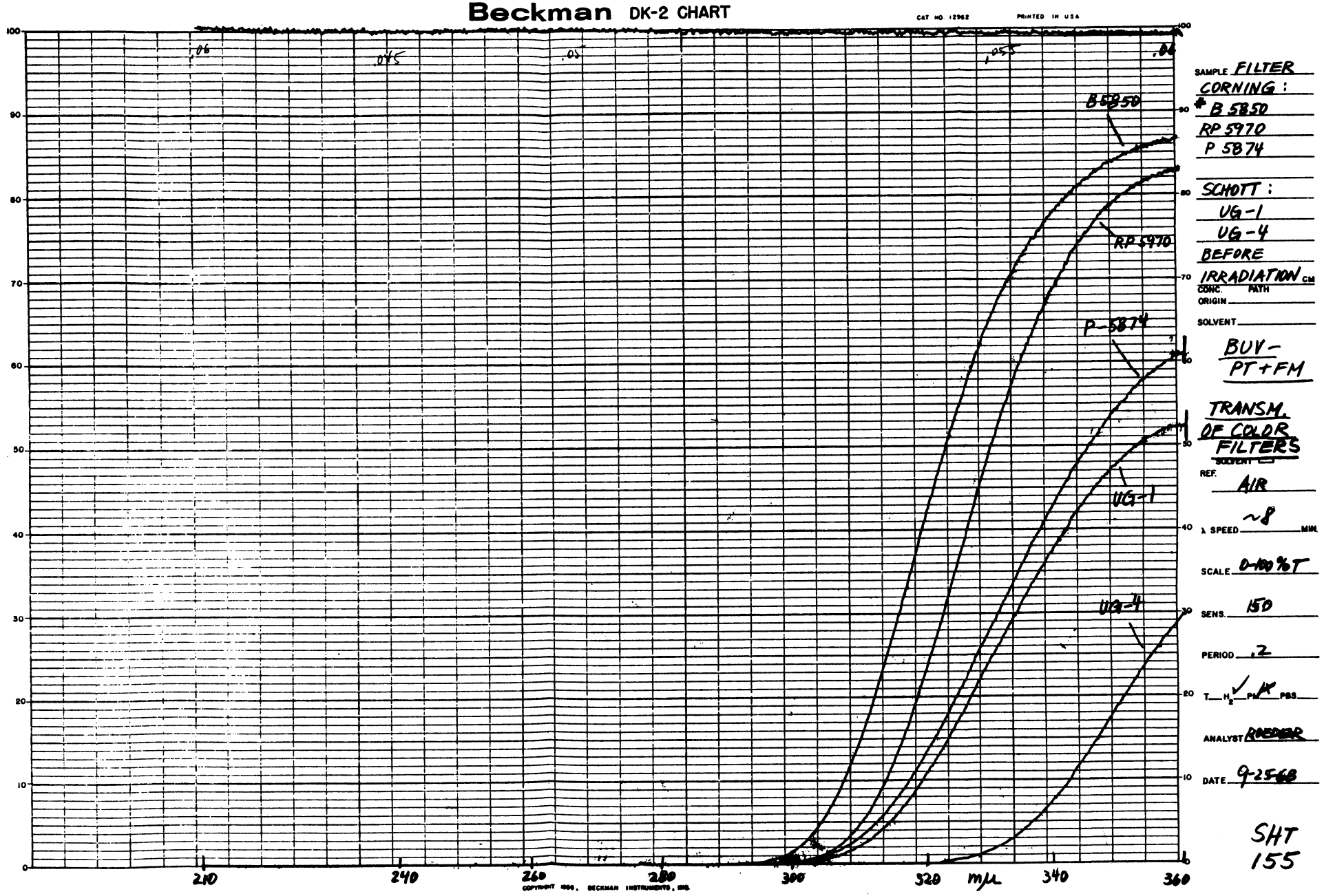

Figure 3-65. Percent Transmission of Corning Filters (Before Irradiation) (2 of 2)

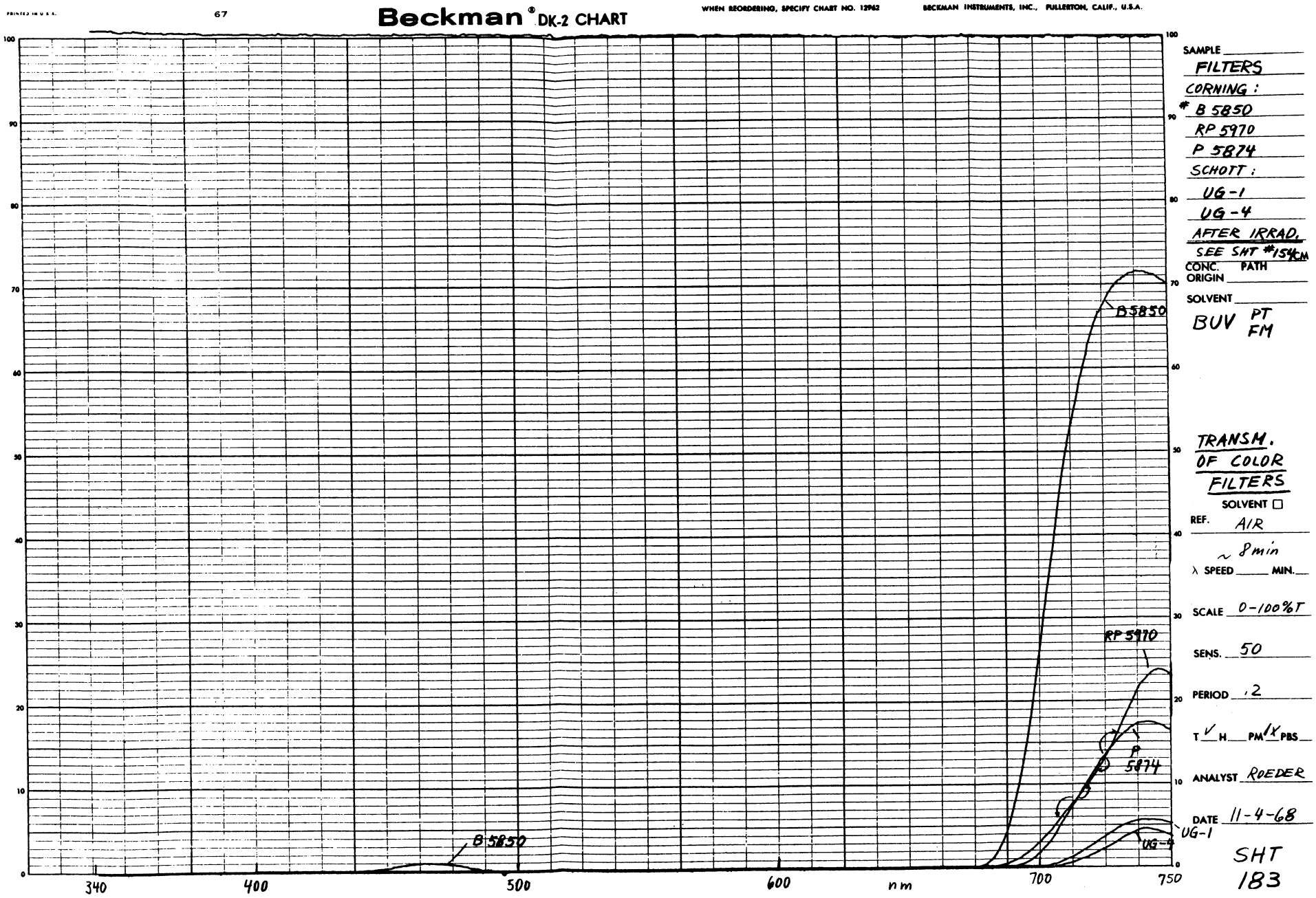

Figure 3-66. Percent Transmission of Corning Filters (After Irradiation)

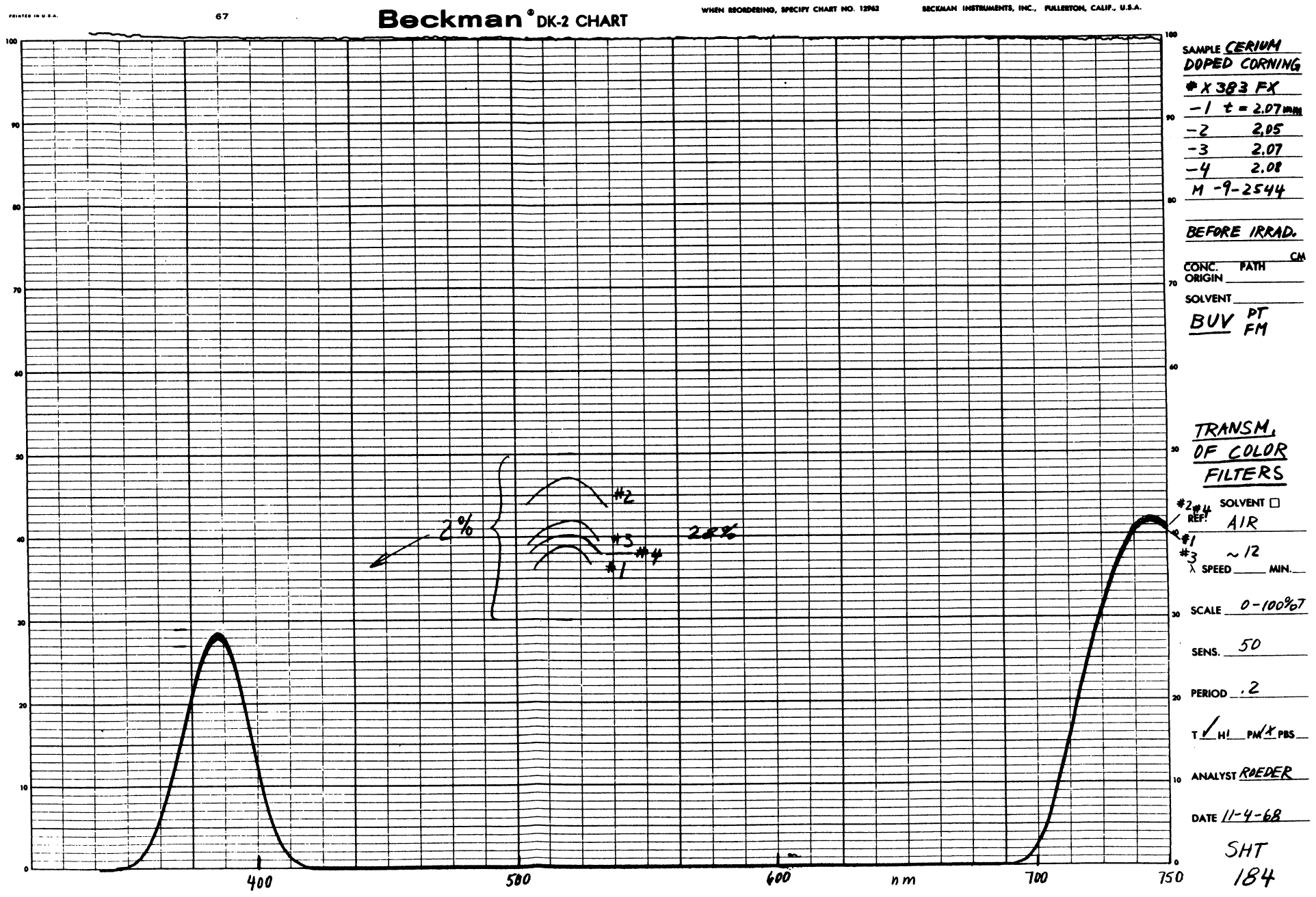

Figure 3-67. Percent Transmission of Cerium Doped Corning Filters (Before Irradiation) (1 of 2)

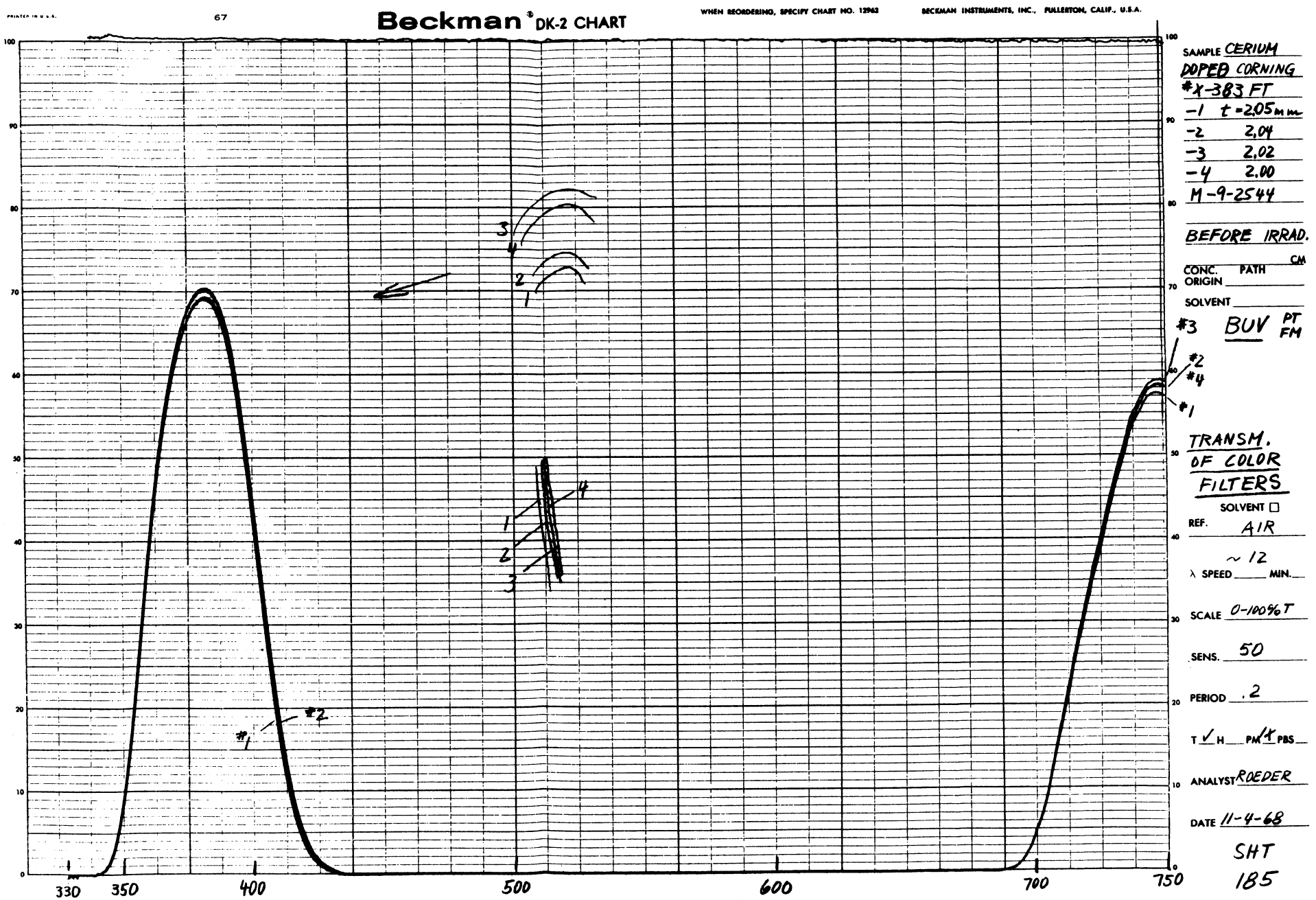

Figure 3-68. Percent Transmission of Cerium Doped Corning Filters (Before Irradiation) (2 of 2)

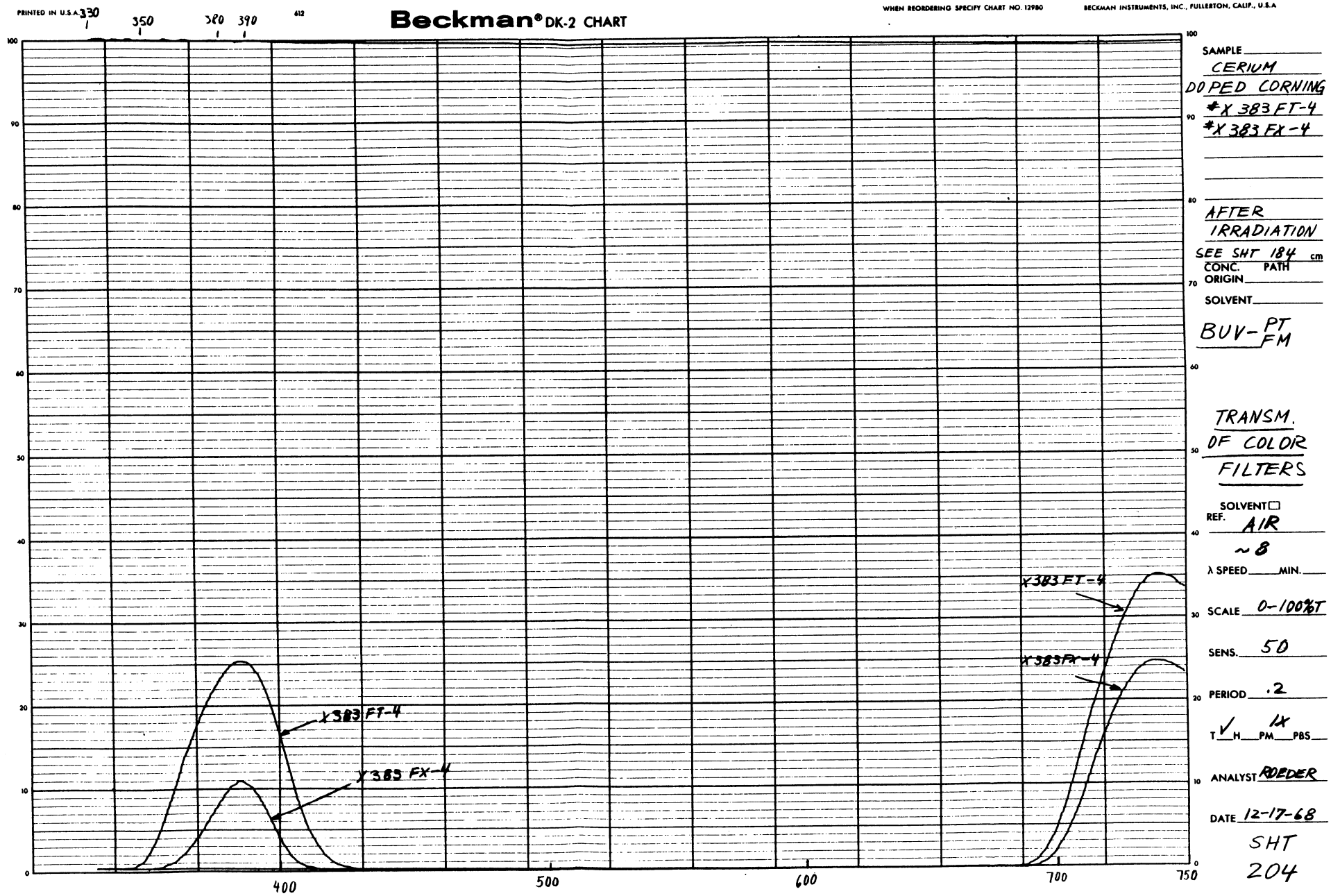

Figure 3-69. Percent Transmission of Cerium Doped Corning Filters (After Irradiation)

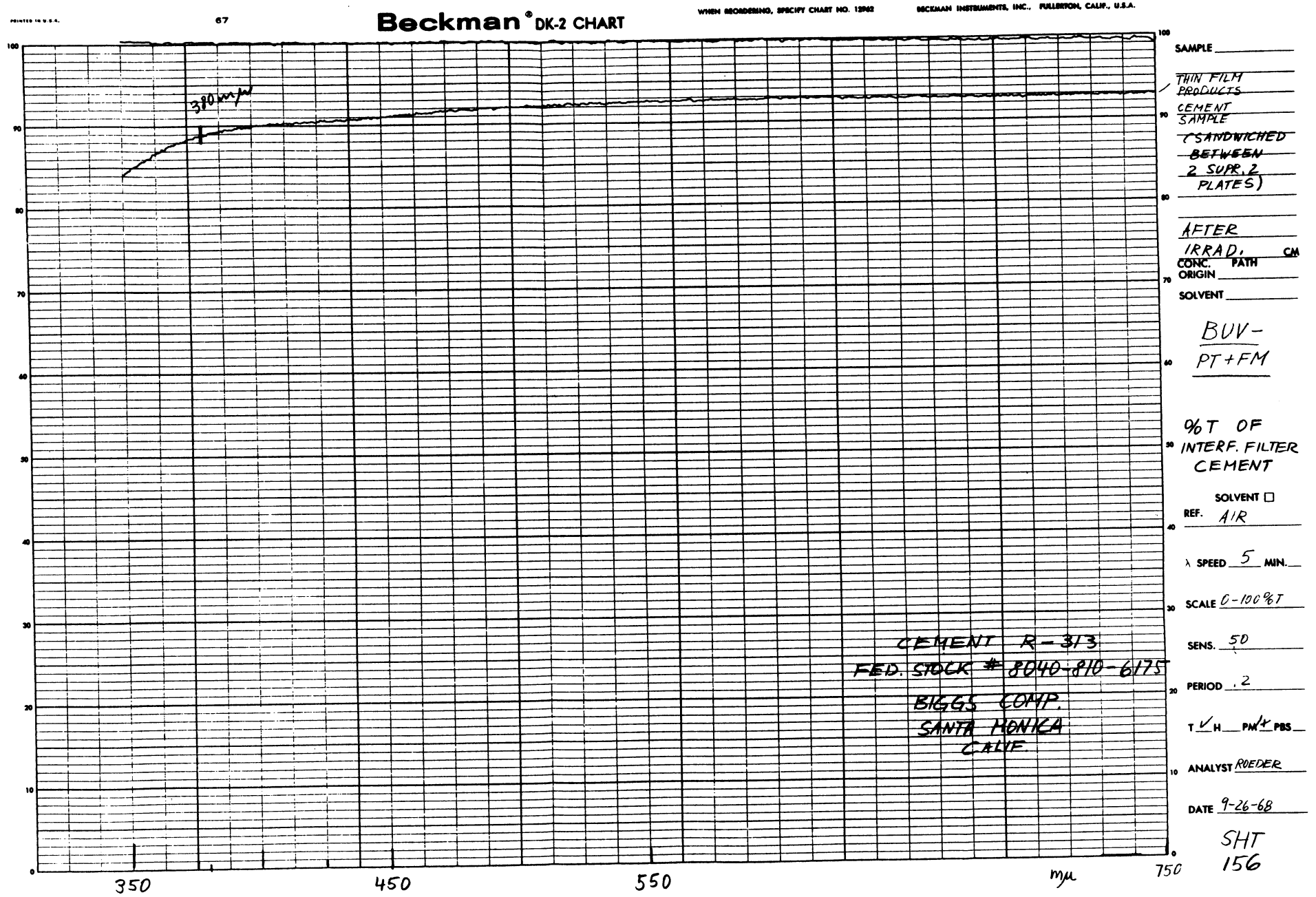

Figure 3-70. Percent Transmission of Interference Filter Cement (After Irradiation) (1 of 2)

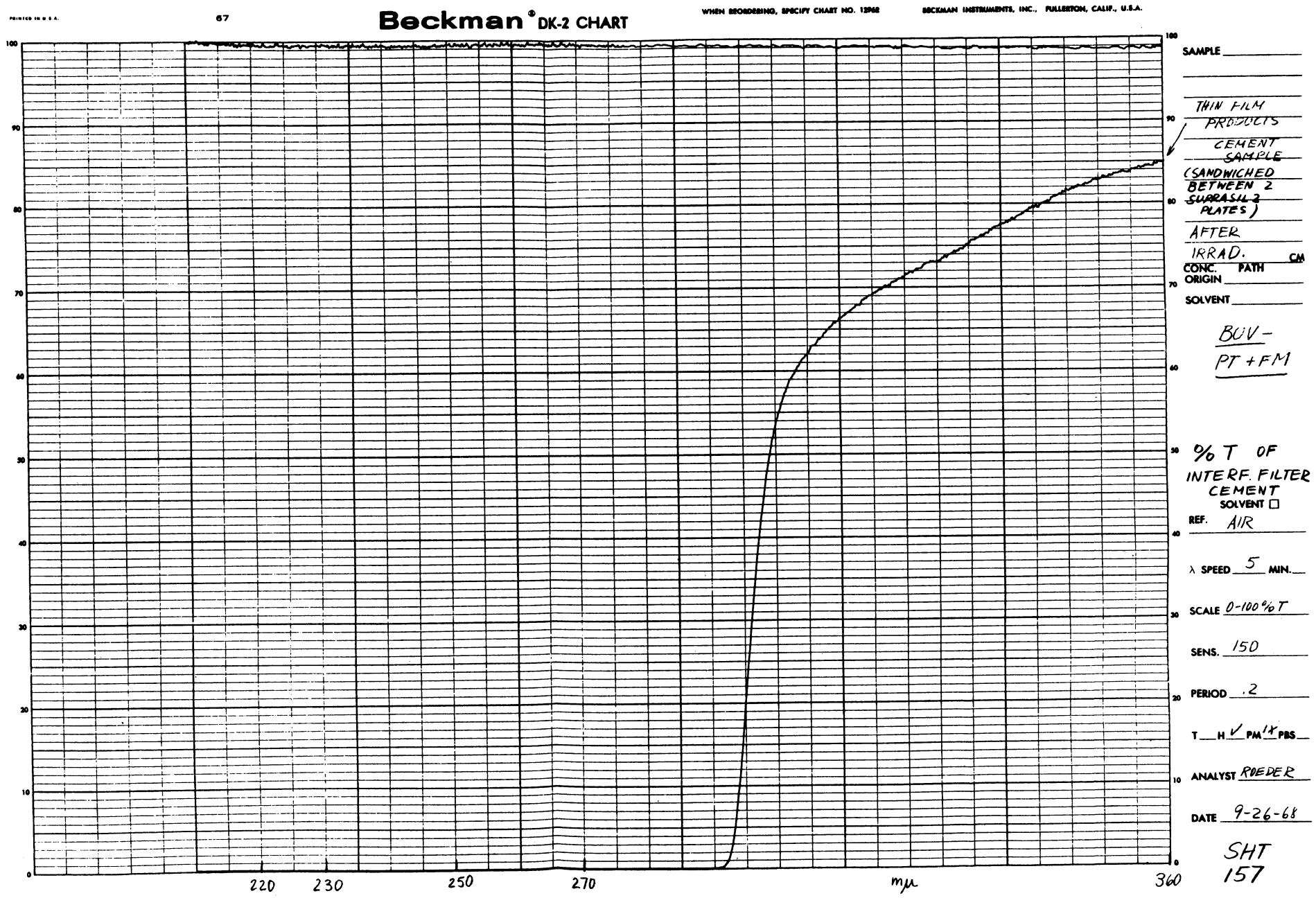

Figure 3-71. Percent Transmission of Interference Filter Cement (After Irradiation) (2 of 2)

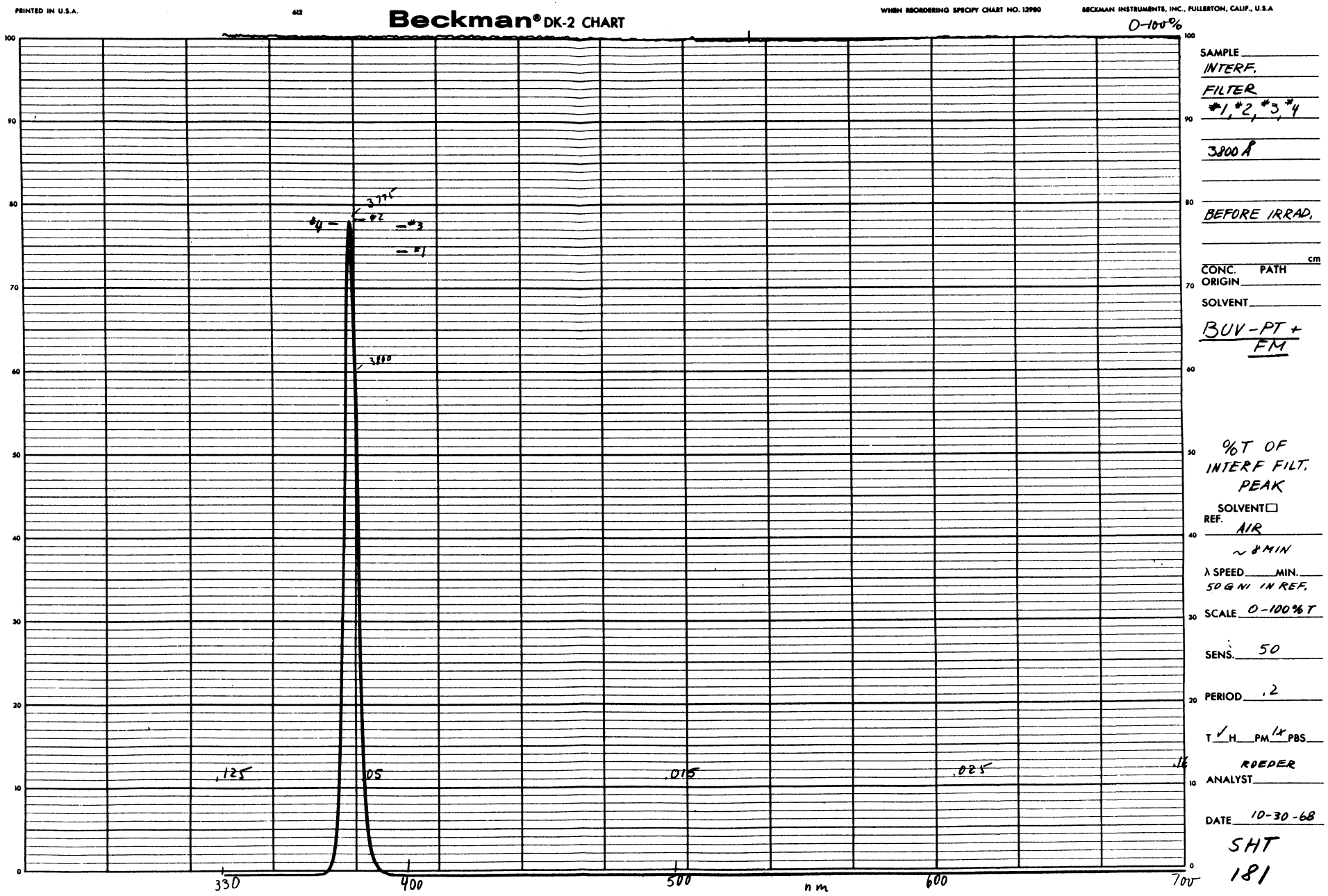

Figure 3-72. Percent Transmission of Interference Filter Peak (Before Irradiation)

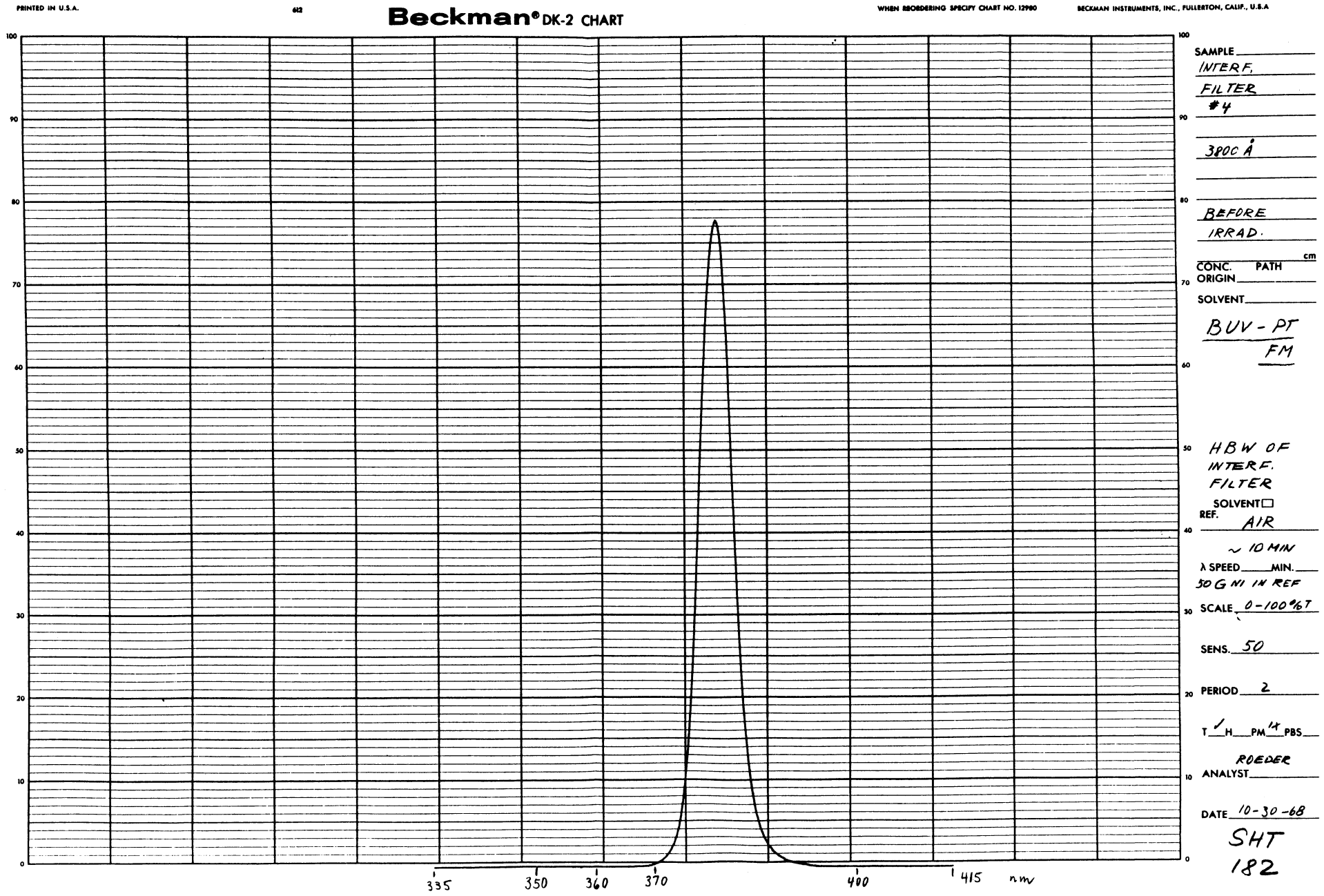

Filter 3-73. Half-Bandwidth of Interference Filter (Before Irradiation)

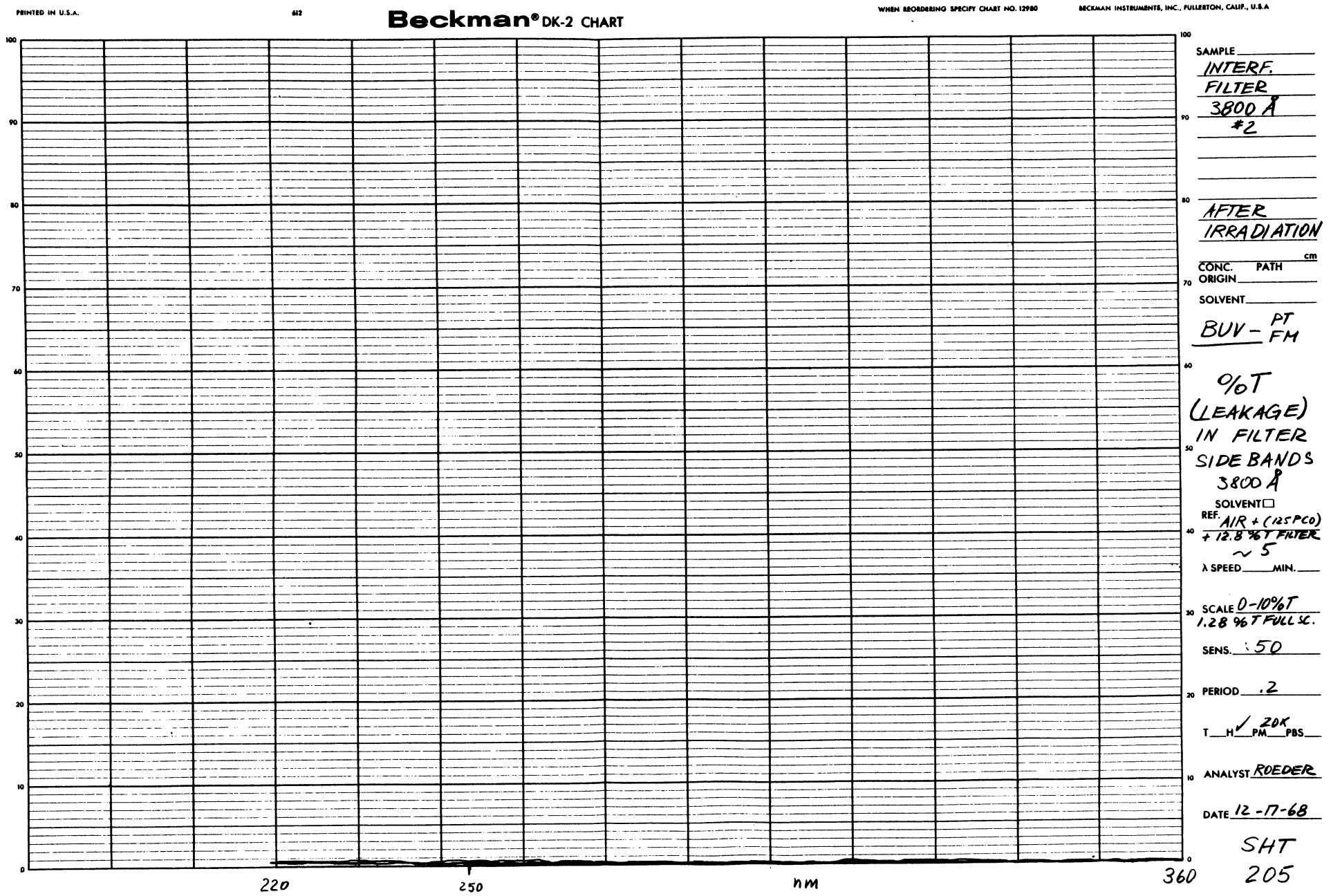

Figure 3-74. Percent Transmission (Leakage) in Filter Sidebands (After Irradiation)

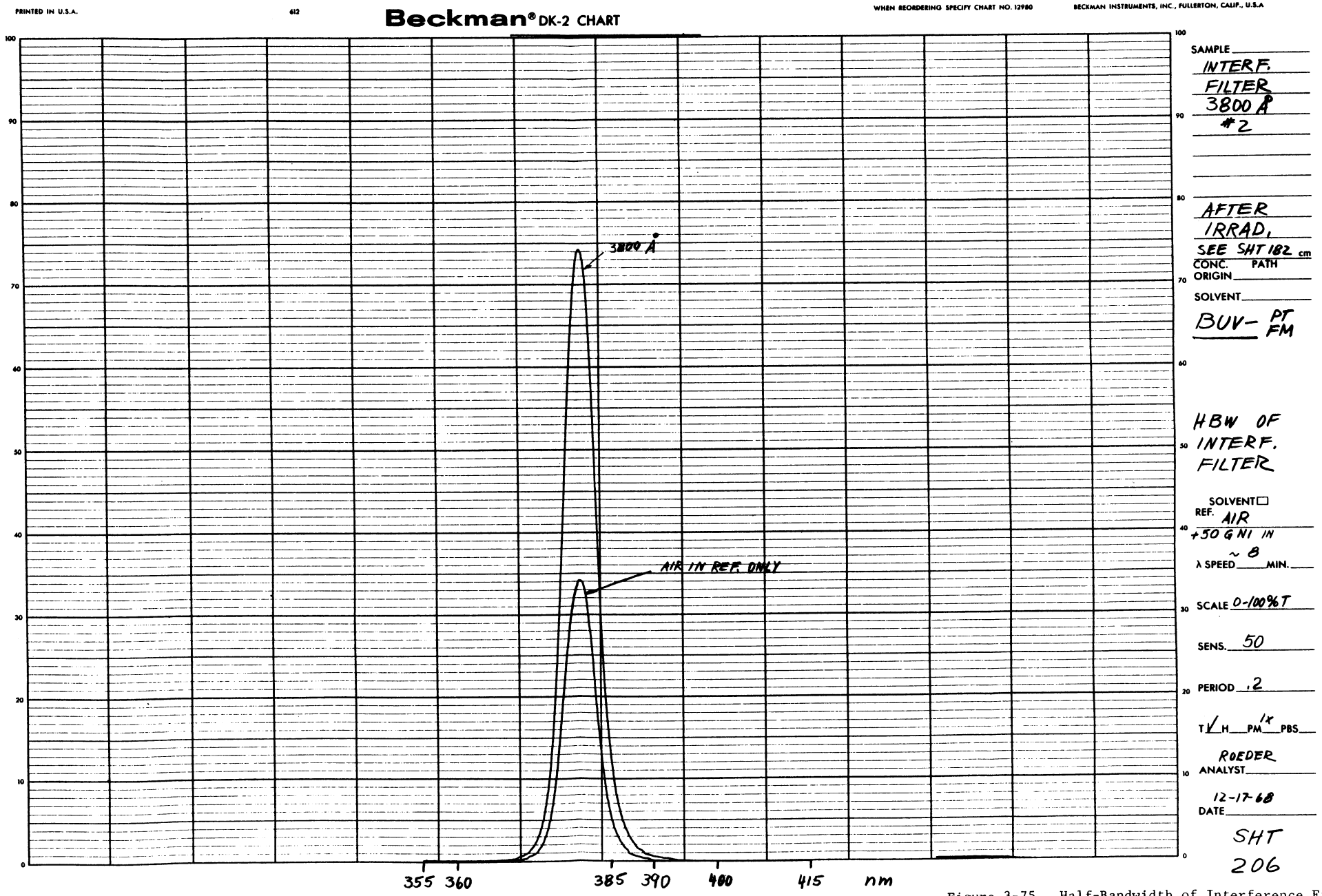

Figure 3-75. Half-Bandwidth of Interference Filter (After Irradiation)

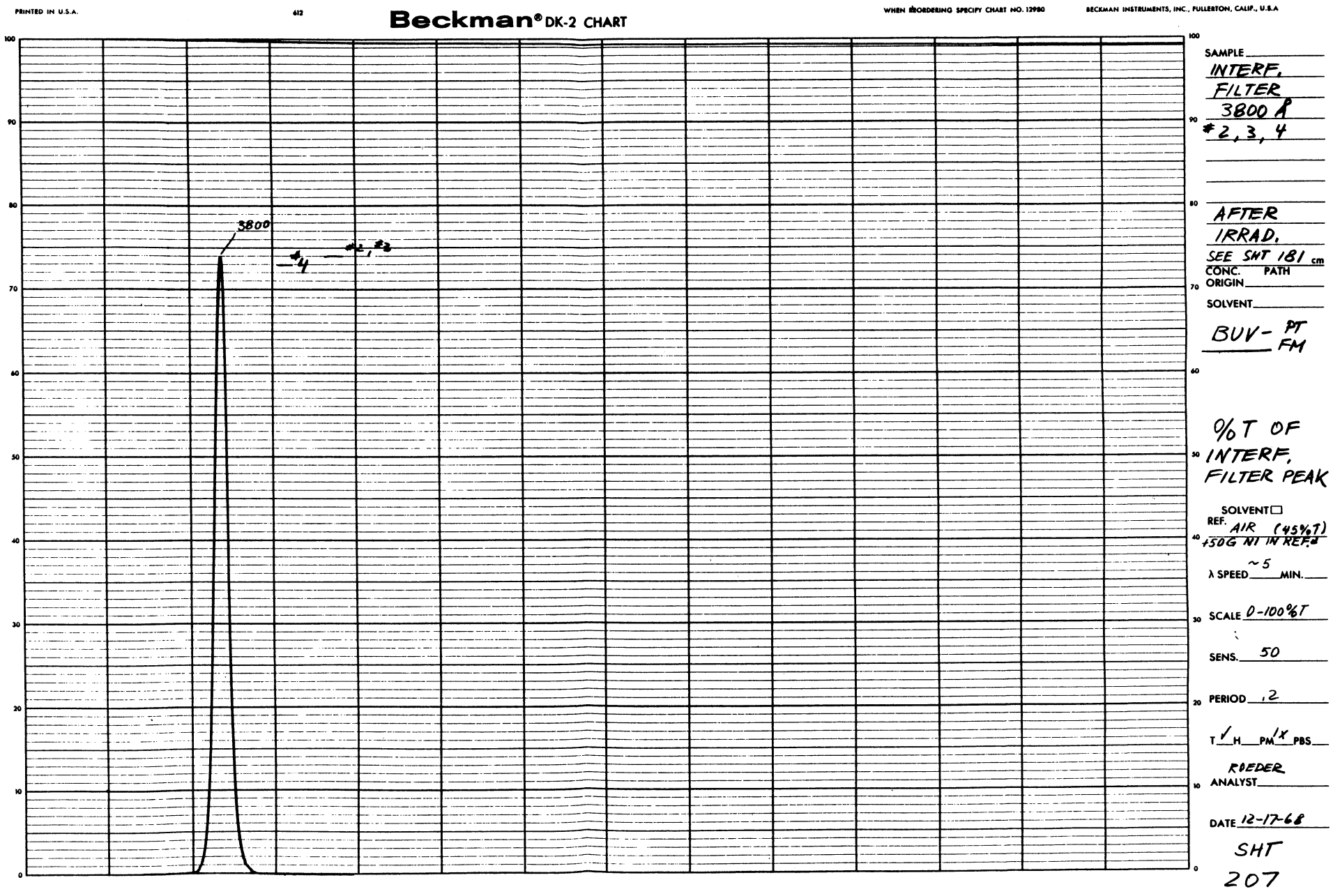

Figure 3-76. Percent Transmission of Interference Filter Peak (After Irradiation)

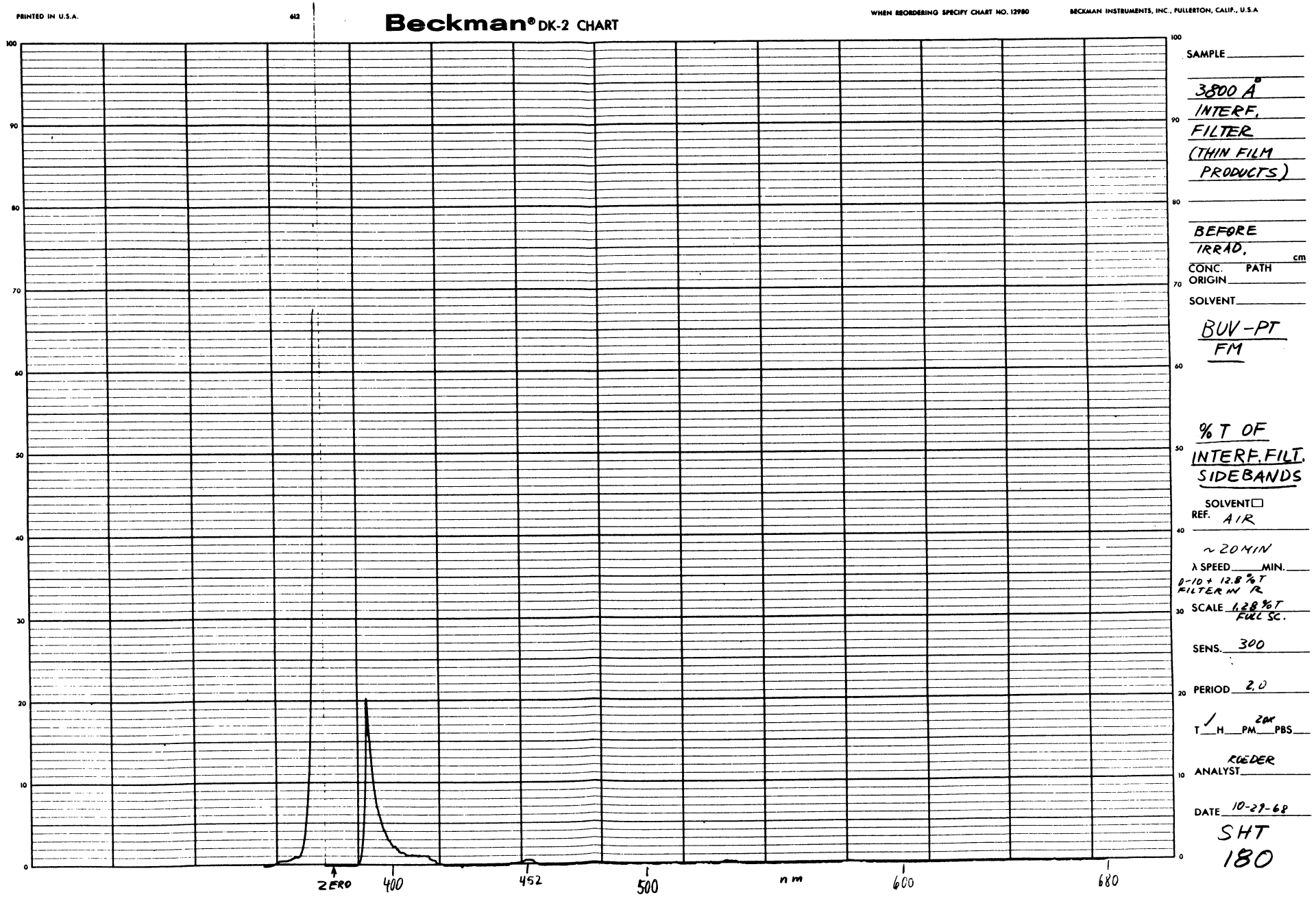

Figure 3-77. Percent Transmission of Interference Filter Sidebands (Before Irradiation)

and were selected from filters 5 to 10, the scans of which are shown in Figures 3-78 through 3-80. Selection of the final filters was also based on location of pinholes in the filters. The filters were selected in such a way that the pinholes were outside the transmission area of the filter.

3.2.8 Diffuser Plate ($BaSO_4$)

Several candidate materials were under consideration for the diffuser plate in the BUV Instrument. These plates are exposed to solarization and irradiation effects since they are located outside of the Instrument. Candidate materials were black Carrera, polished and ground; sandblasted aluminum and anodized aluminum; ground glass; white Carrera, polished and ground; magnesium oxide; Lucalox; and Barium Sulfate. All these materials were investigated for their reflectance characteristics and resistance to irradiation and solarization effects. The only material which proved to be satisfactory was Barium Sulfate ($BaSO_4$). Barium Sulfate stood up very well to the irradiation tests; however, it experienced some solarization damage (reflectance degradation) in the lower wavelength region of the instrument. A material which did not exhibit degradation to any of these destructive tests was sought. New materials considered were ground SUPRASIL fused silica plates; a special paint, potassium hexafluorotitanate; and aluminized ground aluminum plates. The fused silica plates were not considered strong enough to stand the vibration at launch, and the special paint exhibited an unwanted absorbtion at the lower wavelength range of the Instrument. This absorbtion is evident in scans 33 and 34 of Figure 3-81.

Figures 3-81 through 3-84 show the different reflection characteristics of the candidate materials.

The absolute measurements of several types of diffuser plates are performed on a specially modified DK-2A Spectroreflectometer which employs an end assembly with rotating instead of oscillating mirror. This keeps the image at the exit port of the $BaSO_4$ sphere perfectly stable. A special high-gain photomultiplier (RCA C70109) with 2-inch diameter cathode was used at 1500 V for all measurements.

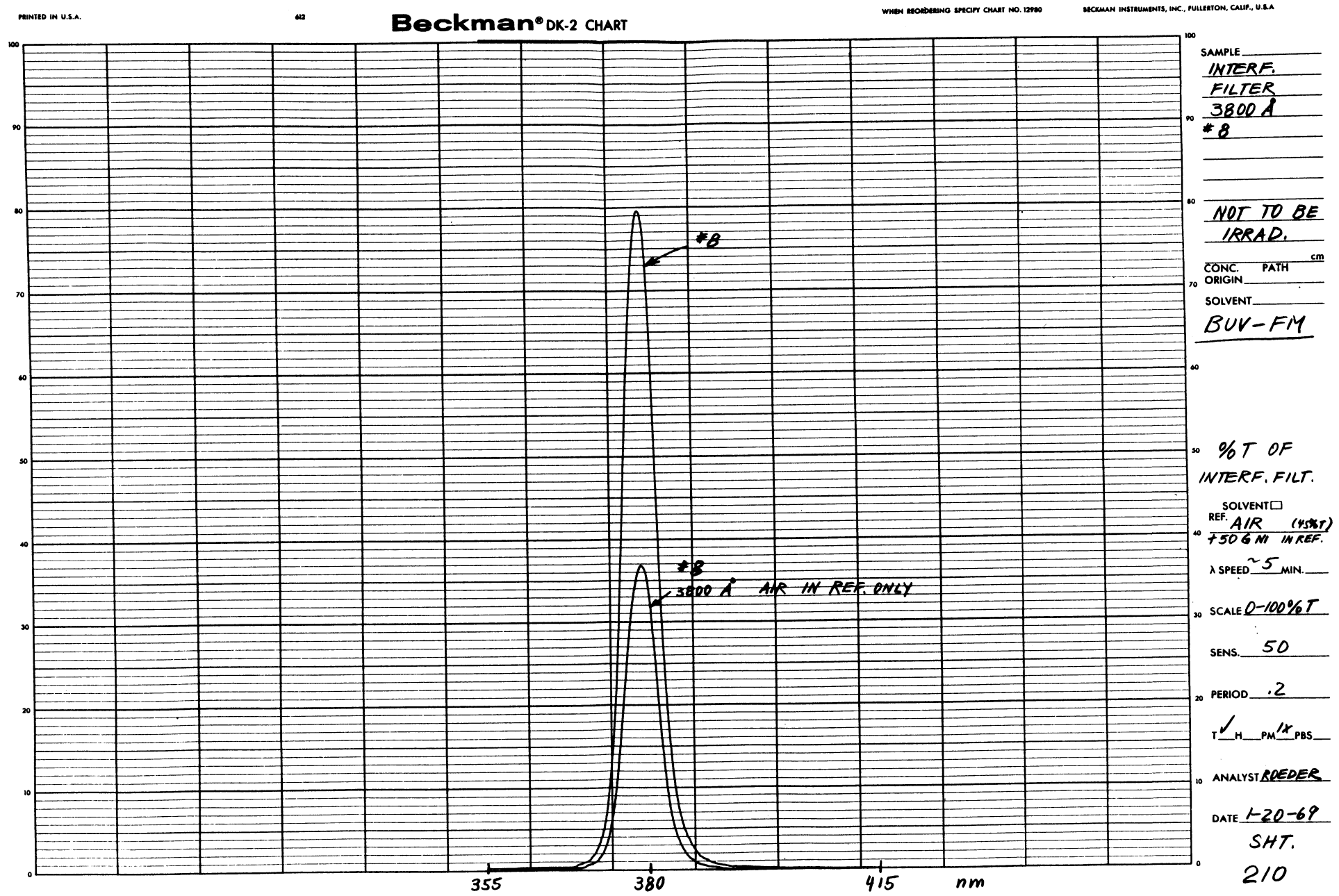

Figure 3-78. Percent Transmission of Interference Filters (No Irradiation) (1 of 3)

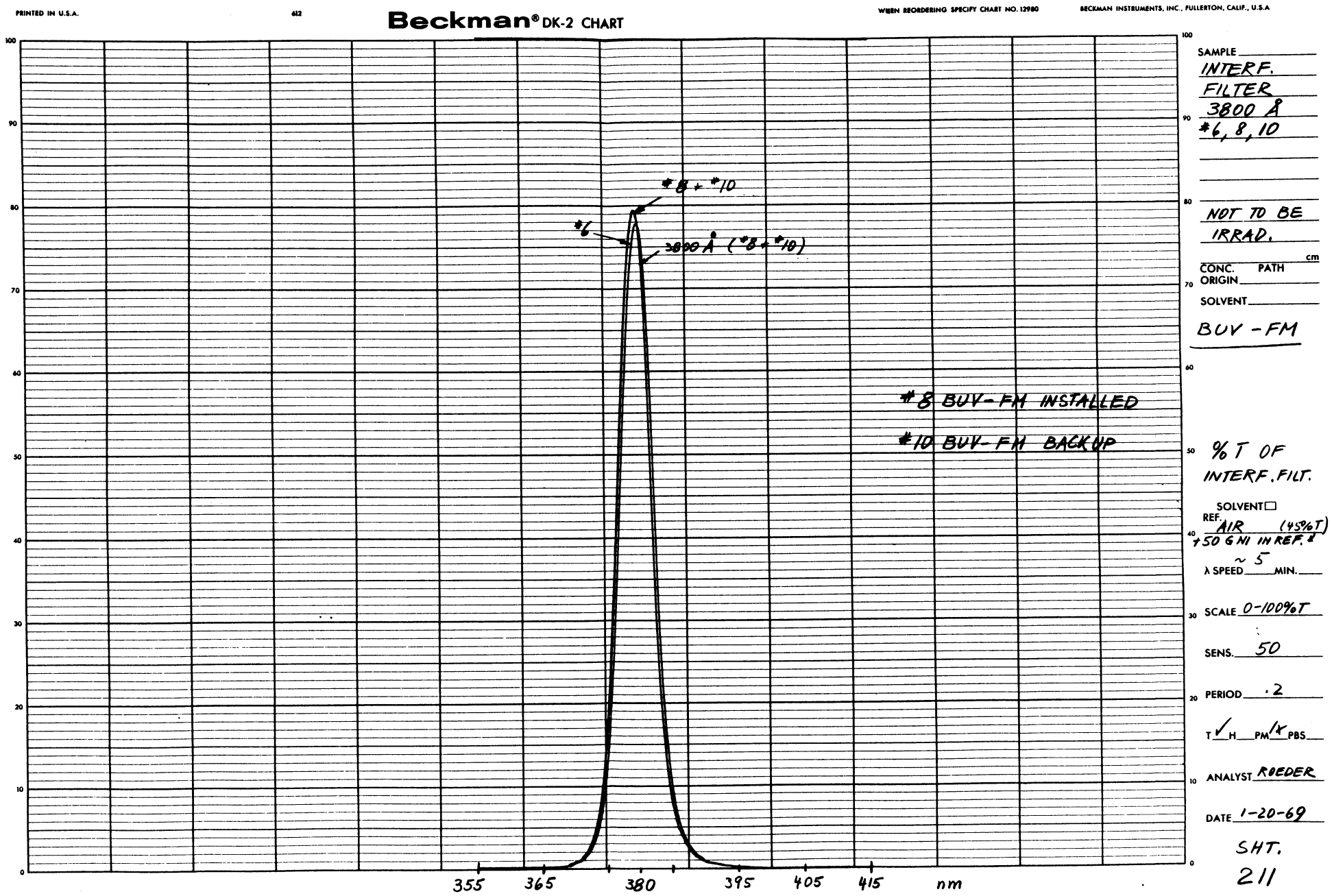

Figure 3-79. Percent Transmission of Interference Filters (No Irradiation) (2 of 3)

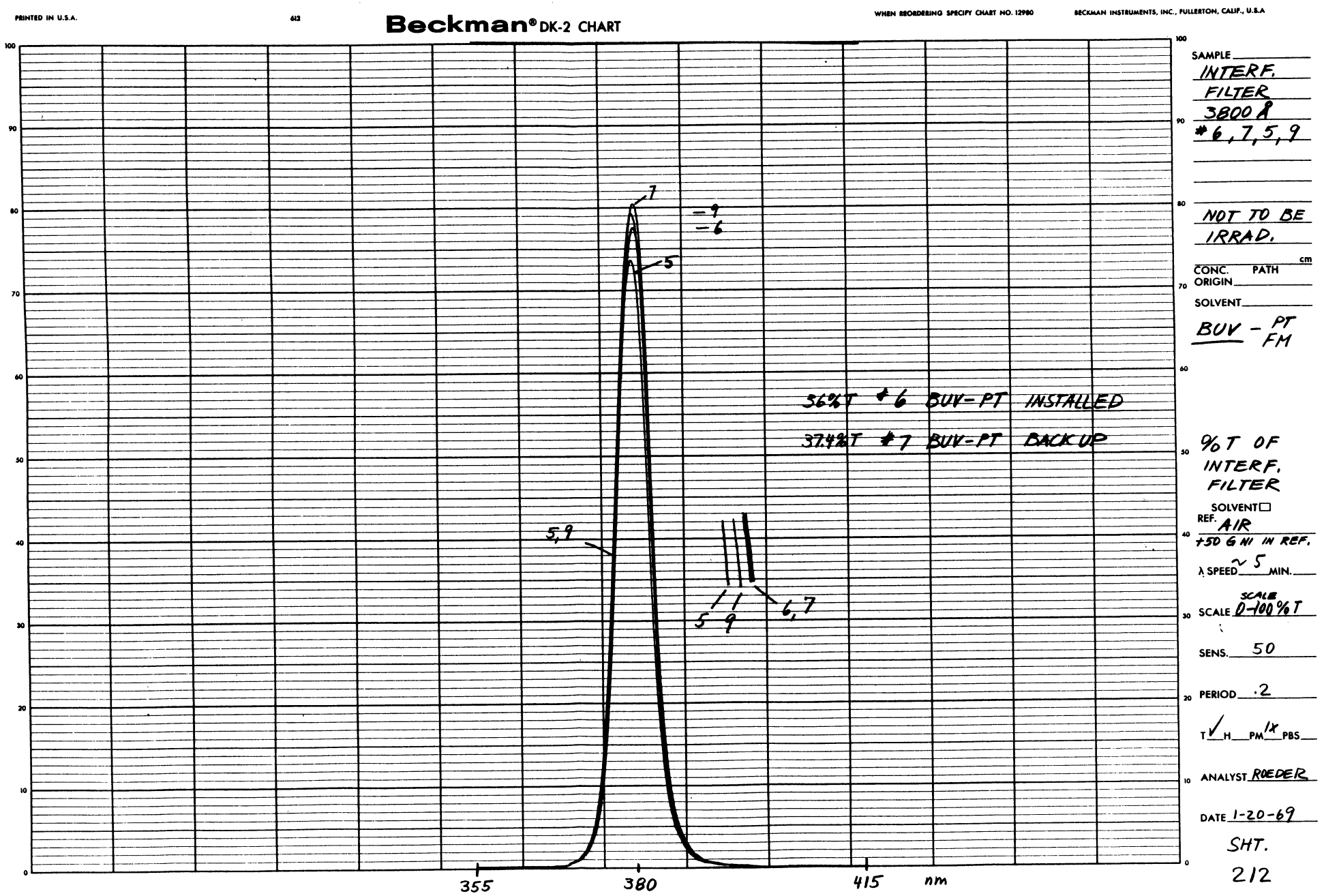

Figure 3-80. Percent Transmission of Interference Filter (No Irradiation) (3 of 3)

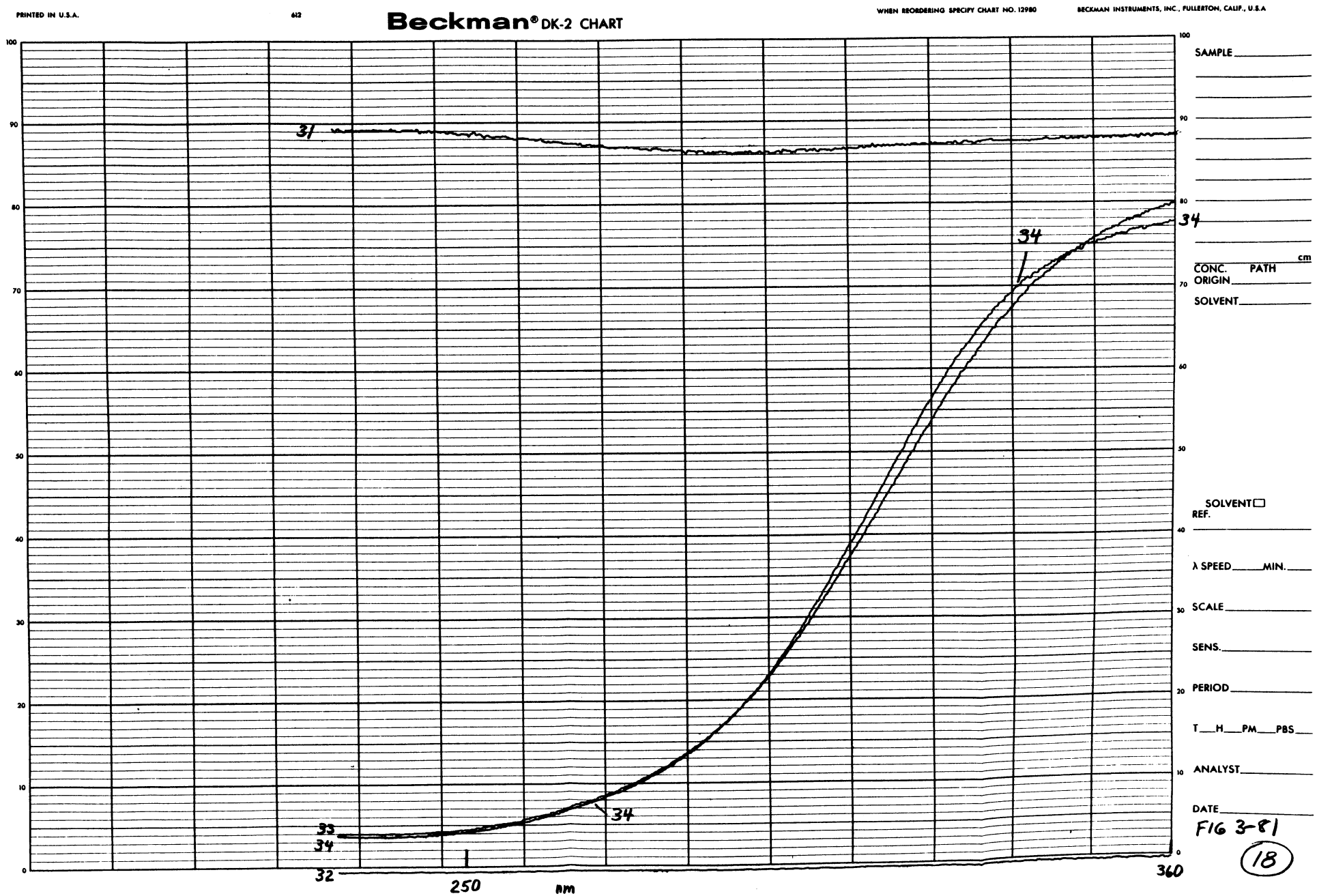

Figure 3-81. Reflection Characteristics (1 of 4)

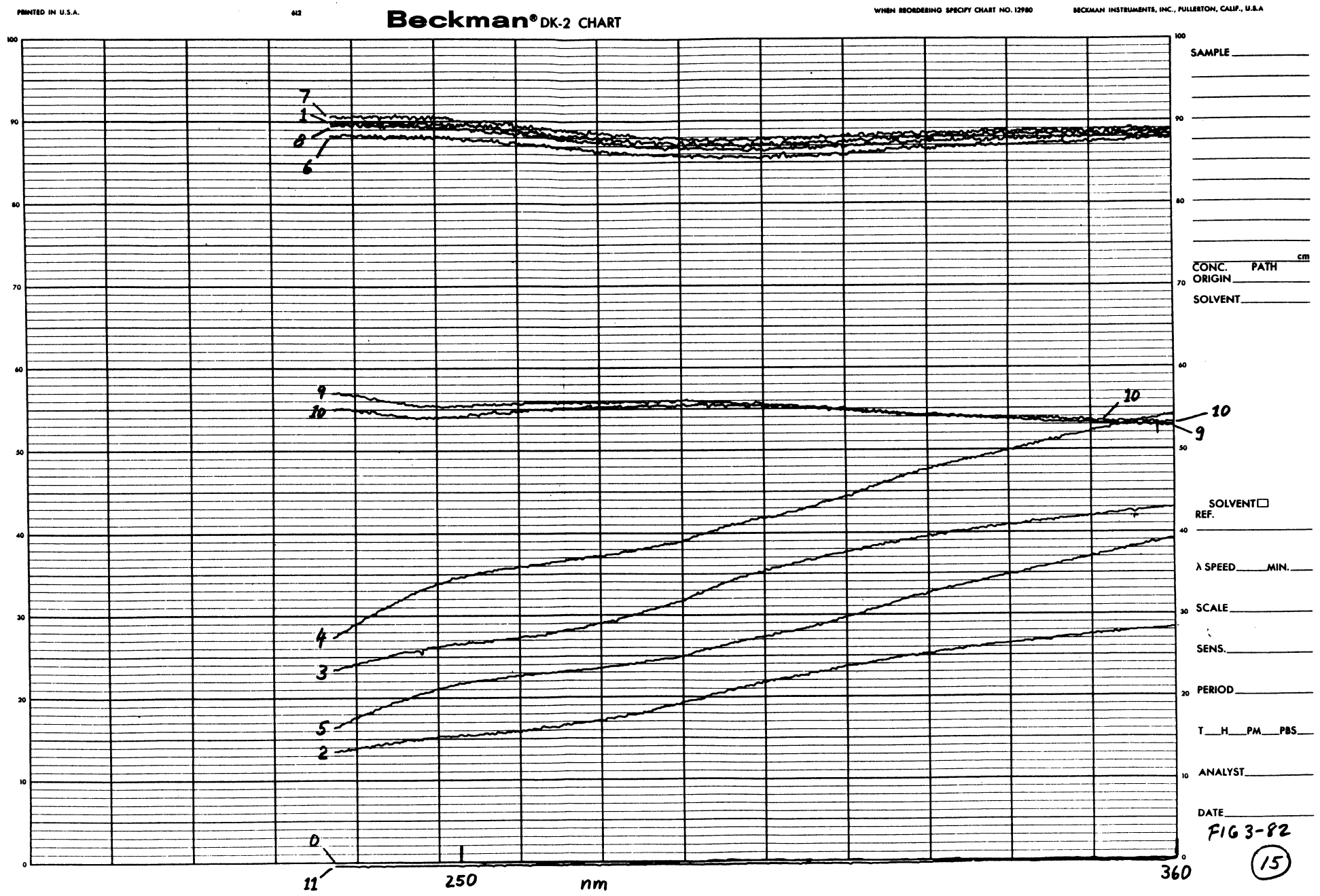

Figure 3-82. Reflection Characteristics
(2 of 4)

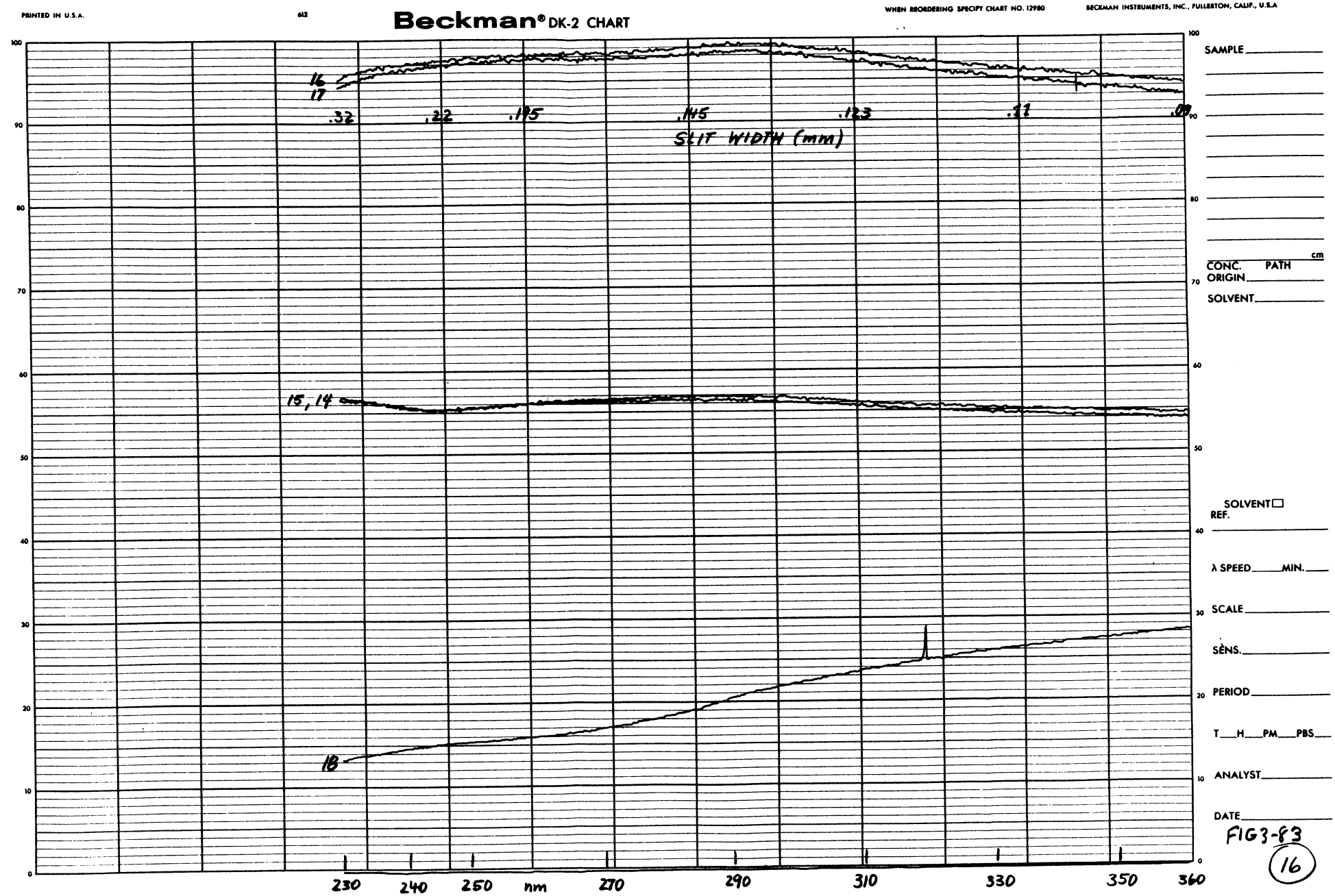

Figure 3-83. Reflection Characteristics (3 of 4)

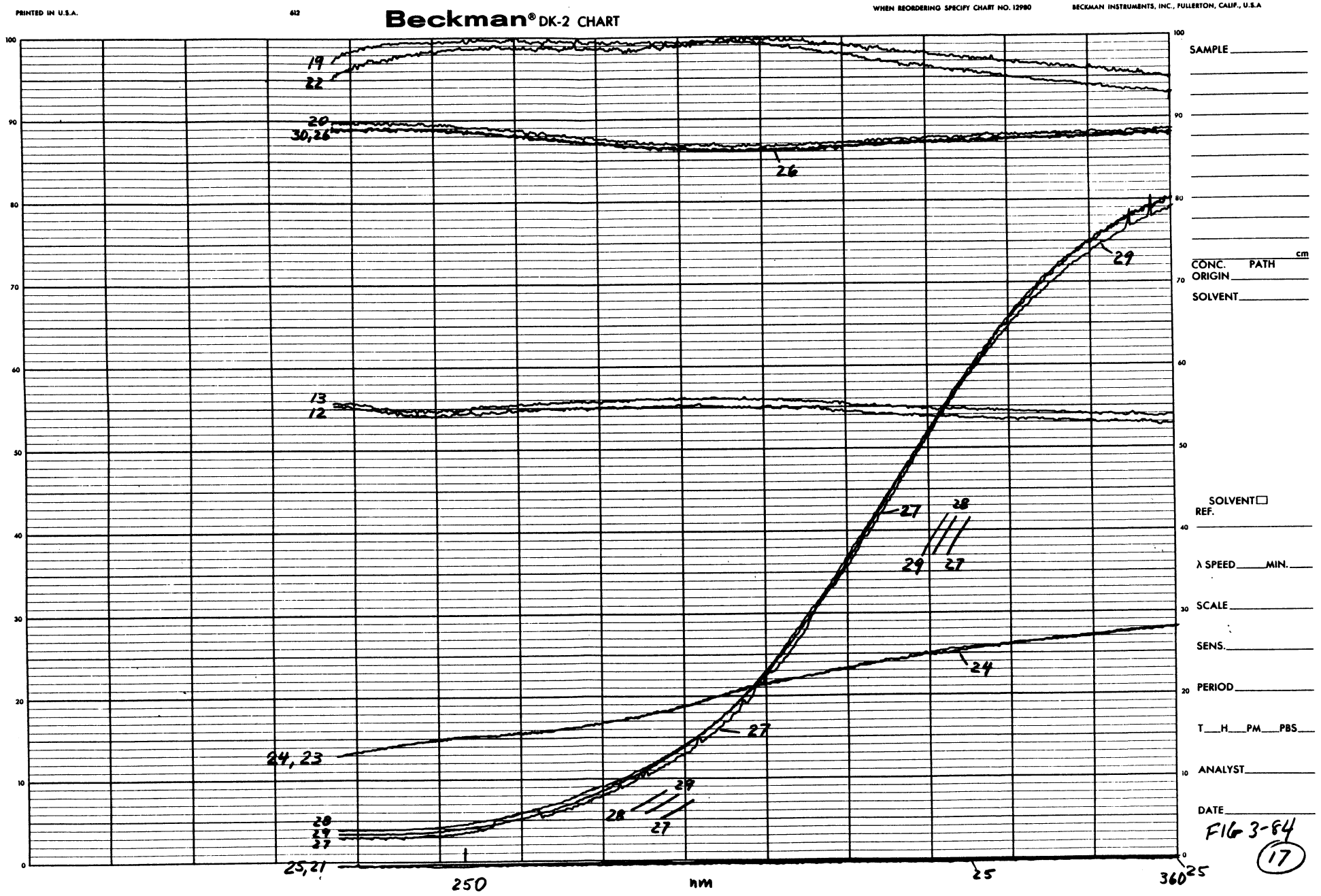

Figure 3-84. Reflection Characteristics (4 of 4)

From scan 8, all the samples are offset from the sphere by the thickness of the masking tape which prevents the active surface of the diffuser plates from touching the sphere. All scans are performed using the center of the sample plates unless noted otherwise in the Remarks column.

The aluminized aluminum diffuser plates are designated AAP No. 1 through No. 7, except for plate No. 3 which received a scratch and was not used. All scans are performed on the candidate final diffuser plates except where noted otherwise in the Sample column.

Conditions of Measurement Setup:

Reference Plate:	Aged $BaSO_4$ plate (10 months old)
100% Line:	Two aged $BaSO_4$ plates
Total & Diffuse Measurements:	No shift plates were used for any of the measurements in Ref. and Sample position
Scanning Speed:	5 min for each scan
Scale:	0-100 percent reflectivity
Sensitivity:	50
Period:	0.2
Source:	Hydrogen
Detector:	RCA C70109 at 1500 V and 20X gain
Reference:	The same aged $BaSO_4$ reference plate was used for all measurements
Analyst:	H. A. Roeder

Scans:

No.	Sample	Remarks	Date	Time
0	Zero line	$BaSO_4$ vs. $BaSO_4$	1-7-70	8:30
1	100% line	$BaSO_4$ vs. $BaSO_4$	"	8:40
2	$BaSO_4$ Sphere #1 Small Aperture	Centered in exit port	"	8:52
3	$BaSO_4$ Sphere #1 Large Aperture	" " " "	"	9:05
4	$BaSO_4$ Sphere #2 Large Aperture	" " " "	"	9:24

No.	Sample	Remarks	Date	Time
5	$BaSO_4$ Sphere #2 Small Aperture	Centered in exit port	1-7-70	9:39
6	100% line	Recheck, diff. area of $BaSO_4$ plate used	"	9:46
7	100% line	Recheck, another diff. area of $BaSO_4$ plate used	"	9:56
8	100% line	Recheck, same area of $BaSO_4$ plate used as in scan 1 but offset by thickness of tape	"	10:20
9	Aluminized alum. plate AAP #1		"	11:02
10	AAP #2		"	11:07
11	Zero Line	AAP #2 in sample port	"	11:11
12	AAP #4		"	11:30
13	AAP #5		"	11:35
14	AAP #6		"	11:42
15	AAP #7		"	11:46
16	BUV-FM P Plate		"	11:53
17	BUV-FM M Plate		"	12:00
18	$BaSO_4$ Sphere #1 Small Aperture	Recheck	"	12:11
19	BUV-PT M Plate		"	12:18
20	100% line	Same as scans 1 & 8	"	12:25
21	Zero Line	$BaSO_4$ in sample port (scan 20)	"	12:30
22	BUV-PT P Plate		"	15:10
23	$BaSO_4$ Sphere #1 Small Aperture	Recheck	"	15:16
24	$BaSO_4$ Sphere #1 Small Aperture	Recheck	1-8	10:15
25	Zero line		"	10:19
26	100% line	Recheck	"	10:25
27	Disregard--light leak		"	10:35
28	Paint Plate "5C" B		"	10:43
29	Paint Plate "5C" C		"	10:49

No.	Sample	Remarks	Date	Time
30	100% line	Recheck	1-8-70	11:02
31	100% line	Recheck	"	13:07
32	Zero line	Recheck	"	13:12
33	Paint disc (1" dia) 5C-2		"	13:16
34	Paint disc (1" dia) 5C-3		"	13:23

The final diffuser plate chosen was ground aluminum plate manufactured from 6061-T6 Aluminum machined out of the center section of 2-inch by 1/2-inch bar stock. The reason for this was because it was suspected that the oil embedded in the rolling process could not be adequately removed from the surface of the aluminum and would tend to darken under solarization.

The abrasive used to hand-grind the diffuser surface was 180 mesh (65 microns) aluminum oxide. The abrasive was washed in nitric acid to remove iron impurities. The 65-micron designation refers to an average particle size. The range of the particle sizes is actually 100 micron maximum to about 40 micron minimum. The grinding surface used was especially machined 6060-T6 aluminum surface which had 1/4 inch of the surface thickness removed. After the plates had been ground in the standard figure eight fashion, they were washed with distilled water. The plates were then coated with a high purity aluminum film approximately 1000 Å thickness. These plates experienced approximately 1 percent reflection degradation under irradiation and solarization. The absolute reflection of the plates is shown in Figure 3-85 and Table 3-15.

The BUV breadboard was used to make goniometric sensitivity measurements on the Barium sulfate plates, the aluminum plates, and specially painted plates. Graphs for these goniometric sensitivity characteristics are shown in Figures 3-86 through 3-89. Test setup and orientation drawings are shown in Figures 3-90 through 3-92.

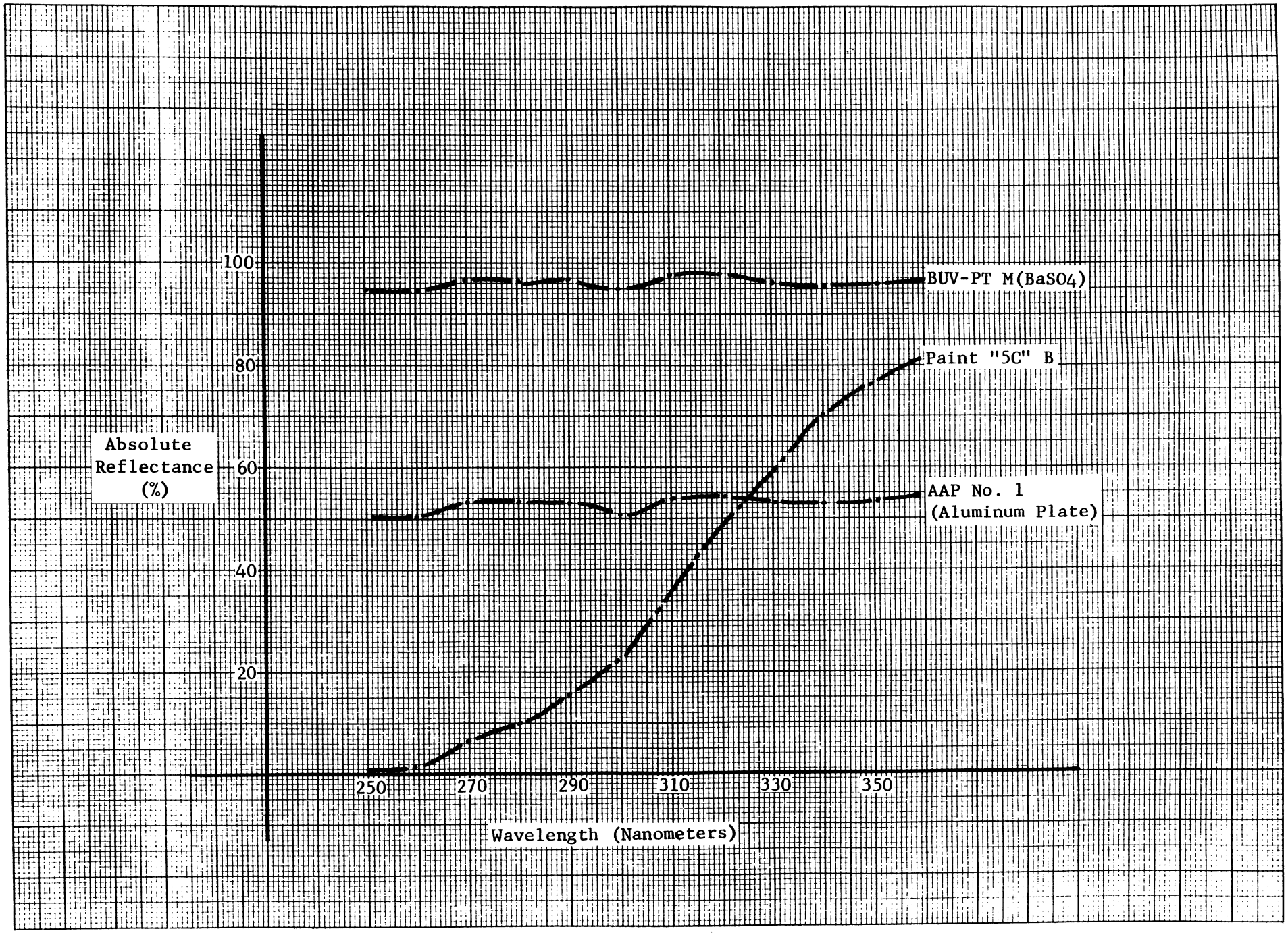

Figure 3-85. Absolute Reflectance of Diffuser

		λ_1	λ_2	λ_3	λ_4	λ_5	λ_6	λ_7	λ_8	λ_9	λ_{10}	λ_{11}	λ_{12}
	Alumin. Alum.	Refl.	Refl.	Refl.	Refl.	Refl.	Refl.	Refl.	Refl.	Refl.	Refl.	Refl.	Refl.
1)	AAP #1	51.0%	50.3%	53.4%	53.4%	53.7%	50.5%	54.0%	54.2%	53.1%	53.0%	53.4%	54.4%
2)	(9)	.555	.556	.558	.560	.558	.554	.549	.543	.540	.534	.533	.530
	AAP #2	49.5%	49.6%	52.9%	52.8%	53.4%	50.5%	54.0%	54.2%	53.1%	53.5%	53.4%	54.4%
	(10)	.540	.549	.553	.554	.555	.554	.549	.543	.540	.539	.533	.530
	AAP #4	40.0%	49.5%	52.6%	52.4%	53.0%	50.1%	53.5%	53.9%	52.7%	53.0%	53.1%	54.2%
	(12)	.545	.548	.550	.550	.551	.550	.544	.540	.536	.534	.530	.528
	AAP #5	50.0%	50.2%	53.4%	53.4%	53.9%	51.1%	54.5%	54.9%	53.6%	53.9%	54.1%	55.4%
	(13)	.545	.555	.558	.560	.560	.560	.554	.550	.545	.543	.540	.540
	AAP #6	51.0%	50.7%	53.9%	53.8%	54.5%	51.1%	54.6%	54.9%	53.9%	54.0%	54.2%	55.4%
	(14)	.555	.560	.563	.564	.566	.560	.555	.550	.548	.544	.541	.540
	AAP #7	51.0%	50.7%	53.9%	54.0%	54.7%	51.6%	55.1%	55.5%	54.4%	54.6%	54.9%	55.9%
	(15)	.555	.560	.563	.566	.568	.565	.560	.556	.553	.550	.548	.545
	$BaSO_4$ Plates												
	BUV-F104 M (7)	92.5%	92.5%	95.4%	95.4%	96.1%	93.1%	96.1%	96.0%	94.3%	94.2%	94.1%	94.4%
		.970	.978	.978	.980	.982	.980	.970	.961	.952	.946	.940	.930
	BUV-F104 P (16)	93.0%	92.7%	96.1%	96.0%	97.1%	94.1%	97.4%	96.9%	95.6%	95.6%	95.1%	95.7%
		.975	.980	.985	.986	.992	.990	.983	.970	.965	.960	.950	.943
	BUV-P103 M (19)	95.0%	94.3%	97.0%	96.6%	97.1%	94.5%	98.1%	97.9%	96.4%	96.2%	96.1%	96.4%
		.995	.996	.994	.992	.992	.994	.990	.980	.973	.966	.960	.950
	BUV-P103 P (22)	94.0%	93.3%	96.2%	96.4%	97.3%	94.1%	97.1%	96.4%	94.7%	94.1%	94.1%	94.4%
		.985	.986	.986	.990	.994	.990	.980	.965	.956	.945	.940	.930
	Paint Plates												
	"5C" B	0.5%	1.2%	6.6%	9.9%	15.4%	21.6%	36.1%	48.9%	59.6%	70.1%	76.6%	81.9%
	(28)	.050	.065	.090	.125	.175	.265	.370	.490	.605	.705	.765	.805
	"5C" C	-0.5%	0.2%	5.6%	8.9%	14.4%	20.6%	35.1%	48.4%	59.6%	68.6%	75.6%	80.9%
	(29)	.040	.055	.080	.115	.165	.255	.360	.485	.605	.690	.755	.795
	"5C" 2	0.5%	1.4%	6.2%	9.5%	15.9%	21.6%	37.7%	51.7%	62.1%	71.6%	77.6%	81.9%
	(33)	.050	.067	.086	.121	.180	.265	.386	.518	.630	.720	.775	.805
	"5C" 3	0.1%	0.7%	6.2%	9.5%	15.9%	21.6%	39.1%	54.4%	64.6%	72.6%	76.6%	79.6%
	(34)	.046	.060	.086	.121	.180	.265	.400	.545	.655	.730	.765	.782
1)	AUX.SPH.	.220	.222	.262	.279	.314	.311	.368	.390	.396	.410	.424	.444
2)	#1; (3)	.265	.275	.286	.305	.335	.360	.377	.391	.405	.414	.423	.430
	Change	-.045	-.053	-.024	-.026	-.021	-.049	-.009	-.001	-.009	-.004	+.001	+.014

1) Absolute value = original value + difference of (absolute value of auxillary sphere less original value of auxillary sphere)

2) Original value as recorded on DK runs

Table 3-15. Absolute Reflectance Diffuser

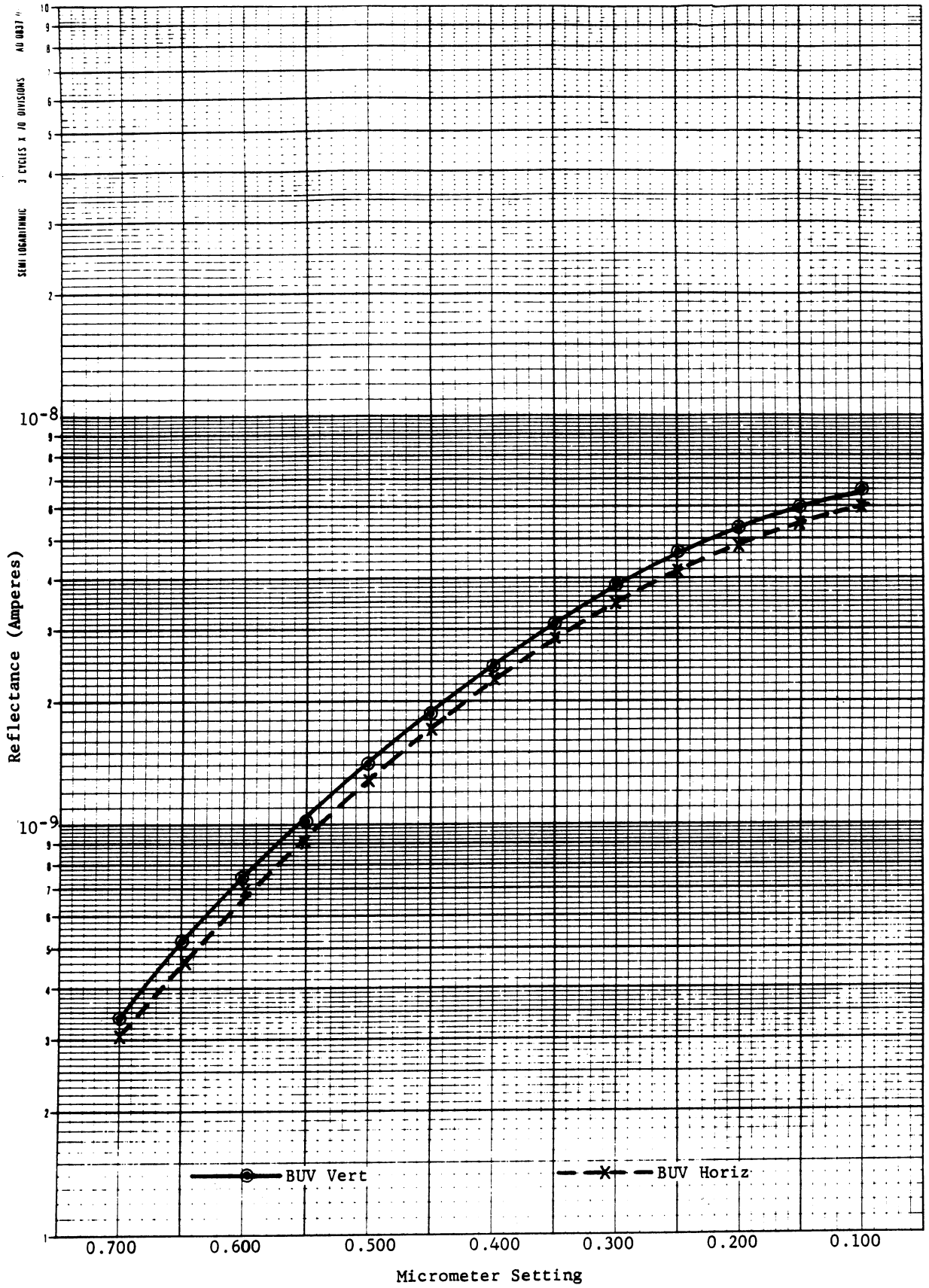

Figure 3-86. Aluminum Diffuser Plate Reflectance vs. Wavelength

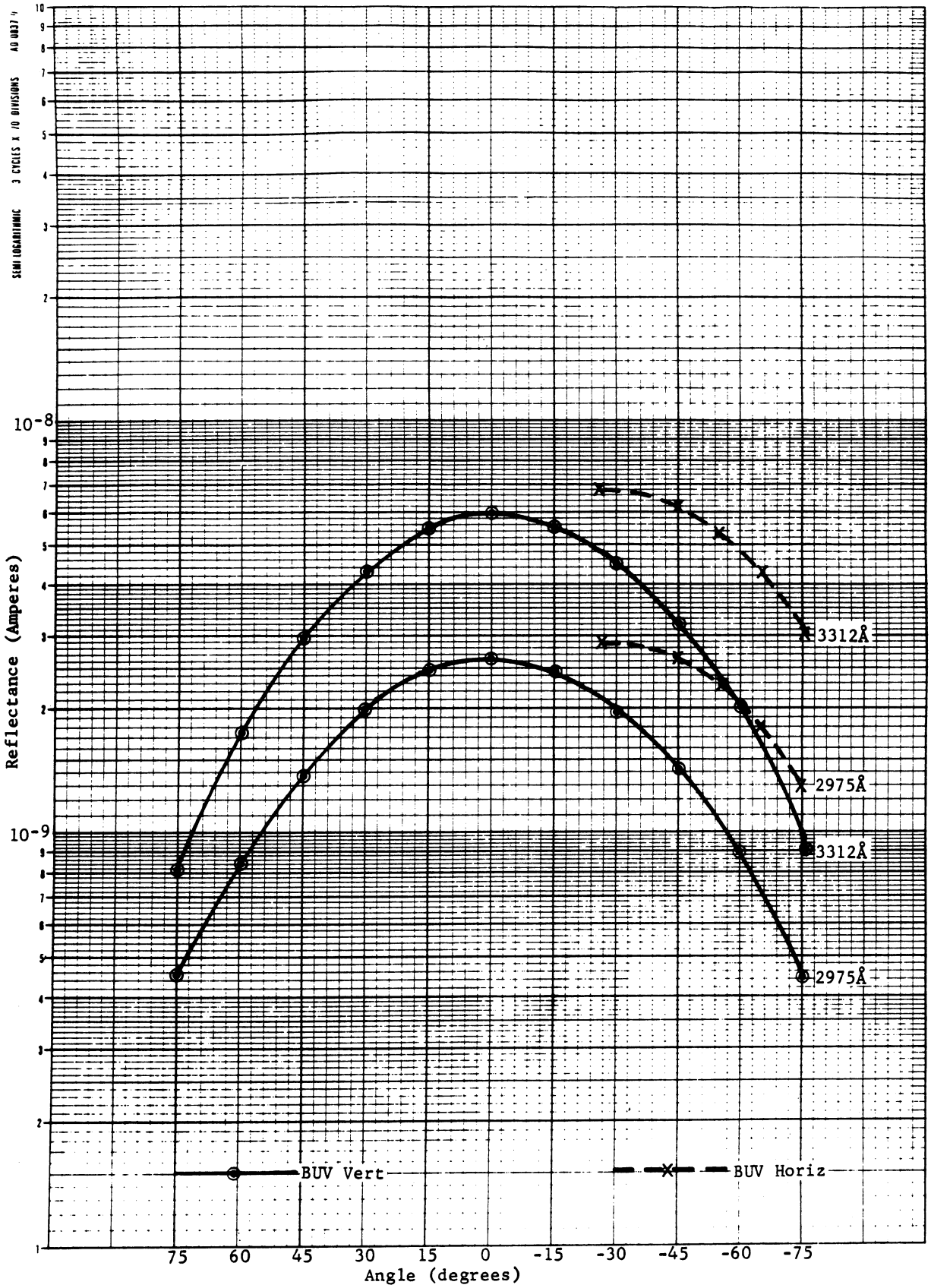

Figure 3-87. Aluminum Diffuser Plate Reflectance vs. Instrument Position

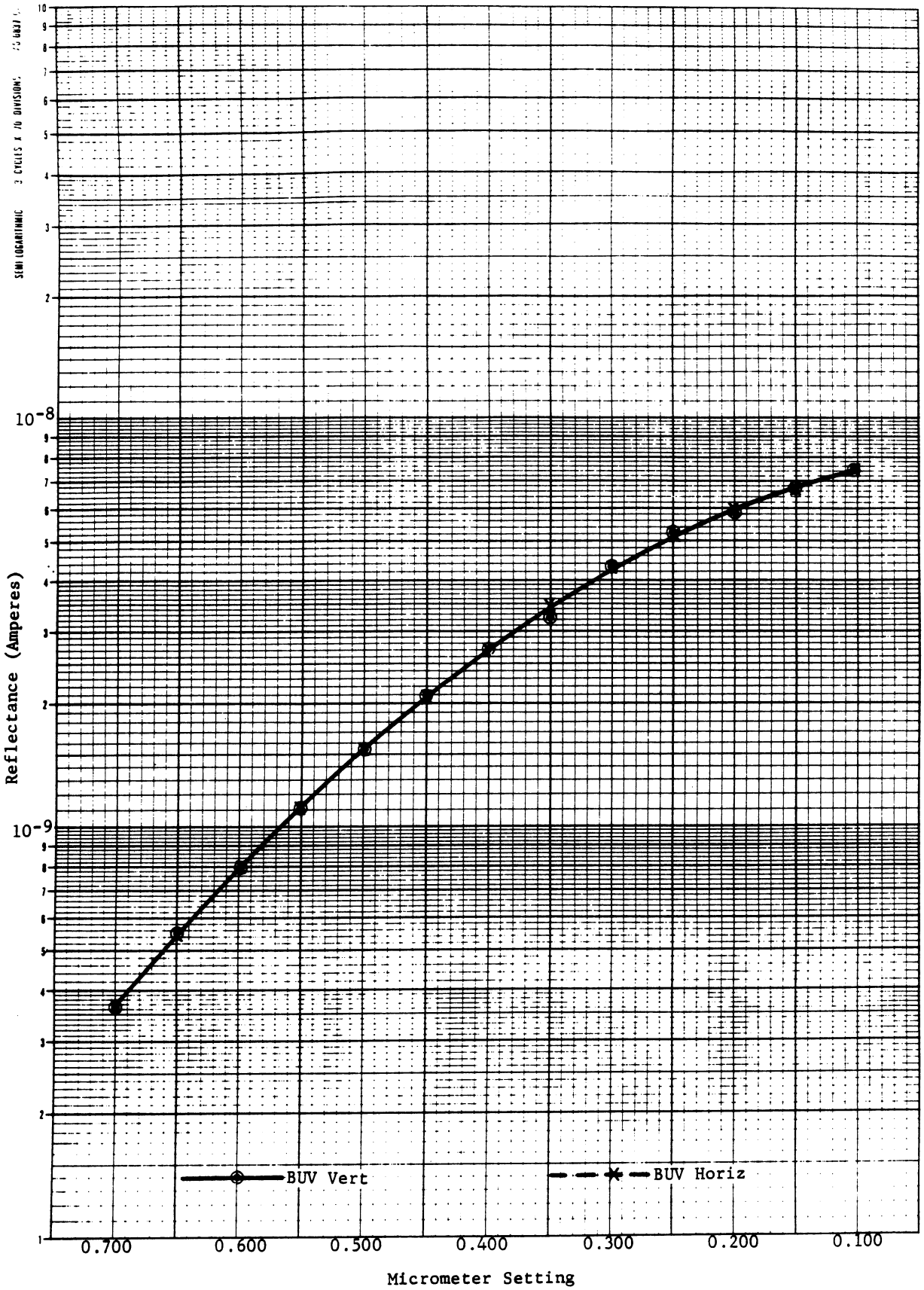

Figure 3-88. Barium Diffuser Plate--Reflectance vs. Wavelength

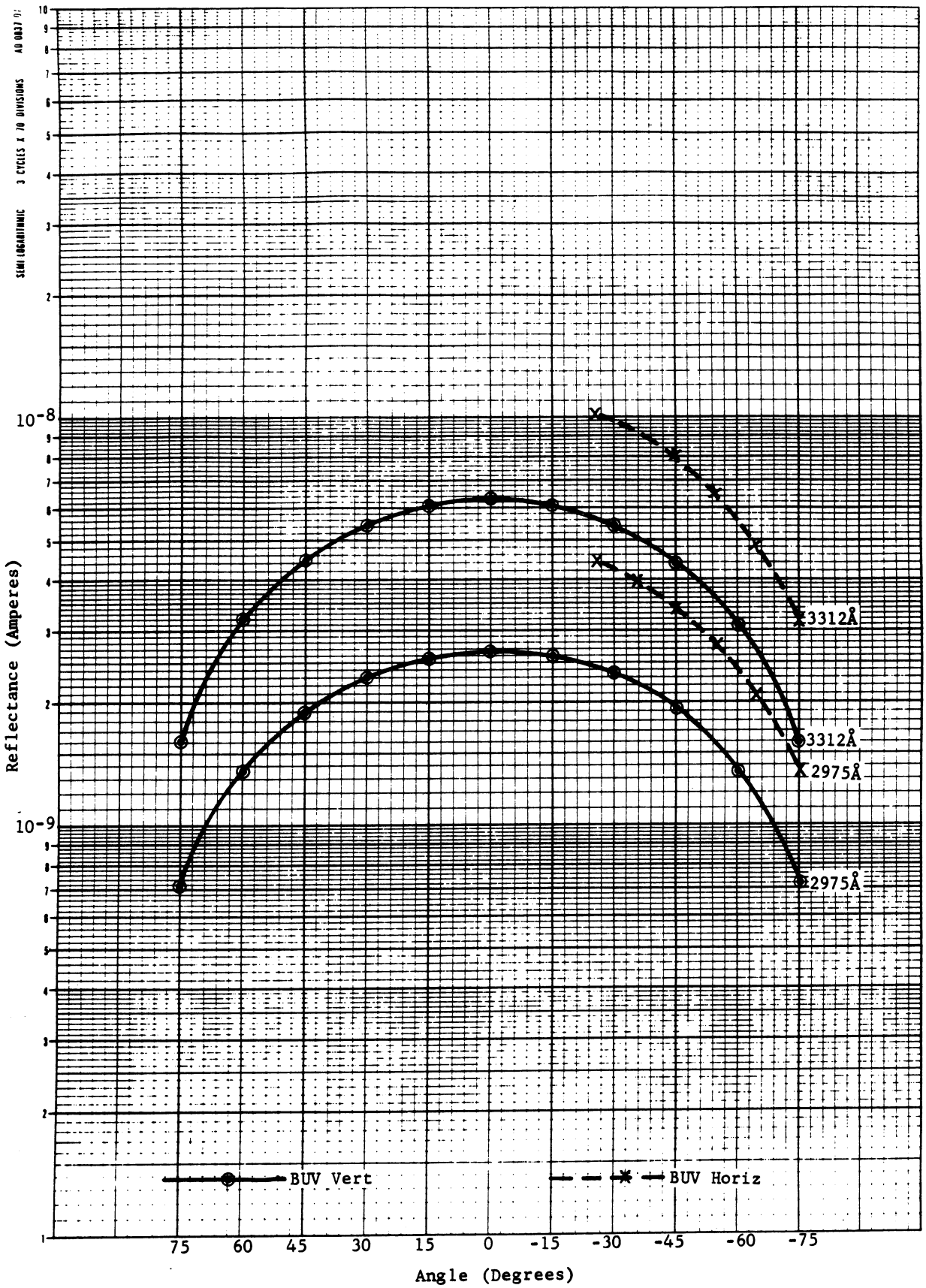

Figure 3-89. Barium Diffuser Plate--Reflectance vs. Instrument Position

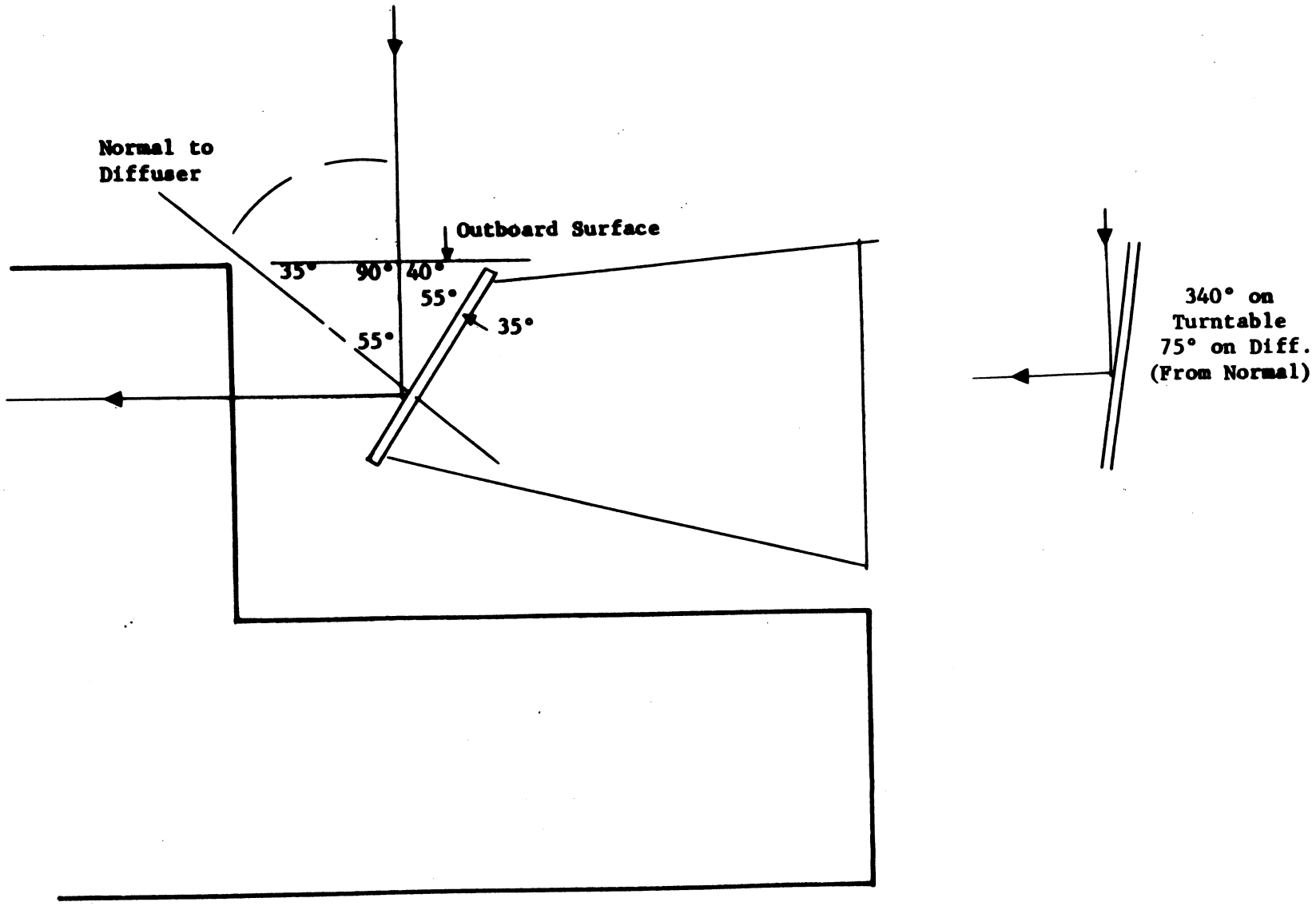

Figure 3-90. Angular Relationship Between Incident Energy and the BUV Breadboard

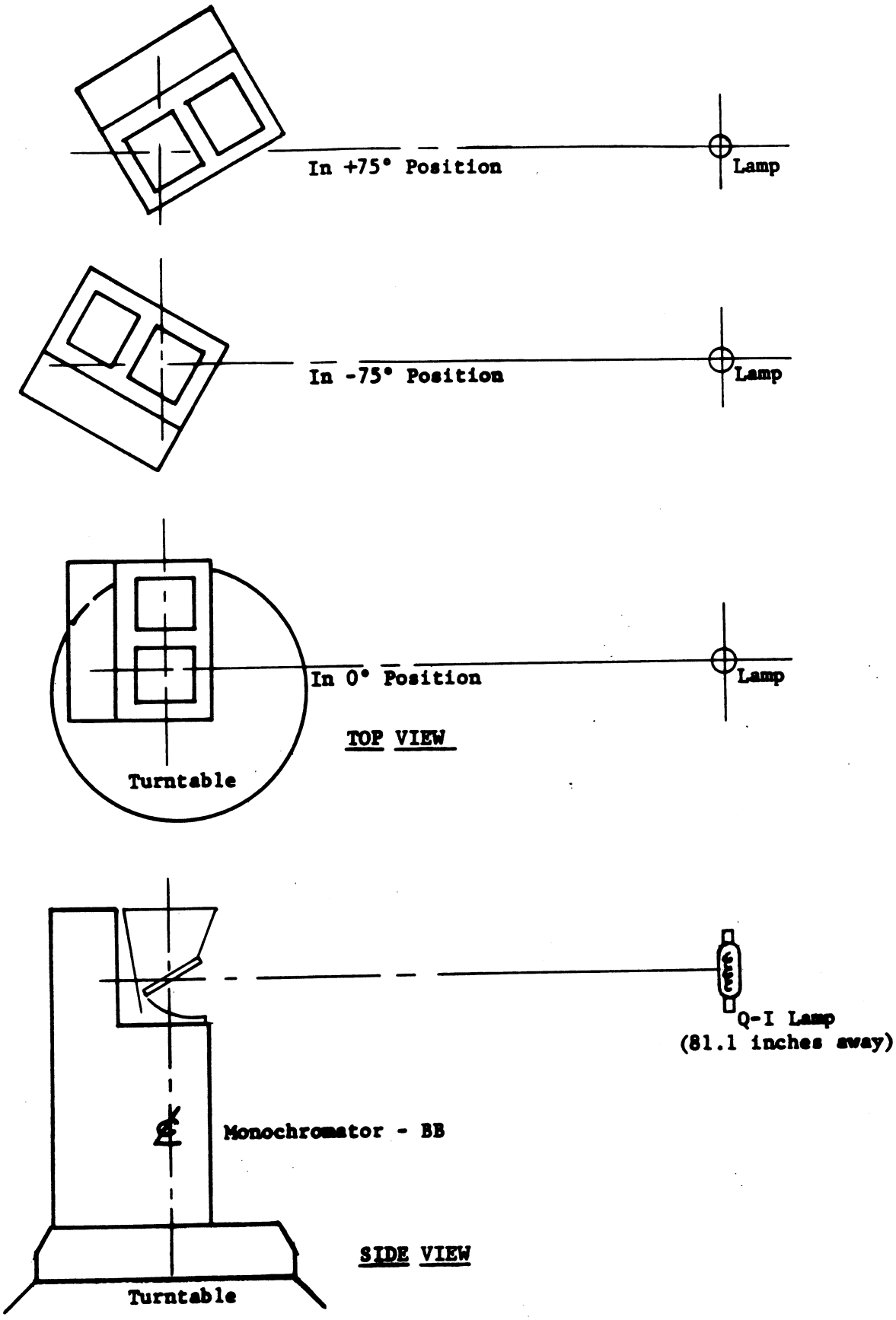

Figure 3-91. BUV in Vertical Position for Goniometric Sensitivity Measurements

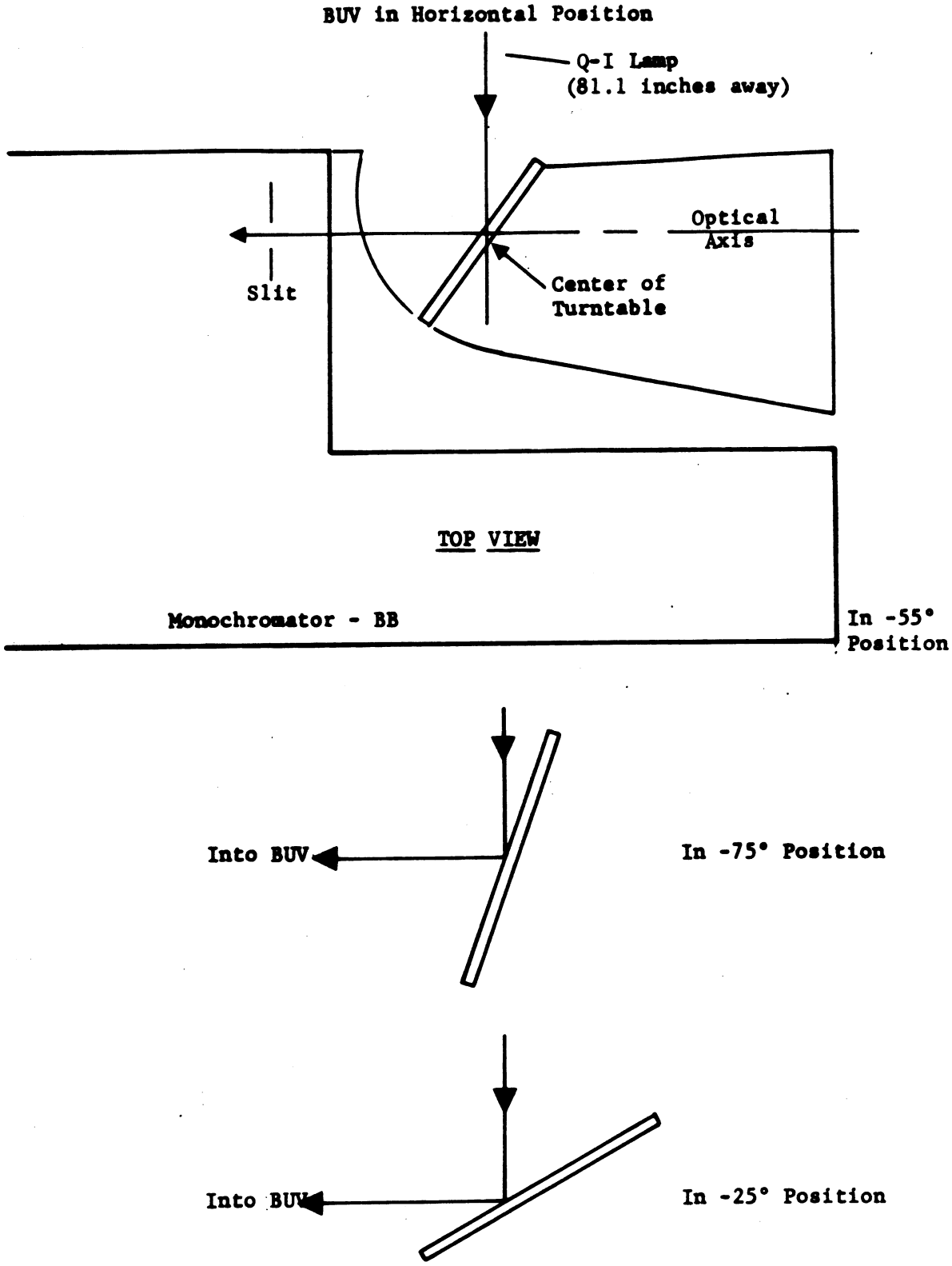

Figure 3-92. BUV in Horizontal Position for Goniometric Sensitivity